Trans-Dihydride Complexes of Ruthenium Bearing N-Heterocyclic Carbene Ligands

Davies, Caroline

Award date:
2014

Awarding institution:
University of Bath

Trans-Dihydride Complexes of Ruthenium Bearing N-Heterocyclic Carbene Ligands

Caroline Jessica Elizabeth Davies

A thesis submitted in partial fulfilment of the requirements for the degree of Doctor of Philosophy

Department of Chemistry

UNIVERSITY OF BATH

October 2014

Signed…… Date……..

Table of Contents

Acknowledgments

First, I thank Professor Mike Whittlesey for giving me the opportunity to commence research in his group as a project student and subsequently as a PhD student. Your support, depth of knowledge, experience and encouragement have helped me keep my sanity and focus. I have greatly appreciated working with such a caring and hard working supervisor.

I thank Dr. Mike Page for introducing me to the lab and for helping me through my BSc project and the first few months of my PhD. I also thank Dr. Araminta Ledger, Dr. Elena Mas-Marzá, Dr. Charlie Ellul and Dr. Tom Martin for establishing a welcoming and helpful working atmosphere..

I am very grateful to Dr. John Lowe for his massive amount of help with all things NMR and for putting up with so many questions from me.

I thank Dr. Mary Mahon for teaching me how to use the X-ray machines, solving my crystal structures and for offering advice and a friendly ear at some of the tougher times.

I thank soon to be Dr. Nicola Bramananthan, Rebecca Poulten, Lee Collins and Dr Ian Riddlestone for being great friends and co-workers. I thank Mateusz Cybulski for being such a motivated project student and a brilliant lab mate.

I thank my partner Steve for his love, endless support and tolerance of many late nights of working. I thank my parents for always being there when I need them.

Abstract

Addition of 1,3,4,5-tetramethylimidazol-2-ylidene (IMe_4) to $Ru(PPh_3)_3HCl$ (in the presence of H_2) or $Ru(PPh_3)_4H_2$ gave the all-*trans* isomer of $Ru(IMe_4)_2(PPh_3)_2H_2$, whereas 1,3-diethyl-4,5-dimethylimidazol-2-ylidene (IEt_2Me_2) reacted with $Ru(PPh_3)_4H_2$ to form *cis*, *cis*, *trans*-$Ru(IEt_2Me_2)_2(PPh_3)_2H_2$. The previously reported *trans* dihydride complex, $Ru(IMe_4)_4H_2$, was synthesized by a new method involving the reduction of $Ru(IMe_4)_4Cl_2$ with KC_8/H_2.

CO reacted with $Ru(IMe_4)_2(PPh_3)_2H_2$ to give a mixture of $Ru(IMe_4)_2(PPh_3)(CO)H_2$, $Ru(IMe_4)(PPh_3)_2(CO)H_2$ and $Ru(IMe_4)_2(CO)_3$; $Ru(IEt_2Me_2)_2(PPh_3)_2H_2$ reacted in a similar manner, although more slowly, allowing isolation of the monocarbonyl species $Ru(IEt_2Me_2)_2(PPh_3)(CO)H_2$. Insertion of CO_2 into one of the Ru-H bonds of $Ru(NHC)_2(PPh_3)H_2$ (NHC = IMe_4, IEt_2Me_2) generated mixtures of major and minor isomers of the κ^2-formate complexes $Ru(IMe_4)_2(PPh_3)(OCHO)H$ and $Ru(IEt_2Me_2)_2(PPh_3)(OCHO)H$. The hydridic nature of $Ru(NHC)_2(PPh_3)_2H_2$ (NHC = IMe_4, IEt_2Me_2) was apparent by their reactivity toward MeI, which gave $[Ru(IMe_4)_2(PPh_3)_2H]I$, $Ru(IEt_2Me_2)_2(PPh_3)HI$, $[Ru(IEt_2Me_2)_2(PPh_3)_2H]I$, and $Ru(IEt_2Me_2)(PPh_3)_2HI$.

H/D exchange of $Ru(IMe_4)_2(PPh_3)_2H_2$ with C_6D_6 (elevated temperature) or D_2 (room temperature) gave $Ru(IMe_4)_2(PPh_3)_2HD$ and $Ru(IMe_4)_2(PPh_3)_2D_2$. Addition of $P(C_6D_5)_3$ to a solution of the dihydride precursor resulted in the rapid substitution of the PPh_3 ligands. Addition of D_2 to $Ru(IMe_4)_4H_2$ gave $Ru(IMe_4)_4HD$ and $Ru(IMe_4)_4D_2$. The dihydride complex activated benzene and toluene at room temperature and could catalyse H/D exchange between the two solvents.

The catalytic activity of $Ru(NHC)_2(PPh_3)_2H_2$ (NHC = IMe_4, IEt_2Me_2) for the reduction of CO_2 by pinacolborane has been contrasted with that of the all-NHC analogue $Ru(IMe_4)_4H_2$. Despite the latter being substitutionally inert, it affords a far more active catalyst and yields a wider array of reduction products. These findings suggest that access to vacant coordination sites on the metal centre may not be a prerequisite for catalytic activity in the reduction of CO_2 and that, in this case, the presence of a highly nucleophilic hydride ligand may be of greater relevance. The dihydridoborate hydride complexes $Ru(IMe_4)_2(PPh_3)(H_2Bpin)H$ and $Ru(IEt_2Me_2)_2(PPh_3)(H_2Bpin)H$ were isolated by reaction of pinacolborane with $Ru(NHC)_2(PPh_3)_2H_2$ (NHC = IMe_4, IEt_2Me_2) and were structurally characterized.

List of Abbreviations

Å	angström
Ar	unspecified aryl group
atm.	atmospheres
BAr_4^F	$B(3,5\text{-}C_6H_3(CF_3)_2)_4$
br	broad
COD	1,5-cyclooctadiene
COE	cyclooctene
COSY	correlation spectroscopy
cm^{-1}	wavenumber
Cy	cyclohexyl
Cyp	cyclopentyl
d	doublet
δ	NMR chemical shift
dcpe	1,2-bis(dicyclohexylphosphino)-ethane
DFT	density functional theory
DPEphos	bis(2-diphenylphospinophenyl)ether
dmpe	$Me_2PCH_2CH_2PMe_2$
equiv	equivalents
EXSY	exchange spectroscopy
g	grams
h	hour(s)
HMBC	heteronuclear multiple bond correlation
HMQC	heteronuclear multiple quantum correlation
HSQC	heteronuclear single quantum correlation
Hz	hertz
i-	ipso
IAd	1,3-bis-adamantylimidazol-2-ylidene
ICy	1,3-dicyclohexylimidazol-2-ylidene
IEt_2Me_2	1,3-diethyl-4,5-dimethylimidazol-2-ylidene
$I^iPr_2Me_2$	1,3-diisopropyl-4,5-dimethylimidazol-2-ylidene
IMe_4	1,3,4,5-tetramethylimidazol-2-ylidene
IMes	1,3-dimesityl-imidazol-2-ylidene
^{i}Pr	*iso*-propyl
^{i}Pr-PONOP	$C_5H_3N\text{-}1,3\text{-}(OP^iPr_2)_2$

IPr	1,3-*bis*(2,6-diisopropylphenyl)imidazol-2-ylidene
IR	infra-red
I^{t}Bu	1,3-*bis*(*tert*-butyl)imidazol-2-ylidene
K	Kelvin
kJ	kilojoule(s)
L	generic metal ligand
m	multiplet
m-	meta
Me	methyl
mg	milligrams
MHz	megahertz
min	minute(s)
mL	milliliter
µl	microlitre
mmol	millimoles
mol	moles
NOESY	Nuclear Overhauser Effect Spectroscopy
NHC	N-heterocyclic carbene
o-	ortho
p-	para
PENDANT	Polarisation Enhancement During Attached Nucleus Testing
Ph	phenyl
PNP	2, 6-bis-(di-*tert*-butylphosphinomethyl)pyridine)
ppm	parts per million
q	quartet
R	unspecified generic group
s	singlet
t	triplet
$\nu_{(XY)}$	IR shift of XY bond
VT	variable temperature
Xantphos	9,9-dimethyl-4,5-bis(diphenylphosphino)xanthene

Chapter 1

Chapter 1: Transition Metal hydride complexes

Given the important role of transition metal phosphine hydride complexes such as $Rh(PPh_3)_3(CO)H$[1] and $Ru(PPh_3)_3(CO)H_2$[2] in catalytic applications, it is unsurprising that there has been considerable interest shown in the preparation and reactivity of related species in which one or more phosphines are substituted by N-heterocyclic carbenes (NHCs).[3] In this introduction, a brief overview of NHC-M-H chemistry will be given, as an entrée to a discussion on *trans* metal dihydride complexes, the topic that lies at the heart of this thesis.

1.1. Synthesis and reactivity of NHC-M-H complexes

Two conventional routes exist for the synthesis of NHC metal hydride complexes. In light of the favourable energetics of PR_3 substitution for NHC described many years ago by Nolan,[4] there are now many examples in which reaction of R_3P-M-H with carbene affords a corresponding NHC-M-H derivative (Scheme 1.1).[3,5]

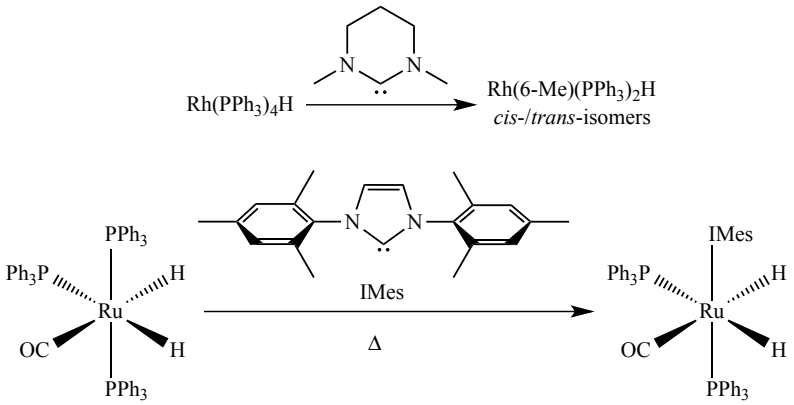

Scheme 1.1: PPh_3 substitution by NHC.

In these cases, the hydride ligand is already present in the precursor. An alternate approach is to introduce hydride through the oxidative addition of an imidazolium salt to a coordinatively unsaturated precursor (Scheme 1.2).[6]

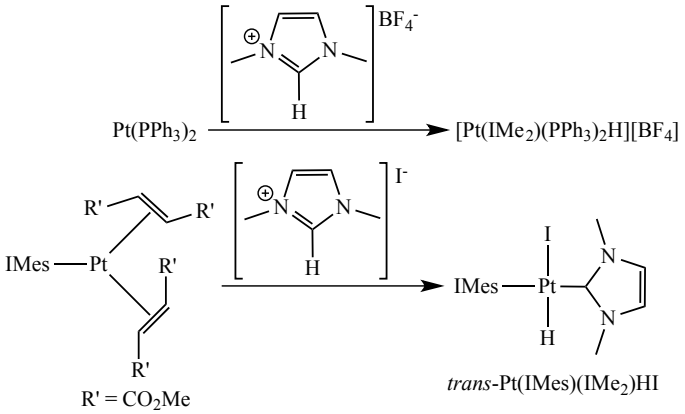

Scheme 1.2: Direct intermolecular C-H activation of the C2-H carbon in an imidazolium salt.

Under certain circumstances, the expected product is not formed, as in the case of Scheme 1.3, which illustrates the work by Crabtree *et al*. that led to the first example of so-called abnormal coordination through a backbone C4 or C5 position rather than via the "normal" C2 position.[7]

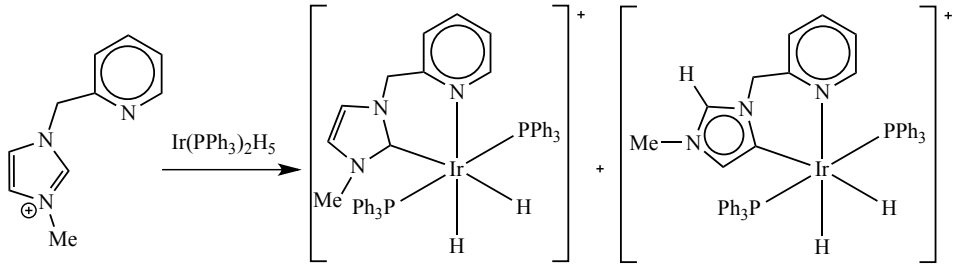

Scheme 1.3: Preparation of an Ir complex with the imidazole ring bound via C5 rather than the usual C2.

The reverse process in which the ligands in NHC-M-H combine to form $[NHCH]^+$ and M is one of the well-established reactions associated with this type of complex.[8] Two representative examples are shown in Scheme 1.4, although whether these involve true reductive elimination processes or deprotonation steps (i.e. hydrogen abstraction by the NHC acting as a base) is often not altogether clear.[9]

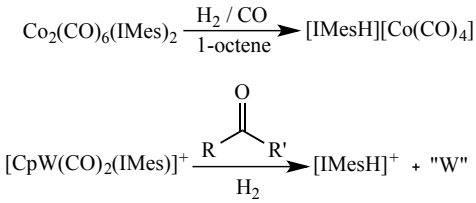

Scheme 1.4: Decomposition of the NHC-M-H complex via formation of $[IMesH]^+$.

Alongside reductive elimination, a series of intramolecular bond activation reactions of the N-substituents form perhaps the most well-known types of processes observed for NHC-M-H species.[4b,8] Most common is C-H activation which is particularly associated with the platinum group metals, especially Ru, Rh, Ir and Ni (Scheme 1.5).[10]

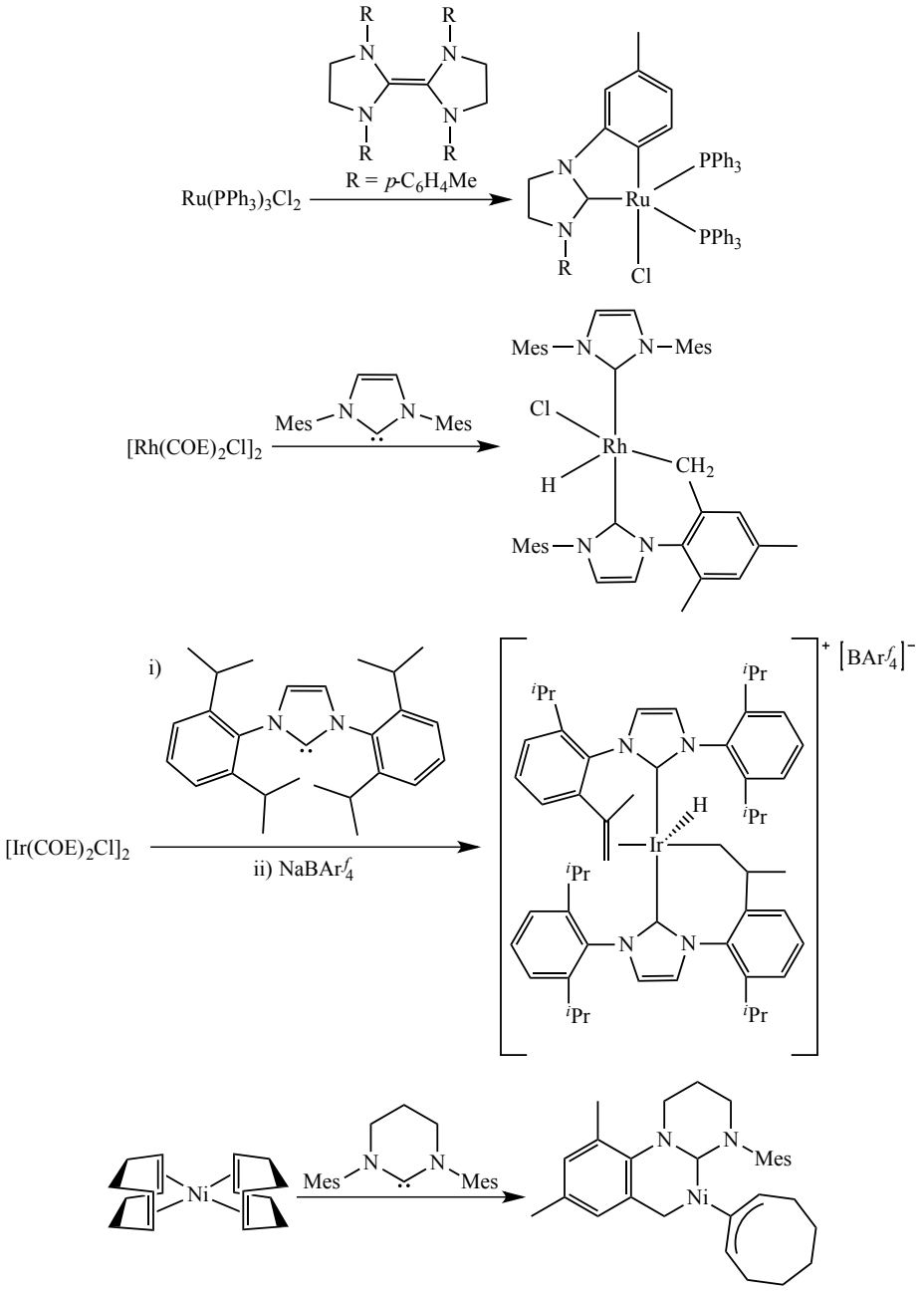

Scheme 1.5: Representative examples of C-H activation of NHCs in platinum group metal compounds.

C-H, as well as C-N activation, has been observed in NHC-Ni complexes although a Ni-H species has only been proposed as an intermediate in the reaction (Scheme 1.6).[11] In the case of Ru, C-H activation occurs alongside C-N activation, as shown in Scheme 1.7.[12]

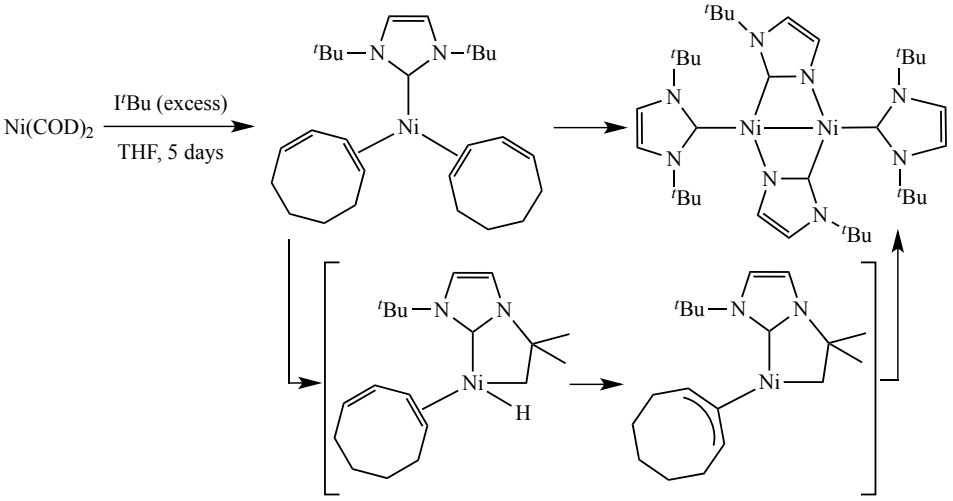

Scheme 1.6: C-H and C-N activation of I^{t}Bu by Ni(COD)$_2$ reported by Caddick and Cloke in 2004.

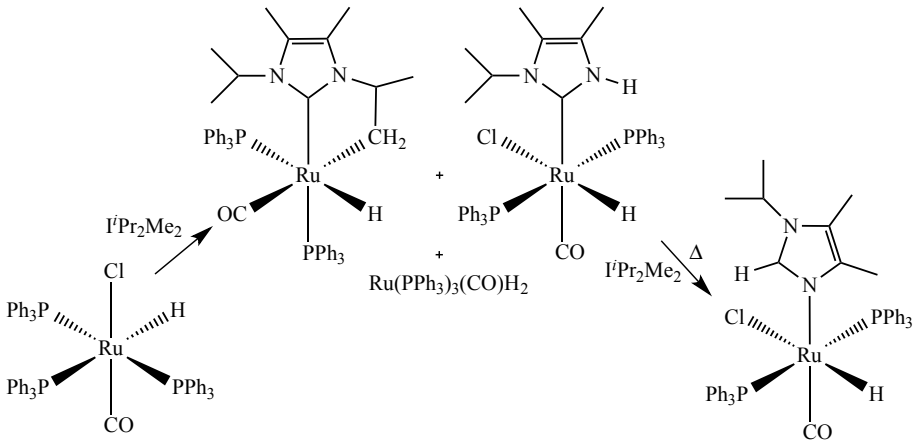

Scheme 1.7: Intramolecular C-N activation of the NHC in a Ru hydride complex.

Formation of the C-H activated Ru complex can also be achieved spontaneously by treatment of $Ru(PPh_3)_3(CO)H_2$ with $I^iPr_2Me_2$, although addition of H_2 reverses the process to generate $Ru(I^iPr_2Me_2)(PPh_3)_2(CO)H_2$ (Scheme 1.8).[13] This reversibility allows these species to be employed in the catalytic borrowing of hydrogen, and demonstrates that in some cases, decomposition of an NHC ligand by intramolecular activation need not be catastrophic for catalyst activity.

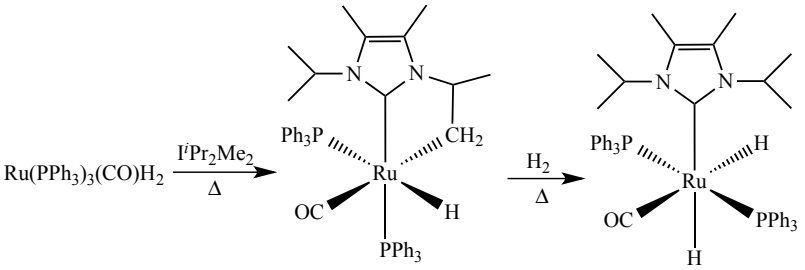

Scheme 1.8: Reversible C-H activation of the isopropyl methyl group of the NHC ligand.

1.1.1. Catalytic activity of NHC-M-H complexes

NHC-M-H species have been reported to be active catalyst precursors for other transformations. Leitner *et al*. synthesized Ru(IMes)(PCy_3)(η^2-H_2)$_2$(H_2) and Ru(IMes)$_2$(η^2-H_2)$_2$(H_2), the carbene analogues of Chaudret's complex Ru(PCy_3)$_2$(η^2-H_2)$_2$(H_2).[14] Ru(IMes)(PCy_3)(η^2-H_2)$_2H_2$ catalysed H/D exchange between H_2 and toluene-d_8. Activation of the *meta* C-D bond in toluene resulted in incorporation of D at both the metal centre and ultimately in the *o*-Me groups of the IMes ligand, indicative again of reversible intramolecular C-H activation. This reactivity contrasted to that of Chaudret's complex which showed no significant exchange with toluene-d_8 under the same reaction conditions.[15] This comparison provides another example of the remarkable effect substituting a PR_3 ligand for an NHC ligand can have on the properties of a metal complex.

Sabo-Etienne compared Ru(PCy_3)$_2$(η^2-H_2)$_2H_2$ and Ru($PCyp_3$)$_2$(η^2-H_2)$_2H_2$ in their reactions with C_6D_6, D_2 and their abilities to catalyse the deuteration of silanes. The $PCyp_3$ complex rapidly exchanged with C_6D_6 whereas the PCy_3 complex needed 24 h. When D_2 was used instead of C_6D_6 the exchange took place at the hydride sites instead of on the Cyp rings.[16] The PCyp complex was a more efficient catalyst for the deuteration of silanes.[17]

In 2012, Stephan *et al*. published the syntheses of a series of Ru hydride complexes (Figure 1.1) containing carbene-diether ligands that were effective catalysts for the hydrogenation of alkenes.[18] The ability of the carbene-ether substituents to coordinate to the metal (as in **A** and **B**) enhanced the catalytic activity. The electron-donating ability of the carbene in **B** could be changed by modifying the backbone substituents. These modifications did not have a dramatic impact on the catalytic activity, although for the select substrate cyclohexene, the catalyst with the most electron-donating carbene was significantly better. Introducing a CO ligand to the complex (**C**) generated a catalyst selective for terminal alkenes. Replacing the PPh_3

ligand with a second carbene ligand (*trans* to the existing NHC, **D**) stabilized the catalyst but reduced the catalytic activity, indirectly showing the advantages of having a mixed NHC/PR_3 system. However, the zwitterionic *bis*-carbene species (**E**, *cis* NHCs) enhanced reactivity selectively towards terminal alkenes.

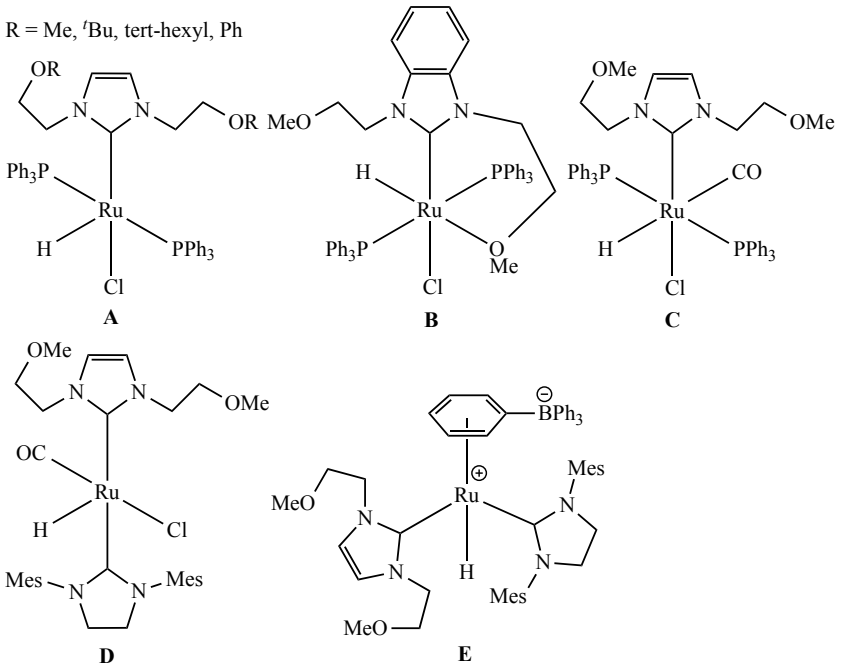

Figure 1.1: Series of Ru hydride complexes prepared by Stephan et al.

Nolan *et al*. in 2012 reported the catalytic deuteration of silanes as well as the hydrosilylation of ketones, aldehydes and imines using a Rh hydride complex as the catalyst (Scheme 1.9). Remarkably, the cyclometalated complex dissolved in the silane resulting in solvent free reaction conditions.[19]

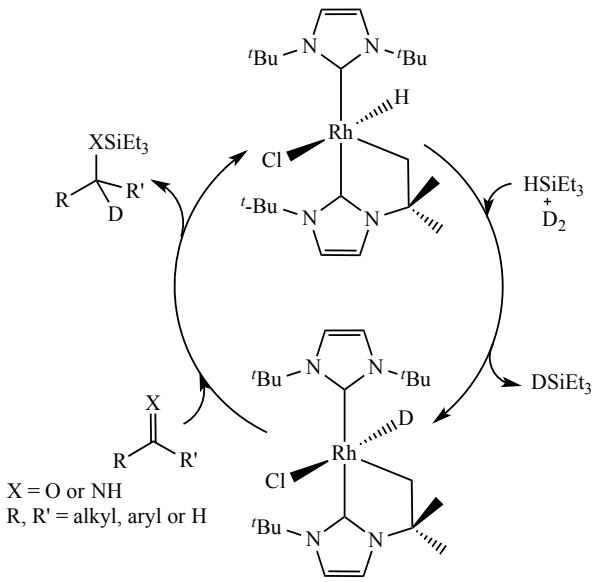

Scheme 1.9: A two step, one pot deuteration and hydrosilylation reaction.

1.2. Metal dihydride complexes: *cis* and *trans* isomers

In complexes such as $Ru(IMes)_2(\eta^2\text{-}H_2)_2H_2$ and $Ru(IMes)(PPh_3)_2(CO)H_2$, the hydride ligands are *cis*. This has implications for reactivity as such complexes are most likely to react via reductive elimination of H_2.

In most transition metal complexes bearing an NHC ligand and two hydride ligands, the hydrides are in a *cis* orientation. This is seen in some of the examples above. Another example of this was reported by Whittlesey *et al*. in 2006. UV irradiation of the complex, $Ru(IEt_2Me_2)(PPh_3)_2(CO)H_2$, resulted in isomerization involving loss of either H_2 or phosphine (Figure 1.2).[20] The phosphine analogue of this complex ($Ru(PPh_3)_3(CO)H_2$) has very different photochemistry, only losing H_2 on the way to postulated dimeric products.[21]

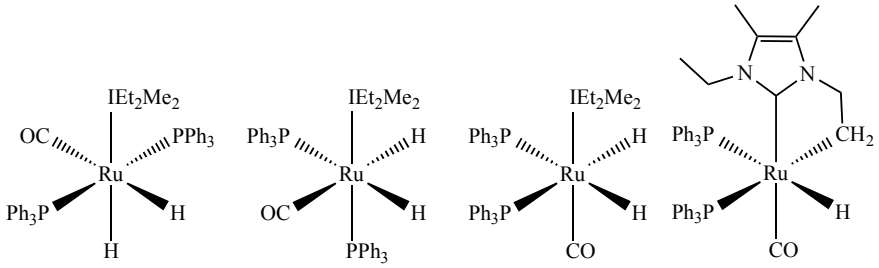

Figure 1.2: Product distribution resulting from irradiation with UV light of $Ru(IEt_2Me_2)(PPh_3)_2(CO)H_2$.

In contrast, *trans*-dihydride compounds are far less common and are likely to have quite different chemistry due to the nucleophilic properties of hydride when it is *trans* to another M-H ligand in a complex bearing strongly donating ligands such as NHCs. It is not possible to synthesise *trans* dihydride transition metal complexes directly from oxidative addition of H_2 to the metal centre, as a rearrangement from the *cis* dihydride isomer would be necessary. Due to the high *trans* influence and *trans* effect of hydride, a *cis* configuration of hydride ligands is more stable, unless dominant steric factors disfavour it. The use of either bulky ligands or pincer ligands are two commonly employed methods of synthesizing *trans* dihydride species.

1.2.1. Using Pincer ligands

Milstein *et al*. have reported a number of *trans* dihydride transition metal complexes using PNP type pincer ligands. In 1997 a neutral, 6-coordinate Ir *trans* dihydride complex (**H**, Scheme 1.10) was shown to be not only more thermodynamically favourable than the corresponding *cis* isomer (**G**) (the *cis* dihydride isomer converted to the *trans* dihydride complex with heating at 90 °C under 35 psi of

H_2), but also kinetically more stable. This was deduced by analysing two different synthetic pathways to the complex.[22] The first method was to react H_2 with the Ir(I) pincer complex **F**, which gave only **G**. This could be converted to **H** with heating. Removal of the H_2 atmosphere from **G** resulted in reformation of **F**. The second method involved reaction of $Ir(PPh_3)_3(CO)H$ with the pincer phosphine ligand. The product ratio (**H**:**G**) was 95:5. The latter immediately converted (in the absence of H_2) to **F**, indicating that the formation of the *trans* dihydride species was kinetically controlled.

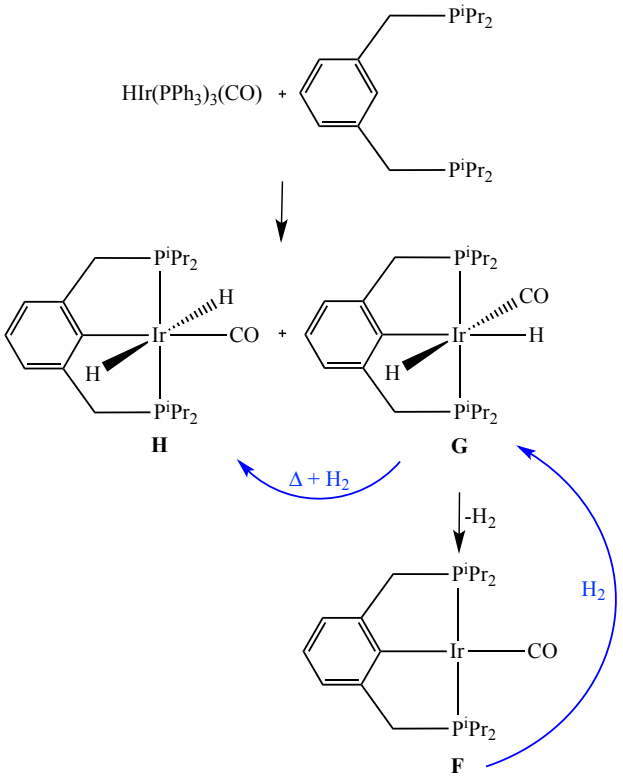

Scheme 1.10: Methods of synthesis of an Ir trans dihydride complex.

Goldberg reported the synthesis of the cationic Ir *trans* dihydride complex **I** based on a PNP pincer ligand upon decarbonylation and dehydrogenation of MeOH.[23] Interestingly, they also showed that the complex was more kinetically stable than its *cis* counterpart **J** since the latter could not be formed by oxidative addition of H_2 to the Ir(I) carbonyl complex **K** (Scheme 1.11).[24]

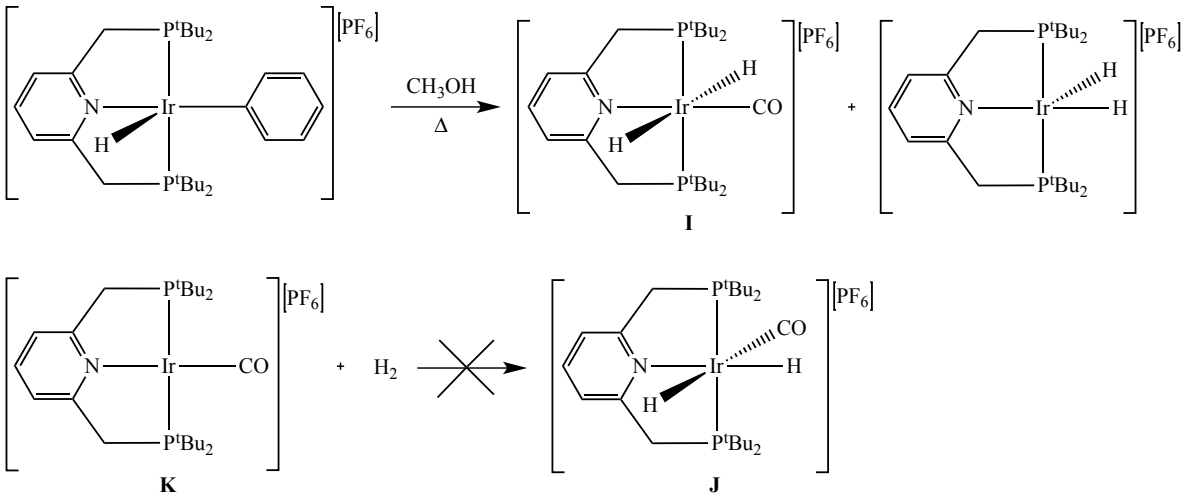

*Scheme 1.11: Method of synthesis of the Ir trans dihydride complex (**I**) reported by Goldberg in 2006.*

In 2006, Milstein *et al.* reported the synthesis of an Ir(III) *trans* dihydride complex upon addition of H_2 to an Ir(I) complex bearing the same tridentate phosphine ligand, with a monohydride species as a transition state (Scheme 1.12). The transition state was formed by water-assisted proton transfer. The PNP ligand had an active role in the activation of the H_2 involving aromatization/dearomatization of the ligand with proton migration from the ligand "arm" to the metal. In 2010, Brookhart published a different method for synthesising a similar *trans* dihydride Ir complex with a different phosphine ligand (Scheme 1.12). Since the bridge atoms of the phosphine ligand were oxygen in Brookhart's complex, the proton migration described by Milstein was not applicable. Instead the H_2 cleavage was proton-catalyzed. It was striking that two different water mediated mechanisms could apply to such similar systems.[25]

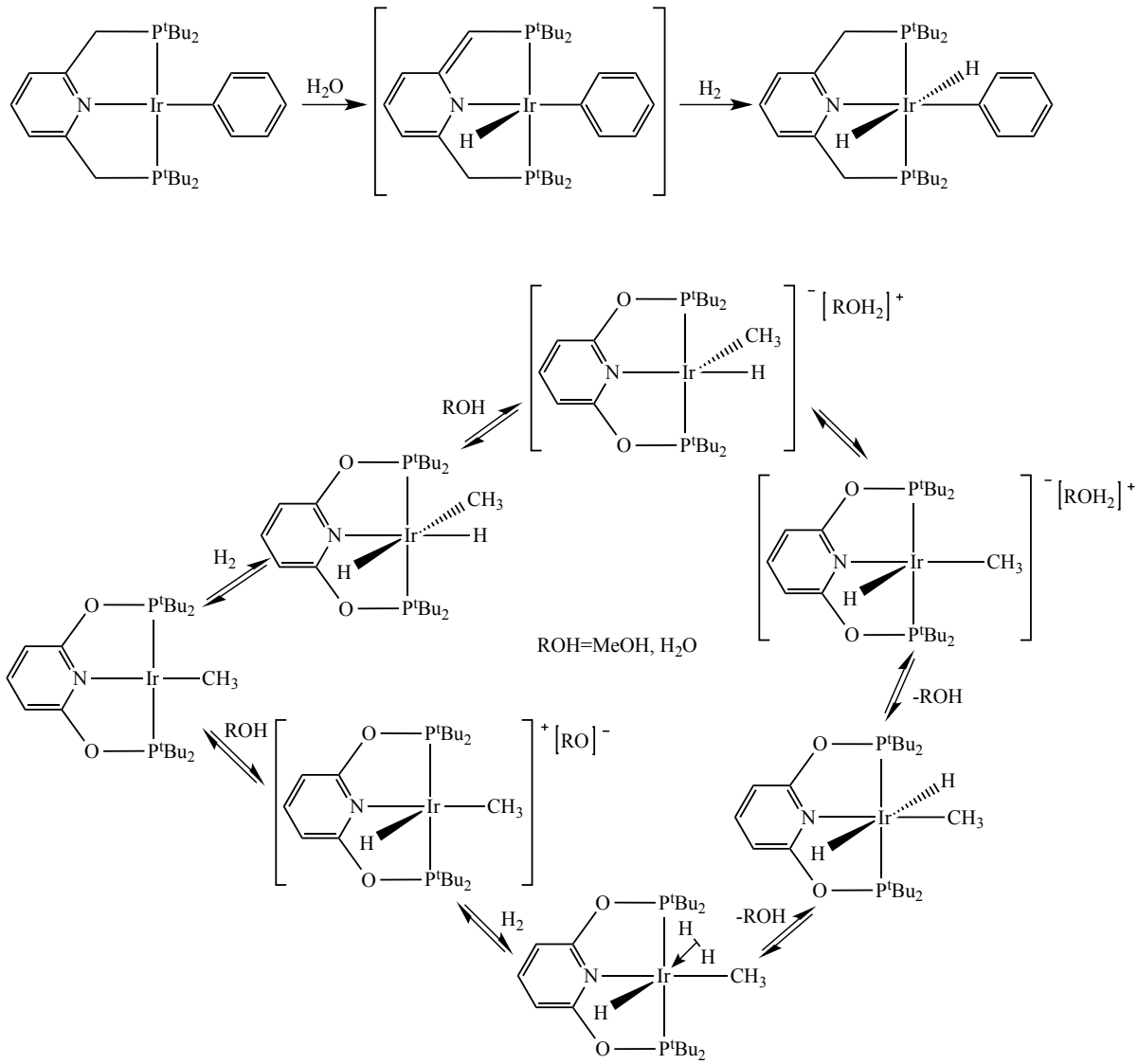

Scheme 1.12: Methods of synthesis of two trans dihydride Ir complexes by Milstein (top) and Brookhart (bottom) respectively.

In 2012, Milstein *et al*. reported the synthesis of *cis* and *trans* dihydride isomers of the pincer complex Fe(PNP)(CO)H_2 from the reaction of the borohydride hydride precursor with aniline (Scheme 1.13).[26] At room temperature, the equilibrium between the isomers lay heavily towards the *trans* isomer as the *cis* isomer was only detectable at low temperature.

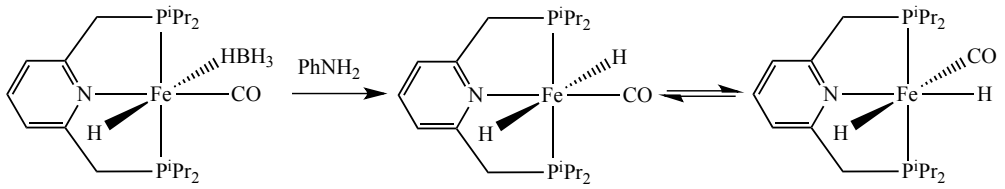

Scheme 1.13: Trans and cis Fe dihydride complexes described by Milstein et al. in 2012.

1.2.2. Using bulky ligands

Seven Pt *trans* dihydride complexes of the form PtL_2H_2 were synthesized by Shaw in 1974 by employing, different bulky phosphine ligands (L = P^tBuMe_2, P^tBuEt_2, $P^tBu(CH_2Ph)_2$, P^tBu_2Pr, $P^tBu_2CH_2Ph$ and $P(C_6H_{11})_3$), starting from either *cis*-PtL_2Cl_2 or *trans*-PtL_2HCl complexes. The more bulky the phosphine ligand the more stable the *trans* dihydride product.[27] Additional derivatives were later prepared by Otsuka in 1977 where L was either $P(C_6H_{11})_3$ or P^iPr_3 through the oxidative addition of MeOH to either two coordinate PtL_2 or three coordinate PtL_3, followed by the room temperature β-hydrogen elimination of the methoxy ligand.[28]

In 2004, Dahlenburg and Gotz used chelating phosphine-amine ligands to enforce a *trans* geometry in the Ir(III) cationic dihydride complexes $[Ir(P\text{-}N)_2H_2]^+$ (Scheme 1.14). Interestingly, the choice of hydrogen source dictated the selectivity for the *trans* H-Ir-H isomer. Use of KOH / ^{i}PrOH gave exclusively the *trans*-product, whereas K[BH(*s*-Bu)$_3$] gave a 3:1 isomeric mixture of *trans* and *cis* dihydride products.[29]

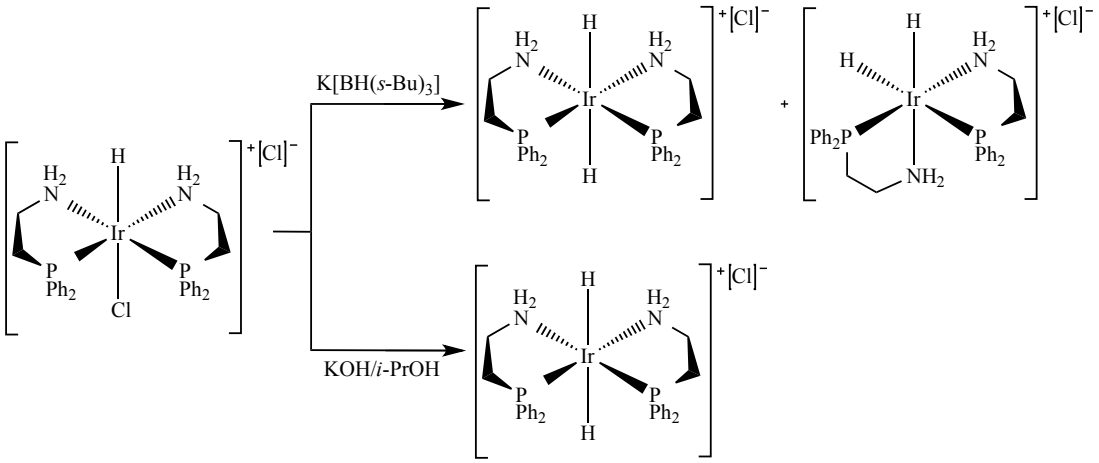

Scheme 1.14: Methods of synthesis of a trans $[Ir(P\text{-}N)_2H_2]^+$ complex.

Sabo-Etienne reported the isolation of a Ru *trans* dihydride with bulky $PCyp_3$ ligands ($Ru\{PCy_2(\eta^2\text{-}C_5H_7)\}_2H_2$) from the exposure of $Ru(PCyp_3)_2(H_2)_2H_2$ to C_2H_4 for only 2 minutes. In solution the *trans* dihydride was in equilibrium with the *cis* dihydride isomer.[30]

1.2.3. Stoichiometric and catalytic reactivity of *trans* H-M-H complexes

Milstein *et al.* reported the reactivity of the *trans*-dihydride Ir complex $IrC_6H_3(CH_2P(^iPr_2)_2)(CO)H_2$, with $CDCl_3$, PhC(O)Cl, CS_2 and MeI (Scheme 1.15).[22]

They proposed a direct attack of these electrophiles on the hydride ligand since the Ir complex was 18-electron with ligands which did not dissociate at ambient temperature. They noted that the monohydrides formed as a result of the reactions were inert to any excess of the electrophilic reagents, suggesting that the hydridic reactivity was a unique property of the *trans*-dihydride configuration. The *trans* influence of the hydride ligands weakened the normally strong Ir-H bonds rendering the hydrides more susceptible to electrophilic attack.

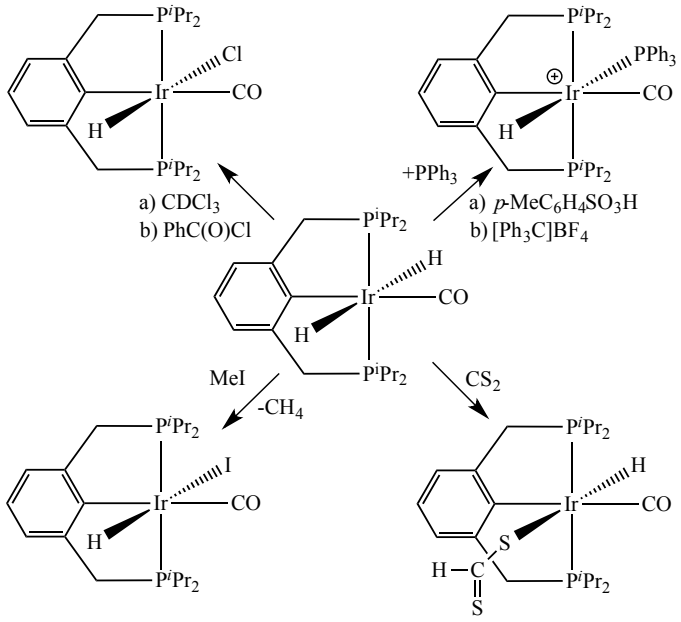

Scheme 1.15: Reaction of electrophiles with trans dihydride Ir complex.

In 2011 Yang reported the successful hydrogenation of ketones (specifically acetophenone) using the *trans* dihydride Fe complex shown in Scheme 1.16 as the catalyst.[31] The complex was initially observed by Milstein (Scheme 1.13) but was not considered in the mechanism they proposed for ketone hydrogenation.[32]

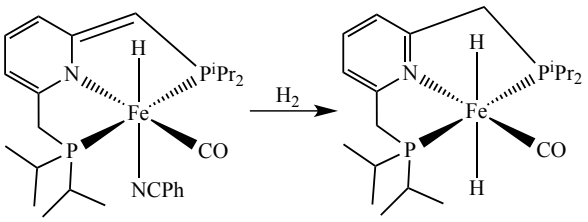

Scheme 1.16: Synthesis of the trans dihydride Fe complex reported by Milstein.

A series of Os and Ru *trans* dihydride complexes with tridentate PNP or POP ligands (Figure 1.3) were prepared by Gusev *et al* in 2011.[33] The Os PNP complex was

an excellent transfer hydrogenation catalyst for acetophenone (giving a TOF *ca*. x 10 higher than the Ru analogue) and also demonstrated high efficiency for the amination and dehydrogenative coupling of primary alcohols, producing secondary amines and symmetrical esters, respectively.

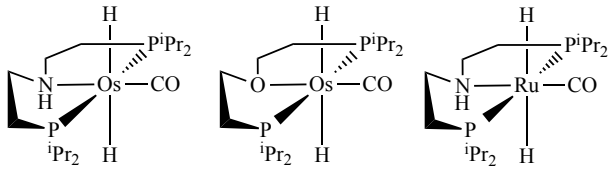

Figure 1.3: Group 8 metal trans dihydride complexes for alcohol dehydrogenation.

A *trans* H-Fe-H complex bearing a PNP pincer ligand was synthesized by Guan (Scheme 1.17) that was active as a hydrogenation catalyst for unactivated esters under mild conditions.[34] The catalytic efficiency was comparable to many Ru catalysts but was not as competitive as the most active Ru catalysts.[35]

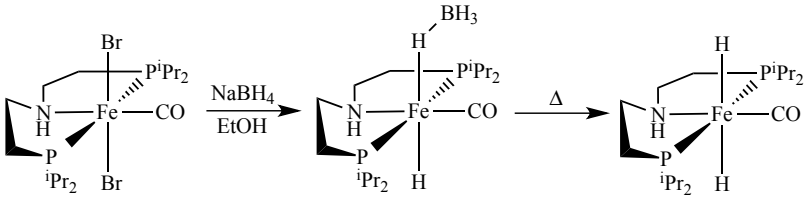

Scheme 1.17: One possible route to the active trans dihydride catalyst.

Morris reported characterisation of the *trans*-dihydride complexes **L** and **M** in equilibrium with their amido counterparts **N** and **O** via the transfer of H_2. This "Noyori" mixture was used for the enantioselective hydrogenation of ketones. A model of $H^{\delta+}\cdots H^{\delta-}$ transfer from the *trans* dihydridediamine complex to a prochiral ketone was proposed to explain the stereochemistry of the chiral alcohols produced (Scheme 1.18).[36] In 2002 they described the mechanism of the ketone hydrogenation in more detail for two Ru *trans* dihydride complexes (the previously reported dihydridediamine complex **L** and the analogous $Ru(PPh_3)_2$) complex **M**) which both showed elongated Ru-H bonds and were active catalysts for the hydrogenation of acetophenone with clean conversion to the alcohol (Scheme 1.18).

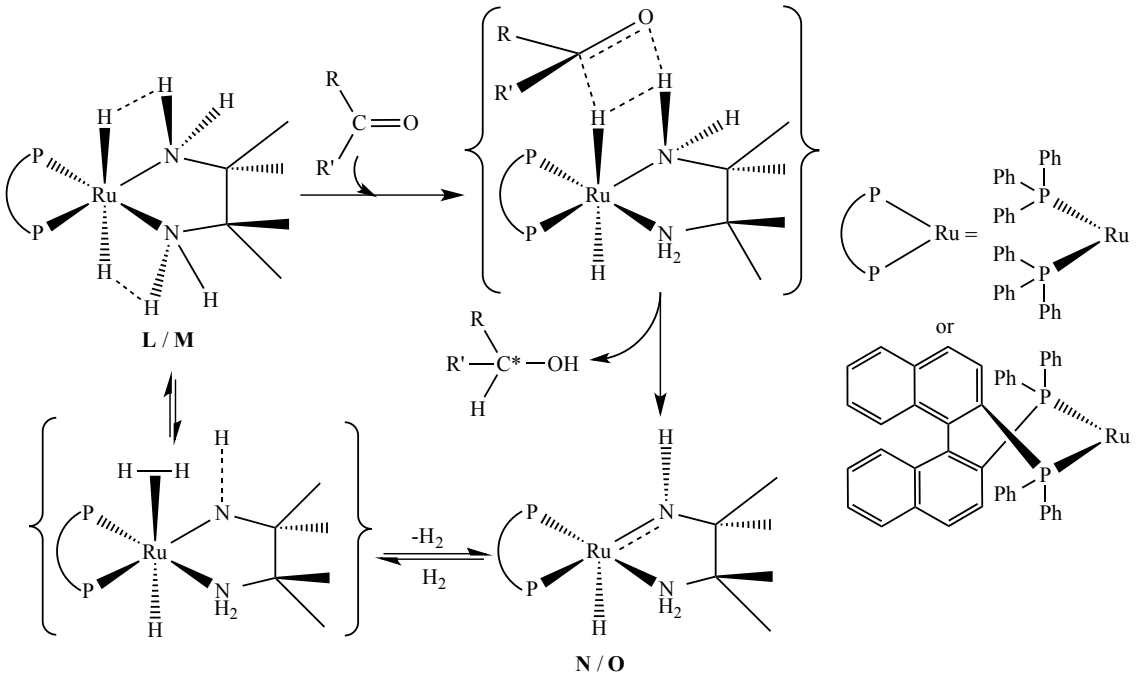

Scheme 1.18: Mechanism proposed by Morris for the catalytic hydrogenation of ketones catalysed by the trans dihydride complexes and the hydridoamido complexes.

Three years later Morris reported the synthesis of two tetradentate Ru *trans* dihydrides with bulky ligands (Figure 1.4). Both were shown to be catalytically active for ketone hydrogenation.[37] The precatalyst was the analogous HCl complex (*trans*-Ru($PPh_2C_6H_4CH_2NHC_6H_{10}NHCH_2C_6H_4PPh_2$)HCl) which reacted with a base to produce a reactive hydridoamido complex (Ru($PPh_2C_6H_4CH_2NC_6H_{10}NHCH_2C_6H_4PPh_2$)H) which subsequently added hydrogen across the Ru-amido bond forming the *trans* dihydride complex, **P**. **Q** was formed in much the same way, however the complex was only stable under H_2. Both **P** and **Q** formed along with other hydride-containing products.

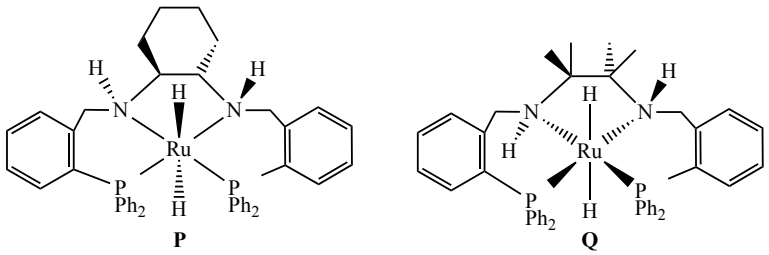

Figure 1.4: Trans dihydride Ru complexes with bulky ligands.

Further work on ketone hydrogenation using a Ru hydride chloride complex as the precatalyst yielded a succession of Ru dihydride complexes, one of which had *trans*

dihydride ligands. Investigating each step of the reaction as well as the conversion of the isomers revealed that the *trans* dihydride complex along with the corresponding amido-amine complex were the active hydrogenation catalysts and the analogous *cis* isomers were the precatalysts (Scheme 1.19).[38]

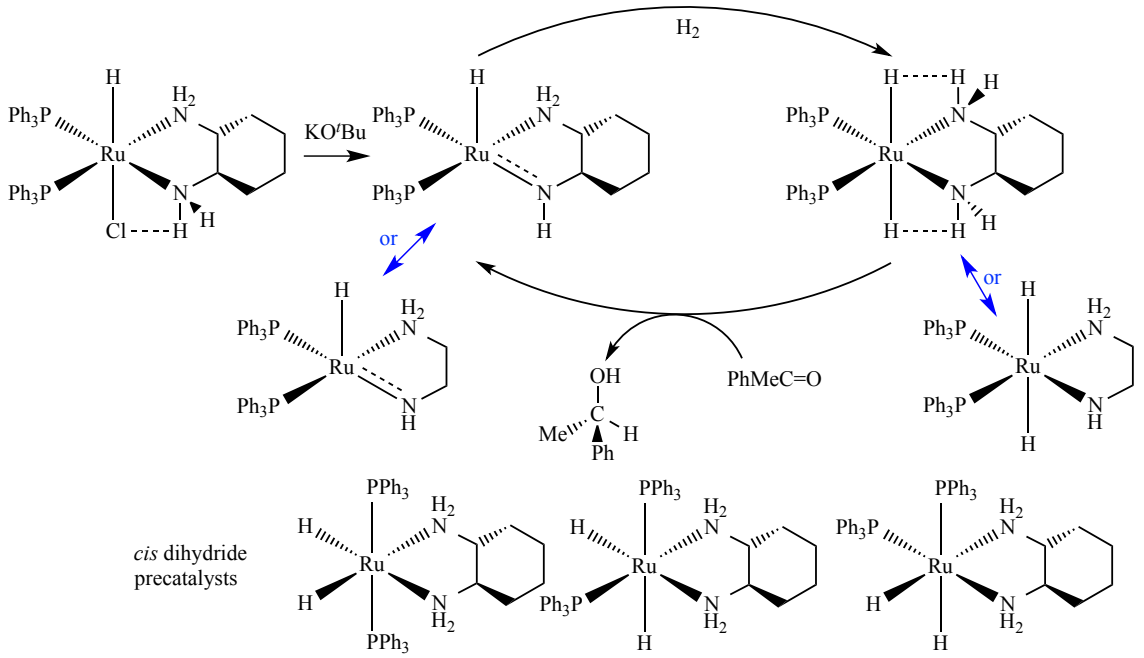

Scheme 1.19: Reaction of Ru hydride chloride producing a mixture of dihydride complexes and successful ketone hydrogenation catalysed by the trans dihydride complex.

Schneider *et al*. shed some light on the mechanism of ketone hydrogenation catalysed by the Ru amido chelate complexes illustrated in Scheme 1.20.[39] The heterolytic H_2 activation was shown to be reversible and resulted in hydrogenation and dehydrogenation of the ethylene bridges of the complexes. A similar equilibrium was reported by Milstein *et al.* in 2006, in which the complexes contained a pyridine based PNP ligand and a CO ligand in place of the PMe_3 ligand.[40]

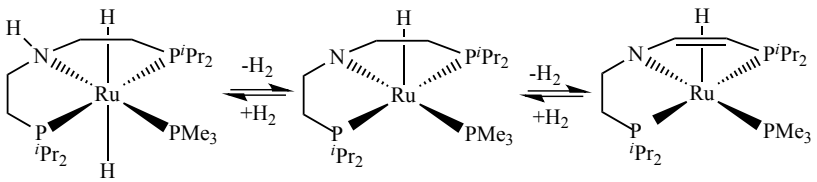

Scheme 1.20: Hydrogenation and dehydrogenation of the ethylene bridges in Ru PNP complex.

Schneider also reported proton exchange between water and the hydride ligand of $Ru(HN(CH_2CH_2P^iPr_2)_2)(PMe_3)H_2$ which was evident by broadening of the hydride resonance in the ^1H NMR spectrum. The hydride that exchanged with H_2O was on the same side of the Ru centre as the substituent proton on the adjacent tridentate phosphine ligand. The hydride the other side of the metal centre did not exchange with H_2O.[41]

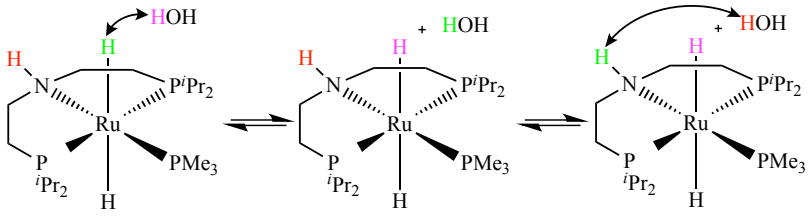

Scheme 1.21: Interaction between a hydride ligand of a trans dihydride complex with the adjacent ligand substituent.

In 2011 Beller *et al*. reported alcohol dehydrogenation under mild conditions using the product formed upon reaction of $Ru(PPh_3)_3(CO)H_2$ and the PNP pincer ligand $(P^iPr_2CH_2CH_2)_2NH$. They proposed the formation of the *trans* dihydride complex, $Ru(PNP)(CO)H_2$ after phosphine exchange, followed by the loss of H_2 upon heating, consistent with the mechanism reported by Schneider *et al*. The resultant Ru(PNP)(CO)H complex then reacted with the alcohol to reform the *trans* dihydride species.[42]

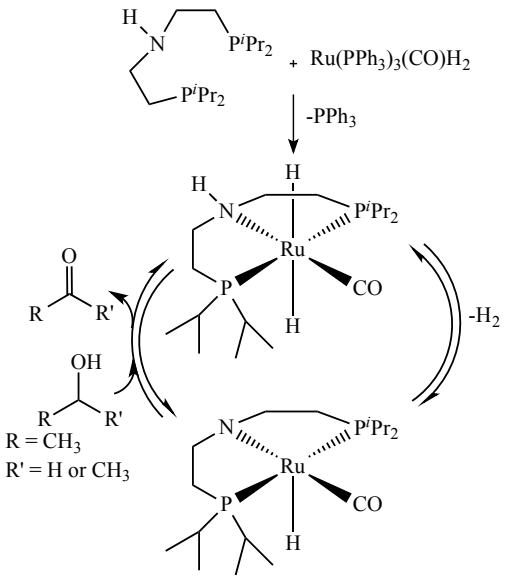

Scheme 1.22: Alcohol dehydrogenation catalysed by a trans dihydride Ru complex.

In 2008, Leitner *et* al. described the catalytic H/D exchange between arenes, alkenes and deuterated benzene under mild conditions using Ru(dtbpmp)(η^2-H_2)(H_2), Figure 1.5. When isoquinoline was used as a substrate, two *trans* dihydride complexes were the transition states, one of which was 19.6 kcal mol^{-1} more stable than the other.[43]

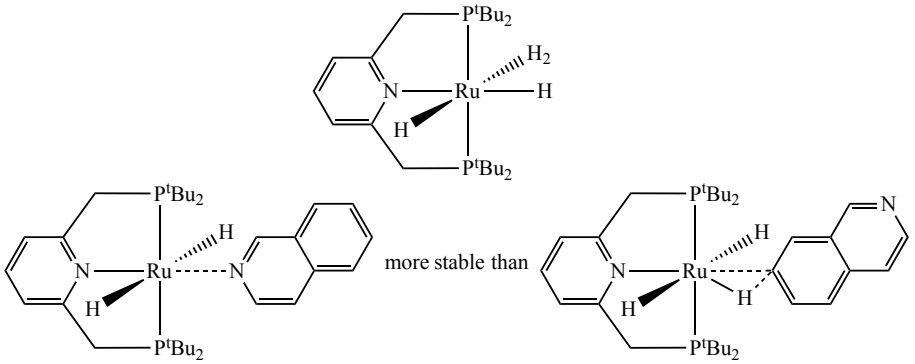

Figure 1.5:Trans dihydride Ru complexes reported by Leitner.

1.3. *Trans* dihydride transition metal complexes with an NHC ligand

There are remarkably few examples of *trans*-H-M-H complexes containing NHC ligands. During attempts to hydrogenate the C-H activated N-Et carbene complex Ru(IEt_2Me_2)'(PPh_3)$_2$(CO)H (**R**), it was reported that reaction with EtOH gave the thermally unstable *trans*-dihydride isomer of Ru(IEt_2Me_2)(PPh_3)$_2$(CO)H_2 (**S**). Only spectroscopic characterisation was provided as this rapidly isomerised at 323 K to the *cis* isomer **T** and ultimately to **U**.[44]

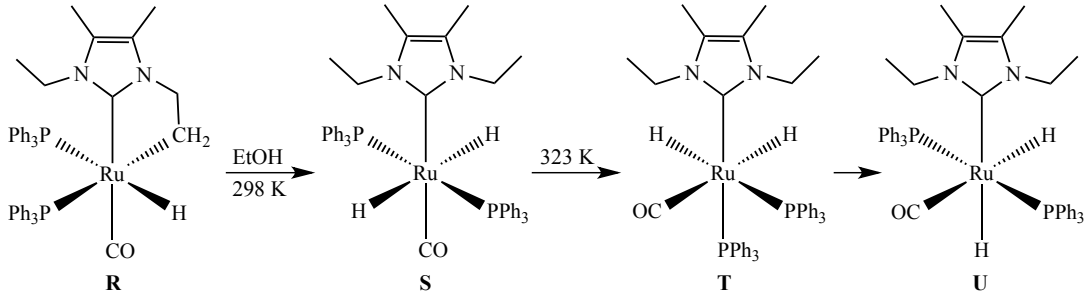

*Scheme 1.23: Synthesis of the short lived trans dihydride NHC Ru complex **T** and the subsequent more stable cis isomers.*

Following on from the approach of generating *trans*-Pd(PPh_3)$_2H_2$ complexes with bulky phosphines,[27,28] Cazin reported that addition of H_2 to Pd(IPr)(PCy_3) gave the structurally characterised *trans*-dihydride species Pd(IPr)(PCy_3)H_2 (Scheme 1.24).[45] Use

of HD gave the isotopomer Pd(IPr)(PCy_3)HD, which exhibited a *trans* $^2J_{HD}$ coupling constant of 7 Hz.

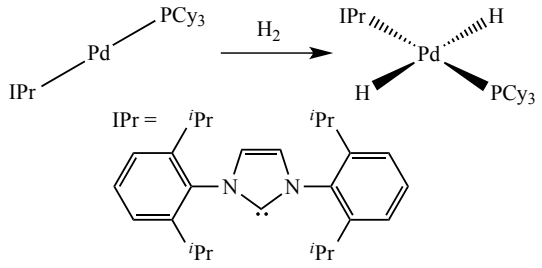

Scheme 1.24: Formation of a mixed NHC/PR_3 trans dihydride Pd complex.

Of particular relevance to this thesis, was the report by Wolf and co-workers on the reduction of *trans*-Ru(IMe_4)$_4Cl_2$ by $LiAlH_4$ to give *trans*-Ru(IMe_4)$_4H_2$.[46] Despite the relatively small size of the IMe_4 ligand, the propeller arrangement of the four NHCs helped to stabilise the *trans* H-Ru-H geometry. DFT calculations were carried out comparing the stability with the theoretical *cis* isomer. This is discussed further at the beginning of Chapter 2.

1.4. Project outline

Given Wolf's findings above, the aim of the work described in this thesis was to prepare analogues of Ru(IMe_4)$_4H_2$ incorporating phosphine ligands to provide a series of potentially more substitutionally labile and stereoelectronically tuneable ruthenium *trans*-dihydride complexes for study. Chapter 2 reports on the synthesis of all-*trans* Ru(IMe_4)$_2$(PPh_3)$_2H_2$ and *cis*, *cis*, *trans*-Ru(IEt_2Me_2)$_2$(PPh_3)$_2H_2$, as well as an improvement to the preparation of Ru(IMe_4)$_4H_2$. Chapter 3 describes the stoichiometric reactions of these compounds with CO, CO_2 and MeI. Their susceptibility to H/D exchange with deuteroarenes and D_2 is reported in Chapter 4. Chapter 5 discusses the application of these complexes as catalysts for the reduction of CO_2 with pinacolborane.

1.5. References

1. (a) Arisawa, M.; Kuwajima, M.; Toriyama, F.; Li, G.; Yamaguchi, M., *Org. Lett.* **2012**, *14,* 3804; (b) Burling, S.; Whittlesey, M. K.; Williams, J. M. J., *Adv. Synth. Catal.* **2005**, *347,* 591; (c) Trzeciak, A. M.; Olejnik, Z.; Ziolkowski, J. J.; Lis, T., *Inorg. Chim. Acta* **2003**, *350,* 339; (d) Menglet, D.; Bond, A. M.; Coutinho, K.; Dickson, R. S.; Lazarev, G. G.; Olsen, S. A.; Pilbrow, J. R., *J. Am. Chem. Soc.* **1998**, *120,* 2086; (e) Evans, D.; Osborn, J. A.; Wilkinson, G., *J. Chem. Soc.* **1968**, 3133.

2. (a) Kakiuchi, F.; Murai, S., *Acc. Chem. Res.* **2002**, *35,* 826; (b) Sonoda, M.; Kakiuchi, F.; Chatani, N.; Murai, S., *Bull. Chem. Soc. Jpn.* **1997**, *70,* 3117; (c) Kakiuchi, F.; Sekine, S.; Tanaka, Y.; Kamatani, A.; Sonoda, M.; Chatani, N.; Murai, S., *Bull. Chem. Soc. Jpn.* **1995**, *68,* 62.

3. Jazzar, R. F. R.; Macgregor, S. A.; Mahon, M. F.; Richards, S. P.; Whittlesey, M. K., *J. Am. Chem. Soc.* **2002**, *124,* 4944.

4. (a) Clavier, H.; Nolan, S. P., *Chem. Commun.* **2010**, *46,* 841; (b) Scott, N. M.; Nolan, S. P., *Eur. J. Inorg. Chem.* **2005**, 1815.

5. Segarra, C.; Mas-Marzá, E.; Lowe, J. P.; Mahon, M. F.; Poulten, R. C.; Whittlesey, M. K., *Organometallics* **2012**, *31,* 8584.

6. (a) Hahn, F. E.; Jahnke, M. C., *Angew. Chem., Int. Ed.* **2008**, *47,* 3122; (b) Duin, M. A.; Clement, N. D.; Cavell, K. J.; Elsevier, C. J., *Chem. Commun.* **2003**, 400.

7. (a) Appelhans, L. N.; Zuccaccia, D.; Kovacevic, A.; Chianese, A. R.; Miecznikowski, J. R.; Macchioni, A.; Clot, E.; Eisenstein, O.; Crabtree, R. H., *J. Am. Chem. Soc.* **2005**, *127,* 16299; (b) Chianese, A. R.; Kovacevic, A.; Zeglis, B. M.; Faller, J. W.; Crabtree, R. H., *Organometallics* **2004**, *23,* 2461; (c) Crabtree, R. H., *Pure Appl. Chem.* **2003**, *75,* 435; (d) Grundemann, S.; Kovacevic, A.; Albrecht, M.; Faller, J. W.; Crabtree, R. H., *J. Am. Chem. Soc.* **2002**, *124,* 10473; (e) Kovacevic, A.; Grundemann, S.; Miecznikowski, J. R.; Clot, E.; Eisenstein, O.; Crabtree, R. H., *Chem. Commun.* **2002**, 2580.

8. Crudden, C. M.; Allen, D. P., *Coord. Chem. Rev.* **2004**, *248,* 2247.

9. (a) Wu, F.; Dioumaev, V. K.; Szalda, D. J.; Hanson, J.; Bullock, R. M., *Organometallics* **2007**, *26,* 5079; (b) van Rensburg, H.; Tooze, R. P.; Foster, D. F.; Slawin, A. M. Z., *Inorg. Chem.* **2004**, *43,* 2468.

10. (a) Davies, C. J. E.; Page, M. J.; Ellul, C. E.; Mahon, M. F.; Whittlesey, M. K., *Chem. Commun.* **2010**, *46,* 5151; (b) Tang, C. Y.; Smith, W.; Vidovic, D.; Thompson, A. L.; Chaplin, A. B.; Aldridge, S., *Organometallics* **2009**, *28,* 3059; (c) Huang, J. K.; Stevens, E. D.; Nolan, S. P., *Organometallics* **2000**, *19,* 1194; (d) Hitchcock, P. B.; Lappert, M. F.; Pye, P. L.; Thomas, S., *J. Chem. Soc., Dalton Trans.* **1979**, 1929.

11. Caddick, S.; Cloke, F. G. N.; Hitchcock, P. B.; Lewis, A. K. D., *Angew. Chem., Int. Ed.* **2004**, *43,* 5824.

12. Burling, S.; Mahon, M. F.; Powell, R. E.; Whittlesey, M. K.; Williams, J. M. J., *J. Am. Chem. Soc.* **2006**, *128,* 13702.

13. Burling, S.; Paine, B. M.; Nama, D.; Brown, V. S.; Mahon, M. F.; Prior, T. J.; Pregosin, P. S.; Whittlesey, M. K.; Williams, J. M. J., *J. Am. Chem. Soc.* **2007**, *129,* 1987.

14. Giunta, D.; Holscher, M.; Lehmann, C. W.; Mynott, R.; Wirtz, C.; Leitner, W., *Adv. Synth. Catal.* **2003**, *345,* 1139.

15. (a) Guari, Y.; Sabo-Etienne, S.; Chaudret, B., *Eur. J. Inorg. Chem.* **1999**, 1047; (b) Guari, Y.; Sabo-Etienne, S.; Chaudret, B., *J. Am. Chem. Soc.* **1998**, *120,* 4228; (c) Chaudret, B.; Poilblanc, R., *Organometallics* **1985**, *4,* 1722; (d) Chaudret, B.; Devillers, J.; Poilblanc, R., *J. Chem. Soc., Chem Commun.* **1983**, 641.

16. Grellier, M.; Mason, S. A.; Albinati, A.; Capelli, S. C.; Rizzato, S.; Bijani, C.; Coppel, Y.; Sabo-Etienne, S., *Inorg. Chem.* **2013**, *52,* 7329.

17. Smart, K. A.; Mothes-Martin, E.; Annaka, T.; Grellier, M.; Sabo-Etienne, S., *Adv. Synth. Catal.* **2014**, *356,* 759.

18. Wang, T.; Pranckevicius, C.; Lund, C. L.; Sgro, M. J.; Stephan, D. W., *Organometallics* **2013**, *32,* 2168.

19. (a) Egbert, J. D.; Nolan, S. P., *Chem. Commun.* **2012**, *48,* 2794; (b) Fortman, G. C.; Jacobsen, H.; Cavallo, L.; Nolan, S. P., *Chem. Commun.* **2011**, *47,* 9723.

20. Ampt, K. A. M.; Burling, S.; Donald, S. M. A.; Douglas, S.; Duckett, S. B.; Macgregor, S. A.; Perutz, R. N.; Whittlesey, M. K., *J. Am. Chem. Soc.* **2006**, *128,* 7452.

21. (a) Colombo, M.; George, M. W.; Moore, J. N.; Pattison, D. I.; Perutz, R. N.; Virrels, I. G.; Ye, T. Q., *J. Chem. Soc., Dalton Trans.* **1997**, 2857; (b) Geoffroy, G. L.; Bradley, M. G., *Inorg. Chem.* **1977**, *16,* 744.

22. Rybtchinski, B.; Ben-David, Y.; Milstein, D., *Organometallics* **1997**, *16,* 3786.

23. Kloek, S. M.; Heinekey, D. M.; Goldberg, K. I., *Organometallics* **2006**, *25,* 3007.

24. (a) Mazet, C.; Smidt, S. P.; Meuwly, M.; Pfaltz, A., *J. Am. Chem. Soc.* **2004**, *126,* 14176; (b) Paterniti, D. P.; Francisco, L. W.; Atwood, J. D., *Organometallics* **1999**, *18,* 123; (c) Kimmich, B. F. M.; Somsook, E.; Landis, C. R., *J. Am. Chem. Soc.* **1998**, *120,* 10115; (d) Deutsch, P. P.; Eisenberg, R., *Chem. Rev.* **1988**, *88,* 1147; (e) Johnson, C. E.; Eisenberg, R., *J. Am. Chem. Soc.* **1985**, *107,* 3148; (f) Chin, C. S.; Park, H. K.; Joo, W. C., *Polyhedron* **1985**, *4,* 1673; (g) Park, S. H.; Park, H. K.; Chin, C. S., *Inorg. Chem.* **1985**, *24,* 1120; (h) Crabtree, R., *Acc. Chem. Res.* **1979**, *12,* 331; (i) Crabtree, R. H.; Felkin, H.; Morris, G. E., *J. Chem. Soc., Chem Commun.* **1976**, 716; (j) Vaska, L.; Catone, D. L., *J. Am. Chem. Soc.* **1966**, *88,* 5324.

25. (a) Findlater, M.; Bernskoetter, W. H.; Brookhart, M., *J. Am. Chem. Soc.* **2010**, *132,* 4534; (b) Ben-Ari, E.; Leitus, G.; Shimon, L. J. W.; Milstein, D., *J. Am. Chem. Soc.* **2006**, *128,* 15390.

26. Langer, R.; Iron, M. A.; Konstantinovski, L.; Diskin-Posner, Y.; Leitus, G.; Ben-David, Y.; Milstein, D., *Chem.-Eur. J.* **2012**, *18,* 7196.

27. Shaw, B. L.; Uttley, M. F., *J. Chem. Soc., Chem Commun.* **1974**, 918.

28. Yoshida, T.; Otsuka, S., *J. Am. Chem. Soc.* **1977**, *99,* 2134.

29. Dahlenburg, L.; Gotz, R., *Inorg. Chim. Acta* **2004**, *357,* 2875.

30. Grellier, M.; Vendier, L.; Sabo-Etienne, S., *Angew. Chem., Int. Ed.* **2007**, *46,* 2613.

31. Yang, X., *Inorg. Chem.* **2011**, *50,* 12836.

32. Langer, R.; Leitus, G.; Ben-David, Y.; Milstein, D., *Angew. Chem., Int. Ed.* **2011**, *50,* 2120.

33. Bertoli, M.; Choualeb, A.; Lough, A. J.; Moore, B.; Spasyuk, D.; Gusev, D. G., *Organometallics* **2011**, *30,* 3479.

34. Chakraborty, S.; Dai, H.; Bhattacharya, P.; Fairweather, N. T.; Gibson, M. S.; Krause, J. A.; Guan, H., *J. Am. Chem. Soc.* **2014**, *136,* 7869.

35. (a) Saudan, L. A.; Saudan, C. M.; Debieux, C.; Wyss, P., *Angew. Chem., Int. Ed.* **2007**, *46,* 7473; (b) Saudan, L.; Dupau, P.; Riedhauser, J.; Wyss, P.; Lionel, S.; Sauda, L.; Wyss, R. WO2006106483-A1; (c) Saudan, L.; Dupau, P.; Riedhauser, J.; Wyss, P. WO2006106484-A1.

36. Abdur-Rashid, K.; Faatz, M.; Lough, A. J.; Morris, R. H., *J. Am. Chem. Soc.* **2001**, *123,* 7473.

37. Li, T. S.; Churlaud, R.; Lough, A. J.; Abdur-Rashid, K.; Morris, R. H., *Organometallics* **2004**, *23,* 6239.

38. (a) Abbel, R.; Abdur-Rashid, K.; Faatz, M.; Hadzovic, A.; Lough, A. J.; Morris, R. H., *J. Am. Chem. Soc.* **2005**, *127,* 1870; (b) Abdur-Rashid, K.; Abbel, R.; Hadzovic, A.; Lough, A. J.; Morris, R. H., *Inorg. Chem.* **2005**, *44,* 2483.

39. Kaess, M.; Friedrich, A.; Drees, M.; Schneider, S., *Angew. Chem., Int. Ed.* **2009**, *48,* 905.

40. Zhang, J.; Leitus, G.; Ben-David, Y.; Milstein, D., *Angew. Chem., Int. Ed.* **2006**, *45,* 1113.

41. Friedrich, A.; Drees, M.; auf der Guenne, J. S.; Schneider, S., *J. Am. Chem. Soc.* **2009**, *131,* 17552.

42. Nielsen, M.; Kammer, A.; Cozzula, D.; Junge, H.; Gladiali, S.; Beller, M., *Angew. Chem., Int. Ed.* **2011**, *50,* 9593.

43. Prechtl, M. H. G.; Hoelscher, M.; Ben-David, Y.; Theyssen, N.; Milstein, D.; Leitner, W., *Eur. J. Inorg. Chem.* **2008**, 3493.

44. Burling, S.; Mahon, M. F.; Paine, B. M.; Whittlesey, M. K.; Williams, J. M. J., *Organometallics* **2004**, *23,* 4537.

45. Fantasia, S.; Egbert, J. D.; Jurcik, V.; Cazin, C. S. J.; Jacobsen, H.; Cavallo, L.; Heinekey, D. M.; Nolan, S. P., *Angew. Chem., Int. Ed.* **2009**, *48,* 5182.

46. Wolf, R.; Plois, M.; Hepp, A., *Eur. J. Inorg. Chem.* **2010**, 918.

Chapter 2

Chapter 2: Synthesis and Characterisation of $Ru(IMe_4)_4H_2$, $Ru(IMe_4)_2(PPh_3)_2H_2$ and $Ru(IEt_2Me_2)_2(PPh_3)_2H_2$

2.1. Introduction

Ruthenium hydride complexes of the type RuL_nH_2 or $[RuL_nH]^+$ where L is a phosphine ligand (monodentate up to tetradentate) are known to catalyse organic transformations and to bind small molecules.[1] It is well-known that NHCs can replace phosphine ligands. In 1999, Grubbs published a new generation of Ru-based alkene metathesis catalysts which differed from the previous generation by replacement of the PCy_3 ligand with a range of NHC ligands.[2] In 2010, Wolf synthesized the NHC analogue of $Ru(PR_3)_4H_2$, $Ru(NHC)_4H_2$, thereby altering the steric and electronic properties of the complex, potentially enhancing the catalytic applications and ability to coordinate and activate small molecules.[3] In contrast to the *cis* hydride geometry adopted by related phosphine complexes, the preferred geometry of the NHC complex, $Ru(IMe_4)_4H_2$, was one featuring *trans* hydride ligands. This was confirmed both spectroscopically and by X-ray crystallography.[4] Furthermore, DFT calculations showed that the hypothetical *cis* dihydride would be *ca*. 14 kcal mol^{-1} higher in energy than the *trans* dihydride product. Calculations were also applied to a theoretical "small" model in which the IMe_4 ligands were replaced with IH_4 ligands as well as an "abnormal" model where the IH_4 ligands were bound to the metal through the backbone of the NHC. Both models showed no energy difference between their respective *cis* and *trans* dihydride isomers indicating that the preference for the *trans* hydride arrangement in $Ru(IMe_4)_4H_2$ was steric in nature.

Trans hydride complexes of ruthenium with comparatively small ligands (e.g. IMe_4) are much less common and compounds featuring exclusively NHCs and hydride ligands are exceedingly rare.[5] The majority of hydridoruthenium complexes containing NHCs also have a carbon monoxide or halide ligand. [3,6a-d]

Transition metal complexes with an NHC *trans* to a phosphine ligand can have better catalytic activity than the analogous *bis*-phosphine complexes. A well established example of this is Grubbs' first and second generation catalysts,[7] as well as a striking contrast between $Ru(NHC)(PPh_3)_2(CO)H_2$ and $Ru(PPh_3)_3(CO)H_2$ as highly active and totally inactive hydrodefluorination catalysts respectively.[8] Isolating species of the form $Ru(NHC)_2(PR_3)_2H_2$ represents an interesting synthetic challenge. In addition to a mixed NHC/phosphine complex having possibly enhanced catalytic abilities, the potential for having such a species with *trans* hydrides could also be advantageous. A recent computational study on the mechanism of hydrodefluorination

by $Ru(NHC)(PPh_3)_2(CO)H_2$ showed nucleophilic attack of the hydride ligand to be a key feature.[9] Having a hydride *trans* to another hydride would increase both nucleophilicity, as well as hydricity, of each hydride.

Another point worth mentioning is the possibility of accessing the very reactive Ru(0) fragment complex $[Ru(NHC)_4]$ from $Ru(NHC)_4H_2$. The phosphine analogue $[Ru(dmpe)_2]$ was the first species to undergo intermolecular C-H bond activation.[10] However, the preference for the hydrides to be *trans* in the NHC complex means that reductive elimination of dihydrogen to afford $Ru(NHC)_4$ could not occur without prior isomerisation.

2.2. Results and Discussion

2.2.1. Synthesis of $Ru(IMe_4)_4Cl_2$ (**1**)

When 4 equiv. of IMe_4 were stirred with $Ru(PPh_3)_3Cl_2$ in toluene for 24 h, a colour change from purple to orange was observed, along with the formation of an orange/yellow precipitate. This was isolated and following work up, identified as *trans*-$Ru(IMe_4)_4Cl_2$ (**1**). Compound **1** was characterised spectroscopically; the ^1H NMR spectrum (C_6D_6) showed two singlet resonances in a 1:1 ratio at δ_H 3.69 and 1.79 for the N-Me and backbone methyl groups of the IMe_4 ligands respectively (Figure 2.2). The $^{13}C\{^1H\}$ NMR spectrum showed a distinctive high frequency carbenic carbon resonance at δc 199.0. These data were consistent with those previously reported by Wolf *et al.* who reported the preparation of **1** in 44% yield following thermolysis of $[Ru(COD)Cl_2]_x$ with 4 equiv. of IMe_4.[4] Starting from $Ru(PPh_3)_3Cl_2$ gave a slightly higher yield of 67%.

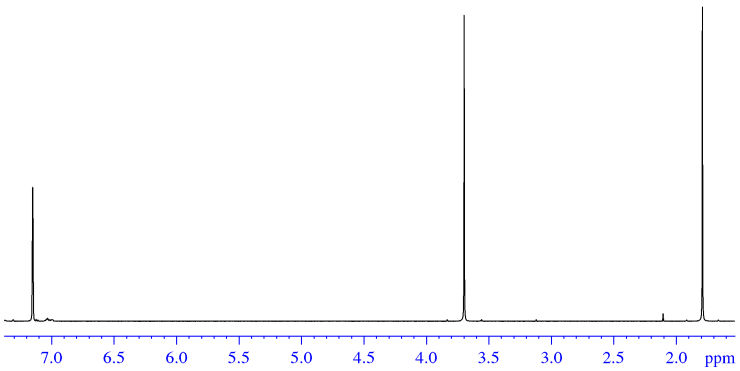

*Figure 2.2: ^1H NMR spectrum of $Ru(IMe_4)_4Cl_2$, **1** (C_6D_6, 298 K, 500 MHz).*

2.2.2. Synthesis of $Ru(IMe_4)_4H_2$ (**3**)

The reaction of **1** with excess potassium graphite (KC_8) in THF under 1 atm of H_2 for 24 h resulted in a colour change from an orange suspension to a yellow solution

with a black precipitate (graphite and KCl). A ^{1}H NMR spectrum of a portion of the reaction mixture (dried and re-dissolved in C_6D_6) showed two hydride resonances: a singlet at δ_H -7.45 and a broad singlet at δ_H -22.10. After removing the black precipitate by filtration and stirring hexane with the filtrate for a short time, a very small amount of orange solid precipitated (compound **2**). Upon re-dissolving this precipitate in C_6D_6, the ^{1}H NMR spectrum now showed only the lower frequency Ru hydride signal at δ_H -22.10 (**2**, Figure 2.3). Removal of the solvent from the remaining filtrate afforded a yellow solid, which upon dissolution in C_6D_6, displayed a singlet Ru-H resonance at δ_H -7.45. (compound **3**, Figure 2.4) This chemical shift was consistent with that of *trans*-Ru(IMe$_4$)$_4$H$_2$ (**3**) reported by Wolf upon reaction of *trans*-Ru(IMe$_4$)$_4$Cl$_2$ with LiAlH$_4$.[4] Interestingly, Wolf also reported that a second species with a Ru-H peak at δ_H -16.20 was formed as a by-product in the reduction, which they proposed was *trans*-Ru(IMe$_4$)$_4$HCl.

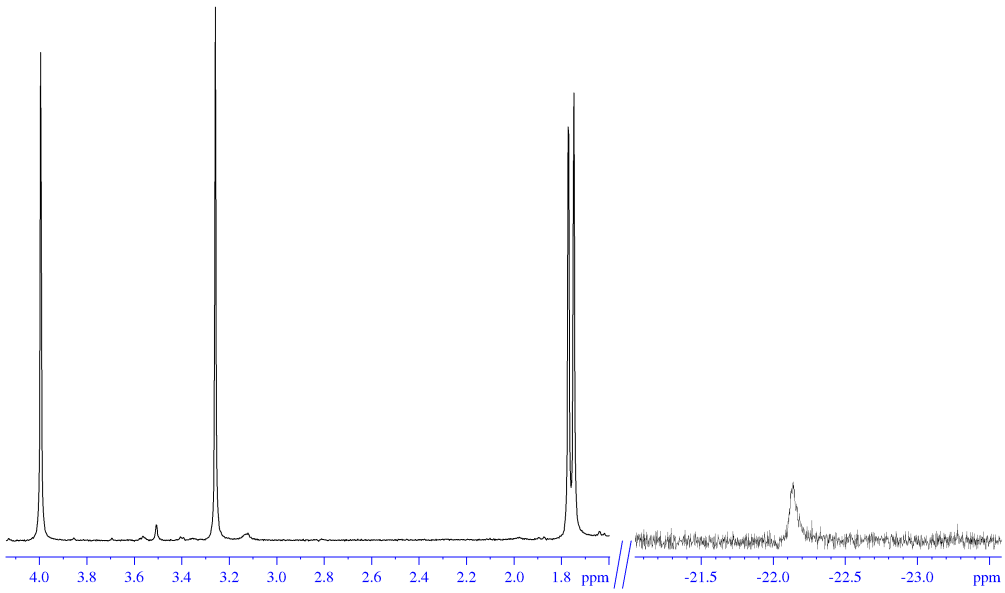

*Figure 2.3: ^{1}H NMR spectrum of compound **2** formed upon reaction of **1** with KC_8 and H_2 (C_6D_6, 298 K, 500 MHz).*

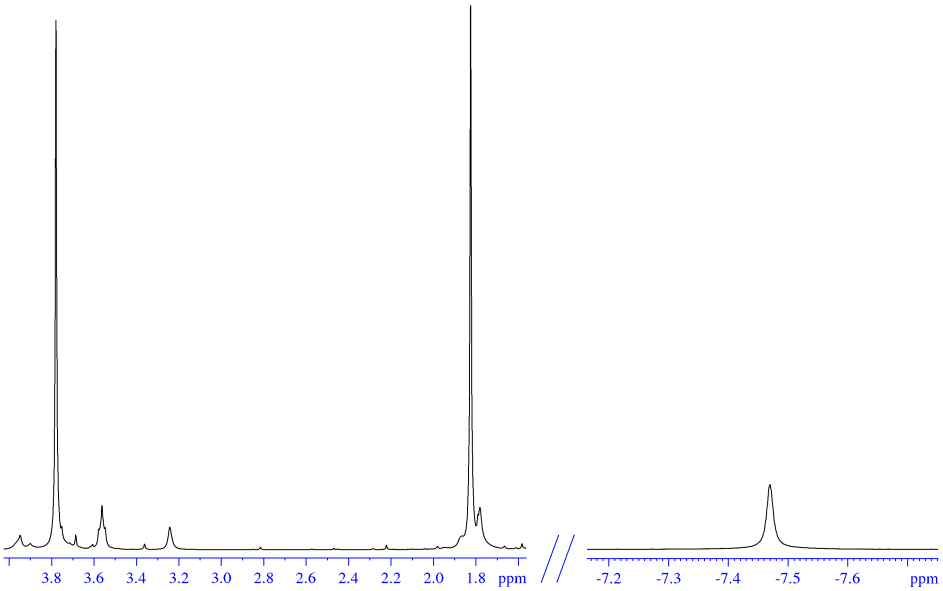

*Figure 2.4: ^1H NMR spectrum of $Ru(IMe_4)_4H_2$ (**3**) formed upon treatment of $Ru(IMe_4)_4Cl_2$ (**1**) with KC_8 under H_2 (C_6D_6, 298 K, 400 MHz).*

The identity of the hydride species **2** (δ_H -22.10) remains to be established. However, relative integrals of 1:12:12:12:12 for the hydride versus four IMe_4 signals at δ_H 3.99, 3.26, 1.77 and 1.75 suggest it is a Ru *mono*-hydride complex with four IMe_4 ligands. The hydride resonances of three ruthenium hydride chloride species previously reported[11] ranged from about δ_H -16 to -17 depending upon the ancillary ligand set on the ruthenium (see Table 2.1 for comparison of hydride resonance values), so it appeared reasonable to suggest that **2** corresponded to *trans*-$Ru(IMe_4)_4HCl$. It is worth noting that $[Ru(IMe_4)_4H]^+$, in which the hydride is *trans* to a vacant site, exhibited a hydride resonance at a much lower frequency of δ_H -40.70.[3] This was further evidence that a resonance at δ_H -22.10 involved a hydride with a ligand *trans* to it. It was difficult to rationalize what the product could be, if not $Ru(IMe_4)_4HCl$. With this rationalisation, a summary of the reaction is shown in Scheme 2.1.

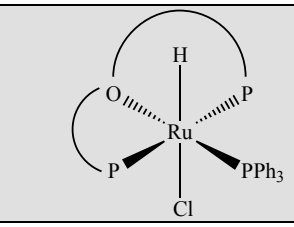	RuHCl complex	Hydride resonance
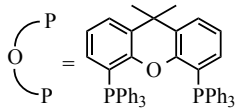	Ru(xantphos)(PPh$_3$)HCl	δ_H -16.20[11a]
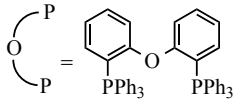	Ru(DPEphos)(PPh$_3$)HCl	δ_H -16.30[11a]
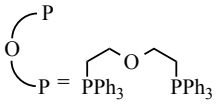	Ru((Ph$_2$PCH$_2$CH$_2$)$_2$O)(PPh$_3$)HCl	δ_H -17.50[11a]

Table 2.1: Comparison of hydride shifts of previously reported Ru hydride chloride complexes.

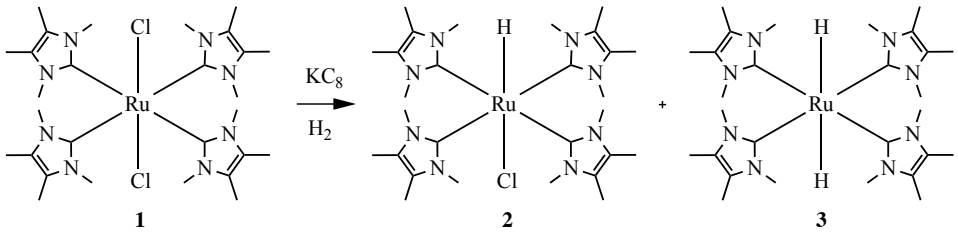

1 **2** **3**

*Scheme 2.1: Summary of Ru containing products formed from the reaction of **1** with KC_8 in THF under 1 atmosphere of H_2.*

It is plausible that KH formed in the reaction from the KC_8 and H_2 and was partially responsible for the reduction of **1**.[12] Some evidence for this came from the same mixture of products (**2** and **3**) being formed from the direct reaction of **1** with KH in THF. However, the yield of **3** was much lower from this reaction; even after an extended reaction time of 96 h (*c.f.* 24 h), residual **1** was still present.

2.2.3. Synthesis of Ru(IMe$_4$)$_2$(PPh$_3$)$_2$H$_2$ (**4a-d**)

2.2.3.1. Characterisation of all-*trans* Ru(IMe$_4$)$_2$(PPh$_3$)$_2$H$_2$ (**4a**)

The reaction of Ru(PPh$_3$)$_3$HCl with 2-4 equiv. of IMe$_4$ in THF under an 1 atm. of hydrogen formed a mixture of products over 15 h. During the course of the reaction, a yellow precipitate formed which was shown by NMR spectroscopy to be a mixture of **1** and **2**. This yellow precipitate was removed by filtration to leave an orange/yellow solution which was shown to contain a mixture of all-*trans* Ru(IMe$_4$)$_2$(PPh$_3$)$_2$H$_2$ (**4a**)

and $Ru(PPh_3)_4H_2$. The latter corresponds to the ^1H NMR resonance at δ_H -10.10 in Figure 2.5, which is complex due to the second-order AA'BB'XX' spin system.[13] A ^{31}P-^1H HSQC experiment showed that two triplet resonances in the $^{31}P\{^1H\}$ NMR spectrum at δ_P 48.8 ($^2J_{PP}$ = 14 Hz) and 40.6 ($^2J_{PP}$ = 14 Hz) correlated to the hydride signal at δ_H -10.10. These data are consistent with that reported for $Ru(PPh_3)_4H_2$ by Linn in 1999.[14]

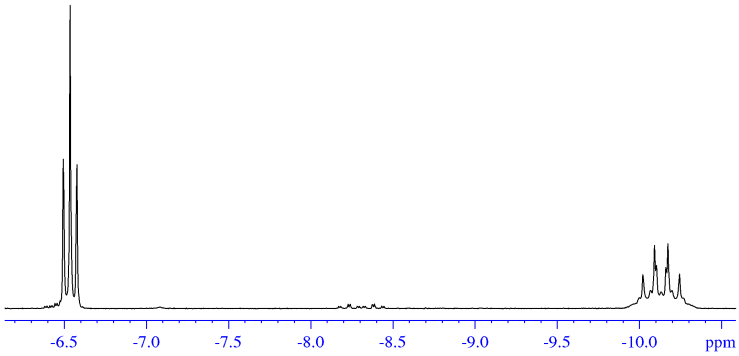

*Figure 2.5: Hydride region of the ^1H NMR spectrum of the mixture of $Ru(IMe_4)_2(PPh_3)_2H_2$ (**4a**) and $Ru(PPh_3)_4H_2$ (C_6D_6, 298 K, 500 Hz).*

4a was extracted into Et_2O to separate it from $Ru(PPh_3)_4H_2$ and isolated in a 12 % yield. The ^1H NMR spectrum of **4a** showed two Me signals (at δ_H 3.75 for the NMe group and at δ_H 1.34 for the backbone Me groups) that integrated in a 12:12:2 ratio with a triplet hydride resonance at δ_H -6.54 ($^2J_{HP}$ = 20.4 Hz). HSQC and HMBC experiments showed correlations between this Ru-H resonance and a singlet at δ_P 72.0 in the $^{31}P\{^1H\}$ NMR spectrum and a triplet at δ_C 197.9 ($^2J_{CP}$ = 15 Hz) in the $^{13}C\{^1H\}$ NMR spectrum. These data are indicative of each carbenic carbon of the two NHC ligands coupling to two equivalent PPh_3 ligands and are consistent with an all-*trans* arrangement of ligands in $Ru(IMe_4)_2(PPh_3)_2H_2$ (**4a**).[15]

Characterisation by single crystal X-ray diffraction (Figure 2.6) of crystals grown from slow diffusion of hexane into a concentrated benzene solution of **4a** confirmed the mutual *trans* arrangement of the IMe_4, PPh_3 and hydride ligands. The Ru-C and Ru-P distances of 2.107(2) and 2.2836(4) Å are comparable to the values reported for other $Ru(NHC)(PR_3)$ complexes.[6a,6d,11b,16a-f]

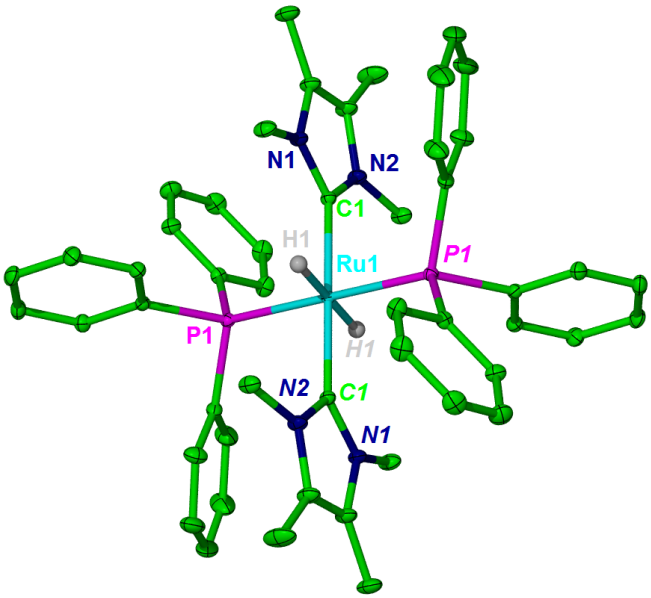

*Figure 2.6: Molecular structure of **4a**. Thermal ellipsoids are shown at the 30 % probability level. Hydrogen atoms except for Ru-H are removed for clarity. Atoms labelled in italics are related to those in the asymmetric unit by the 1-x, 1-y, 1-z symmetry operation. Selected bond lengths (Å) and angles (deg): Ru-C(1) 2.107(2), Ru-P(1) 2.2836(4), C(1)-Ru-P(1) 90.10(4).*

2.2.3.2. Characterisation of $Ru(IMe_4)_2(PPh_3)_2H_2$ (**4a-d**)

In an effort to achieve a higher yield of **4a**, $Ru(PPh_3)_4H_2$ was investigated as a precursor. Two equiv. of IMe_4 were added to a THF solution of $Ru(PPh_3)_4H_2$ at room temperature and after 15 h, the resulting reaction mixture comprised **4a** as the minor product alongside three additional Ru hydride containing species. These were identified as alternative isomers of **4a** on the basis of NMR studies. Figure 2.7 shows the hydride resonances of each of the isomers and Figure 2.8 shows their geometries, the deduction of which, is subsequently explained.

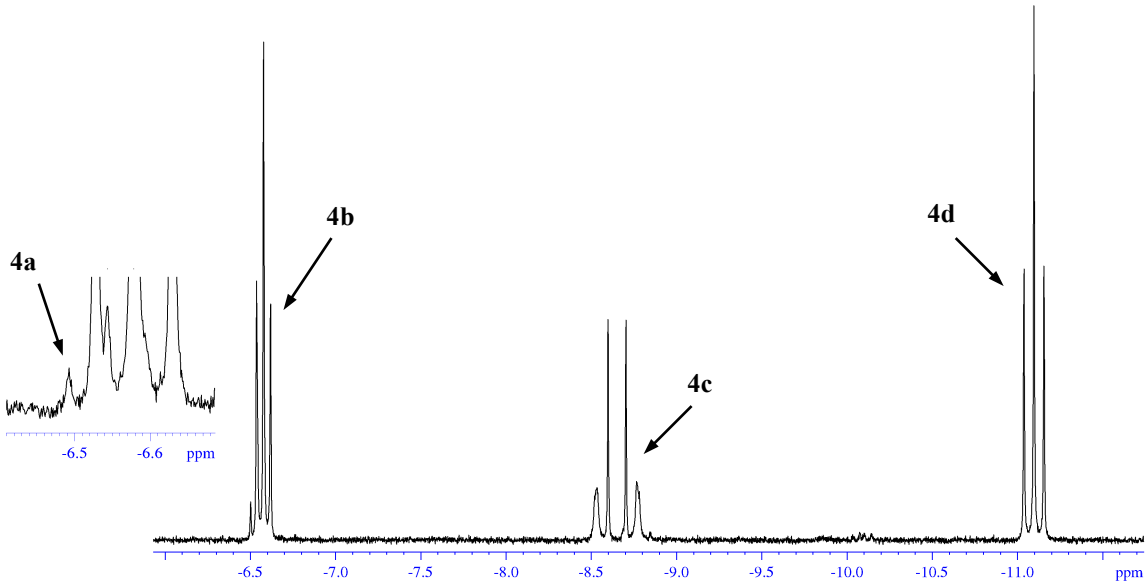

*Figure 2.7: Hydride region of the ^{1}H NMR spectrum of the reaction mixture 15 h after the addition of IMe_4 to $Ru(PPh_3)_4H_2$ (C_6D_6, 298 K, 400 MHz). Inset: expansion of hydride resonance at δ_H -6.54 corresponding to complex **4a**.*

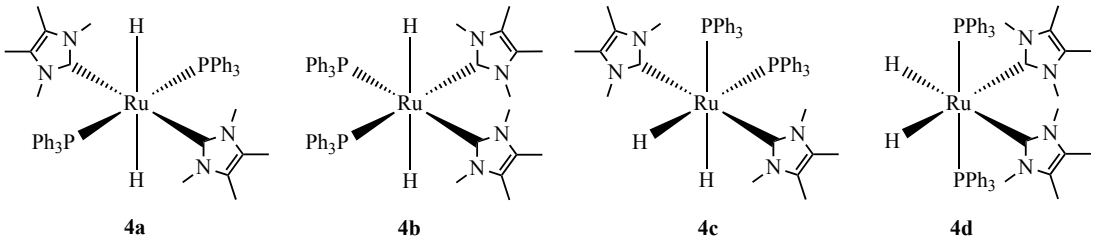

*Figure 2.8: Geometries of isomers **4a-d**.*

As can be seen in Figure 2.7, isomers **4b** and **4d** were initially the major products formed in a 1:1 ratio with isomers **4a** and **4c** formed in smaller amounts. The NMR characterization of the different isomers is discussed below.

NMR characterization of **4b** (*cis*-IMe_4, *cis*-PPh_3, *trans*-H)

The *cis*, *cis*, *trans* isomer of $Ru(IMe_4)_2(PPh_3)_2H_2$ (**4b**) showed a triplet resonance at δ_H -6.58 ($^{2}J_{HP}$ = 20.2 Hz) which correlated to a singlet in the $^{31}P\{^{1}H\}$ NMR spectrum at δ_P 69.0 in a ^{1}H-^{31}P HSQC experiment. A selectively ^{1}H coupled ^{31}P NMR spectrum (shown in Figure 2.9) split the δ_P 69.0 resonance into a triplet with a 20 Hz splitting which was consistent to the splitting of the hydride resonance in the ^{1}H NMR spectrum. A ^{1}H-^{13}C HMBC experiment showed a correlation between the hydride resonance and a second order Ru-C_{NHC} resonance (AA'XX' spin system) at δ_C 197.6. These data, along

with the integrals of the hydride signal compared to the resonances for the Me groups of IMe_4 in the ^1H NMR spectrum, were consistent with two equivalent hydrides coupling to two equivalent PPh_3 ligands, with two IMe_4 ligands on the Ru centre. The second order ^{13}C resonance for the carbenic carbon indicated magnetically inequivalent PPh_3 ligands, consistent with the *cis*, *cis*, *trans* geometry shown below.

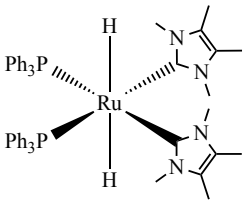

4b

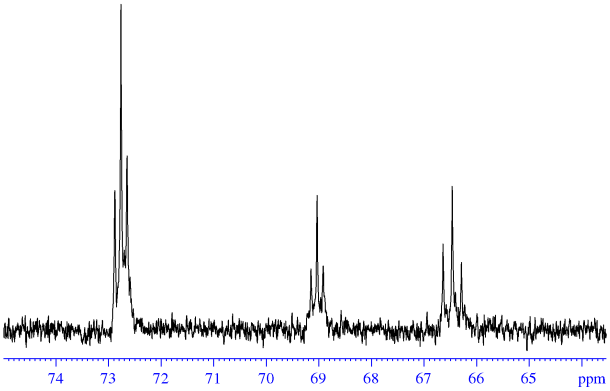

*Figure 2.9: Selected region of the selectively ^1H coupled ^{31}P NMR spectrum showing resonances for **4a**, **4b** and **4d** (from left to right, C_6D_6, 202 MHz, 298 K).*

NMR characterization of **4c** (*trans*-IMe_4, *cis*-PPh_3, *cis*-H)

The second order hydride resonance at δ_H -8.65 suggested *cis* hydride and *cis* phosphine ligands in **4c**. A ^1H-^{31}P HSQC experiment correlated the hydride resonance to a singlet phosphorus resonance at δ_P 45.1. This isomer was never present in large enough concentrations to allow the carbenic signal to be observed by $^{13}C\{^1H\}$ NMR spectroscopy. It's solubility in hexane hindered separation from free PPh_3.

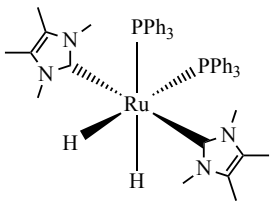

4c

NMR characterization of **4d** (*cis*-IMe_4, *trans*-PPh_3, *cis*-H)

HSQC experiments revealed that the triplet hydride resonance at δ_H -11.01 ($^2J_{HP}$ = 29.4 Hz) correlated to a single phosphorus resonance at δ_P 66.0 and a triplet resonance

at δ_C 201.1 ($^2J_{CP}$ = 8 Hz) in the $^{13}C\{^1H\}$ NMR spectrum. These data are consistent with (i) a species containing two equivalent hydrides coupling to two equivalent PPh_3 ligands and (ii) with the carbenic carbons and the PPh_3 ligands being both chemically and magnetically equivalent, consistent with **4d** having a *cis, trans, cis* geometry as shown below.

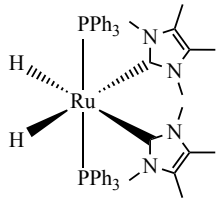

4d

Conversion of the isomers

It was noted that an NMR sample of **4a-d** left on the bench top for an extended period of time showed a depletion of complexes **4b-d** and an increase in the amount of **4a** in solution. This prompted a repeat of the experiment for the purpose of a ^1H EXSY NMR spectrum of the initial reaction mixture. The EXSY experiment showed cross peaks between **4b** and **4d**, confirming the presence of isomerization on an NMR time scale, presumably via PPh_3 dissociation. This intramolecular conversion of isomers was supporting evidence for an equilibrium existing between **4a**, **4b** and **4d** and the resulting solution being of the most stable isomer (**4a**).

Removal of the solvent after 15 h of reaction time (i.e. at the initial stage of the reaction, after all $Ru(PPh_3)_4H_2$ had reacted and before any conversion between the isomers) and washing the sticky orange residue with a minimum amount of hexane resulted in a yellow powder consisting of **4b** and **4d** (with trace amounts of **4a**) in a 65 % yield. **4c** was more soluble in hexane than the other isomers so was removed during the workup along with any excess free PPh_3.

Dissolving a portion of the isolated mixture in C_6D_6 provided a more controlled means of monitoring the conversion of the isomers. After a week at room temperature the initial mixture (**4b**, **4d** with trace amounts of **4a**) had completely converted to **4a**. This conversion was faster at 70 °C with full conversion to **4a** taking only 15 h. **4a** was isolated in 80 % yield from the mixture of isomers.

The formation of **4a-d** from $Ru(PPh_3)_4H_2$ prompted investigation into the conditions that brought about their respective formations. A preliminary experiment to compare the conversion of the isomers in the presence or absence of light at both room and a lower temperature of 5 °C was carried out. Unsurprisingly, the conversion to **4a**

was slower at the lower temperature. More interestingly, **4c** did not form in the dark, suggesting light plays a role in the mechanism of the formation of **4c**.

Further work was done to investigate the effect of excess free PPh_3 (10 equiv.) on the conversion of the isomers in both the light and the dark, as well as at the different temperatures. With exposure to daylight and excess PPh_3, there was a significant preference for the formation of isomer **4c** during the conversion to **4a**. At comparable times there was a greater concentration of **4c** present in the solution with excess PPh_3 compared to the solution without excess free PPh_3, as shown in Figure 2.10. This experiment confirmed that **4c** did not form in the absence of light, even with excess free PPh_3 present.

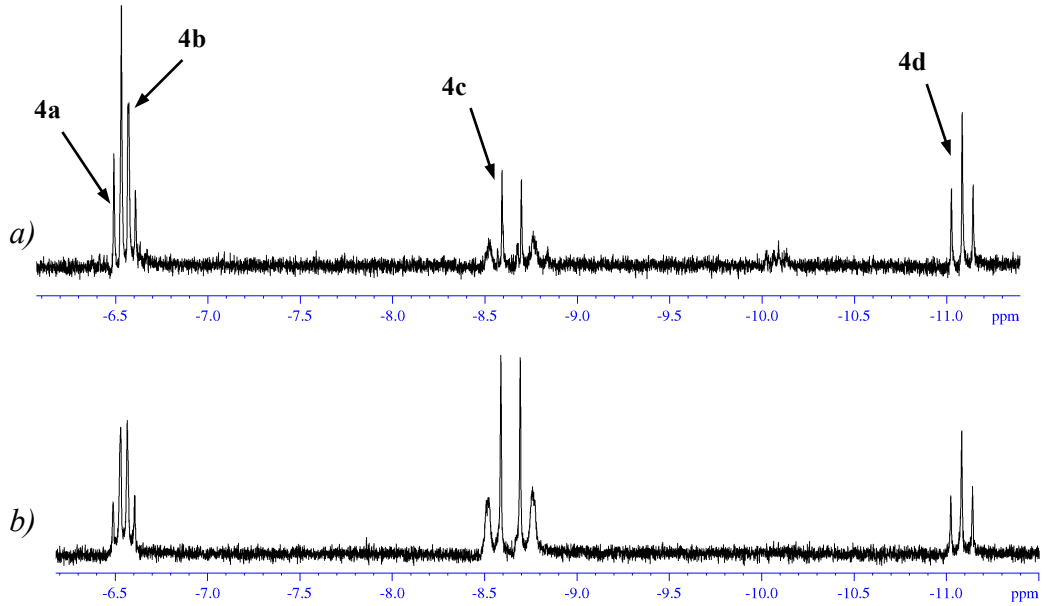

*Figure 2.10: Hydride regions of the ^1H NMR spectra of **4a-d** after 1 day of conversion in solution a) without excess PPh_3 and b) with 10 equiv. of excess free PPh_3 (C_6D_6, 298 K, 500 MHz).*

Density functional theory (DFT)[1] was employed to rationalize the conversion to **4a**. Calculations were done on two models: a 'full model' and a 'small model' as shown in Table 2.2. When the 'full model' was used (with IMe_4 and PPh_3 ligands), the calculations gave **4a** as the lowest energy structure, in agreement with the experimental findings. In contrast, using a 'small model' (in which IH_4 and PH_3 were used as ligands) and with the energy of **4a** set to 0 kcal mol^{-1}, the calculations showed **4c** to be

[1] DFT calculations : Gaussian 09; BP86 functional; SDD pseudopotential / basis sets (Ru, P with polarization on P); 6-31g** (C, H, N). Performed by Prof Stuart Macgregor and Dr. Andrés Algarra at Heriot-Watt University.

the most stable structure, at -5.5 kcal mol^{-1}. However, the difference in energy between the isomers remained relatively small, consistent with the equilibrium behaviour identified between **4b** and **4d** spectroscopically. The energies were also calculated for the theoretical fifth isomer (**4e**) with the ligands in an *all cis* arrangement, although this isomer was never seen experimentally.

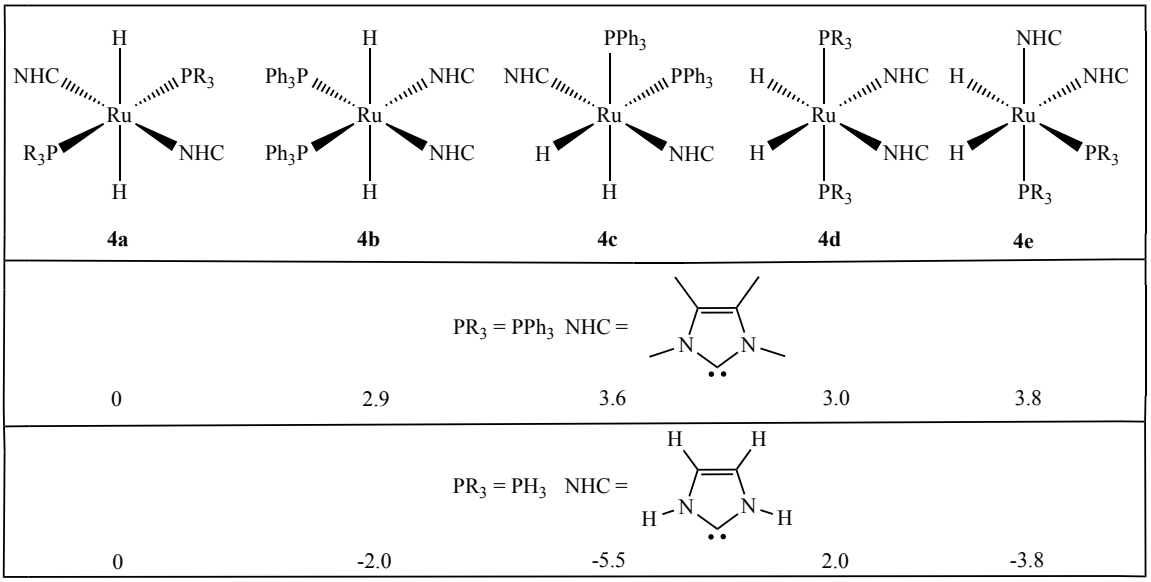

Table 2.2: Computed energies for $Ru(NHC)_2(PPh_3)_2H_2$ ($PR_3 = PPH_4$, NHC = IH_4; $PR_3 = PPh_3$, NHC = IMe_4, $kcalmol^{-1}$).

4c was the lowest energy structure when any steric bulk of the ligands was removed (in the 'small model'), showing that steric effects must be the driving force for the preference of **4a** in the 'full model', overriding the fact that a *trans* arrangement of hydrides is electronically disfavoured. This influence of steric factors matches Wolf's observations on $Ru(IMe_4)_4H_2$ described previously.[4]

2.2.4. Synthesis of $Ru(IEt_2Me_2)_2(PPh_3)_2H_2$ (**5b**)

The formation of isomers **4a-d** from the reaction of $Ru(PPh_3)_4H_2$ with IMe_4 prompted investigation into the reaction of the same precursor with the N-Et substituted carbene, IEt_2Me_2. Two equiv. of IEt_2Me_2 were added to a THF solution of $Ru(PPh_3)_4H_2$ which, overnight, afforded an orange solution. Concentrating the solution in the presence of hexane afforded a yellow precipitate which was characterised as the *cis*, *cis*, *trans* isomer of $Ru(IEt_2Me_2)_2(PPh_3)_2H_2$, **5b**. This showed a triplet Ru-H resonance at δ_H -6.70 ($^2J_{HP}$ = 20.4 Hz), which correlated to a singlet in the $^{31}P\{^1H\}$ NMR spectrum at δ_P 69.7 and a doublet of doublets resonance at δ_C 196.3 ($^2J_{CP}$ = 96 Hz, $^2J_{CP}$ = 24 Hz) in

the $^{13}C\{^1H\}$ NMR spectrum for the two equivalent carbenic carbons. The ^1H NMR spectrum displayed very different chemical shifts for the methylene groups of the N-Et substituents, with one observed at δ_H 3.00 and the other shifted to significantly higher frequency at δ_H 6.49. This was explained by the close proximity of the methylene protons to the hydride, which was seen by a strong NOESY interaction to the Ru-H signal suggestive of *exo* and *endo* diastereotopic -CH_2 protons (Figure 2.11).

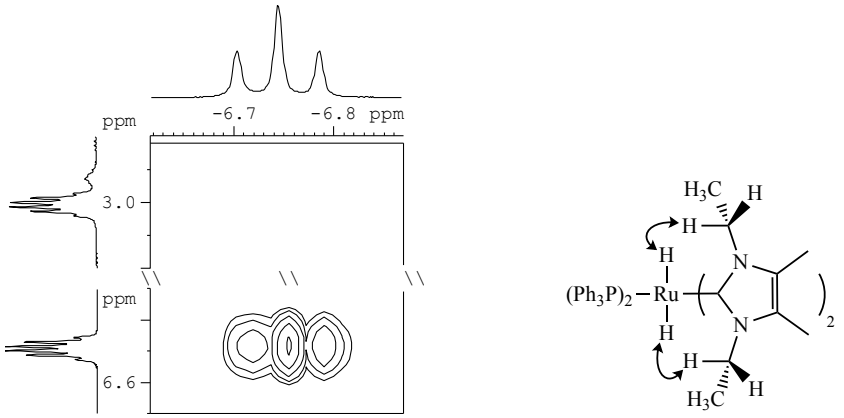

*Figure 2.11: Section of a ^1H NOESY NMR spectrum of **5b** showing the correlation between the hydrides and one of the CH_2 protons of the carbenes (C_6D_6, 298 K, 500 MHz)*

Crystals of **5b** suitable for X-ray diffraction were grown by slow diffusion of hexane into a concentrated THF solution of the complex. The solid-state structure confirmed the *cis*-NHC, *cis*-phosphine and *trans*-hydride geometry. A slightly more distorted octahedral structure was apparent than in **4a**, with C_{NHC}-Ru-C_{NHC} and P-Ru-P angles of 87.49(7)° and 97.393(2)° respectively (*cf.* C_{NHC}-Ru-P angle of 89.90(4) in **4a**). The angle of 14.2° between the mean planes comprising C10, Ru1 and C1 and atoms P1, P2 and Ru1 further illustrate the deviation from the ideal octahedral geometry. The longer Ru-P distances observed in **5b** (2.3189(5) and 2.3042(5) Å *cf.* 2.2836(4) Å in **4a**) are consistent with the change in the nature of the *trans* ligand from PPh_3 to NHC.

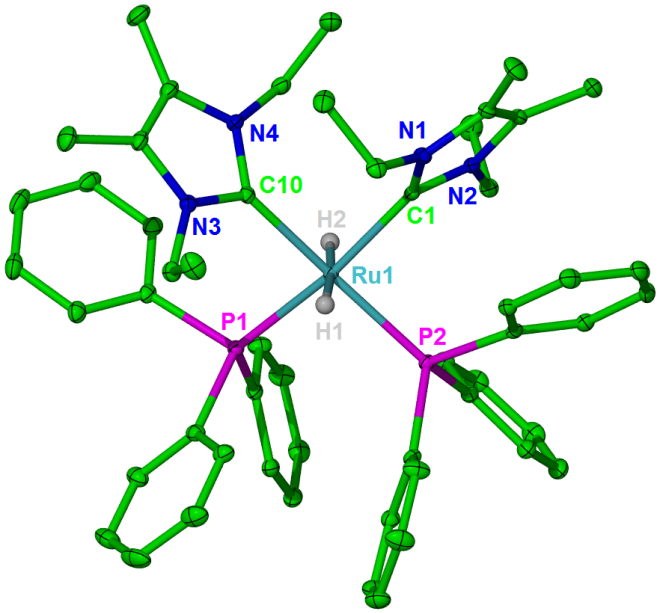

Figure 2.12: Molecular structure of ***5b****. Ellipsoids are shown at the 30 % probability level. Hydrogen atoms except for Ru-H are removed for clarity. Selected bond lengths (Å) and angles (deg): Ru-P(1) 2.3189(5), Ru-P(2) 2.3042(5), Ru-C(1) 2.097(2), Ru-C(10) 2.105(2), C(1)-Ru-C(10) 87.49(7), C(1)-Ru-P(1) 169.03(5), P(1)-Ru-P(2) 97.393(7).*

2.3. Summary and Conclusions of Chapter 2

Three ruthenium complexes (**3, 4a** and **5b**) with unusual *trans* dihydride geometries have been synthesized. Characterisation of $Ru(IMe_4)_2(PPh_3)_2H_2$ (**4a**), and subsequent DFT calculations of **4a-d** have shown that despite the high *trans* influence of hydride ligands, the most stable isomer is dictated by steric factors, rather than electronics at the ruthenium centre. Use of the slightly larger IEt_2Me_2 ligand resulted in a change in position of both the carbene and phosphine ligands with a *cis* arrangement being observed in $Ru(IEt_2Me_2)_2(PPh_3)_2H_2$, **5b**.

A cleaner and higher yielding route to the all-carbene complex $Ru(IMe_4)_4H_2$ (**3**) than that found in the literature[4] was developed which will allow direct comparisons of reactivity to the mixed NHC/phosphine analogues to be drawn. This work forms the basis of chapters 3-5. The differing geometries of **4a** and **5b** provide an insight into just how subtle the changes that are required to alter the geometry at the ruthenium centre need to be.

2.4. Experimental

The following is common to the work described in chapters 2 to 5 and is given here. All experiments were carried out using standard Schlenk, high-vacuum and glovebox techniques using dried and degassed solvents, unless otherwise stated. Solvents were dried using either an MBraun SPS solvent system (CH_2Cl_2, Et_2O, hexane, pentane and toluene), an Innovative Technologies PS-400-7 solvent system (THF and acetonitrile) or under a nitrogen atmosphere from purple solutions of sodium benzophenone ketyl (C_6H_6) or Mg/I_2 (methanol and ethanol). Deuterated solvents (Aldrich) were vacuum transferred from potassium (C_6D_6, toluene-d_8, THF-d_8) or calcium hydride (CD_2Cl_2, $CDCl_3$). The following were acquired from commercial sources and used as received: CO, CO_2, H_2, N_2 and O_2 (BOC, 99.9 %); HBpin, $P(C_6F_5)_3$, D_2 and $^{13}CO_2$ (Sigma-Aldrich, 98 %).

NMR spectra were recorded on Bruker Avance 300, 400 and 500 MHz NMR spectrometers (at 298 K unless otherwise stated) and referenced to residual solvent signals for ^1H and ^{13}C spectra for C_6D_6 (δ_H 7.15, δ_C 128.0), CD_2Cl_2 (δ_H 5.31, δ_C 54.0), $CDCl_3$ (δ_H 7.26, δ_C 77.7), THF-d_8 (δ_H 3.58, δ_C 25.4), CD_3CN (δ_H 1.94, δ_C 118.7) and toluene-d_8 (δ_H 2.10, δ_C 20.4). $^{31}P\{^1H\}$ spectra were referenced externally to 85% H_3PO_4 at δ_P 0.0, while ^{19}F spectra were referenced to $CFCl_3$ at δ_F 0. PPh_3 resonances have been excluded, except in cases where definitive assignments could be made in the ^1H and ^{13}C NMR spectra. IR spectra were recorded as nujol mulls or in C_6D_6 solution on a Nicolet Nexus spectrometer. Elemental analyses were performed at London Metropolitan University, London, U.K. $Ru(PPh_3)_3Cl_2$,[13b] $Ru(PPh_3)_3HCl$,[17] $Ru(PPh_3)_4H_2$,[18] IMe_4, and IEt_2Me_2[19] were prepared according to literature methods.

2.4.1. Synthesis of $Ru(IMe_4)_4Cl_2$ (**1**)

A toluene (15 mL) solution of IMe_4 (200 mg, 1.6 mmol) and $Ru(PPh_3)_3Cl_2$ (390 mg, 0.4 mmol) was transferred to an ampoule fitted with a J. Youngs PTFE valve containing a magnetic stirrer bar. The solution was stirred overnight to generate a yellow/orange precipitate and an orange/red solution. The solution was cannula filtered to isolate **1** as an orange solid, which was washed with hexane and dried *in vacuo*. NMR data were in agreement with those in the literature.[4] Yield 160 mg (67 %). ^1H NMR (CD_2Cl_2, 500 MHz): δ 3.30 (s, 24H, NCH_3), 2.20 (s, 24H, NCCH_3=NCCH_3). ^1H NMR (C_6D_6, 500 MHz): δ 3.69 (s, 24H, NCH_3), 1.79 (s, 24H, NCCH_3=NCCH_3). ^1H NMR (CD_3CN, 500 MHz): δ 3.00 (s, 24H, NCH_3), 2.10 (s, 24H, NCCH_3=NCCH_3).

$^{13}C\{^1H\}$ NMR (C_6D_6, 125 MHz): δ 199.1 (s, Ru-C_{NHC}), 124.3 (s, N*C*CH_3=N*C*CH_3), 35.8 (s, N*C*H_3), 10.1 (s, NC*C*H_3=NC*C*H_3).

2.4.2. Synthesis of $Ru(IMe_4)_4H_2$ (**3**)

An ampoule fitted with a J. Youngs resealable valve was charged with $Ru(IMe_4)_4Cl_2$ (100 mg, 0.15 mmol), KC_8 (40 mg, 0.3 mmol) and THF (10 mL) was added. The solution was freeze-pump-thaw degassed (3 cycles), 1 atm of H_2 was added and the mixture stirred at room temperature for 15 h. The solution changed from orange to yellow with the appearance of a fine black precipitate (graphite). This was removed by cannula filtration and the solvent removed *in vacuo* to yield a highly air sensitive orange/yellow solid. Yield: 45 mg (52 %). ^1H NMR (500 MHz, THF-d_8): δ 3.34 (s, 24H, NC*H*$_3$), 1.97 (s, 24H, NCC*H*$_3$=NCC*H*$_3$), -8.14 (s, 2H, Ru*H*). $^{13}C\{^1H\}$ NMR (125 MHz, THF-d_8): δ 212.4 (s, Ru-C_{NHC}), 120.7 (s, N*C*CH_3=N*C*CH_3), 35.9 (s, N*C*H_3), 10.2 (s, NC*C*H_3=NC*C*H_3). ^1H NMR (500 MHz, C_6D_6): δ 3.78 (s, 24H, NC*H*$_3$), 1.82 (s, 24H, NCC*H*$_3$=NCC*H*$_3$), -7.46 (s, 2H, Ru*H*). $^{13}C\{^1H\}$ NMR (125 MHz, C_6D_6): δ 212.3 (s, Ru-C_{NHC}), 120.8 (s, N*C*CH_3=N*C*CH_3), 36.9 (s, N*C*H_3) 10.2 (s, NC*C*H_3=NC*C*H_3). Anal. Calcd (%) for $C_{28}H_{50}N_8Ru$ (599.83): C, 56.06; H, 8.40; N, 18.68; found: C, 55.63; H, 8.92; N, 18.42.

2.4.3. Synthesis of $Ru(IMe_4)_2(PPh_3)_2H_2$ (**4a**–**d**)

$Ru(PPh_3)_4H_2$ (400 mg, 0.35 mmol) and IMe_4 (86 mg, 0.70 mmol) were suspended in THF (20 mL) in an ampoule fitted with a J. Youngs resealable valve, and stirred at ambient temperature for 15 h. Removal of the solvent *in vacuo* yielded a sticky orange oil. Hexane (20 mL) was added and the suspension heated at 323 K for 4 h to afford an orange solution containing a yellow precipitate. The precipitate was isolated by cannula filtration and dried under vacuum to afford 200 mg of a mixture of **4a-d**. The isomer **4a** was prepared by heating a mixture of **4a**–**d** (200 mg, 0.23 mmol) in THF (15 mL) in an ampoule fitted with a J. Youngs resealable valve at 343 K for 15 h. After cooling to room temperature, the solvent was removed *in vacuo* and the residue washed with hexane (30 mL). 160 mg (80% yield) of **4a** as a yellow solid. NMR data for **4a**: ^1H NMR (400 MHz, C_6D_6): δ 7.80 (br m, 12H, PC$_6$*H*$_5$), 6.99–6.92 (m, 18 H, PC$_6$*H*$_5$), 3.75 (s, 12H, NC*H*$_3$), 1.34 (s, 12H, NCC*H*$_3$=NCC*H*$_3$), -6.54 (t, $^2J_{HP}$ = 20.4 Hz, 2H, Ru*H*). $^{31}P\{^1H\}$ NMR (162 MHz, C_6D_6): δ 72.4 (s). $^{13}C\{^1H\}$ NMR (126 MHz, C_6D_6): δ 197.9 (t, $^2J_{CP}$ = 15 Hz, Ru-C_{NHC}), 142.3 (vt, *J* = 15 Hz, P*C*$_6$H$_5$), 134.8 (br m, P*C*$_6$H$_5$), 127.0 (br m, P*C*$_6$H$_5$), 126.3 (br m, P*C*$_6$H$_5$), 122.3 (s, N*C*CH_3=N*C*CH_3), 36.9 (s,

NCH$_3$), 9.9 (s, NC*C*H$_3$=NC*C*H$_3$). Anal. Calcd (%) for $C_{50}H_{56}N_4P_2Ru$ (876.02): C, 68.55; H, 6.44; N, 6.40. Found: C, 68.54; H, 6.57; N, 6.24. Selected NMR data for other isomers: **4b**: ^{1}H NMR (500 MHz, C_6D_6): δ 3.75 (s, 12H, NC*H*$_3$), 1.31 (s, 12H, NCC*H*$_3$=NCC*H*$_3$), -6.58 (t, $^2J_{HP}$ = 20.2 Hz, Ru*H*). ^{31}P{^{1}H} NMR (202 MHz, C_6D_6): δ 68.9 (s). ^{13}C{^{1}H} NMR (126 MHz, C_6D_6): δ 197.6 (dd, $^2J_{CP}$ = 94 Hz, $^2J_{CP}$ = 24 Hz, Ru-*C*$_{NHC}$), 121.9 (s, N*C*CH$_3$=N*C*CH$_3$), 37.0 (s, N*C*H$_3$), 10.0 (s, NC*C*H$_3$=NC*C*H$_3$). **4d**: ^{1}H NMR (500 MHz, C_6D_6): δ 3.46 (s, 6H, NC*H*$_3$), 3.10 (s, 6H, NC*H*$_3$), 1.56 (s, 6H, NCC*H*$_3$=NCC*H*$_3$), 1.42 (s, 6H, NCC*H*$_3$=NCC*H*$_3$), -11.01 (t, $^2J_{HP}$ = 29.4 Hz, Ru*H*). ^{31}P{^{1}H} NMR (202 MHz, C_6D_6): δ 66.3 (s). ^{13}C{^{1}H} NMR (126 MHz, C_6D_6): δ 201.1 (t, $^2J_{CP}$ = 8 Hz, Ru-*C*$_{NHC}$), 123.5 (s, N*C*CH$_3$=N*C*CH$_3$), 122.2 (s, N*C*CH$_3$=N*C*CH$_3$), 37.3 (s, N*C*H$_3$), 36.1 (s, N*C*H$_3$), 10.0 (s, NC*C*H$_3$=NC*C*H$_3$), 9.7 (s, NC*C*H$_3$=NC*C*H$_3$). **4c**: ^{1}H NMR (500 MHz, C_6D_6): δ 4.10 (s, 6H, NC*H*$_3$), 3.20 (s, 6H, NC*H*$_3$), 1.69 (s, 6H, NCC*H*$_3$=NCC*H*$_3$), 1.21 (s, 6H, NCC*H*$_3$=NCC*H*$_3$), -8.65 (m, Ru*H*). ^{31}P{^{1}H} NMR (202 MHz, C_6D_6): δ 45.1 (s).

2.4.4. Synthesis of Ru(IEt$_2$Me$_2$)$_2$(PPh$_3$)$_2$H$_2$ (**5b**)

Ru(PPh$_3$)$_4$H$_2$ (400 mg, 0.35 mmol) and IEt$_2$Me$_2$ (106 mg, 0.70 mmol) were suspended in THF (15 mL) in an ampoule fitted with a J. Youngs resealable valve, and stirred at ambient temperature for 15 h. Removal of the solvent left an orange oil. Hexane (20 mL) was added and the suspension was stirred at ambient temperature for 1 h to afford a yellow precipitate. The suspension was concentrated to half volume to induce more solid, which was isolated by cannula filtration and dried under vacuum to afford 200 mg (62% yield). ^{1}H NMR (500 MHz, C_6D_6): δ 7.97-7.91 (br, 10H, PPh$_3$), 7.06-7.02 (br, 3H, PPh$_3$), 6.96–6.90 (br, 17H, PPh$_3$), 6.49 (dq, $^2J_{HH}$ = 13.2 Hz, $^3J_{HH}$ = 6.5 Hz, 4H, NC*H*HCH$_3$), 3.00 (dq, $^2J_{HH}$ = 13.2 Hz, $^3J_{HH}$ = 6.5 Hz, 4H, NCH*H*CH$_3$), 1.40 (s, 12H, NCC*H*$_3$=NCC*H*$_3$), 0.79 (br t, $^3J_{HH}$ = 6.5 Hz, 12H, NCH$_2$C*H*$_3$), -6.74 (t, $^2J_{HP}$ = 20.4 Hz, 2H, Ru*H*). ^{31}P{^{1}H} NMR (202 MHz, C_6D_6): δ 69.7 (s). ^{13}C{^{1}H} NMR (126 MHz, C_6D_6): δ 196.3 (dd, $^2J_{CP}$ = 96 Hz, $^2J_{CP}$ = 24 Hz, Ru-*C*$_{NHC}$), 142.7 (m, P*C*$_6$H$_5$), 135.4 (m, P*C*$_6$H$_5$), 126.7 (br, P*C*$_6$H$_5$), 126.1 (m, P*C*$_6$H$_5$), 122.8 (s, NC*C*H$_3$=*C*NCH$_3$), 44.2 (s, N*C*H$_2$CH$_3$), 13.9 (s, NC*C*H$_3$=CN*C*H$_3$), 9.6 (s, N*C*H$_2$CH$_3$). Anal. Calcd (%) for $C_{54}H_{64}N_4P_2Ru$ (932.11): C, 69.57; H, 6.92; N, 6.00. Found: C, 69.52; H, 7.05; N, 5.92.

2.5. References

1. (a) Noyori, R.; Hashiguchi, S., *Acc. Chem. Res.* **1997**, *30,* 97; (b) Saburi, M.; Ohnuki, M.; Ogasawara, M.; Takahashi, T.; Uchida, Y., *Tetrahedron Lett.* **1992**, *33,*

5783; (c) Bautista, M. T.; Cappellani, E. P.; Drouin, S. D.; Morris, R. H.; Schweitzer, C. T.; Sella, A.; Zubkowski, J., *J. Am. Chem. Soc.* **1991**, *113,* 4876; (d) Ueda, W.; Yokoyama, T.; Morikawa, Y.; Morooka, Y.; Ikawa, T., *J. Mol. Catal.* **1988**, *44,* 197; (e) Albers, M. O.; Singleton, E.; Viney, M. M., *J. Mol. Catal.* **1985**, *33,* 77.

2. Scholl, M.; Ding, S.; Lee, C. W.; Grubbs, R. H., *Org. Lett.* **1999**, *1*.

3. Burling, S.; Haller, L. J. L.; Mas-Marzá, E.; Moreno, A.; Macgregor, S. A.; Mahon, M. F.; Pregosin, P. S.; Whittlesey, M. K., *Chem.-Eur. J.* **2009**, *15,* 10912.

4. Wolf, R.; Plois, M.; Hepp, A., *Eur. J. Inorg. Chem.* **2010**, 918.

5. Giunta, D.; Holscher, M.; Lehmann, C. W.; Mynott, R.; Wirtz, C.; Leitner, W., *Adv. Synth. Catal.* **2003**, *345,* 1139.

6. (a) Wang, T.; Pranckevicius, C.; Lund, C. L.; Sgro, M. J.; Stephan, D. W., *Organometallics* **2013**, *32,* 2168; (b) Blacquiere, J. M.; Higman, C. S.; Gorelsky, S. I.; Beach, N. J.; Dalgarno, S. J.; Fogg, D. E., *Angew. Chem., Int. Ed.* **2011**, *50,* 916; (c) Haller, L. J. L.; Mas-Marzá, E.; Moreno, A.; Lowe, J. P.; Macgregor, S. A.; Mahon, M. F.; Pregosin, P. S.; Whittlesey, M. K., *J. Am. Chem. Soc.* **2009**, *131,* 9618; (d) Abdur-Rashid, K.; Fedorkiw, T.; Lough, A. J.; Morris, R. H., *Organometallics* **2004**, *23,* 86.

7. Scholl, M.; Trnka, T. M.; Morgan, J. P.; Grubbs, R. H., *Tetrahedron Lett.* **1999**, *40,* 2247.

8. Reade, S. P.; Mahon, M. F.; Whittlesey, M. K., *J. Am. Chem. Soc.* **2009**, *131,* 1847.

9. Panetier, J. A.; Macgregor, S. A.; Whittlesey, M. K., *Angew. Chem., Int. Ed.* **2011**, *50,* 2783.

10. Chatt, J.; Davidson, J. M., *J. Chem. Soc.* **1965**, 843.

11. (a) Ledger, A. E. W.; Moreno, A.; Ellul, C. E.; Mahon, M. F.; Pregosin, P. S.; Whittlesey, M. K.; Williams, J. M. J., *Inorg. Chem.* **2010**, *49,* 7244; (b) Burling, S.; Kociok-Kohn, G.; Mahon, M. F.; Whittlesey, M. K.; Williams, J. M. J., *Organometallics* **2005**, *24,* 5868.

12. Herold, A.; Saehr, D., *C. R. Hebd. Seances Acad. Sci.* **1960**, *250,* 545.

13. (a) Knoth, W. H., *J. Am. Chem. Soc.* **1972**, *94,* 104; (b) Stephenson, T. A.; Hallman, P. S.; Wilkinson, G., *Inorg. Synth.* **1970**, *12,* 237.

14. Linn, D. E., *J. Chem. Ed.* **1999**, *76,* 70.

15. Davies, C. J. E.; Lowe, J. P.; Mahon, M. F.; Poulten, R. C.; Whittlesey, M. K., *Organometallics* **2013**, *32,* 4927.

16. (a) Lund, C. L.; Sgro, M. J.; Cariou, R.; Stephan, D. W., *Organometallics* **2012**, *31,* 802; (b) Benhamou, L.; Wolf, J.; Cesar, V.; Labande, A.; Poli, R.; Lugan, N.;

Lavigne, G., *Organometallics* **2009**, *28,* 6981; (c) Burling, S.; Mas-Marzá, E.; Valpuesta, J. E. V.; Mahon, M. F.; Whittlesey, M. K., *Organometallics* **2009**, *28,* 6676; (d) Reade, S. P.; Nama, D.; Mahon, M. F.; Pregosin, P. S.; Whittlesey, M. K., *Organometallics* **2007**, *26,* 3484; (e) Burling, S.; Mahon, M. F.; Paine, B. M.; Whittlesey, M. K.; Williams, J. M. J., *Organometallics* **2004**, *23,* 4537; (f) Jazzar, R. F. R.; Macgregor, S. A.; Mahon, M. F.; Richards, S. P.; Whittlesey, M. K., *J. Am. Chem. Soc.* **2002**, *124,* 4944.

17. Schunn, R. A.; Wonchoba, E. R.; Wilkinson, G., *Inorg. Synth.* **1971**, *13,* 131.
18. Young, R.; Wilkinson, G., *Inorg. Synth.* **1990**, *28,* 337.
19. Kuhn, N.; Kratz, T., *Synthesis* **1993**, 561.

Chapter 3

Chapter 3: Reactivity of $Ru(IMe_4)_2(PPh_3)_2H_2$, $Ru(IMe_4)_4H_2$ and $Ru(IEt_2Me_2)_2(PPh_3)_2H_2$ with small molecules: CO, CO_2, MeI

3.1 Introduction

Initial studies on the synthesized *trans* dihydride Ru complexes started with an investigation into their reactivity with the small molecules CO and CO_2. This followed on from previous investigations into small molecule reactivity done in the Whittlesey group on the cationic tetracarbene ruthenium hydride compound, $[Ru(IMe_4)_4H]^+$ which showed NHC dependant reactivity.[1]

CO is ubiquitous in organometallic chemistry and has a key function in many catalytic processes, either as a carbon source (Fischer-Tropsch) or as a spectator ligand.[2] Transition metal carbonyl complexes also have an important role as intermediates in homogeneous catalytic processes.[3] For example, $Ru(PPh_3)_3(CO)H_2$ has a 45 year history of useful catalytic applications.[4]

The functionalization of CO_2 is currently popular due to the undesirable increase of the amount of CO_2 in the atmosphere and its potential to act as a C1 feedstock.[5] The potential use of CO_2 as an abundant and inexpensive source of carbon is a very attractive goal because of its low critical temperature and the potential for a wide variety of products to be synthesized. One that has gained particular attention is formic acid.[6] A key step in catalytic cycles that result in the functionalization of CO_2 is often the insertion of CO_2 into a metal-carbon or metal-hydride bond.[7] This insertion is often reversible (which is desirable for a catalytic cycle) and provides access to a much more reactive formate species than the very stable free CO_2 molecule.[6b] The *all*-phosphine analogue of complexes **3**, **4a** and **5b**, $Ru(PPh_4)_4H_2$, has already proven to be an active catalyst for the homogeneous hydrogenation of CO_2 to formic acid.[8] It is reasonable to hypothesise that complexes **4a** and **5b** having phosphine and NHC ligands could be better catalysts than $Ru(PPh_4)_4H_2$.

3.2 Results and Discussion

3.2.1. Reactions of $Ru(IMe_4)_2(PPh_3)_2H_2$ (**4a**)

3.2.1.1. Reaction of **4a** with CO

Addition of 1 atm CO to a C_6D_6 solution of **4a** resulted in the formation of the monocarbonyl dihydride complex $Ru(IMe_4)_2(PPh_3)(CO)H_2$ (**6**) and subsequent onward reaction yielded the tricarbonyl complex $Ru(IMe_4)_2(CO)_3$ (**8**). A week at room temperature led to full conversion to **8**, which was isolated as a pale yellow, air-sensitive solid.

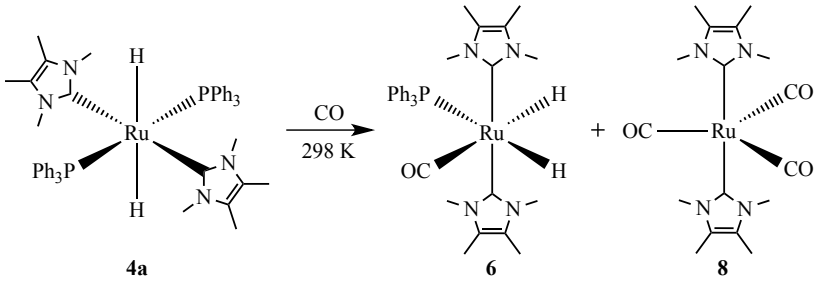

*Scheme 3.1: Reaction of **4a** with CO at 298 K.*

The monocarbonyl complex **6** was only present in a mixture along with **4a** or **8** so could not be isolated, but was characterized unambiguously by NMR spectroscopy. Thus, two hydride resonances were observed at δ_H -5.12 and -7.14 (at 298 K) with *cis* ($^2J_{HP}$ = 36.7 Hz) and *trans* ($^2J_{HP}$ = 94.9 Hz) phosphine couplings respectively (Figure 3.1a). A ^{1}H-^{31}P HSQC experiment showed correlations from both hydride resonances to a ^{31}P{^{1}H} singlet at δ_P 51. Surprisingly, no $^2J_{HH}$ coupling was observed between the two hydride resonances although their presence in the same molecule was confirmed by the appearance of a strong cross-peak in the ^{1}H,^{1}H-NOESY spectrum. Presumably, the coupling between the *cis* hydrides was not seen as it was < 2 Hz and therefore lost within the line width of the signal. There is a literature precedent for this in work by Mayer and Kaska, which reports the synthesis of three iridium complexes with *cis* hydride ligands, only one of which shows a J_{HH} coupling on the hydride resonance in the ^{1}H NMR spectrum.[9]

Further evidence for the structure of **6** came from employing ^{13}CO, which enabled the *trans*-^{13}C-Ru-H and *cis*-^{13}C-Ru-H splittings (24 and 6 Hz respectively) to be measured from the hydride resonances in the ^{1}H NMR spectrum (Figure 3.1b). Peaks in a ^{1}H-^{13}C HSQC spectrum showed correlations between both hydride signals and a doublet at δ_C 211 in the ^{13}C{^{1}H} NMR spectrum. This was further evidence for both hydride ligands being in the same molecule, as well as that of the CO ligand. These data are consistent with the geometry of **6** shown in Scheme 3.1.

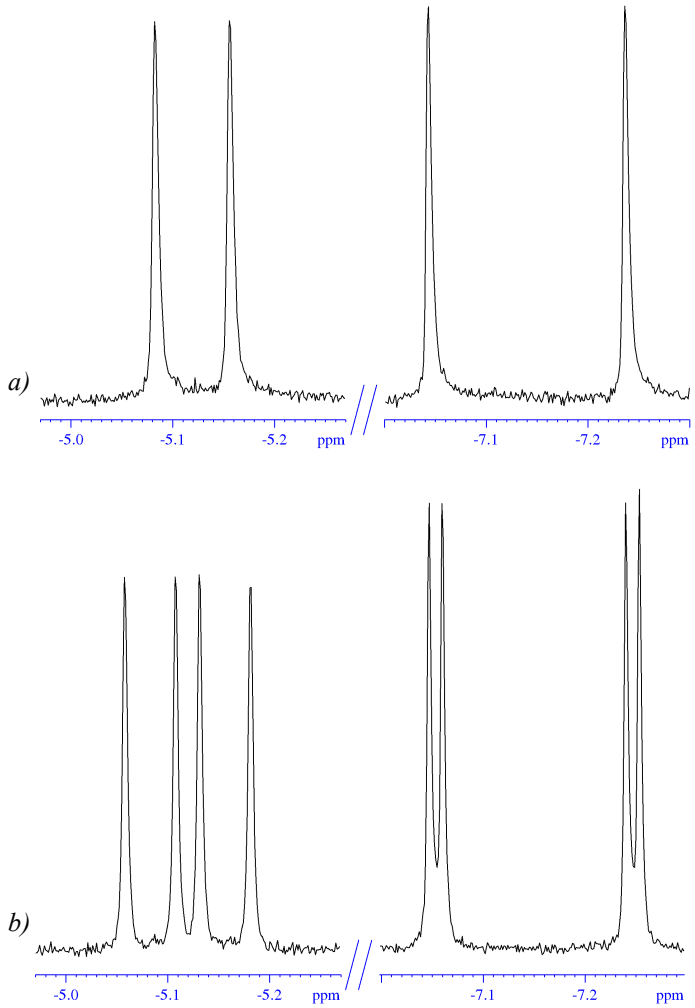

Figure 3.1: a) Hydride region of the ^{1}H NMR spectrum (C_6D_6, 298 K, 500 MHz) of ***6*** *prepared with ^{12}CO and b) upon use of ^{13}CO (C_6D_6, 298 K, 500 MHz).*

The spectroscopic properties of the tricarbonyl complex **8** (resonances in the ^{13}C NMR spectrum at δ_C 217 for the carbonyl and δ_C 182 for the carbenic carbon and a single ν_{CO} IR band at 1840 cm^{-1}) were similar to those for the previously reported analogues with IE_2Me_2 and ICy ligands which suggested that **8** had a trigonal bipyramidal structure with the IMe_4 ligands being *trans* and axial.[10]

In an attempt to speed up the conversion of **4a** to **8**, the reaction mixture was heated. After 15 h at 313 K (Scheme 3.2) or 2 h at 343 K, an additional monocarbonyl complex (**7**) was identified from the appearance of two doublet of triplet hydride resonances in the ^{1}H NMR spectrum and in a ^{13}CO labeled reaction, an additional triplet resonance in the $^{13}C\{^{1}H\}$ NMR spectrum. A ^{1}H-^{31}P HSQC spectrum showed the hydride signals (at δ_H -5.35 ($^{2}J_{HH}$ = 4.6 Hz, *cis*-$^{2}J_{HP}$ = 36.4 Hz) and δ_H -8.49 ($^{2}J_{HH}$ = 4.7 Hz, *cis*-$^{2}J_{HP}$ = 26.2 Hz) correlated with a singlet in the $^{31}P\{^{1}H\}$ NMR spectrum at δ_P 65.5. A ^{1}H-^{13}C HSQC experiment showed weak correlations between the hydride

resonances and the triplet resonance at δ_C 209.8 in the $^{13}C\{^1H\}$ NMR spectrum. This resonance had a *cis* $^2J_{CP}$ coupling of 9.3 Hz. All data imply that **7** is the *bis*-phosphine monocarbonyl complex shown in Scheme 3.2.

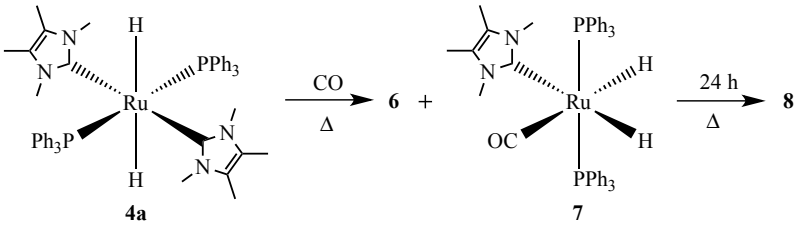

*Scheme 3.2: Complexes **6**, **7** and **8** produced from a heated reaction of **4a** with CO.*

Heating the reaction to the higher temperature of 343 K gave complete conversion of the mixture of **6** and **7** to **8** after 24h.

3.2.1.2. Reaction of **4a** with CO_2

The addition of 1 atm CO_2 to a C_6D_6 solution of **4a** at room temperature resulted in a rapid insertion reaction into one of the Ru-H bonds to afford the formate hydride complex $Ru(IMe_4)_2(PPh_3)(\kappa^2\text{-OCHO})H$, as a mixture of two isomers, **9** and **10**, in a 2.4:1 ratio respectively (Scheme 3.3).

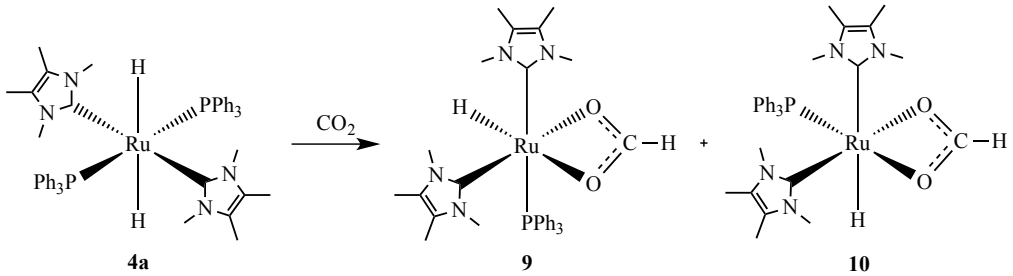

*Scheme 3.3: Reaction of **4a** with CO_2 forming two isomers of $Ru(IMe_4)_2(PPh_3)(\kappa^2\text{-OCHO})H$, **9** and a proposed structure for **10**.*

As shown in Figure 3.2, a ^1H NMR spectrum (at 298 K) of the reaction mixture displayed two characteristic high frequency formate resonances at δ_H 8.73 (**9**) and δ_H 8.70 (**10**). The hydride region of the spectrum showed two partially overlapping doublet resonances at δ_H -23.35 ($^2J_{HP}$ = 29.5 Hz) for **9** and δ_H -23.30 ($^2J_{HP}$ = 49.5 Hz) for **10** in the same 2.4:1 ratio (Figure 3.2).

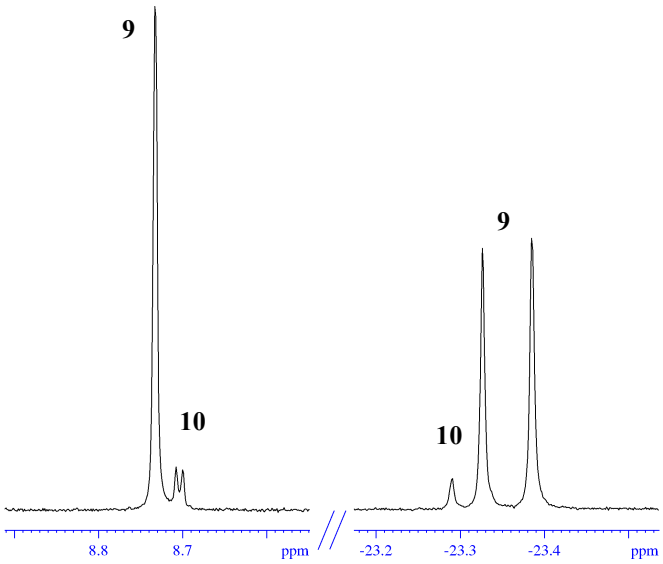

*Figure 3.2: Formate and hydride resonances of **9** and **10** (C_6D_6, 298 K, 500 MHz).*

A ^{1}H-^{31}P HSQC NMR spectrum (with the average coupling value set to 45 Hz) showed a correlation between the hydride resonance for **9** and a singlet resonance in the ^{31}P{^{1}H} NMR spectrum at δ_P 48.4. Changing the average coupling value from 45 Hz to 5 Hz revealed a correlation of this ^{31}P signal to the formate resonance at δ_H 8.73. A ^{1}H-^{13}C HSQC NMR spectrum showed a correlation between the formate resonance at δ_H 8.73 and a singlet resonance at δ_C 170.3 in the ^{13}C{^{1}H} NMR spectrum for the formate carbon.

When $^{13}CO_2$ was used, the formate resonances of **9** and **10** (δ_H 8.73 and δ_H 8.70) split with large doublet couplings of 192 and 190 Hz, respectively. ^{13}C enhanced formate resonances at δ_C 170.3 and δ_C 170.2, split with the same $^{1}J_{CH}$ couplings in the ^{1}H coupled ^{13}C NMR spectrum (Figure 3.3).

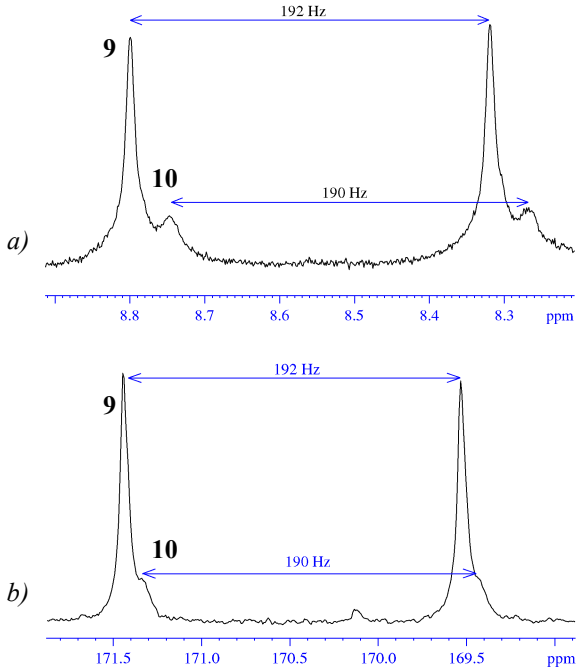

*Figure 3.3: a) Formate regions of (a) the ^{1}H NMR spectrum (toluene-d_8, 298 K, 400 MHz) of ^{13}C labeled **9** and **10** and (b) the ^{13}C NMR spectrum (toluene-d_8, 298 K, 126 MHz) showing the same J values.*

These large $^{1}J_{HC}$ couplings of *ca*. 190 Hz are consistent with a κ^2-bonded formate.[7b,11a-d] Additional evidence for the κ^2-coordination of the formate ligand came from the appearance of a strong $\nu_{(CO2)asym}$ IR absorption band at 1566 cm^{-1}.[12]

These data confirmed the presence of a Ru complex with a hydride, a phosphine and a formate ligand but a series of sharp and broad resonances were observed between *ca*. δ_H 1 and 4 in the room-temperature ^{1}H NMR spectrum for the IMe_4 groups. Upon cooling to 258 K, the resonances for the major species **9** resolved into eight sharp methyl signals (Figure 3.4), each of integral 3H relative to the 1H formate resonance indicative of two IMe_4 ligands on the metal being in different magnetic environments. The *cis* geometry of the IMe_4 ligands shown in Scheme 3.3 seemed most likely.

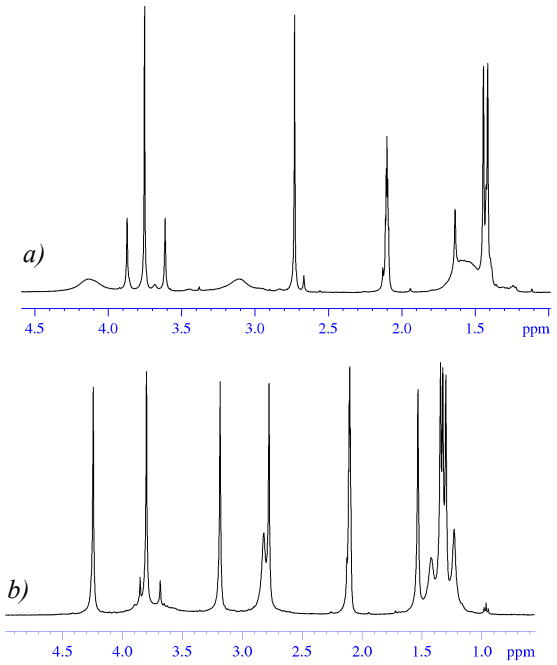

*Figure 3.4: Methyl region of the ^{1}H NMR spectrum of the major isomer **9** and the minor isomer **10** at a) 298 K and b) 258 K (toluene-d_8, 400 MHz).*

Whilst the spectroscopic data obtained for the minor isomer **10** is slightly ambiguous in regard to the geometry of the complex, a suitable structure can be proposed on the basis of ^{1}H-^{31}P HSQC NMR spectrum which showed a correlation between the formate resonance at δ_H 8.70 and a small singlet resonance in the ^{31}P{^{1}H} NMR spectrum at δ_P 84.2. Exchanging the hydride and phosphine positions in **9** to give **10** (Scheme 3.3) is a reasonable deduction, as the most notable spectroscopic difference between the two species is the different shifts of the PPh_3 ligand in their ^{31}P{^{1}H} NMR spectra (*c.f.* δ_P 48.4 for **9** and δ_P 84.2 for **10**). This might also be reasoning for why a small $^{2}J_{HP}$ coupling of 4 Hz is seen on the formate signal in the ^{1}H NMR spectrum of **10** but not for **9** (Figure 3.2).

A third formate-containing product, **11** (Figure 3.5) was observed by NMR spectroscopy upon cooling toluene-d_8 solutions of **9** and **10** to < 258 K. This species was only ever present at low concentrations and was characterized by the appearance of a higher-frequency formate resonance at δ_H 9.27. Of particular note was that there was no accompanying hydride signal, suggesting that this species is most likely the *bis*-formate complex $Ru(IMe_4)_2(PPh_3)(OCHO)_2$, presumably with two κ^1-bound formate ligands. This was supported by a ^{1}H-^{13}C HSQC correlation of the formate resonance at δ_H 9.27 to a single ^{13}C resonance at δ_C 168.3 ($^{1}J_{CH}$ = 186 Hz, determined upon $^{13}CO_2$ labeling).

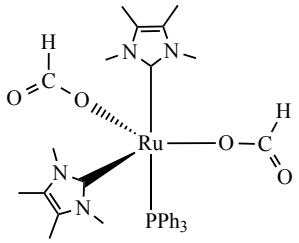

11

*Figure 3.5: Possible structure of **11**.*

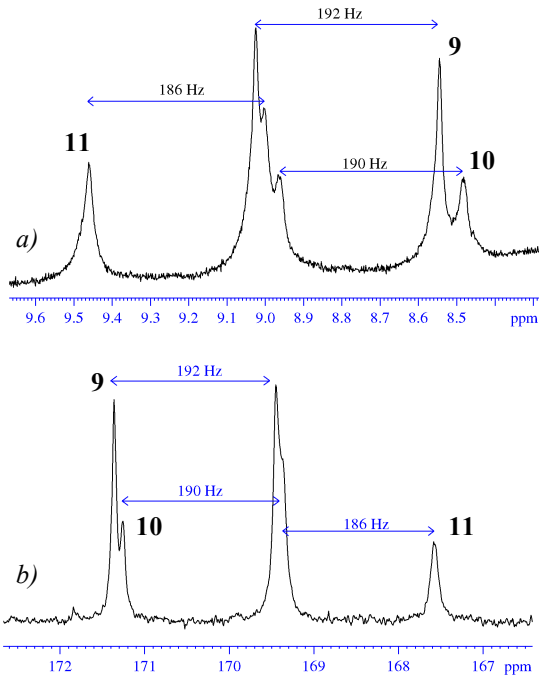

*Figure 3.6: Formate regions of a) the ^{1}H NMR spectrum (toluene-d_8, 234 K, 400 MHz) and b) the ^{13}C NMR spectrum (toluene-d_8, 234 K, 126 MHz) of **9**, **10** and **11**.*

Upon further cooling to 211 K **10** is no longer visible in the NMR spectra, allowing a more precise measurement of the $^{1}J_{CH}$ coupling of **11**. Along with the disappearance of the peaks corresponding to **10** from the ^{1}H and ^{13}C NMR spectra (at δ_H 8.70 and δ_C 170.2 respectively), the peak at δ_P 84.2 in the $^{31}P\{^{1}H\}$ NMR spectrum was also no longer visible at 211 K.

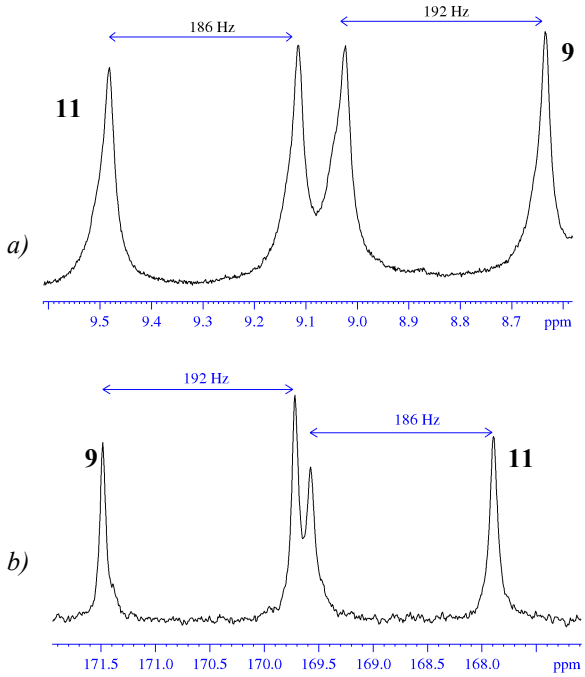

*Figure 3.7: Formate regions of a) the ^{1}H NMR spectrum (toluene-d_8, 211 K, 400 MHz) and b) the ^{13}C NMR spectrum (toluene-d_8, 211 K, 126 MHz) of products **9** and **11**.*

3.2.1.2.1. Characterisation of $Ru(IMe_4)_2(PPh_3)(CO)(CO_3)$ (**12**)

Efforts to push the reaction of **4a** with CO_2 through to a single product by heating (at 353 K), instead resulted in the precipitation of pale yellow crystals from the reaction. Although isolated in good yield (50 %), the limited solubility of the complex prevented NMR characterization. However, IR spectra revealed characteristic carbonyl and carbonate absorption bands at 1915 and 1600 cm^{-1} respectively.[10a] The structure was confirmed by X-ray crystallography to be the ruthenium carbonyl carbonate complex $Ru(IMe_4)_2(PPh_3)(CO)(CO_3)$ (**12**, Figure 3.8), presumably formed via disproportionation of CO_2.[13]

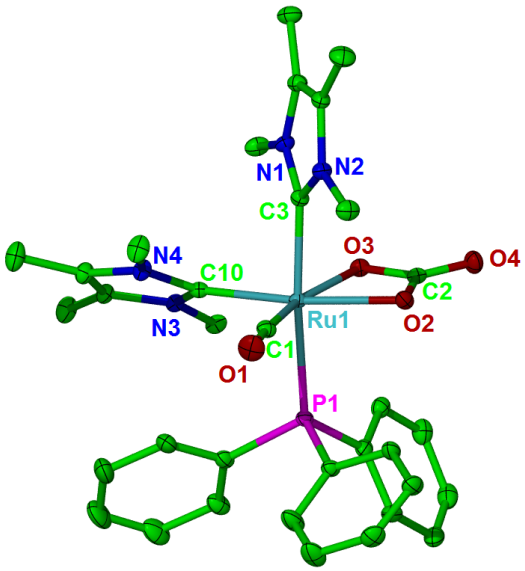

*Figure 3.8: Molecular structure of $Ru(IMe_4)_2(PPh_3)(CO)(CO_3)$ (**12**). Ellipsoids are shown at the 30 % probability level. All hydrogen atoms are removed for clarity. Selected bond lengths (Å) and angles (°): Ru-C(1) 1.821(3), Ru-C(3) 2.086(3), Ru-C(10) 2.071(3), Ru-P(2) 2.4021(7), Ru-O(2) 2.126(2), Ru-O(3) 2.137(2), P(1)-Ru-C(3) 94.88(9), C(1)-Ru-C(10) 175.34(8), C(3)-Ru-C(10) 90.4(2), O(2)-Ru-O(3) 62.16(7).*

3.2.1.3. Reaction of **4a** with MeI

The *trans* H-Ru-H geometry in **4a** should impart high hydridic character because of the good donor ligands on the Ru centre.[14] As a preliminary investigation into this, 2 equiv. of MeI was added to a benzene solution of **4a**, which resulted in an immediate colour change from yellow to red followed by the formation of a red precipitate over a period of *ca.* 2 h. This red precipitate was identified by NMR spectroscopy and X-ray crystallography as $[Ru(IMe_4)_2(PPh_3)_2H]I$ (**13**) and was isolated in 87 % yield (Scheme 3.4). Electrophilic MeI abstracted a hydride from **4a**, presumably with the formation of CH_4, to give the 5-coordinate cationic species **13**.

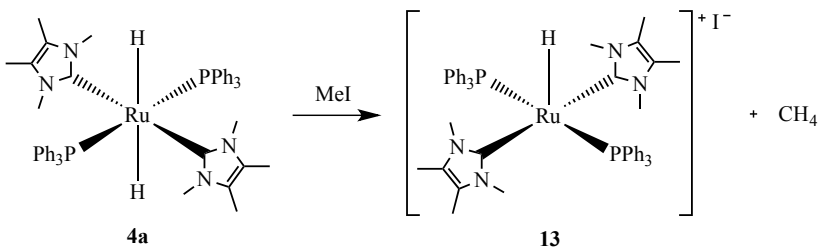

*Scheme 3.4: Reaction of **4a** with MeI to form **13**.*

Complex **13** exhibited a low-frequency triplet hydride signal in THF-d_8 at δ_H -32.32 ($^2J_{HP}$ = 23 Hz). Interestingly, this chemical shift is in line with the values reported for the all-phosphine analogues $[Ru(P\text{-}P)_2H]^+$ (P-P = $R_2PCH_2CH_2PR_2$; R = Cy, ^{i}Pr),[15] rather than the all-carbene derivatives $[Ru(NHC)_4H]^+$ (NHC = IMe_4, IEt_2Me_2, $I^iPr_2Me_2$), which appear at significantly lower frequency (*ca*. δ_H -41), suggesting that the presence of a phosphine ligands significantly influences the electronic environment of the hydride.[1,16] The geometry at Ru was established by the appearance of a triplet rather than a doublet of doublets ^{13}C signal (δ_C 189.0, $^2J_{CP}$ = 14 Hz) implying a *trans* arrangement of NHCs and *trans* disposition of PPh_3 ligands.

X-ray quality crystals formed from a concentrated C_6D_6 or THF solution of **13** and the subsequent structure (Figure 3.9) confirmed the *trans* NHC and *trans* phosphine geometry. There is some evidence of C-H interaction from an N-Me group of the carbene *trans* to the hydride. Both Me groups have a H pointing towards the metal centre, however, one is considerably shorter than the other (2.221 *c.f.* 2.697 Å). The Ru···H-C angle is 122.11° which is in line with values reported for an anagostic interaction.[17]

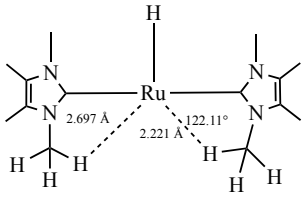

Calculations have been done showing that an anagostic interaction such as this impacts on the shift of the hydride signal in the ^{1}H NMR spectrum.[18] The stronger a ligand *trans* to a hydride the more downfield the hydride resonance is shifted. Even a weak anagostic interaction can shift the resonance. Table 3.1 shows some hydride resonances of a series of Ru complexes from either experimental or computational values. The compounds $[Ru(IMe_4)_4H]^+$ and $Ru[(PH_3)_4H]^+$ do not have any anagostic interation and have hydrides shifts of *ca*. δ -40. In the compounds with an anagostic interaction, the frequency of the hydride resonance shifts downfield to *ca*. δ -32. Therefore with the Ru-H length, the Ru···H-C angle and the chemical shift of δ -32 of the hydride resonance, it is reasonable to suggest there must be an anagostic interaction in compounds $[Ru(IMe_4)_2(PPh_3)_2H]^+$ (**13**) and $[Ru(IEt_2Me_2)_2(PPh_3)_2H]^+$ (**20**), the synthesis and characterisation of which is detailed later.

Ru---H-C interaction?	Ru complex	Hydride resonance value / ppm	
		Experimental	Calculated
✗	$[Ru(IMe_4)_4H]^+$	-40[1]	
✓	$[Ru(dcpe)_2H]^+$	-32[15a]	
✗	$[Ru(PH_3)_4H]^+$		-40[18]
✓	$[Ru(PH_2Et)_4H]^+$		-32[18]
Partial	$[Ru(IMe_4)_2(PPh_3)_2H]^+$	-32	
Partial	$[Ru(IEt_2Me_2)_2(PPh_3)_2H]^+$	-28	

Table 3.1: Chemical shifts of the hydride resonances of five-coordinate Ru complexes.

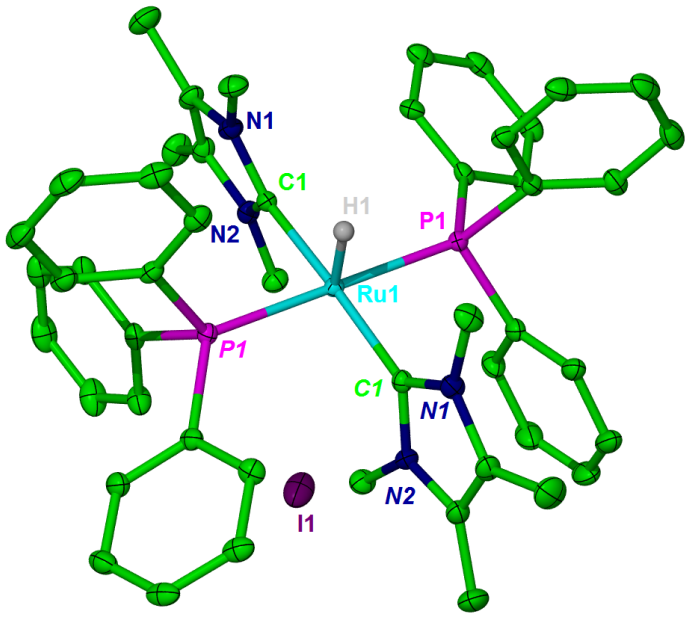

*Figure 3.9: Molecular structure of $[Ru(IMe_4)_2(PPh_3)_2H]I$ (**13**). Ellipsoids are shown at the 30 % probability level. Hydrogen atoms except Ru-H are removed for clarity. Ru1, H1 and I1 are located at a 2-fold rotation axis intrinsic to the space group symmetry. Selected bond lengths (Å) and angles (deg) in **13**: Ru-C(1) 2.084(2), Ru-P(1) 2.3356(5), C(1)-Ru-P(1) 93.31(6). C(1)-N(2)-C(7) 123.0(2), C(1)-N(2)-C(4) 125.3(2).*

3.2.2. Reactions of $Ru(IEt_2Me_2)_2(PPh_3)_2H_2$ (**5b**)

3.2.2.1. Reaction of **5b** with CO

Analogous products were produced in the reaction of **5b** with CO as with **4a** and CO (Scheme 3.5), although the formation of the known Ru(0) tricarbonyl complex[10a] $Ru(IEt_2Me_2)_2(CO)_3$ (**16**) was much slower, allowing the Ru(II) monocarbonyl complex

$Ru(IEt_2Me_2)_2(PPh_3)(CO)H_2$ (**14**) to be isolated and characterized. As with the reaction of **4a**, a minor *bis*-phosphine product (**15**) was also generated.

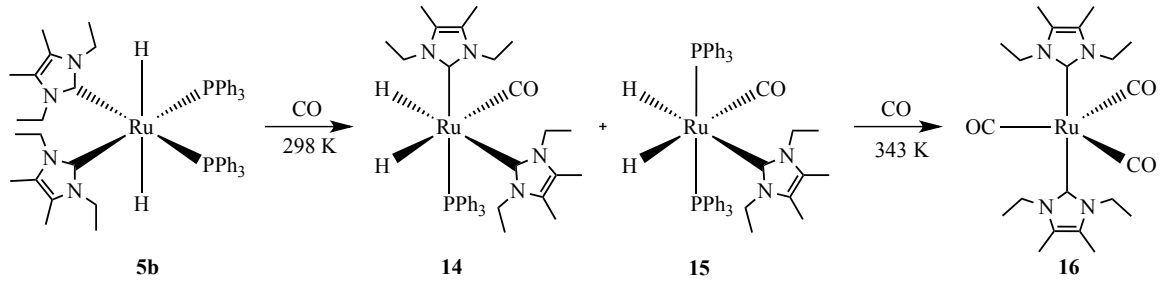

*Scheme 3.5: Reaction of **5b** with CO*

The ^{1}H NMR spectrum of **14** displayed two doublet of doublet hydride resonances at δ_H -5.51 and δ_H -8.92, both of which showed typical *cis*-H-P coupling constants of 39.5 Hz and 27.0 Hz respectively (Figure 3.10). In contrast to the hydride resonances of the IMe_4 analogue, **6**, the $^2J_{HH}$ coupling of 4.6 Hz was now visible. As with the IMe_4 analogue **6**, both the hydride signals correlated with a singlet in the ^{31}P NMR spectrum (δ_P 63.9). A ^{1}H-^{13}C HMQC NMR experiment showed a correlation between the hydride at δ_H = -5.51 and a doublet carbonyl resonance in the $^{13}C\{^1H\}$ NMR spectrum at δ_C 209.5 ($^2J_{CP}$ = 9 Hz) as well as a correlation between the hydride at δ_H -8.92 and the carbenic resonance doublet at δ_C 190.7 ($^2J_{CP}$ = 82 Hz). These data are consistent with the geometry of **14** shown in Scheme 3.5.

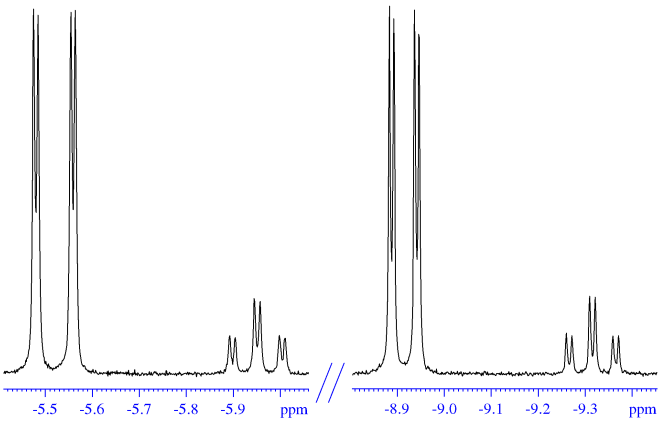

*Figure 3.10: Hydride region of the ^{1}H NMR spectrum of the major product, **14** and the minor product, **15** (C_6D_6, 298 K, 500 MHz).*

Crystals of **14** were grown from slow diffusion of hexane into a concentrated benzene solution of the complex. The structure (Figure 3.11) confirmed the

arrangement of ligands shown in Scheme 3.5. The *trans* C_{NHC}-Ru-P angle of 163.51(8)° reflects the movement of the sterically bulky NHC and PPh_3 ligands toward the space available at the hydride coordination sites. The two Ru-C_{NHC} distances were found to be substantially different (2.145(4) and 2.097(3) Å) due to the relative *trans* influences of the hydride and phosphine ligands, respectively.

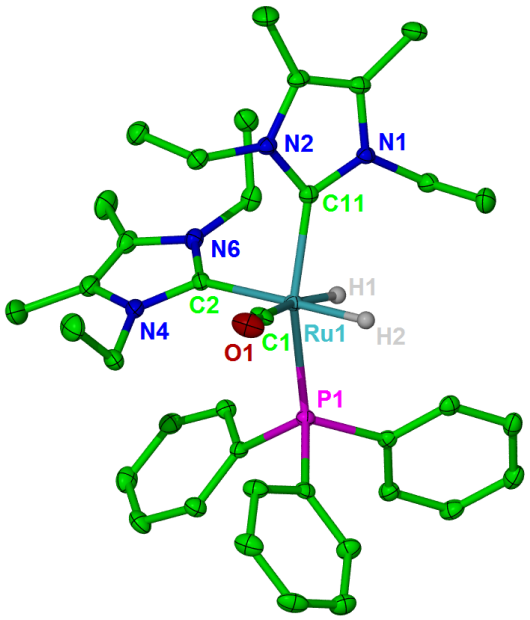

Figure 3.11: Molecular structure of ***14****. Ellipsoids are shown at the 30 % probability level. Hydrogen atoms except for Ru-H are removed for clarity. Selected bond lengths (Å) and angles (deg): Ru(1)-C(1) 1.863(4), Ru(1)-C(2) 2.145(4), Ru(1)-C(11) 2.097(3), Ru(1)-P(1) 2.3035(9), C(1)-Ru(1)-C(2) 105.4(2), C(1)-Ru(1)-C(11) 93.3(2), C(1)-Ru(1)-P(1) 99.6(2), C(11)-Ru(1)-P(1) 163.51(8).*

The reaction was accompanied by the formation of small amounts (<15 %) of a second monocarbonyl product (**15**, Scheme 3.5) which was believed to be the *bis*-phosphine complex $Ru(IEt_2Me_2)(PPh_3)_2(CO)H_2$. **15** showed two doublet of triplet hydride resonances (δ_H -5.95 and δ_H -9.32, Figure 3.10) with similar chemical shifts to **14** and both with typical *cis* H-P coupling constants of 26.7 Hz and 25.0 Hz respectively. This was suggestive of Ru-H being *trans* to IEt_2Me_2 and CO. Further evidence for this geometry came from the carbonyl signal which was a triplet at δ_C 208.4 with a *cis* C-P coupling of 9.9 Hz and the Ru-C_{NHC} resonance, which was also a triplet (δ_C 195.4) with a *cis* C-P coupling of 7.9 Hz. It is worth noting that while **15** could be seen in the room temperature reaction of **5b** with CO, the IMe_4 analogue **7** was only observed at elevated temperature.

Complete conversion through to just the known Ru(0) tricarbonyl complex **16** was achieved upon heating the reaction mixture at 343 K for *ca*. 40 h (*cf.* 24 h for the IMe_4 analogue). The ^1H and ^{13}C NMR data for **16** was in agreement with that in the literature for **16**, formed via the reaction of $Ru_3(CO)_{12}$ with IEt_2Me_2.[10a]

It is noteworthy that the Ru hydrides adopt a *cis* conformation in the IMe_4 and IEt_2Me_2 monocarbonyl complexes **6**, **7**, **14** and **15**. This could be due to the smaller CO ligand replacing a larger NHC or PPh_3 ligand or due to electronic reasons in placing a strong π-acceptor ligand (CO) opposite the strong σ-donating hydride ligand. It would be possible to reductively eliminate hydrogen from these *cis* dihydride complexes which would explain the formation of the Ru(0) tricarbonyl complexes.

3.2.2.2. Reaction of **5b** with CO_2

Complex **5b** reacted with CO_2 in a similar way to the IMe_4 analogue **4a** to give major (**17**) and minor (**18**) isomers of a formate complex (Scheme 3.6).

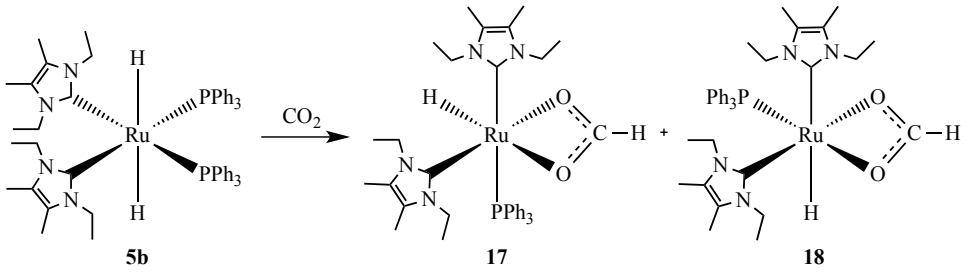

*Scheme 3.6: Reaction of **5b** with CO_2 to give major product **17** and minor product **18**.*

Eight separate multiplets were observed in the ^1H NMR spectrum of **17** (*cf.* **9**) for the diastereotopic methylene protons of the N-Et substituents of the carbene (Figure 3.12). The chemical shifts of the hydride and formate signals (**17**: δ_H -23.36, δ_H 8.61; **18**: δ_H -23.15, δ_H 8.64) were similar to those of **9** and **10**.

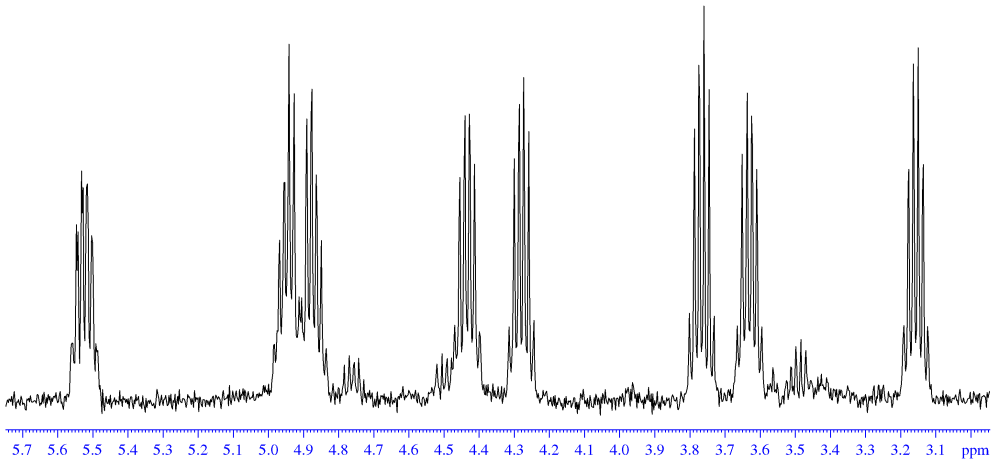

*Figure 3.12: ^{1}H NMR spectrum of **17** showing the eight diastereotopic methylene resonances (C_6D_6, 298 K, 500 MHz).*

As with the IMe_4 analogue **9**, the formate resonance for **17** at δ_H 8.61 correlated to a singlet resonance in the ^{31}P NMR spectrum (δ_P 48.5) by ^{1}H-^{31}P HSQC NMR. Also the formate resonance (δ_H 8.64) of the minor isomer **18** correlated to a singlet in the $^{31}P\{^{1}H\}$ NMR spectrum at δ_P 85.3 which is again a similar chemical shift to that of the IMe_4 analogue **10**.

The carbenic carbon of **17** appeared as a doublet resonance at δ_C 196.2 with a *trans* $^{2}J_{CP}$ coupling constant of 95 Hz. Assignment of the carbon resonance of the formate of **17** was made by ^{1}H-^{13}C HMQC spectroscopy, which showed a correlation between the resonance at δ_H 8.61 and a singlet resonance at δ_C 170.4. Based on the relative intensities of the signals in the $^{13}C\{^{1}H\}$ NMR spectrum, a singlet resonance δ_C 169.9 was assigned to the formate of the minor isomer **18**.

The higher selectivity for **17** to **18** (formed in a ratio of 5:1) compared to that of the analogous IMe_4 complexes **9** and **10** (2.4:1) allowed X-ray quality crystals of **17** to be isolated. These confirmed assignment as the κ^2-formate species $Ru(IEt_2Me_2)_2(PPh_3)(\kappa^2\text{-}OCHO)H$. The structure (Figure 3.13) displayed a highly distorted octahedral structure (with a *trans* C_{NHC}-Ru-P angle of 166.26(10)°), partially resulting from the small bite-angle of the formate ligand (O-Ru-O angle of 56.85(8)°). A combination of electronic and packing effects is the most likely explanation for the different Ru-O (2.379(2) Å (*trans* to H), 2.269(2) Å (*trans* to C_{NHC})) and Ru-C_{NHC} distances (2.083(3) Å (*trans* to P), 1.981(3) Å (*trans* to O)).

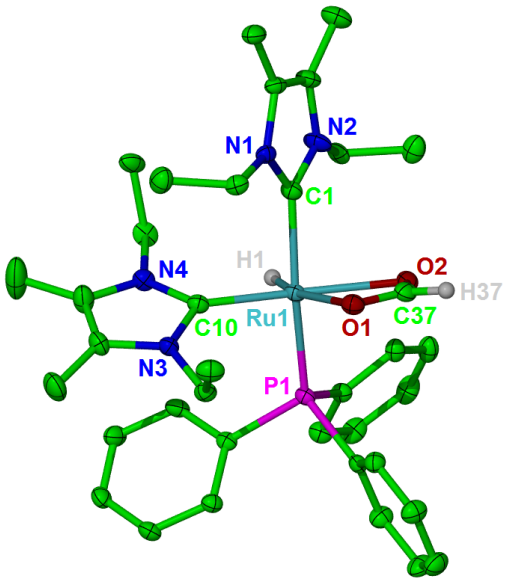

*Figure 3.13: Molecular structure of $Ru(IEt_2Me_2)_2(PPh_3)(\kappa^2\text{-}OCHO)H$ (**17**). Ellipsoids are shown at the 30 % probability level. Minor disordered fractional occupancy atoms and hydrogens except for Ru-H and Ru-OCHO are removed for clarity. Selected bond lengths (Å) and angles (°): Ru-C(1) 2.083(3), Ru-C(10) 1.981(3), Ru-P(1) 2.2997(8), Ru-O(1) 2.379(2), Ru-O(2) 2.269(2), C(1)-Ru-C(10) 92.9(3), C(1)-Ru-P(1) 166.6(2), O(1)-Ru-O(2) 56.85(8).*

Complex **17** has comparable bond lengths and angles to $Ru(IMe_4)_2(PPh_3)(CO)(CO_3)$ (**12**). The C_{axial}-Ru-$C_{equatorial}$ bond angle was slightly bigger in **17** (92.9(3)°) than in **12** (90.4(1)°). The Ru-O bond lengths in **17** (2.269(2), 2.379(2) Å) were longer than those in the carbonate carbonyl complex **12** (2.126(2), 2.137(2) Å)

3.2.2.3. Reaction of **5b** with MeI

In contrast to the simplicity of the reaction of **4a** with MeI, addition of 2 equiv. of MeI to either C_6D_6 or THF solutions of **5b** gave a mixture of up to four Ru-H containing products. However, one major product was consistently formed, the neutral Ru hydride iodide complex $Ru(IEt_2Me_2)_2(PPh_3)HI$, **19**. This could be isolated in good yield (71 %) after leaving the reaction 1 h at room temperature. **19** was fully characterized by standard spectroscopic methods. The ^1H NMR spectrum showed a doublet hydride resonance at δ_H -30.45 ($^2J_{HP}$ = 41 Hz) that correlated to a singlet resonance at δ_P 74.5 in the $^{31}P\{^1H\}$ NMR spectrum. The ^1H NMR spectrum also showed resonances that were assigned to two IEt_2Me_2 ligands; four methylene resonances that integrated 2:1 to the hydride resonance with the corresponding triplet resonances for the Me groups as well as a singlet resonances for the Me groups on the

backbone of the carbene that integrated 12:1 to the hydride resonance. The $^{13}C\{^{1}H\}$ NMR spectrum showed a carbenic carbon signal at δ_C 196.0 with a doublet, *cis* C-P coupling of 13 Hz. These spectroscopic data are consistent with the structure of **19** shown below.

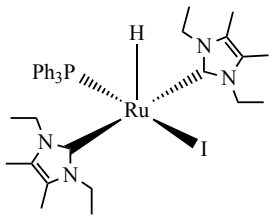

19

All attempts to crystallize this species from either crude reaction mixtures (i.e. ones still containing the PPh_3 dissociated in the reaction) or cleaned-up reaction mixtures (i.e. washed with hexane in efforts to remove the free PPh_3) gave instead deep red crystals of the cationic species $[Ru(IEt_2Me_2)_2(PPh_3)_2H]I$ (**20**), the direct analogue of the IMe_4 complex, **13**. This is perhaps not surprising as charge separation in the solid state is not unreasonable and iodide is a good leaving group.[19]

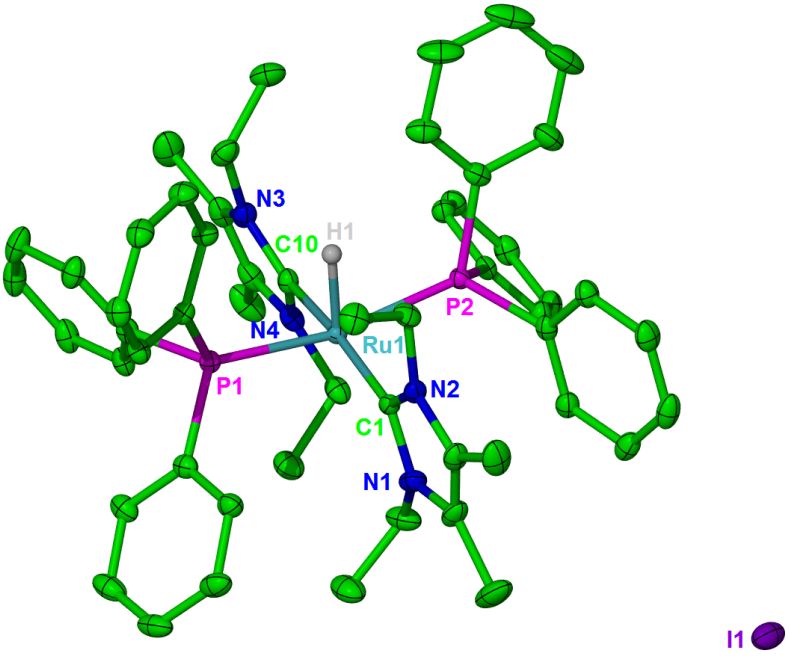

*Figure 3.14: Molecular structure of $[Ru(IEt_2Me_2)_2(PPh_3)_2H]I$ (**20**). Ellipsoids are shown at the 30 % probability level. Hydrogen atoms except Ru-H are removed for clarity. Selected bond lengths (Å) and angles (deg): Ru-C(1) 2.083(3), Ru-C(10) 2.098(3), Ru-P(1) 2.3469(8), Ru-P(2) 2.3242(8), C(1)-Ru-C(10) 169.0(2), C(1)-Ru-P(1) 90.57(8), P(1)-Ru-P(2) 165.56(3).*

Complexes **13** (NHC = IMe_4) and **20** (NHC = IEt_2Me_2) are isostructural, with the mutually *trans* NHC and PPh_3 ligands arranged at the base of a square pyramid with the hydride ligand in an apical position. However, **13** is closer to an ideal square based pyramid than **20**, as evidenced by comparison of the largest deviation of any atom from the mean plane subtended by the Ru, P and C_{NHC} atoms (*c.f.* 0.05 Å in **13**; 0.26 Å in **20**). The accompanying asymmetry of the Ru-C_{NHC}-N angles associated with each of the carbene ligands is also noteworthy in complex **20**, as the smaller angles correspond with bending of these ligands away from the basal square plane and toward the vacant coordination site opposite the hydride. Phosphine movement in the opposite direction offsets this bend.[20] The net result is that two methylene hydrogens move closer to the vacant coordination site on the metal in structure **20** (H4B and H17A, 2.65 and 2.75 Å from Ru1, respectively). The Ru-C_{NHC} distances (**13**: 2.084(2) Å; **20**: 2.083(3) Å, 2.098(3) Å) are comparable to those found in $[Ru(NHC)_4H]^+$ (NHC = IMe_4 average 2.0822(16) Å; NHC = IEt_2Me_2, average 2.0795(4) Å).[1]

Efforts to measure NMR spectra of $[Ru(IEt_2Me_2)_2(PPh_3)_2H]I$ (**20**) by redissolving the crystalline material showed only the characteristic doublet Ru-H signal of the neutral complex **19**. This was consistent with **20** and **19** being in an equilibrium lying heavily toward the latter in solution at room temperature. Upon cooling a toluene solution of crystalline **20** to 245 K, the hydride region of the ^1H NMR spectrum showed a mixture (1:0.6 ratio) of **19** together with a triplet signal at δ_H -27.5 ($^2J_{HP}$ = 22.4 Hz), which was tentatively assigned to **20**. Warming the solution back to ambient temperature resulted in the disappearance of the triplet resonance along with the singlet at δ_P 50 in the $^{31}P\{^1H\}$ NMR spectrum to which it correlated (Figure 3.15).

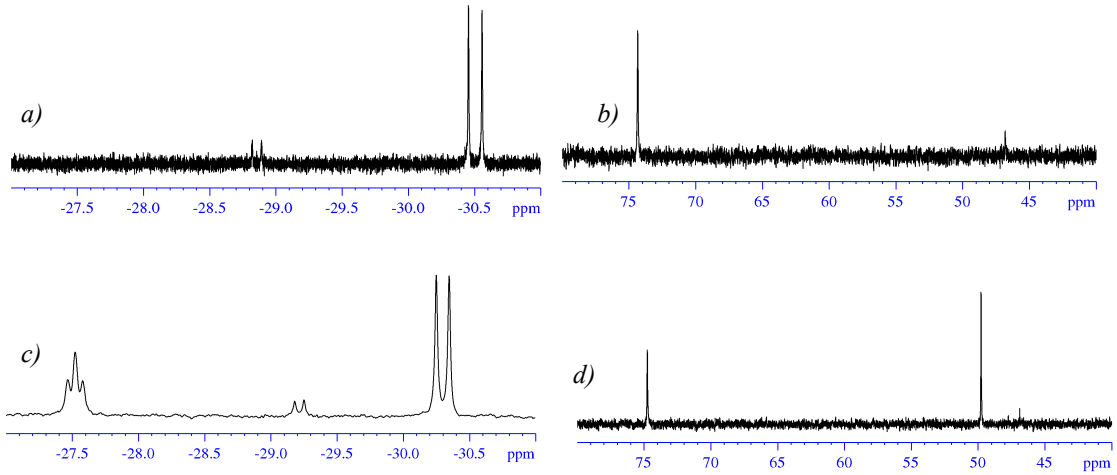

*Figure 3.15: Pertinent regions of the ^1H (toluene-d_8, 298 K, 400 MHz) and $^{31}P\{^1H\}$ (toluene-d_8, 162 Hz) NMR spectra of **19** and **20** at 298 K (a and b) and 245 K (c and d).*

As is evident from Figure 3.15a, even a crystalline sample of the product contained a minor side product formed in the reaction. This hydride containing species (a doublet at *ca*. δ_H -29) was never present in a large enough proportion of the mixture to be characterized spectroscopically. One possibility is that the structure is a different isomer of **19** that maintained *cis* hydride and phosphine ligands but had *cis* IEt_2Me_2 ligands.

Monitoring the reaction of **5b** with MeI over a longer time of 8 h showed the presence of a further hydride containing complex (**21**) in solution by the presence of a small triplet hydride resonance at δ_H -25.5. This resonance showed a typical *cis*-$^2J_{HP}$ coupling of 23.6 Hz and correlated to a singlet resonance in the $^{31}P\{^1H\}$ NMR spectrum at δ_P 47.7. In an attempt to isolate this product, the reaction was repeated with 5 equiv. of MeI. After either 22 days at 298 K in THF or 8 h at 343 K in C_6D_6, there was no starting material (**5b**) remaining and **21** was the major product in solution. **21** was isolated in a low yield because some decomposition had occurred.

As **21** formed after a prolonged reaction time, it seemed possible it formed from reaction of the PPh_3 eliminated from **5b** with **19**. Indeed, addition of a large excess of PPh_3 to an isolated sample of **19** gave complete conversion to **21** over several days. Slow diffusion of hexane into a concentrated THF solution of **21** yielded light brown crystals, which revealed the product to be a Ru hydride iodide complex complete with an agostic interaction from the N-Et arm of the carbene (Figure 3.16). This product provided some additional, albeit circumstantial, support for **19** being a neutral Ru hydride iodide complex. **21** (Figure 3.16) was the iodide analogue of the previously reported $Ru(IEt_2Me_2)(PPh_3)_2HCl$ complex, which displayed the same stabilizing agostic interaction.[17a] A summary of the reactivity of **5b** with MeI is given in Scheme 3.7.

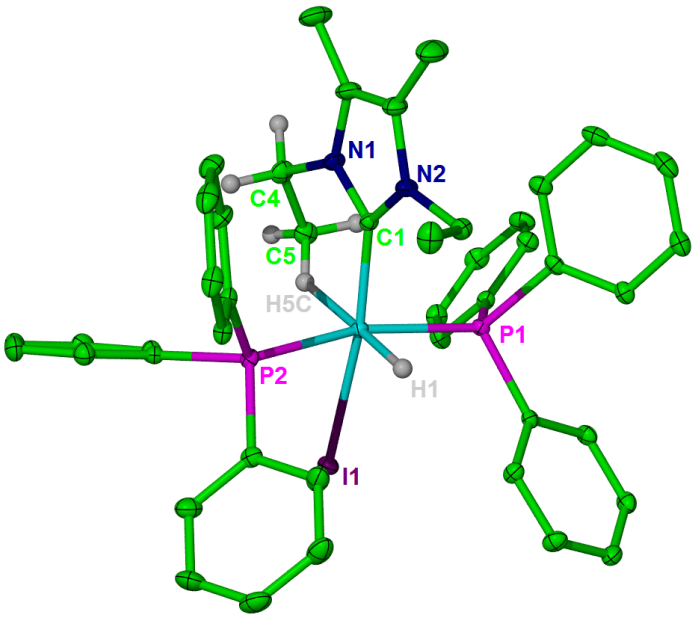

*Figure 3.16: Molecular structure of Ru(IEt$_2$Me$_2$)(PPh$_3$)$_2$HI (**21**). Ellipsoids are shown at the 30 % probability level. Hydrogen atoms except for Ru-H and those in the agostically bound N-Et arm are removed for clarity. Selected bond lengths (Å) and angles (deg): Ru-C(1) 1.996(3), Ru-P(1) 2.3299(7), Ru-P(2) 2.3223(7), Ru-I(1) 2.8187(3), C(1)-Ru-I(1) 170.04(8), C(1)-Ru-P(1) 93.48(8), P(1)-Ru-P(2) 164.65(3).*

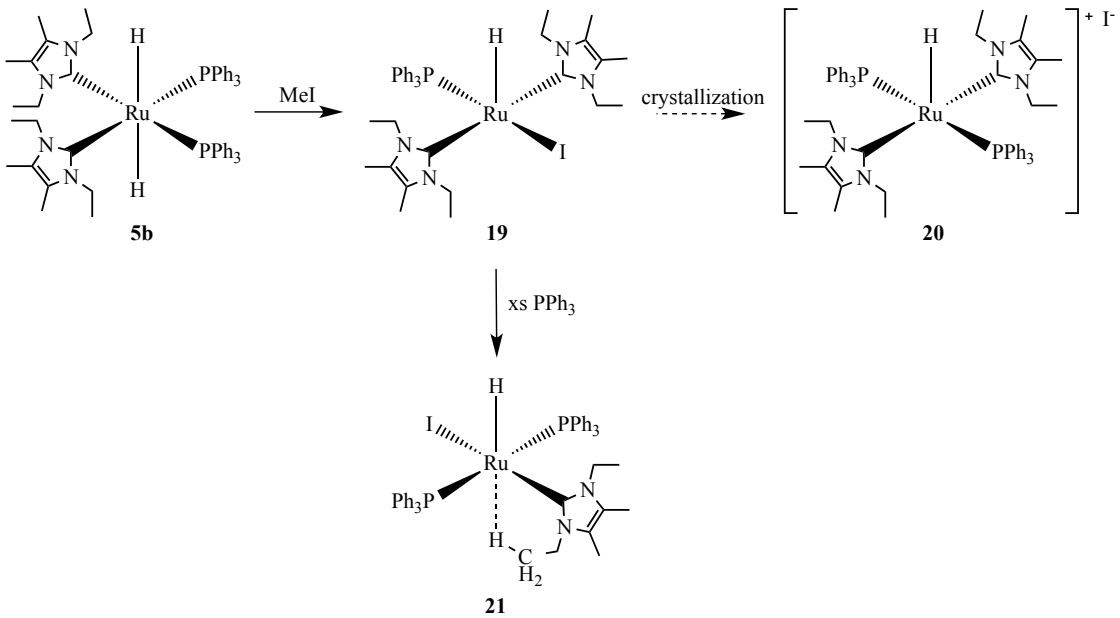

*Scheme 3.7: Summary of reactions of **5b** with MeI.*

3.2.3. Reactions of $Ru(IMe_4)_4H_2$ (**3**)

3.2.3.1. Reaction of **3** with CO

Addition of 1 atm of CO to a benzene (or toluene) solution of **3**, surprisingly resulted in the slow formation (over 3 days) of $[Ru(IMe_4)_4(CO)H]^+X^-$ (**22**) and an off-white precipitate, proposed to be a Ru carbonate species (a speculative formulation as $Ru(IMe_4)_4(CO_3)$ is shown below in Scheme 3.8) The ^1H NMR spectrum of the residue from the filtrate showed resonances for the methyl groups of the carbenes and a hydride resonance (δ_H -3.97) that matched those of the previously reported $[BAr^F_4]$ salt of **22** formed upon addition of CO to $[Ru(IMe_4)_4H][BAr^F_4]$.[1] Cleavage of the Ru-H bond rather than the Ru-NHC bond was surprising. The identity of X^- is not clear.

The insolubilty of the Ru carbonate complex precluded any NMR spectroscopy. However, supporting evidence for the species being a carbonate came from IR spectroscopy, which showed a carbonate stretching frequency at 1611 cm^{-1}, close to the value for **12**.[10a] The formation of a carbonate species hints at water being present somehow as an impurity in the reaction.

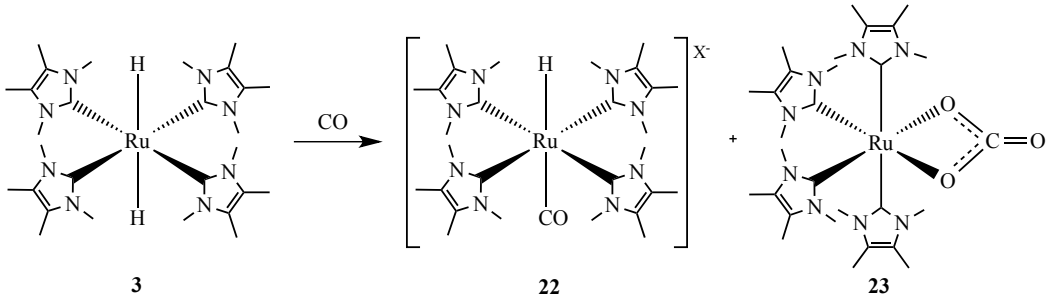

3 **22** **23**

*Scheme 3.8: Proposed products from reaction of **3** with CO.*

Repeating the reaction in THF showed the same products as above, however, during the course of the reaction two unidentified hydride containing products were also seen in the ^1H NMR spectrum, with resonances at δ_H -3.89 and -4.01. Figure 3.17 shows selected regions of the ^1H NMR spectrum of the reaction at different time intervals over a period of 9 days. At 5 h (Figure 3.17a), there was a large proportion of unreacted **3** in the solution and the initial product formed was **22**. After 2 days (Figure 3.17b), all of **3** had reacted with the CO to give the Ru carbonate **23**, **22** and the unidentifed products, the Me signals of which could not be identified due to them overlapping. After 9 days (Figure 3.17c), the major product in solution was **22**, although residual amounts of the other hydride products persisted.

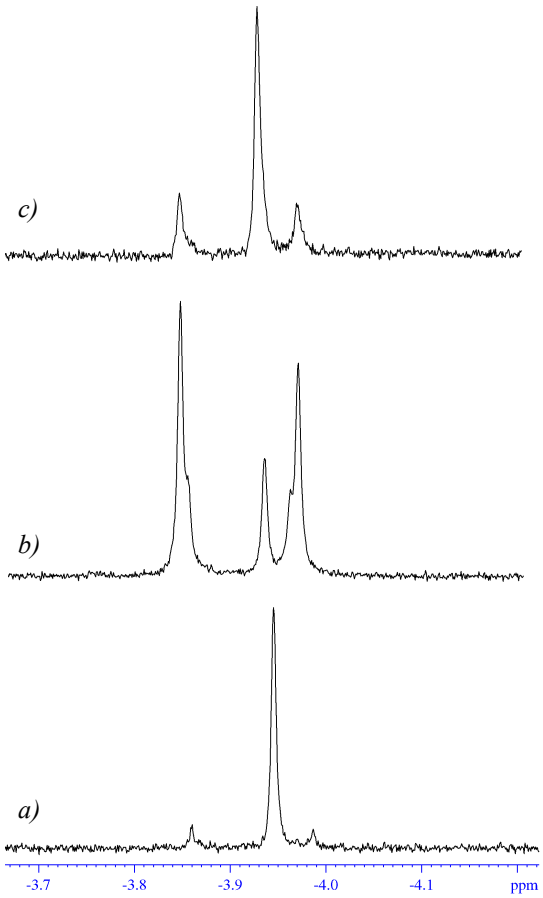

*Figure 3.17: Selected hydride regions of ^{1}H NMR spectra of reaction of **3** with CO after a) 5 h, b) 2 days and c) 9 days (THF-d_8, 298 K, 500 MHz)*

3.2.3.2. Reaction of **3** with CO_2

On addition of 1 atm of CO_2 to a yellow solution of **3**, there was an immediate colour change to red, which over 2 h slowly became orange. Using ^{1}H and ^{13}C{^{1}H} NMR spectroscopy over a range of temperatures, along with $^{13}CO_2$, the course of the reaction was deduced. Initially, the formate hydride species $Ru(IMe_4)_4(OCHO)H$ (**24**) appears to form on the basis of two signals at δ_H 8.66 and δ_H -26.28 in the ^{1}H NMR spectrum. After 1 h, the *bis*-formate complex $Ru(IMe_4)_4(OCHO)_2$, (**25**) is proposed to form, as suggested by the signals for **24** diminishing and the appearance of a broad singlet resonance at δ_H 7.95. After 4 h, complete conversion to **25** was observed. Upon warming to 320 K, extrusion of CO_2 from the *bis*-formate reformed the formate hydride complex **24**. When the solution was cooled back to room temperature, reinsertion of CO_2 into the Ru-H took place, leaving the *bis*-formate as the major species in the solution (Scheme 3.9).

Figure 3.18a-d shows change in the formate region of the ^{1}H NMR spectrum upon starting with the *bis*-formate complex **25**. Figure 3.18b-d shows the decrease in

intensity of the *bis*-formate resonance at δ_H 7.95 and the appearance and increase in intensity of the formate hydride resonance at δ_H 8.66 as the temperature was increased.

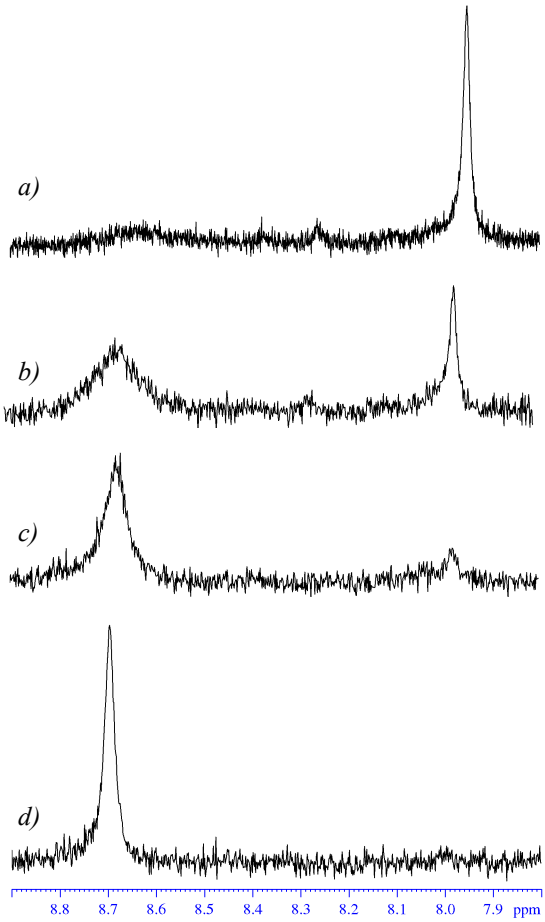

*Figure 3.18: Selected regions of the ^1H NMR spectrum of products from CO_2 insertion into **3** at a) 298 K and b) 308 K c) 318 K and d) 328 K (THF-d_8, 400 MHz).*

Using $^{13}CO_2$, the formate resonances could be assigned in the ^{13}C NMR spectra. A ^1H-^{13}C HMBC experiment showed a correlation between the δ_H 8.66 resonance of **24** and a signal at δ_C 167.6 in the $^{13}C\{^1H\}$ NMR spectrum (Figure 3.19), both of which exhibited a C-H splitting of *ca*. 180 Hz. The *bis*-formate complex **25** showed a correlation of the resonance at δ_H 7.9 to a signal at δ_C 170.1 (Figure 3.19), and now showed a C-H splitting of 190 Hz.

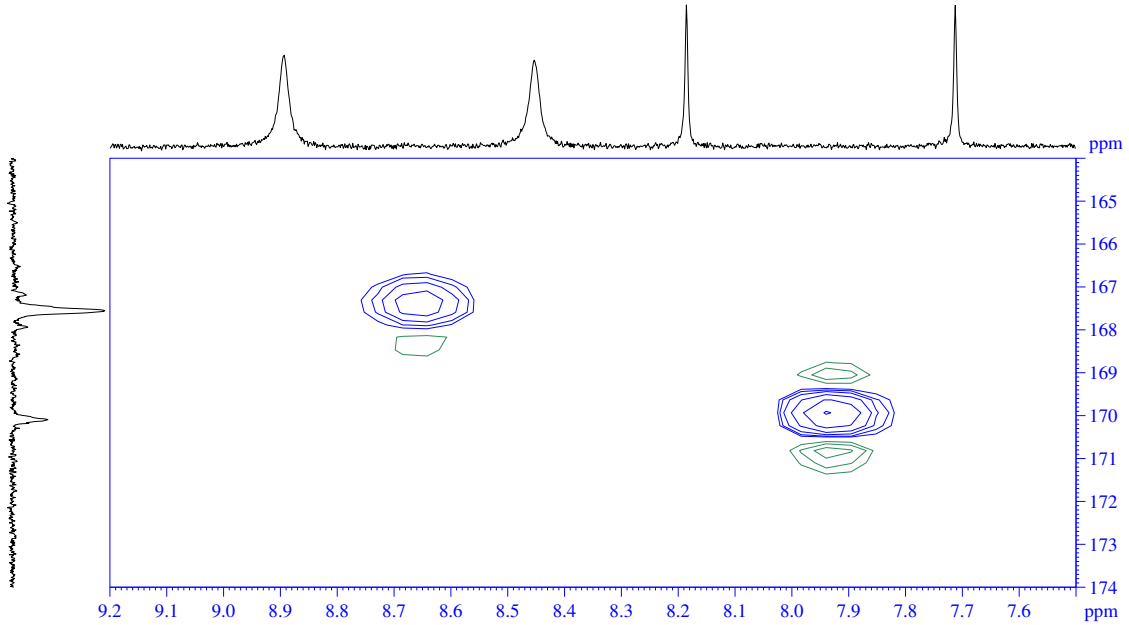

*Figure 3.19: Selected region of the $^{13}CO_2$ enhanced ^{1}H-^{13}C HSQC NMR spectrum of **24** and **25** 1 h into reaction showing the correlation between the respective formate resonances (THF-d_8, 298 K, 400 MHz).*

The reaction was scaled up in an attempt to isolate the *bis*-formate product **25**, however both **24** and **25** were always present thus precluding isolation. Indeed, heating a sample containing a 1:2 ratio of **24**:**25** to 328 K increased the amount of **24**, allowing a small amount of free $^{13}CO_2$ to be seen by $^{13}C\{^{1}H\}$ NMR spectroscopy. On cooling to room temperature and monitoring the solution for 3 days, reformation of **25** was observed.

IR spectroscopy showed the mixture of products with a peak at 1606 cm^{-1}, which is characteristic of a κ^1-bound formate and is consistent with the proposed structures of the complexes.[11c]

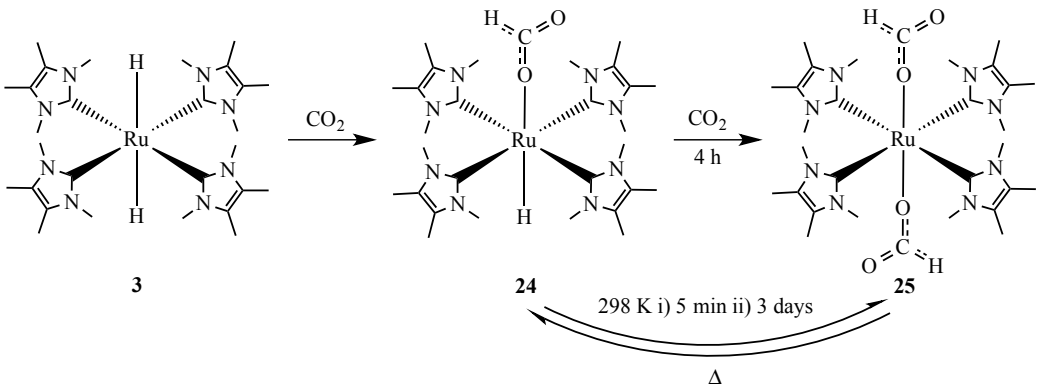

*Scheme 3.9: Reaction of **3** with CO_2 with conversion i) under an atmosphere of CO_2 and ii) under an atmosphere of argon.*

3.3. Summary and Conclusions of Chapter 3

The reactivities of **3**, **4a** and **5b** with CO, CO_2 and MeI have been investigated. The subtle differences in reactivity with CO and CO_2 between **4a** and **5b** could be attributed to both the change in steric demands of their respective carbenes and the differences in geometry.

The small molecule coordination and activation shown by complexes **3**, **4a**, and **5b** in this chapter are, for the most part, in line with the reactivity observed with other Ru-NHC hydride complexes.[10,12] Arguably the most interesting reactivity relates to that with MeI to afford the five-coordinate species $[Ru(NHC)_2(PPh_3)_2H]^+$ as a result of the highly nucleophilic character that results from the *trans* H-Ru-H geometries. This nucleophilic aspect is considered again in Chapter 5.

3.4. Experimental

3.4.1. Formation of $Ru(IMe_4)_2(PPh_3)(CO)H_2$ (**6**) from reaction of **4a** and CO

A sample of **4a** (*ca.* 5 mg) in C_6D_6 (0.6 mL) in a J. Youngs resealable NMR tube was freeze–pump–thaw degassed and placed under 1 atm CO. The formation of **6** was apparent by ^{1}H NMR spectroscopy within 3 h at room temperature, with complete conversion through to a mixture of **6** and **7** taking place over 24 h. Spectroscopic characterization of $Ru(IMe_4)_2(PPh_3)(CO)H_2$ (**6**). ^{1}H NMR (500 MHz, $C_6D_5CD_3$, 200 K): δ 3.92 (s, 6H, NC*H*$_3$), 3.53 (s, 6H, NC*H*$_3$), 1.55 (s, 6H, C*H*$_3$), 1.25 (s, 6H, C*H*$_3$), -5.05 (d, $^2J_{HP}$ = 36.7 Hz, 1H, Ru*H*), -6.91 (d, $^2J_{HP}$ = 94.9 Hz, 1H, Ru*H*). ^{31}P{^{1}H} NMR (202 MHz, $C_6D_5CD_3$, 298 K): δ 51.5 (s). ^{13}C{^{1}H} NMR (126 MHz, C_6D_6, 298 K): δ 211.0 (d, $^2J_{CP}$ = 5 Hz, Ru-*C*O), 193.2 (d, $^2J_{CP}$ = 9 Hz, Ru-*C*$_{NHC}$), 142.8* (d, J_{CP} = 25 Hz, P*C*$_6$H$_5$), 133.9* (d, J_{CP} = 12 Hz, P*C*$_6$H$_5$), 127.1* (d, J_{CP} = 8 Hz, P*C*$_6$H$_5$) 123.0 (s, N*C*CH$_3$=N*C*CH$_3$), 37.5 (s, N*C*H$_3$), 9.6 (s, NC*C*H$_3$=NC*C*H$_3$). *The presence of free PPh_3 precluded complete identification of all PPh_3^{13}C signals of **6**. Spectroscopic characterization of $Ru(IMe_4)(PPh_3)_2(CO)H_2$ (**7**). ^{1}H NMR (500 MHz, C_6D_6, 298 K): δ -5.35 ($^2J_{HH}$ = 4.6 Hz, *cis*-$^2J_{HP}$ = 36.4 Hz, Ru*H*), -8.49 ($^2J_{HH}$ = 4.7 Hz, *cis*-$^2J_{HP}$ = 26.2 Hz, Ru*H*). ^{31}P{^{1}H} NMR (202 MHz, C_6D_6, 298 K): δ 65.5 (s). ^{13}C{^{1}H} NMR (126 MHz, C_6D_6, 298 K): δ 209.8 (t, $^2J_{CP}$ = 9.3 Hz, Ru-*C*O),

3.4.2. Synthesis of $Ru(IMe_4)_2(CO)_3$ (**8**)

A THF or C_6H_6 solution (10 mL) of **4a** (100 mg, 0.1 mmol) in an ampoule fitted with a J. Youngs resealable valve was freeze–pump–thaw degassed, placed under 1 atm CO, and stirred at 343 K for 24 h. After cooling to ambient temperature, the solvent

was removed to leave a yellow solid, which was washed with hexane (10 mL) and dried under vacuum. Yield 35 mg (70%). ^{1}H NMR (500 MHz, C_6D_6): δ 3.76 (s, 12H, NCH_3), 1.36 (s, 12H, NCCH_3=CNCH_3). ^{13}C{^{1}H} NMR (126 MHz, C_6D_6): δ 217.0 (s, Ru-*C*O), 181.9 (s, Ru-C_{NHC}), 124.7 (s, N*C*CH$_3$=N*C*CH$_3$), 37.2 (s, N*C*H$_3$), 9.4 (s, NC*C*H$_3$=NC*C*H$_3$). IR: 1840 cm^{-1} (ν_{CO}). Anal. Calcd (%) for $C_{17}H_{24}N_4O_3Ru$ (433.49): C, 47.10; H, 5.58; N, 12.92. Found: C, 47.02; H, 5.93; N, 12.80.

3.4.3. Reaction of **4a** with CO_2

(i) NMR scale: A sample of **4a** (*ca.* 5 mg) in toluene-d_8 (0.6 mL) in a J. Youngs resealable NMR tube was degassed (freeze–pump–thaw × 3) and placed under 1 atm CO_2. Total consumption of **4a** was apparent by ^{1}H NMR spectroscopy within 20 min at room temperature, to afford a mixture of **9** and **10**. (ii) Preparative scale: A 20 mL toluene solution of **4a** (300 mg, 0.34 mmol) was placed under 1 atm CO_2 in an ampoule fitted with a J. Youngs PTFE valve. Over 16 h at ambient temperature, the stirred solution changed colour from orange to yellow with formation of a yellow precipitate. This was isolated by filtration and dried under vacuum to give 135 mg of a mixture of **9** and **10**, although still containing traces of PPh_3. Redissolution of 80 mg of the solid in toluene and layering with hexane gave 52 mg of an analytically pure mixture of **9** and **10**. Spectroscopic characterization of Ru(IMe$_4$)$_2$(PPh$_3$)$_2$(OCHO)H (**9**). ^{1}H NMR (400 MHz, $C_6D_5CD_3$, 211 K): δ 8.87 (s, 1H, Ru-OC*H*O), 4.24 (s, 3H, NCH_3), 3.80 (s, 3H, CH_3), 3.18 (s, 3H, CH_3), 2.77 (s, 3H, NCH_3), 1.53 (s, 3H, CH_3), 1.34 (s, 3H, CH_3), 1.32 (s, 3H, NCH_3), 1.30 (s, 3H, *CH$_3$*), -23.35 (d, $^{2}J_{HP}$ = 29.5 Hz, 1H, Ru*H*). ^{31}P{^{1}H} NMR (162 MHz, $C_6D_5CD_3$, 211 K): δ 48.4 (s). ^{13}C NMR (100 MHz, C_6D_6, 298 K): δ 197.7 (d, $^{2}J_{CP}$ = 96 Hz, Ru-C_{NHC}), 196.0 (d, $^{2}J_{CP}$ = 11 Hz, Ru-C_{NHC}), 170.3 (s, Ru–O*C*HO; d, $^{1}J_{CH}$ = 192 Hz in ^{1}H-coupled ^{13}C spectrum), 142.8* (d, J_{CP} = 28 Hz, PC_6H_5), 122.0 (s, N*C*CH$_3$=N*C*CH$_3$), 121.1 (s, N*C*CH$_3$=N*C*CH$_3$), 34.1 (s, N*C*H$_3$), 9.6 (s, NC*C*H$_3$=NC*C*H$_3$), 8.8 (s, NC*C*H$_3$=NC*C*H$_3$). *The presence of **10** and free PPh_3 precluded complete identification of all PPh_3 ^{13}C signals of **9**. Spectroscopic characterization of Ru(IMe$_4$)$_2$(PPh$_3$)$_2$(OCHO)H (**10**). ^{1}H NMR (400 MHz, $C_6D_5CD_3$, 272 K): δ 8.60 (br d, *J* = 3.8 Hz, 1H, Ru-OC*H*O), -23.30 (d, $^{2}J_{HP}$ = 49.5 Hz, 1H, Ru*H*). ^{31}P{^{1}H} NMR (162 MHz, $C_6D_5CD_3$, 272 K): δ 84.2 (s). ^{13}C{^{1}H} NMR (100 MHz, $C_6D_5CD_3$, 259 K): δ 170.2 (s, Ru–O*C*HO; d, $^{1}J_{CH}$ = 190 Hz in ^{1}H-coupled ^{13}C spectrum). Spectrosopic characterisation of Ru(IMe$_4$)$_2$(PPh$_3$)(OCHO)$_2$ (**11**): ^{1}H NMR (400 MHz, $C_6D_5CD_3$, 211 K): δ 9.27 (br s, Ru-OC*H*O). ^{31}P{^{1}H} NMR (162 MHz, $C_6D_5CD_3$, 211 K): δ 50.3 (s). ^{13}C{^{1}H} NMR (100 MHz, $C_6D_5CD_3$, 259 K): δ 168.3 (s,

Ru–O*C*HO; d, $^{1}J_{CH}$ = 186 Hz in ^{1}H-coupled ^{13}C spectrum). Anal. Calcd (%) for mixture of **9** and **10**: $C_{33}H_{41}N_4PO_2Ru$ (657.76): C, 60.25; H, 6.28; N, 8.52. Found: C, 60.10; H, 6.27; N, 8.58.

3.4.4. Synthesis of [Ru(IMe$_4$)$_2$(PPh$_3$)$_2$H]I (**13**)

MeI (8.5 μL, 0.14 mmol) was added to a C_6H_6 solution (20 mL) of **3a** (60 mg, 0.07 mmol), and the mixture was stirred at room temperature for 2 h. Over this time, the colour of the solution changed from orange/yellow to red and a red precipitate was formed. This was isolated by cannula filtration and dried under vacuum. Yield: 60 mg (87%). ^{1}H NMR (500 MHz, THF-d_8, 298 K): δ 7.5-7.0 (m, 30H, PC$_6$*H*$_5$), 2.93 (s, 6H, NC*H*$_3$), 2.63 (s, 6H, NC*H*$_3$), 1.78 (s, 6H, NCC*H*$_3$=NCC*H*$_3$), 1.65 (s, 6H, NCC*H*$_3$=NCC*H*$_3$), -32.32 (t, $^{2}J_{HP}$ = 23.0 Hz, 1H, Ru*H*). ^{31}P{^{1}H} NMR (202 MHz, THF-d_8, 298 K): δ 47.6 (s). ^{13}C{^{1}H} NMR (126 MHz, THF-d_8, 298 K): δ 189.0 (t, $^{2}J_{CP}$ = 14 Hz, Ru-C_{NHC}), 138.7 (vt, *J* = 18 Hz, P*C*$_6$H$_5$), 134.3 (vt, *J* = 6 Hz, P*C*$_6$H$_5$), 129.4 (s, P*C*$_6$H$_5$), 128.5 (vt, *J* = 4 Hz, P*C*$_6$H$_5$), 126.3 (s, N*C*CH$_3$=N*C*CH$_3$), 125.0 (s, NCCH$_3$=*C*NCH$_3$), 35.9 (s, N*C*H$_3$), 34.6 (s, N*C*H$_3$), 9.3 (s, NC*C*H$_3$=CN*C*H$_3$), 8.8 (s, NC*C*H$_3$=CN*C*H$_3$). Anal. Calcd (%) for $C_{50}H_{55}N_4P_2RuI$ (1001.9): C, 59.94; H, 5.53; N, 5.59. Found C, 59.69; H, 5.63; N, 5.67.

3.4.5. Synthesis of Ru(IEt$_2$Me$_2$)$_2$(PPh$_3$)(CO)H$_2$ (**14**)

1 atm CO was added to a freeze–pump–thaw degassed THF solution (10 mL) of **5b** (100 mg, 0.11 mmol) in an ampoule fitted with a J. Youngs resealable valve. After stirring for 2 h at room temperature, the solution was reduced to dryness and the resulting yellow oil was washed with hexane (10 mL) to leave **14** as a yellow, microcrystalline solid. Yield 30 mg (40%). ^{1}H NMR (500 MHz, C$_6$D$_6$): δ 5.17 (m, 1H, NC*H*$_2$CH$_3$), 4.59 (m, 4H, NC*H*$_2$CH$_3$), 4.32 (m, 1H, NC*H*$_2$CH$_3$), 3.45 (m, 1H, NC*H*$_2$CH$_3$), 3.00 (m, 1H, NC*H*$_2$CH$_3$), 1.67 (s, 6H, NCCH$_3$=CNC*H*$_3$), 1.59 (s, 3H, NCCH$_3$=CNC*H*$_3$), 1.57 (s, 3H, NCCH$_3$=CNC*H*$_3$), 1.31 (t, $^{3}J_{HH}$ = 7.0 Hz, 3H, NCH$_2$C*H*$_3$), 1.16 (t, $^{3}J_{HH}$ = 7.0 Hz, 6H, NCH$_2$C*H*$_3$), 0.54 (t, $^{3}J_{HH}$ = 7.2 Hz, 3H, NCH$_2$C*H*$_3$), −5.51 (dd, $^{2}J_{HP}$ = 39.5 Hz, $^{2}J_{HH}$ = 4.6 Hz, 1H, Ru-*H*), −8.92 (dd, $^{2}J_{HP}$ = 27.0 Hz, $^{2}J_{HH}$ = 4.6 Hz, 1H, Ru-*H*). ^{31}P{^{1}H} NMR (202 MHz, C$_6$D$_6$, 298 K): δ 63.9 (s). ^{13}C{^{1}H} NMR (126 MHz, C$_6$D$_6$, 298 K): δ 209.5 (d, $^{2}J_{CP}$ = 9 Hz, Ru-*C*O), 190.7 (d, $^{2}J_{CP}$ = 82 Hz, Ru-C_{NHC}) 144.0 (d, $^{2}J_{CP}$ = 33 Hz, P*C*$_6$H$_5$), 134.2 (d, $^{2}J_{CP}$ = 11 Hz, P*C*$_6$H$_5$), 127.6 (s, P*C*$_6$H$_5$), 127.1 (d, $^{2}J_{CP}$ = 8 Hz, P*C*$_6$H$_5$), 123.1 (s, N*C*CH$_3$=N*C*CH$_3$), 123.0 (s, N*C*CH$_3$=N*C*CH$_3$), 44.3 (s, N*C*H$_2$CH$_3$), 43.8 (s, N*C*H$_2$CH$_3$), 43.3 (s, N*C*H$_2$CH$_3$), 15.8 (s,

NCH_2CH_3), 14.6 (s, NCH_2CH_3), 14.3 (s, NCH_2CH_3), 9.4 (s, $NCCH_3{=}NCCH_3$), 9.3 (s, $NCCH_3{=}NCCH_3$). IR: 1870 cm^{-1} (ν_{CO}).

3.4.6. Synthesis of $Ru(IEt_2Me_2)_2(PPh_3)(OCHO)H$ (**17**/**18**)

A 20 mL toluene solution of **5b** (100 mg, 0.11 mmol) was placed under 1 atm CO_2 in an ampoule fitted with a J. Youngs PTFE valve and stirred for 24 h at ambient temperature. The solution was reduced to dryness to leave an orange oil, which was redissolved in hexane (10 mL), concentrated to 5 mL, and stirred for 1 h to afford a yellow precipitate. This was isolated by filtration and dried under vacuum to give 30 mg of a mixture of **17** and **18** (yield: 40%). NMR data for **17**: ^{1}H NMR (500 MHz, C_6D_6, 298 K): δ 8.61 (s, 1H, Ru-OC*H*O), 5.53 (m, 1H, NCH_2CH_3), 5.00–4.83 (m, 2H, NCH_2CH_3), 4.44 (m, 1H, NCH_2CH_3), 4.29 (m, 1H, NCH_2CH_3), 3.77 (m, 1H, NCH_2CH_3), 3.63 (m, 1H, NCH_2CH_3), 3.16 (m, 1H, NCH_2CH_3), 1.72 (s, 3H, $NCCH_3{=}CNCH_3$), 1.59 (s, 3H, $NCCH_3{=}CNCH_3$), 1.55 (s, 3H, $NCCH_3{=}CNCH_3$), 1.51 (s, 3H, $NCCH_3{=}CNCH_3$), 1.30 (t, $^3J_{HH}$ = 7.3 Hz, 3H, NCH_2CH_3), 0.67 (t, $^3J_{HH}$ = 7.2 Hz, 3H, NCH_2CH_3), 0.53 (br, 3H, NCH_2CH_3), 0.43 (t, $^3J_{HH}$ = 7.3 Hz, 3H, NCH_2CH_3), −23.36 (d, $^2J_{HP}$ = 29.7 Hz, 1H, Ru-*H*). ^{31}P{^{1}H} NMR (202 MHz, C_6D_6, 298 K): δ 48.5 (s). NMR data for **18**: ^{1}H NMR (500 MHz, C_6D_6, 298 K): δ 8.64 (d, $^4J_{HP}$ = 3.8 Hz, 1H, Ru-OC*H*O), 4.77 (m, 2H, NCH_2CH_3), 4.40 (m, 2H, NCH_2CH_3), 3.49 (m, 2H, NCH_2CH_3),* 2.10 (s, 12H, $NCCH_3{=}CNCH_3$), 1.49 (t, $^3J_{HH}$ = 7.2 Hz, 6H, NCH_2CH_3), 1.20 (t, $^3J_{HH}$ = 7.2 Hz, 6H, NCH_2CH_3), −23.15 (d, $^2J_{HP}$ = 49.0 Hz, 1H, Ru-*H*). *Remaining methylene resonance overlaps with signals for **17** at δ 5.00–4.83. ^{31}P{^{1}H} NMR (202 MHz, C_6D_6, 298 K): δ 85.3 (s). ^{13}C{^{1}H} NMR for **17** and **18** (126 MHz, C_6D_6, 298 K: assignments made where possible based on relative signal intensities): δ 196.2 (d, $^2J_{CP}$ = 95 Hz, Ru-C_{NHC}, **17**), 194.5 (d, $^2J_{CP}$ = 12 Hz, Ru-C_{NHC}, **17**),* 170.4 (s, Ru-O_2CH, **17**), 169.9 (s, Ru-O_2CH, **18**), 143.5 (d, $^1J_{CP}$ = 36 Hz, PC_6H_5, **18**), 142.6 (d, $^1J_{CP}$ = 29 Hz, PC_6H_5, **17**), 134.2 (d, J_{CP} = 12 Hz, PC_6H_5, **17**), 133.9 (d, J_{CP} = 10 Hz, PC_6H_5, **18**), 127.3 (d, J_{CP} = 8 Hz, PC_6H_5, **17**), 126.7 (d, J_{CP} = 8 Hz, PC_6H_5, **18**), 123.8 (s, $NCCH_3{=}CNCH_3$), 123.6 (s, $NCCH_3{=}CNCH_3$), 122.8 (s, $NCCH_3{=}CNCH_3$), 122.5 (s, $NCCH_3{=}CNCH_3$), 122.4 (s, $NCCH_3{=}CNCH_3$), 121.7 (s, $NCCH_3{=}CNCH_3$), 43.3 (s, NCH_2CH_3), 43.2 (s, NCH_2CH_3), 42.6 (s, NCH_2CH_3), 42.4 (s, NCH_2CH_3), 42.3 (s, NCH_2CH_3), 41.6 (s, NCH_2CH_3), 16.8 (s, NCH_2CH_3), 15.8 (s, NCH_2CH_3), 15.7 (s, NCH_2CH_3), 15.5 (s, NCH_2CH_3), 15.4 (s, NCH_2CH_3), 13.9 (s, NCH_2CH_3), 9.4 (s, $NCCH_3{=}CNCH_3$), 9.2 (s, $NCCH_3{=}CNCH_3$), 9.1 (s, $NCCH_3{=}CNCH_3$), 9.0 (s,

NC*C*H$_3$=CN*C*H$_3$), 8.8 (s, NC*C*H$_3$=CN*C*H$_3$). *Ru-C$_{NHC}$ signals for **18** could not be observed. Anal. Calcd (%) for mixture of **17** and **18**: $C_{37}H_{49}N_4O_2PRu$ (713.82): C, 62.25; H, 6.92; N, 7.85. Found C, 62.33; H, 7.01; N, 7.72.

3.4.7. Ru(IEt$_2$Me$_2$)$_2$(PPh$_3$)HI (**19**) and [Ru(IEt$_2$Me$_2$)$_2$(PPh$_3$)$_2$H]I (**20**)

MeI (13.3 μL, 0.21 mmol) was added to a THF solution (30 mL) of **5b** (100 mg, 0.11 mmol), resulting in an immediate colour change from yellow to red. The solution was stirred at room temperature for 1 h and then pumped to dryness. The resulting red/orange oil was washed with hexane (10 mL) and filtered, and the residue was dried in vacuo. Yield 80 mg (71%). **19**: ^{1}H NMR (500 MHz, C_6D_6, 298 K): δ 4.59 (m, 2H, NC*H*$_2$CH$_3$), 3.79 (m, 2H, NC*H*$_2$CH$_3$), 3.68 (m, 2H, NC*H*$_2$CH$_3$), 3.34 (m, 2H, NC*H*$_2$CH$_3$), 1.59 (s, 12H, NCC*H*$_3$=NCC*H*$_3$), 1.39 (t, $^3J_{HH}$ = 7.2 Hz, 6H, NCH$_2$C*H*$_3$), 1.34 (t, $^3J_{HH}$ = 7.3 Hz, 6H, NCH$_2$C*H*$_3$), -30.45 (d, $^2J_{HP}$ = 40.6 Hz, 1H, Ru*H*). ^{31}P{^{1}H} NMR (202 MHz, C_6D_6, 298 K): δ 74.5 (s). ^{13}C{^{1}H} NMR (126 MHz, C_6D_6, 298 K): δ 196.0 (d, $^2J_{CP}$ = 13 Hz, Ru-*C*$_{NHC}$), 123.4 (s, NC*C*H$_3$=*C*NCH$_3$), 123.1 (s, NC*C*H$_3$=*C*NCH$_3$), 42.6 (s, NC*H*$_2$CH$_3$), 42.1 (s, NC*H*$_2$CH$_3$), 15.6 (s, *C*H$_3$), 15.0 (s, *C*H$_3$), 9.1 (s, *C*H$_3$), 8.8 (s, *C*H$_3$). **20**: Anal. Calcd (%) for $C_{54}H_{63}N_4P_2RuI$ (1058.01): C, 61.30; H, 6.00; N, 5.30. Found C, 61.23; H, 6.21; N, 5.21.

3.4.8. Synthesis of Ru(IEt$_2$Me$_2$)(PPh$_3$)$_2$HI (**21**)

MeI (*ca.* 1.7 μL, 0.025 mmol) was added to a THF-*d*$_8$ solution of **5b** (*ca.* 5 mg) in a J. Youngs resealable NMR tube. After 9 days at room temperature, the major species present in solution was Ru(IEt$_2$Me$_2$)(PPh$_3$)$_2$HI. Layering with hexane afforded a small number of X-ray quality crystals of the complex. ^{1}H NMR (500 MHz, THF-*d*$_8$, 298 K): δ 4.59 (m, 2H, NC*H*$_2$CH$_3$), 2.91 (q, $^3J_{HH}$ = 7.4 Hz, 2H, NC*H*$_2$CH$_3$), 2.81 (q, $^3J_{HH}$ = 7.4 Hz, 2H, NC*H*$_2$CH$_3$), 1.41 (s, 6H, NCC*H*$_3$=NCC*H*$_3$), 0.33 (t, $^3J_{HH}$ = 7.4 Hz, 3H, NCH$_2$C*H*$_3$), -0.23 (t, $^3J_{HH}$ = 7.4 Hz, 3H, NCH$_2$C*H*$_3$), -25.54 (t, $^2J_{HP}$ = 23.6 Hz, 1H, Ru*H*). ^{31}P{^{1}H} NMR (202 MHz, THF-*d*$_8$, 298 K): δ 47.7 (s).

3.4.9. Reaction of **3** with CO_2

A sample of **3** (10 mg, 0.02 mmol) in THF-*d*$_8$ in a J. Youngs resealable NMR tube was freeze-pump-thaw degassed and placed under 1 atm of CO_2. The formation of **24** and subsequently **25** was apparent by ^{1}H and ^{13}C NMR spectroscopy. Spectroscopic characterization of Ru(IMe$_4$)$_4$(OCOH)H, **24**. ^{1}H NMR (400 MHz, THF-*d*$_8$, 298 K): δ$_H$ 8.66 (s, 1H, Ru-OC*H*O), 3.33 (s, 12H, NC*H*$_3$), 3.02 (s, 12H, NC*H*$_3$), 2.01 (s, 24H,

CH_3), -26.30 (br s, 1H, Ru-*H*). $^{13}C\{^1H\}$ NMR (100 MHz, THF-d_8, 298 K): δ_C 210.4 (s, Ru-C_{NHC}), 167.6 (s, Ru-O*C*HO; d, $^1J_{CH}$ = 180 Hz in ^{1}H-coupled ^{13}C spectrum), 34.5 (s, N*C*H$_3$), 34.4 (s, N*C*H$_3$), 9.7 (s, *C*H$_3$). Spectroscopic characterization of Ru(IMe$_4$)$_4$(OCOH)$_2$ (**25**). ^{1}H NMR (400 MHz, THF-d_8, 258 K): δ_H 7.90 (s, 2H, Ru-O*C*HO), 3.98 (s, 9H, NCH_3), 3.31 (s, 6H, NCH_3), 3.24 (s, 6H, NCH_3), 3.04 (s, 6H, NCH_3), 2.22 (s, 9H, CH_3), 2.05 (s, 12H, CH_3). $^{13}C\{^1H\}$ NMR (100 MHz, THF-d_8, 298 K): δ_C 211.2 (s, Ru-C_{NHC}), 170.1 (s, Ru-O*C*HO; d, $^1J_{CH}$ = 190 Hz in ^{1}H-coupled ^{13}C spectrum), 34.8 (s, N*C*H$_3$), 34.1 (s, N*C*H$_3$), 9.9 (s, *C*H$_3$), 9.6 (s, *C*H$_3$). IR (mixture of **24** and **25**): 1606 cm^{-1} (ν_{OCHO}).

3.5. References

1. Burling, S.; Haller, L. J. L.; Mas-Marzá, E.; Moreno, A.; Macgregor, S. A.; Mahon, M. F.; Pregosin, P. S.; Whittlesey, M. K., *Chem.-Eur. J.* **2009**, *15,* 10912.

2. (a) Krylova, A. Y., *Kinet. Catal.* **2012**, *53,* 742; (b) Lu, X.; Hildebrandt, D.; Liu, X.; Glasser, D., *Ind. Eng. Chem. Res.* **2012**, *51,* 16544; (c) Schulz, H., *Appl. Catal., A* **1999**, *186,* 3; (d) Radius, U.; Bickelhaupt, F. M.; Ehlers, A. W.; Goldberg, N.; Hoffmann, R., *Inorg. Chem.* **1998**, *37,* 1080; (e) Cornils, B.; Herrmann, W. A.; Rasch, M., *Angew. Chem., Int. Ed. Engl.* **1994**, *33,* 2144; (f) Elschenbroich, C.; Salzer, A., *Organometallics. A Concise Introduction, 2nd ed.* Weinheim, Germany, 1992; Chapter 17.9, 17.12.

3. Crabtree, R. H., *The Organometallic Chemistry of the Transition Metals*. 4th ed.; Wiley-Interscience: Hoboken, 2005.

4. (a) Samouei, H.; Grushin, V. V., *Organometallics* **2013**, *32,* 4440; (b) Nixon, T. D.; Whittlesey, M. K.; Williams, J. M. J., *Dalton Trans.* **2009**, 753; (c) Kakiuchi, F.; Murai, S., *Acc. Chem. Res.* **2002**, *35,* 826; (d) Murai, S.; Kakiuchi, F.; Sekine, S.; Tanaka, Y.; Kamatani, A.; Sonoda, M.; Chatani, N., *Nature* **1993**, *366,* 529; (e) Hallman, P. S.; McGarvey, B. R.; Wilkinson. G, *J. Chem. Soc.* **1968**, 3143.

5. Tolman, W. B., *Activation of Small Molecules*. Weinheim: Wiley-VCH: Weinheim, Germany, 2006.

6. (a) Urakawa, A.; Jutz, F.; Laurenczy, G.; Baiker, A., *Chem.-Eur. J.* **2007**, *13,* 3886; (b) Aresta, M.; Dibenedetto, A., *Dalton Trans.* **2007**, 2975; (c) Omae, I., *Catal. Today* **2006**, *115,* 33; (d) Arakawa, H.; Aresta, M.; Armor, J. N.; Barteau, M. A.; Beckman, E. J.; Bell, A. T.; Bercaw, J. E.; Creutz, C.; Dinjus, E.; Dixon, D. A.; Domen, K.; DuBois, D. L.; Eckert, J.; Fujita, E.; Gibson, D. H.; Goddard, W. A.; Goodman, D. W.; Keller, J.; Kubas, G. J.; Kung, H. H.; Lyons, J. E.; Manzer, L. E.; Marks, T. J.;

Morokuma, K.; Nicholas, K. M.; Periana, R.; Que, L.; Rostrup-Nielson, J.; Sachtler, W. M. H.; Schmidt, L. D.; Sen, A.; Somorjai, G. A.; Stair, P. C.; Stults, B. R.; Tumas, W., *Chem. Rev.* **2001**, *101,* 953; (e) Baiker, A., *Appl. Organomet. Chem.* **2000**, *14,* 751; (f) Cornils, B.; Herrmann, W., *Applied Homogeneous Catalysis with Organometallic Compounds*. Wiley-VCH: Weinheim, Germany, 1996; Vol 2.

7. (a) Field, L. D.; Jurd, P. M.; Magill, A. M.; Bhadbhade, M. M., *Organometallics* **2013**, *32,* 636; (b) Field, L. D.; Lawrenz, E. T.; Shaw, W. J.; Turner, P., *Inorg. Chem.* **2000**, *39,* 5632; (c) Sullivan, B. P.; Meyer, T. J., *Organometallics* **1986**, *5,* 1500.

8. Inoue, Y.; Izumida, H.; Sasaki, Y.; Hashimoto, H., *Chem. Lett.* **1976**, 863.

9. (a) Nemeh, S.; Flesher, R. J.; Gierling, K.; Maichle-Mossmer, C.; Mayer, H. A.; Kaska, W. C., *Organometallics* **1998**, *17,* 2003; (b) Stossel, P.; Heins, W.; Mayer, H. A.; Fawzi, R.; Steimann, M., *Organometallics* **1996**, *15,* 3393.

10. (a) Ellul, C. E.; Saker, O.; Mahon, M. F.; Apperley, D. C.; Whittlesey, M. K., *Organometallics* **2008**, *27,* 100; (b) Burling, S.; Kociok-Kohn, G.; Mahon, M. F.; Whittlesey, M. K.; Williams, J. M. J., *Organometallics* **2005**, *24,* 5868.

11. (a) Bontemps, S.; Vendier, L.; Sabo-Etienne, S., *Angew. Chem., Int. Ed.* **2012**, *51,* 1671; (b) Albeniz, M. J.; Esteruelas, M. A.; Lledos, A.; Maseras, F.; Onate, E.; Oro, L. A.; Sola, E.; Zeier, B., *J. Chem. Soc., Dalton Trans.* **1997**, 181; (c) Whittlesey, M. K.; Perutz, R. N.; Moore, M. H., *Organometallics* **1996**, *15,* 5166; (d) Tsai, J. C.; Nicholas, K. M., *J. Am. Chem. Soc.* **1992**, *114,* 5117.

12. (a) Jazzar, R. F. R.; Bhatia, P. H.; Mahon, M. F.; Whittlesey, M. K., *Organometallics* **2003**, *22,* 670; (b) Jia, G. C.; Meek, D. W., *Inorg. Chem.* **1991**, *30,* 1953.

13. (a) Lalrempuia, R.; Stasch, A.; Jones, C., *Chem. Sci.* **2013**, *4,* 4383; (b) Lee, G. R.; Maher, J. M.; Cooper, N. J., *J. Am. Chem. Soc.* **1987**, *109,* 2956.

14. (a) Cheng, T. Y.; Brunschwig, B. S.; Bullock, R. M., *J. Am. Chem. Soc.* **1998**, *120,* 13121; (b) Dedieu, A., *Transition Metal Hydrides*. Wiley-VCH: Weinheim, Germany, 1992.

15. (a) Martelletti, A.; Gramlich, V.; Zurcher, F.; Mezzetti, A., *New J. Chem.* **1999**, *23,* 199; (b) Jimenez-Tenorio, M.; Puerta, M. C.; Valerga, P., *Inorg. Chem.* **1994**, *33,* 3515; (c) Jimenez-Tenorio, M.; Puerta, M. C.; Valerga, P., *J. Am. Chem. Soc.* **1993**, *115,* 9794.

16. (a) Wolf, R.; Plois, M.; Hepp, A., *Eur. J. Inorg. Chem.* **2010**, 918; (b) Haller, L. J. L.; Mas-Marzá, E.; Moreno, A.; Lowe, J. P.; Macgregor, S. A.; Mahon, M. F.; Pregosin, P. S.; Whittlesey, M. K., *J. Am. Chem. Soc.* **2009**, *131,* 9618.

17. (a) Burling, S.; Mas-Marzá, E.; Valpuesta, J. E. V.; Mahon, M. F.; Whittlesey, M. K., *Organometallics* **2009**, *28,* 6676; (b) Brookhart, M.; Green, M. L. H.; Parkin, G., *Proc. Natl. Acad. Sci. U. S. A.* **2007**, *104,* 6908.

18. Personal communication from Professor Stuart Macgregor at Heriot-Watt University, Edinburgh.

19. Wurtemberger, M.; Ott, T.; Doring, C.; Schaub, T.; Radius, U., *Eur. J. Inorg. Chem.* **2011**, 405.

20. Davies, C. J. E.; Lowe, J. P.; Mahon, M. F.; Poulten, R. C.; Whittlesey, M. K., *Organometallics* **2013**, *32,* 4927.

Chapter 4

Chapter 4: Reactivity of $Ru(NHC)_2(PPh_3)_2H_2$ (NHC = IMe_4, IEt_2Me_2) and $Ru(IMe_4)_4H_2$ with H_2, D_2, benzene and toluene

4.1. Introduction

Transition metal dihydride complexes are well known for their ability to activate C-H bonds,[1] through the reductive elimination of H_2 and formation of coordinatively unsaturated fragments such as $Cp^*M(PMe_3)$ ($Cp^*=\eta^5$-C_5Me_5; M = Rh, Ir)[2] and $M(dmpe)_2$ (M = Fe, Ru)[3] In both these cases, the hydrides are *cis* and so, as noted in the introduction, the reactivity would be expected to be quite different for *trans*-dihydride complexes, which could only react via heterolytic cleavage. This Chapter describes the abilities of all *trans* $Ru(IMe_4)(PPh_3)_2H_2$ (**4a**), *cis*, *cis*, *trans*-$Ru(IEt_2Me_2)_2(PPh_3)_2H_2$ (**5b**) and $Ru(IMe_4)_4H_2$ (**3**) to bring about C-H activation of aromatic solvents (benzene, toluene) through the observation of H/D exchange. This reactivity is compared and contrasted with the activation of D_2.

4.2. Results and Discussion

4.2.1. Reactions of $Ru(IMe_4)_2(PPh_3)_2H_2$ (**4a**)

4.2.1.1. H/D exchange of **4a** in C_6D_6.

No change in the ^1H NMR spectrum of **4a** was observed after heating in C_6D_6 at 343 K for 9 h, although upon increasing the temperature to 363 K, depletion of the Ru-H resonance at δ_H -6.54 was seen within 30 min (Figure 4.1). New, broader triplet hydride resonances resulting from H/D exchange emerged at both lower and higher frequencies (Figure 4.1c-f). The higher frequency signal (δ_H -6.43) was assigned (vide infra) to the monodeuteride complex $Ru(IMe_4)_2(PPh_3)_2HD$ (**4a-HD**, Scheme 4.1)[4] and the lower frequency signal was most likely representative of isotopomers of **4a** with (i) deuterium incorporated into the phenyl rings of the PPh_3 ligands, (on the basis of the depletion in intensity of the high-frequency phosphine phenyl resonance at *ca*. δ_H 7.8 Figure 4.1) and (ii) H/D exchange into the N-Me groups of the NHC, as suggested by the resonances that appear at δ_H 3.71 and δ_H 3.68.[5] Figure 4.1 also shows the corresponding $^{31}P\{^1H\}$ NMR spectra and the change in the signal from a sharp singlet at δ_P 72.4 to a much broader resonance, which affords extra evidence for D incorporation into **4a**. Deuteration of all these sites was confirmed by ^2H NMR spectroscopy (Figure 4.2).

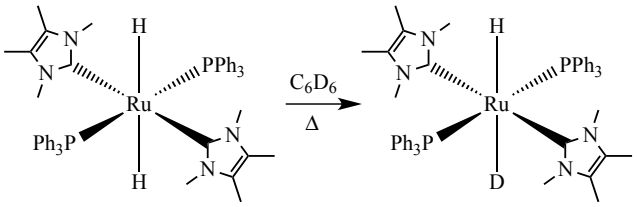

4a **4a-HD**

*Scheme 4.1: Reaction of **4a** with C_6D_6 with heating*

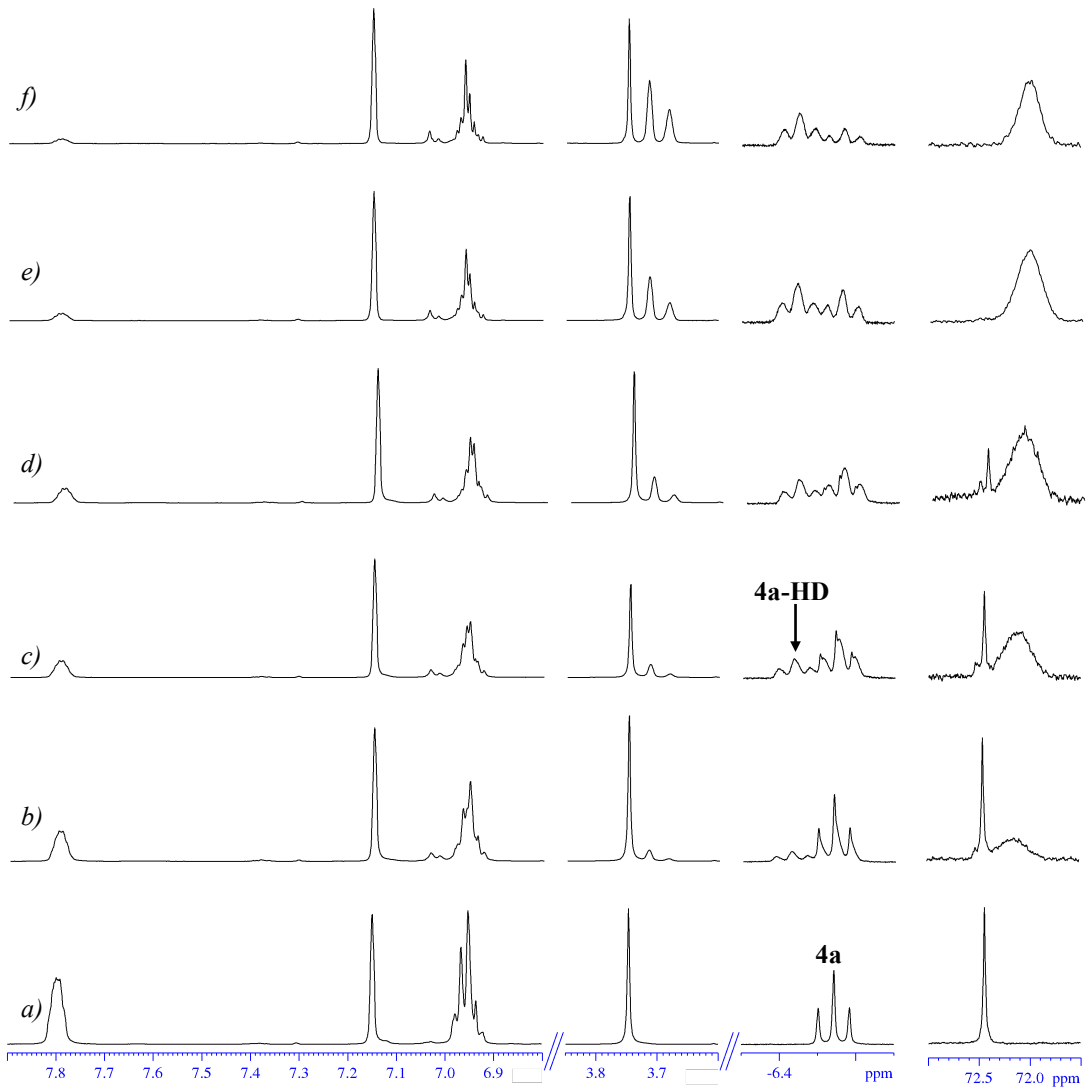

*Figure 4.1: Selected regions of the ^{1}H NMR spectra (298 K, 500 MHz) of **4a** in C_6D_6 a) before heating and then b) 30 min c) 60 min d) 100 min e) 160 min and f) 280 min heating at 363 K. Selected region of the corresponding $^{31}P\{^{1}H\}$ NMR spectra (298 K, 202 MHz) at the same times shown on far right.*

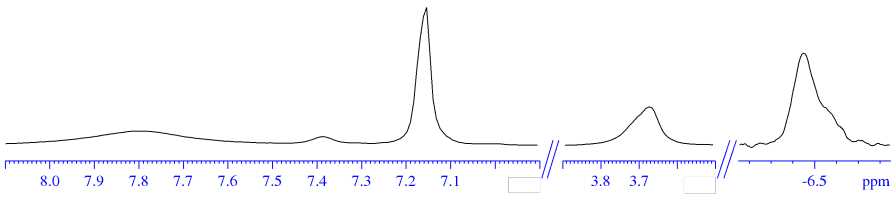

*Figure 4.2: ^{2}H NMR spectrum showing **4a-HD** as well as different isotopologues from deuteration of the Ru-H, N-Me groups and of the aromatic Ph groups (C_6H_6, 298 K, 77 MHz)*

Unsurprisingly, when heating was repeated in the presence of 5 equiv. of PPh_3, a much lower conversion to **4a-HD** was observed even after an extended time of 24 h at 363 K. Further to this, no H/D exchange was now seen in the N-Me groups of the complex. The retardation of the H/D exchange in the presence of PPh_3 might be expected given the 18-electron configuration of **4a** and the need for ligand dissociation to occur prior to any reaction with a C-D bond. The appearance of deuterium in the free PPh_3 by $^{31}P\{^{1}H\}$ NMR spectroscopy (Figure 4.3) was consistent with phosphine dissociation from **4a,** as well as H/D exchange of the PPh_3 ligands.

No H/D exchange was observed upon heating **4a** in THF-d_8 at 363 K over 18 h.

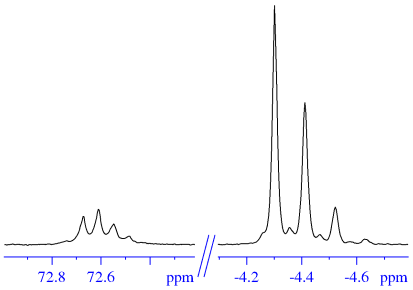

*Figure 4.3: Selected regions of the $^{31}P\{^{1}H\}$ NMR spectrum of a C_6D_6 solution of **4a** with 5 equiv. of PPh_3 after 3 days of heating at 363 K (298 K, 202 MHz).*

4.2.1.2. Phosphine exchange reactions of **4a**

Phosphine dissociation from **4a** was further confirmed by the room-temperature exchange with $P(C_6D_5)_3$ observed within 15 min of adding 5 equiv. of the deuterated phosphine to a C_6D_6 solution of **4a**. In Figure 4.4, **4a** and $P(C_6D_5)_3$ were identified as the two largest singlet resonances, with the two smaller resonances assigned to **4a** with $P(C_6D_5)_3$ incorporated (**4a-D**) and the eliminated, free PPh_3.

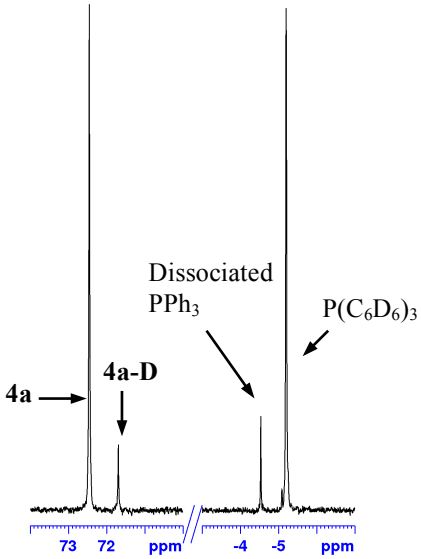

*Figure 4.4: Selected regions of the $^{31}P\{^{1}H\}$ NMR spectrum 15 min after addition of $P(C_6D_5)_3$ to a solution of **4a** (C_6D_6, 298 K, 202 MHz).*

As more $P(C_6D_5)_3$ was incorporated into complex **4a**, a new triplet hydride resonance at slightly lower frequency became increasingly visible in the ^{1}H NMR spectrum (Figure 4.5). As this higher field triplet hydride signal is also seen in the reaction of **4a** with C_6D_6 at 363 K, it stands as additional evidence that D is incorporated into the Ph groups in the reaction of **4a** with C_6D_6. After a reaction time of 5 days, the resonance for **4a-HD** at δ_H -6.43 became apparent (Figure 4.6), consistent with *ortho*-metallation of the phosphine ligand.

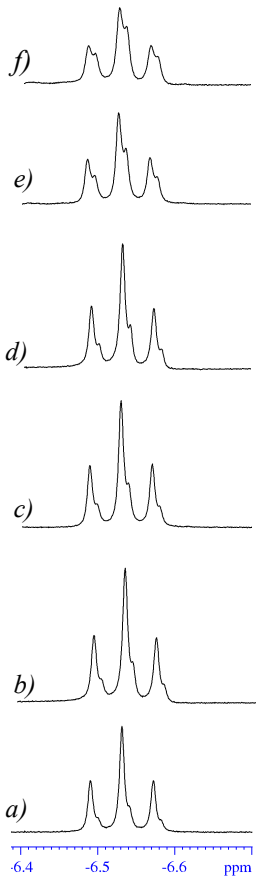

*Figure 4.5: Hydride region of ^{1}H NMR spectrum of the reaction of **4a** with $P(C_6D_6)_3$ after a) 15 min, b) 1.5 h, c) 3.5 h, d) 7h, e) 30.5 h and f) 49.5 h (C_6D_6, 298 K, 500 MHz).*

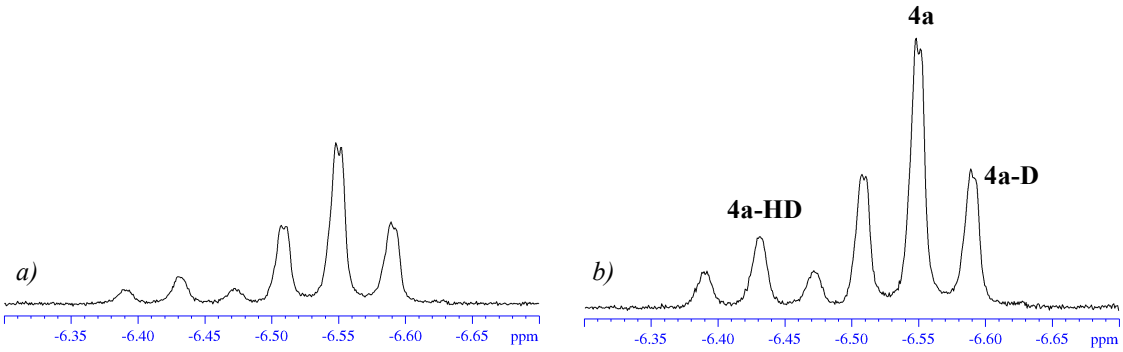

*Figure 4.6: Hydride region of the ^{1}H NMR spectra of the reaction between **4a** and $P(C_6D_5)_3$ after a) 6 days and b) 10 days (C_6H_6, 298 K, 500 MHz).*

4.2.1.3. Reactivity of **4a** with H_2 / D_2

Addition of 1 atm. of H_2 to a toluene-d_8 solution of **4a** resulted in no change to either the ^{1}H or the $^{31}P\{^{1}H\}$ NMR spectra over the temperature range 211-343 K. However, exposure of **4a** to 1 atm. of D_2 resulted in heterolytic H/D exchange at room temperature to afford the monodeuteride and dideuteride complexes $Ru(IMe_4)_2(PPh_3)_2HD$ (**4a-HD**) and $Ru(IMe_4)_2(PPh_3)_2D_2$ (**4a-D_2**) over hours (Scheme

4.2, Figure 4.7). The latter was apparent from a yet higher frequency shoulder in the $^{31}P\{^{1}H\}$ NMR spectrum.[6]

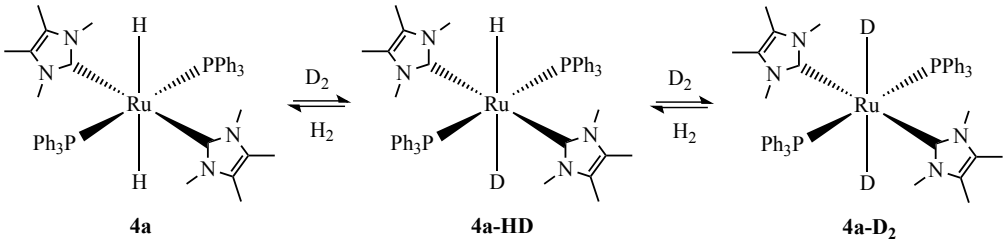

*Scheme 4.2: Reaction of **4a** with D_2.*

Unexpectedly, the rate of H/D exchange between **4a** and D_2 was accelerated by the addition of 5 equiv. of PPh_3. Thus Figure 4.7 shows ^{1}H and $^{31}P\{^{1}H\}$ spectra recorded after addition of D_2 to **4a** in this case and in the absence of any free PPh_3. The resonances show quite clearly higher concentrations of **4a-HD** and **4a-D₂** in the former. This implies that in contrast to exchange between **4a** and C_6D_6, H/D exchange with D_2 appears not to require dissociation of PPh_3 (or the other 2-electron donor present, IMe_4) from **4a** as the presence of added phosphine would be expected to inhibit reaction in such a case. Additional evidence against ligand dissociation being involved came from the observation that **4a** even reacted with D_2 in the solid state, with a ground-up, microcrystalline sample of **4a** found to convert to *ca*. 20 % **4a-HD** upon stirring under 1 atm D_2 for a week.

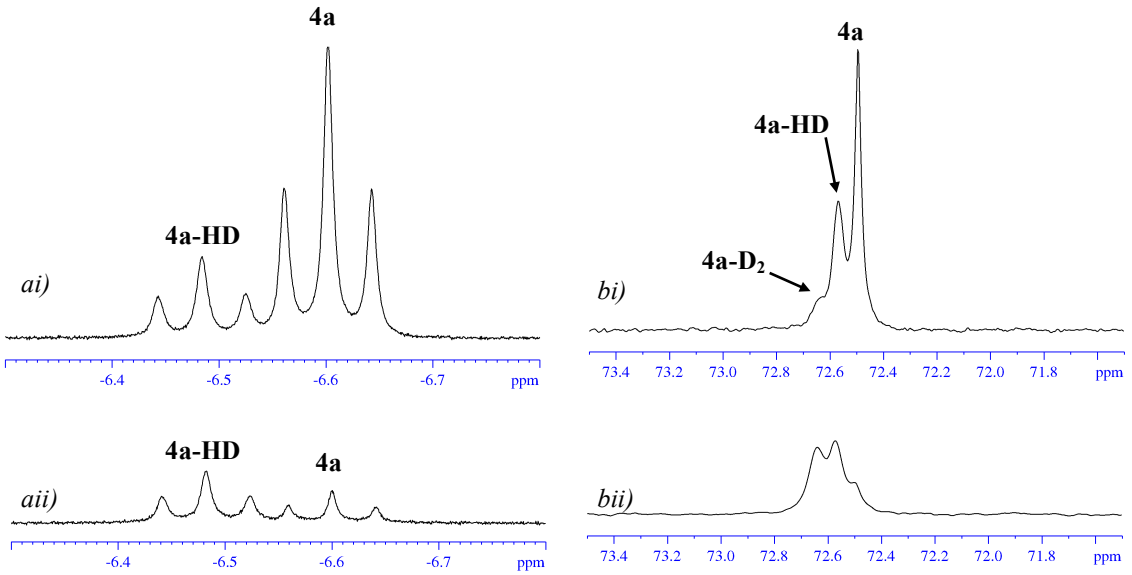

Figure 4.7: ai) Hydride region of ^{1}H NMR spectrum (C_6D_6, 298 K, 500 MHz) and bi) the corresponding $^{31}P\{^{1}H\}$ NMR spectrum (C_6D_6, 298 K, 202 MHz) 5 h after addition of

*1 atm of D_2 to **4a**. The corresponding spectra aii) and bii) were recorded at the same time but following the addition of 1 atm of D_2 to **4a** and 5 equiv. PPh_3 (C_6D_6, 298 K).*

4.2.1.4. Further studies of the phosphine acceleration of the reaction between **4a** and D_2

In an attempt to investigate the generality of the phosphine acceleration of the H/D exchange and whether the basicity of the phosphine influenced the extent of acceleration, tri(*o*-tolyl)phosphine (P(*o*-tolyl)$_3$) and tricyclohexylphosphine (P(C_6H_{11})$_3$) as well as a range of other Lewis bases, including triethylamine (NEt_3), the NHCs 6Mes, ICy and I^{t}Bu, and, finally, the pyrimidinium salt (6MesHBF_4), were investigated. (N.B. none of these ligands reacted with **4a** itself)

Both alternative phosphines (5 equiv.) also enhanced the rate of reaction of **4a** with D_2 compared to when no phosphine was present. The degree of acceleration of PR_3 followed the order PPh_3 > P(*o*-tolyl)$_3$ > P(C_6H_{11})$_3$. Thus, the presence of PPh_3 reduced the intensity of the hydride signal of **4a** by 50 % within 15 min of D_2 addition, with P(*o*-tolyl)$_3$, this took *ca*. 1 h and with P(C_6H_{11})$_3$ *ca*. 2 h. In toluene-d_8 rather than C_6D_6, the rate of acceleration by PPh_3 was much the same, however, that of P(*o*-tolyl)$_3$ was increased, changing the comparative order to P(*o*-tolyl)$_3$ > PPh_3. The toluene order might suggest a correlation to basicity of the phosphine (pKa values for P(C_6H_{11})$_3$ = 9.65, P(*o*-$CH_3C_6H_4$)$_3$ = 3.08, PPh_3 = 2.73),[7] although P(C_6H_{11})$_3$ was not studied under these conditions. Although not only is it unclear as to how PR_3 accelerates exchange, but why the effect in C_6D_6 and toluene-d_8 would change so noticeably.

NEt_3 (pKa = 10.78)[8] also increased the rate of H/D exchange (in C_6D_6) but not as rapidly as PPh_3. Interestingly, all three NHCs completely shut down the exchange reaction (the RuH_2 resonance decreasing by only 15 % after 5 days) whereas [6MesH]BF_4 accelerated the exchange and at a rate comparable to PPh_3.

4.2.1.5. Substitution reaction of **4a** with P(*p*-tolyl)$_3$

In contrast to the lack of reaction between **4a** and P(*o*-tolyl)$_3$, treatment of **4a** with P(*p*-tolyl)$_3$ (1-5 equiv.) resulted in an immediate reaction in which the PPh_3 ligands were substituted (Scheme 4.3).

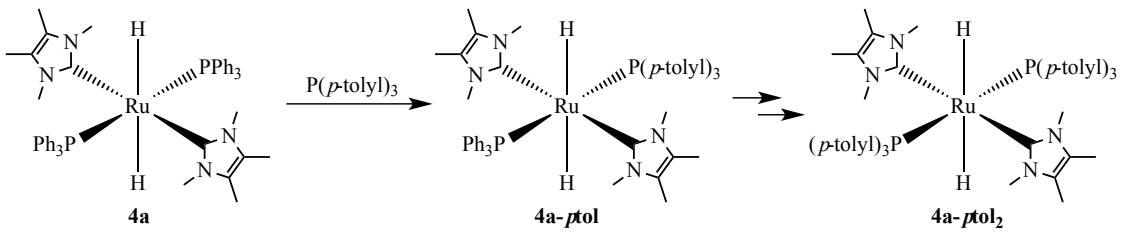

*Scheme 4.3: Reaction of **4a** with P(p-tolyl)$_3$*

The ^{1}H NMR spectrum clearly showed the formation of two new triplet hydride signals (along with the accompanying Me signals) for the new complexes formed (Figure 4.8). On ^{31}P decoupling, the triplet hydride signals simplified to singlets. ^{1}H-^{31}P HSQC spectroscopy (Figure 4.9) allowed the two new triplet hydride resonances to be assigned to the mixed PPh_3-P(*p*-tolyl)$_3$ complex (δ_H -6.58 correlation to an AB resonance centred at *ca*. δ_C 71.5) and *bis* P(*p*-tolyl)$_3$ product at δ_H -6.61 (corresponding ^{31}P singlet at δ_C = 70).

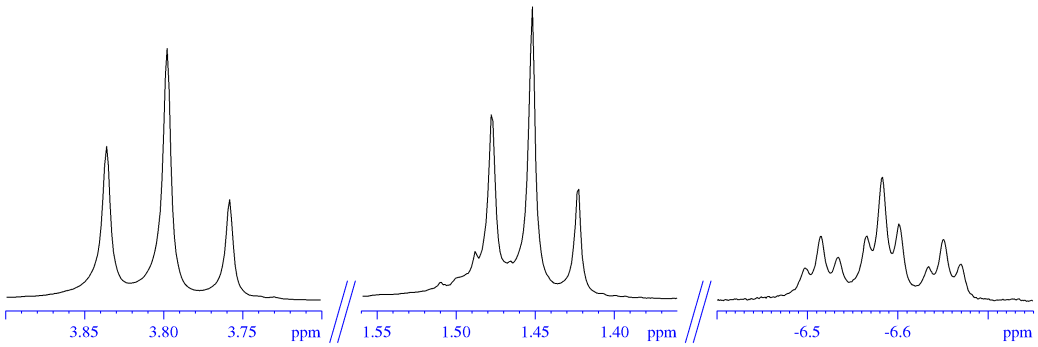

*Figure 4.8: Selected regions of the ^{1}H NMR spectrum of the solution of **4a** and 5 equiv. of P(p-tolyl)$_3$ after 4 days of reaction time (toluene-d$_8$, 298 K, 300 MHz)*

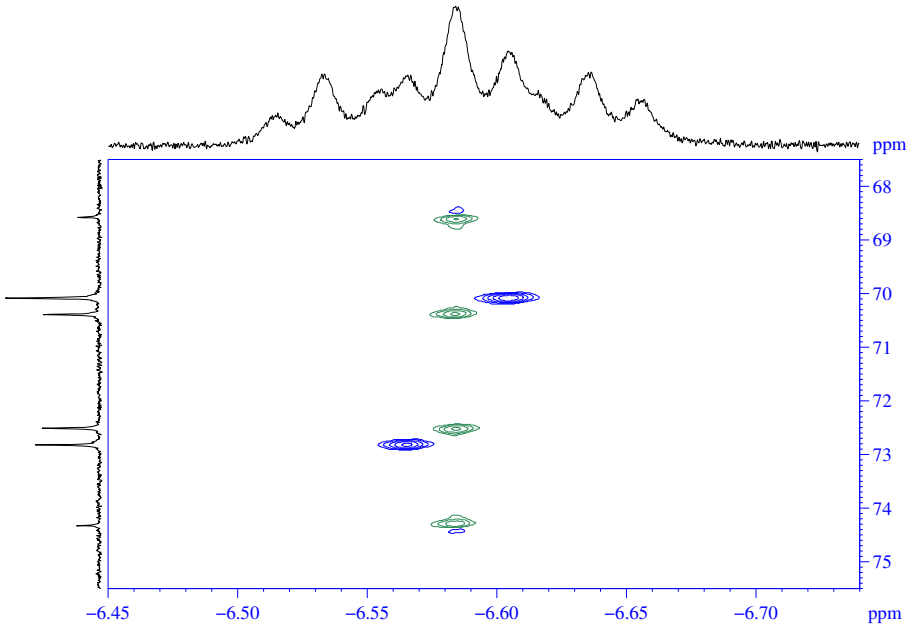

*Figure 4.9: Selected region of the ^{1}H-^{31}P HSQC NMR spectrum of the solution of **4a** and 5 equiv. of P(p-tolyl)$_3$ after 3 days of reaction time (toluene-d$_8$, 298 K, 400 MHz)*

Interestingly, the rate of P(*p*-tolyl)$_3$ substitution into **4a** was found to be accelerated by the presence of H_2. Figure 4.10 shows $^{31}P\{^1H\}$ NMR spectra in the absence and presence of H_2 (1 atm). The latter affords a mixture of **4a**, **4a-*p*tol**, and **4a-(*p*tolyl)$_2$** more quickly. It must be noted that in this case, 2 equiv. P(*p*-tolyl)$_3$ were used which explains why there appears to be rapid formation of **4a-(*p*tolyl)$_2$** followed by a slower reaction to generate the mixed PPh_3 / P(*p*-tolyl)$_3$ species **4a-*p*tolyl** to give an equilibrium mixture of all three species.

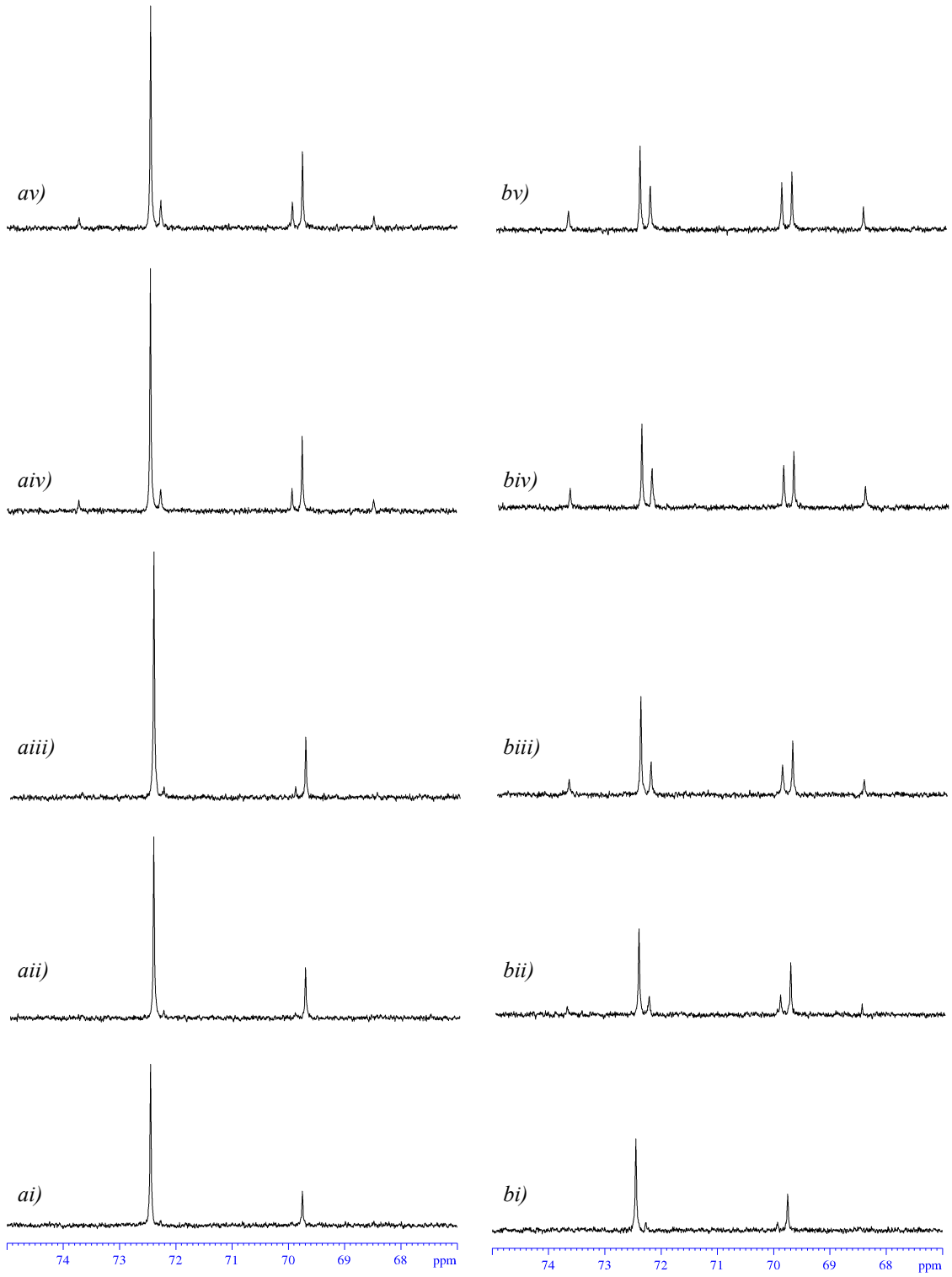

*Figure 4.10: Selected regions of $^{31}P\{^{1}H\}$ NMR spectra of the reaction of **4a** with P(p-tolyl)$_3$ a) without H_2 b) with H_2 at i) 3 min, ii) 30 min, iii) 1 h, iv) 4 h, v) 6 h (C_6D_6, 298 K, 202 Hz).*

Figure 4.11 shows that this acceleration was not restricted to P(*p*-tolyl)$_3$ and that exchange of **4a** with P(C_6D_5)$_3$ was also hastened by the presence of an atmosphere of H_2.

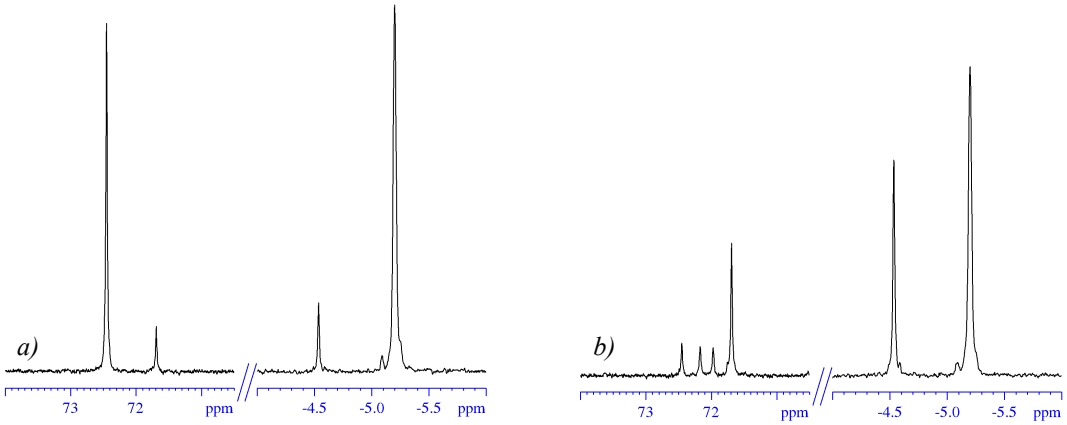

*Figure 4.11: a) 15 min after addition of $P(C_6D_5)_3$ to **4a**. b) 15 min after thawing a mixture of **4a**, $P(C_6D_5)_3$ and H_2 (C_6D_6, 298 K, 202 MHz)*

4.2.1.6. Substitution reaction of **4a** with $P(C_6F_5)_3$

As noted in the previous section, the extent of H/D exchange between **4a** and D_2 as a function of phosphine basicity was probed. $P(C_6F_5)_3$ would offer the possibility of a phosphine of extremely different basicity, however, it was found to react with **4a** over *ca*. 24 h via a remarkable set of bond activation reactions to give, on the basis of NMR spectroscopy, $Ru(IMe_4)_2(PF_2(C_6F_5))(C_6F_5)H$ (**26**).

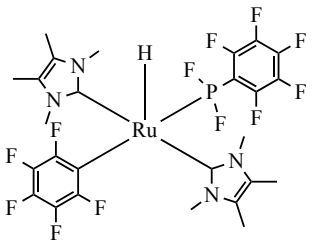

26

*Figure 4.12: Proposed structure of **26** formed from **4a** and $P(C_6F_5)_3$ (the trans-IMe_4 geometry is not definite)*

Thus, addition of 1 to 5 equiv. $P(C_6F_5)_3$ to a C_6D_6 solution of **4a** gave a new Ru-H resonance at δ_H -29.64 with a doublet of triplets multiplicity after 24 h at room temperature. This integrated 1:6:6:6:6 to four new methyl resonances consistent with a $Ru(IMe_4)_2H$ based structure. ^{31}P decoupling left the hydride as a triplet, while ^{19}F decoupling simplified the hydride to a doublet; J_{HP} and J_{HF} were 46.1 and 6.5 Hz respectively. The $^{31}P\{^1H\}$ NMR spectrum is shown in Figure 4.13 and exhibited a very high frequency triplet resonance with a splitting of 1130 Hz, consistent with a PF_2 containing phosphine ligand.[9]

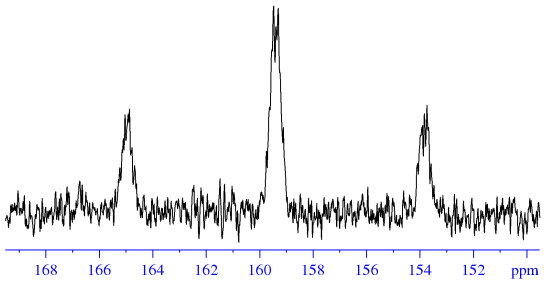

*Figure 4.13: $^{31}P\{^{1}H\}$ NMR spectrum of the product formed from reaction of **4a** and $P(C_6F_5)_3$ (THF-d_8, 298 K, 202 MHz).*

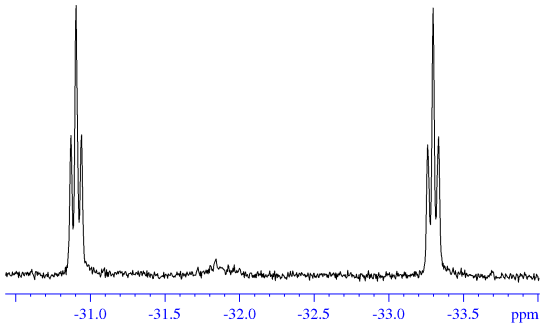

*Figure 4.14: $^{19}F\{^{1}H\}$ NMR spectrum of the product formed from reaction of **4a** and $P(C_6F_5)_3$ (THF-d_8, 298 K, 470 MHz).*

The P bound F atoms appeared at δ_F -32.2 in the $^{19}F\{^{1}H\}$ NMR spectrum as a doublet of triplets; the triplet splitting results from coupling to two *ortho* F atoms of a C_6F_5 group at δ_F -137.2 as shown by ^{19}F COSY. This signal in turn correlated to the *para* and *meta* F atoms of the fluoroaryl ring at δ_F -162.5 and δ_F -154.3 respectively. The presence of the metal bound C_6F_5 group was deduced by a combination of ^{1}H-^{19}F HSQC and ^{19}F COSY experiments. The former showed a correlation of the Ru-H resonance to a broad resonance at δ_F -114.4, which in turn showed COSY cross peaks to two close ^{19}F signals at δ_F -163.0 (*para*-C_6F_5) and δ_F -163.3 (*meta*-C_6F_5).

Despite numerous attempts, isolation of **26** for solid state structural verification or determination of yield was unsuccessful. The latter would be necessary in order to calculate the mass balance of the reaction and to determine the fluoro-organic products that are lost.

4.2.2. Reactions of $Ru(IEt_2Me_2)_2(PPh_3)_2H_2$ (**5b**)

4.2.2.1. H/D exchange reactions of **5b**

5b showed somewhat lower stability in solution compared to **4a**. Leaving a THF solution of **5b** at room temperature for a week resulted in the formation of two

new triplet hydride resonances in the ^{1}H NMR spectrum of the solution (Figure 4.14). The low concentrations of these isomers limited their characterization to ^{1}H and ^{31}P{^{1}H} NMR spectroscopy, but comparison to the chemical shifts of the isomers of **4** led to their assignment as **5a** and **5d**, shown in Figure 4.15.

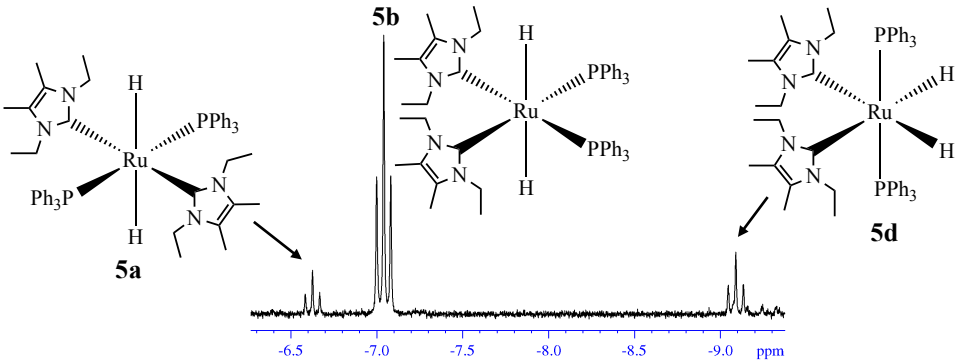

*Figure 4.15: Hydride region of the ^{1}H NMR spectrum of **5b** after 1 week at room temperature (THF-d_8, 298 K, 500 MHz) with suggested structures of the new isomers formed.*

Heating the THF solution of **5b** resulted in decomposition of the compound into many hydride containing products, one of which, was the previously characterized $[Ru(IEt_2Me_2)_4H]^+$ cation with it's distinctive resonance at *ca*. δ -40.[10]

Upon leaving a C_6D_6 solution of **5b** to stand for 4 days at room temperature, isomerization, along with H/D exchange into Ru-H, gave the mixture of species shown in Figure 4.16. The Ru-HD resonances appeared to higher frequency (Δδ 0.13) of their respective dihydride species (*c.f.* **4a-HD** and **4a**, in which Δδ also equal to 0.13). There was no **5d** apparent in C_6D_6.

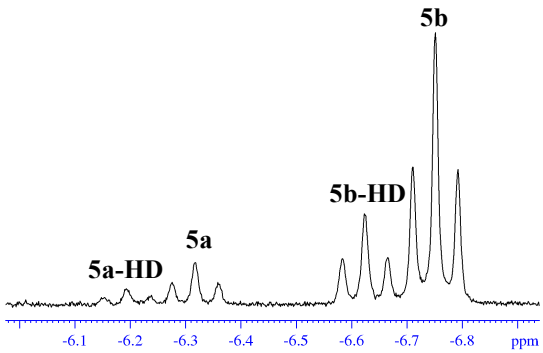

*Figure 4.16: Selected hydride region of ^{1}H NMR spectrum of **5b** after 4 days at room temperature (C_6D_6, 298 K, 500 MHz).*

Warming a C_6D_6 solution of **5b** to 313 K for 5 h also led to additional exchange into the methyl groups of the N-Et substituents, as revealed by ^2H NMR spectroscopy. Some decomposition of the compound was also apparent as shown by the release of free, partially deuterated PPh_3.

4.2.2.2. Reactivity of **5b** with D_2

As **5b** exhibited exchange into a greater number of sites than **4a**, a less-detailed study of H/D exchange chemistry of the former with D_2 was carried out. As with **4a**, **5b** showed room temp H/D exchange with D_2 although into both methylene and methyl groups of the N-Et arms, as well as at the metal centre (Figure 4.17). The formation of a number of small, unidentified, new products was also seen by NMR spectroscopy over *ca*. 24 h along with ^2H-labelled free PPh_3.

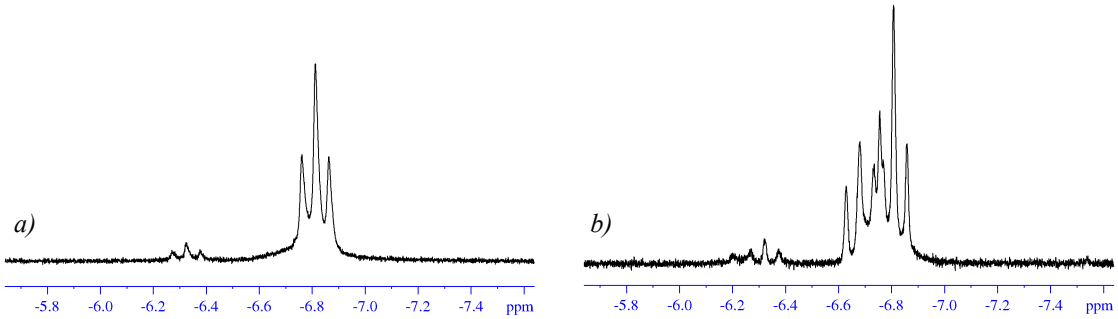

*Figure 4.17: Hydride regions of the ^1H NMR spectra of a toluene-d_8 solution of **5b** after a) 1 day and b) 1 day under 1 atm of D_2 (298 K, 400 Hz)*

4.2.3. Reactions of $Ru(IMe_4)_4H_2$ (**3**)

4.2.3.1. Stability of **3** in deuteroarenes and THF

The all-NHC containing complex $Ru(IMe_4)_4H_2$ was also probed for exchange with solvent and D_2 as, in contrast to both **4a** and **5b**, there is no possibility of facile ligand dissociation. The hydride region of the ^1H NMR spectrum of a sample of **3** in C_6D_6 changed over the course of a week at room temperature with the gradual appearance of a new signal assigned to $Ru(IMe_4)_4HD$ (**3-HD**) at slightly higher frequency ($\Delta\delta$ 0.15), although with little change to the rest of the spectrum. Upon raising the temperature to 323 K, the rate of H/D exchange was increased although this also appeared to lead to D incorporation into the N-Me substituents of the IMe_4 ligands, as shown by the appearance of two new singlet resonances at δ_H 3.79 and δ_H 3.77 in the ^1H NMR spectrum (Figure 4.18).

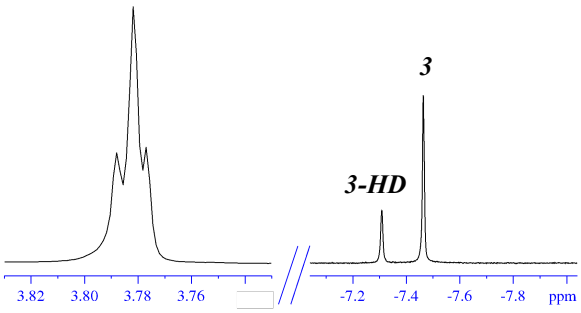

*Figure 4.18: Selected regions of the ^{1}H NMR spectrum of **3** after being heated in C_6D_6 for 21 h (C_6D_6, 298 K, 500 MHz) showing D incorporation into the NMe positions and the hydride resonances of **3-HD** and **3**.*

The corresponding ^{2}H NMR spectrum confirmed the presence of D at these positions (Figure 4.19) and indicated the formation of **3-D$_2$** as well as **3-HD** based on the appearance of two Ru-D signals.

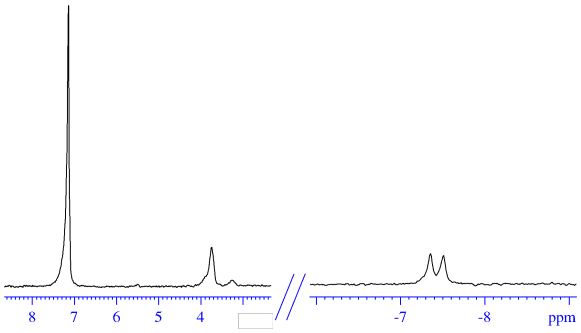

*Figure 4.19: Selected regions of the ^{2}H NMR spectrum of **3** after being heated in C_6D_6 for 4 days (C_6H_6, 298 K, 500 MHz).*

It was also found that **3** activated toluene-d_8 at 323 K (at approximately a comparable rate to C_6D_6) to form **3-HD** (and presumably **3-D$_2$**) and bring about H/D exchange at the Ru and into the NMe groups. No reaction was seen between **3** and THF-d_8 even after 16 h at an increased temperature of 363 K.

4.2.3.2. Reactivity of **3** with H_2 and D_2

The room temperature reaction between **3** and C_6D_6 (albeit slow) resulted in the use of THF as the solvent for reactions with H_2 and D_2. Addition of 1 atm of H_2 to a THF-d_8 solution of **3** resulted in a slight broadening of the hydride resonance in the ^{1}H NMR spectrum, but there was no evidence to indicate any formation of a dihydrogen containing species either at low temperature (198 K) or upon heating to 333 K.

Addition of D_2 to a THF-d_8 solution of **3** resulted in rapid incorporation of D into the Ru-H bond to form the hydride deuteride, **3-HD,** and subsequently the dideuteride, **3-D_2**. A new hydride resonance could be seen in the ^{1}H NMR spectrum at δ_H -7.99 which was assigned to $Ru(IMe_4)_4HD$ (**3-HD**). The ^{2}H NMR spectrum (Figure 4.20b) clearly showed the deuterium incorporation, confirming the identity of the species formed. There was no D incorporation into the NMe group of the IMe_4 ligand.

*Figure 4.20: a) Hydride region of ^{1}H NMR spectrum of **3** and **3-HD**; b) Selected region of ^{2}H NMR spectrum of **3-HD** and **3-D_2**.*

In contrast to what was found for $Ru(IMe_4)_2(PPh_3)_2H_2$ (**4a**), repeating this reaction in the presence of 5 equiv. of either PPh_3 or PCy_3 did not retard the rate of formation of **3-HD** formation.

4.2.3.3. Acceleration of H/D exchange between **3** and deuteroarenes in the presence of H_2

Interestingly, when H/D exchange of **3** with either C_6D_6 or $C_6D_5CD_3$ was carried out under 1 atm H_2, a significant increase in the rate of the reactions was observed as illustrated in the case of C_6D_6 in Figure 4.21. Only minimal formation of **3-HD** was apparent Figure 4.21(a) after 4 days at room temperature in C_6D_6, whereas under 1 atm H_2, 80 % conversion was seen after just 7 h. A similar exchange process took place in toluene-d_8, with reaction being apparent at both the *meta* and *para* sites.

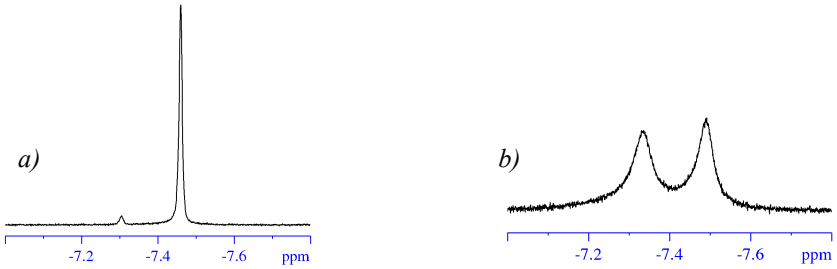

*Figure 4.21: Selected regions of the ^{1}H NMR spectrum of **3** a) after 4 days in C_6D_6 and b) after 7 h in C_6D_6 under an atm of H_2 (298 K, 500 MHz)*

4.2.3.4. Deuterium incorporation into protio solvents mediated by **3**

Initially an investigation into whether deuterium could be incorporated into protio benzene (C_6H_6) from D_2 was carried out. A temperature of 323 K was employed because of the increased rate of H/D exchange into **3** already observed. Over 70 h, the intensity of the C_6H_6 resonances in the ^1H NMR spectrum decreased by *ca*. 30 %, implying D had been incorporated onto the ring.

A study of whether protio toluene could incorporate D from D_2 in the presence of **3** initially showed minimal D incorporation into the *meta* and *para* positions. After 2 h the intensity of the toluene resonances stayed constant suggesting a mixture of HD and D_2 had formed.

4.2.3.5. Catalytic H/D exchange between protio and deuteroarenes with **3**

Given the ability of **3** to bring about H/D exchange between C_6D_6 or toluene-d_8 and H_2, **3** was employed for the H/D exchange of (i) C_6D_6 and toluene-h_8 and (ii) C_6H_6 and toluene-d_8. Results from the former experiment are shown in Figure 4.22 in the form of a stack plot of ^1H NMR spectra recorded over *ca*. 1 day of reaction of a sample of **3** (5 mol%) in a mixture of C_6D_6 (0.6 mL) and toluene-h_8 (44 μL) at 50 °C. It is clear that the signal for C_6D_5H increases, the resonances for the *meta* and *para* C-H groups decrease over time, while that for the *ortho* C-H position is unaffected.

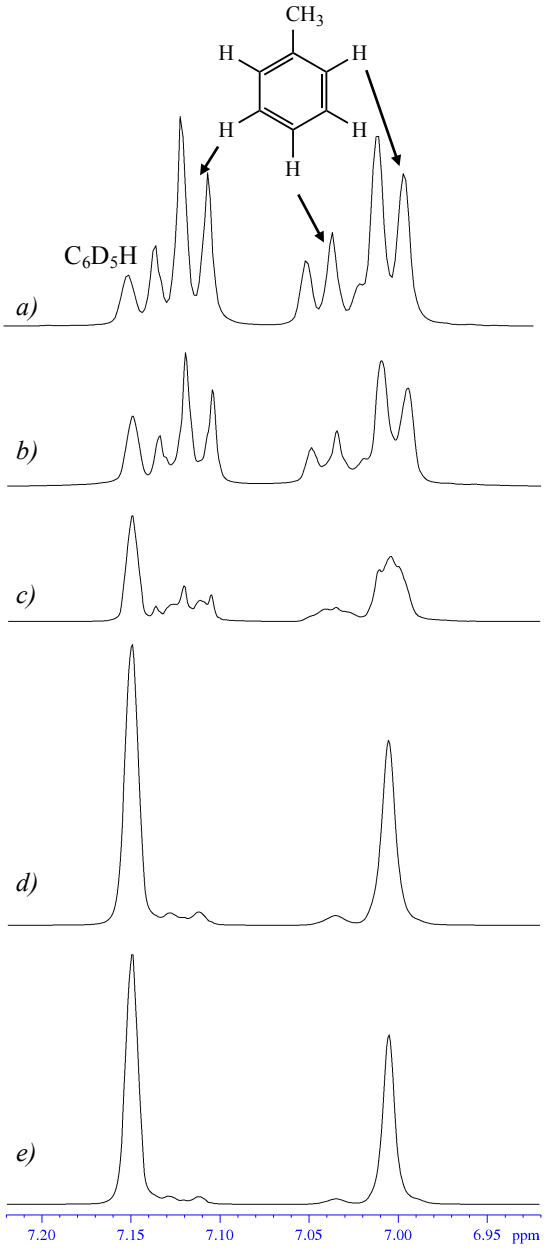

Figure 4.22: Selected regions of ^1H NMR spectra showing change in intensities of C_6D_5H and toluene-h_8 resonances over a) 0 h, b) 0.5 h, c) 4.5 h, d) 19.5 h, e) 28.5 h. (C_6D_6, 298 K, 500 MHz)

4.2.4. Summary and conclusions of Chapter 4

All three *trans* dihydride complexes **3**, **4a** and **5b** exhibit H/D exchange reactions with deuteroarenes and D_2 to incorporate deuterium not only at the metal centres but also on both NHC/phosphine ligands depending on the complex and source of deuterium. While mechanisms of these reactions remains to be elucidated, the fact that benzene activation in **4a** is retarded by the addition of PPh_3 is entirely consistent with a dissociative pathway to form $Ru(IMe_4)_2(PPh_3)H_2$ as a reactive 16 electron fragment for C-H activation. In contrast, **3** must react via a different mechanism which,

on the basis of the results presented in Chapters 3 and 5, could well be related to the highly nucleophilic hydride ligand.

Other observations are even less clear cut. The acceleration of H/D exchange in **4a** in the presence of some Lewis basic ligands cannot be explained at this time, and neither can the enhancement of the rate of phosphine exchange in the same compound by addition of H_2. A full kinetic survey is warranted in which rate is monitored as a function of ligand concentration and H_2 pressure, but such measurements are beyond the scope of this thesis.

4.3. Experimental

4.3.1. Reactivity of $Ru(IMe_4)_2(PPh_3)_2H_2$

4.3.1.1. H/D exchange of **4a** with C_6D_6

4a (*ca*. 5 mg) in a solution of C_6D_6 (0.4 mL) was heated at 363 K for 5 h and periodically monitored by ^1H and $^{31}P\{^1H\}$ NMR spectroscopy. The solvent was removed and replaced with C_6H_6 and the D incorporation analysed by ^2H NMR spectroscopy. Spectroscopic characterization of **4a-HD**: ^1H NMR (500 MHz, C_6D_6): δ 3.71 (s, NC*H*$_2$D), 3.68 (s, NC*H*D$_2$), 1.34 (s, C*H*$_3$), -6.43 (t, $^2J_{HP}$ = 20.7 Hz, Ru-*H*). $^{31}P\{^1H\}$ NMR (202 MHz, C_6D_6): 72.1 (br s). Spectroscopic characterization of **4a-D_2**: ^2H NMR (77 Hz, C_6H_6): δ 3.7 (br s, NC*D*$_x$H$_{3-x}$), δ -6.46 (s, Ru*D*)

4.3.1.2. H/D exchange of **4a** with C_6D_6 in the presence of PPh_3

Two J. Youngs NMR tubes were prepared with **4a** (*ca*. 5 mg) and C_6D_6 (0.4 mL). The second tube also had PPh_3 (15 mg, 5 equiv.) added. Both tubes were heated at 363 K and monitored periodically by NMR spectroscopy. After 24 h heating the solvent was removed from both NMR tubes and replaced with C_6H_6 for analysis by ^2H NMR spectroscopy.

4.3.1.3. Reaction of **4a** with $P(C_6D_5)_3$ without / with H_2

4a (5 mg, 0.006 mmol), $P(C_6D_5)_3$ (7.5 mg, 0.027 mmol) and C_6D_6 (0.4 mL) was put into two J. Youngs NMR tubes. Both NMR tubes were placed into liq N_2 as soon as the solvent was added. Both tubes were degassed (freeze-pump-thaw) and the second tube was put under 1 atm of H_2. The reactions were monitored by NMR spectroscopy. Spectroscopic characterization of **4a-D**, $Ru(IMe_4)_2(P(C_6D_5)_3)PPh_3H_2$: ^1H NMR

spectrum (500 MHz, C_6D_6): δ 7.38 (br m, PC_6H_5), δ 7.07-7.01 (br m, PC_6H_5), δ 3.75 (s, NCH_3), δ 1.35 (s, CH_3), δ -6.55 (s, Ru*H*). $^{31}P\{^1H\}$ NMR (202 Hz, C_6D_6): δ 71.7 (s).

4.3.1.4. Reaction of **4a** with P(*p*-tolyl)$_3$

4a (5 mg), P(*p*-tolyl)$_3$ (3.5 mg, 2 equiv.), C_6H_{12} (2 μL) and C_6D_6 (0.4 mL) were placed in two NMR tubes. Both were degassed (freeze-pump-thawed, 3 cycles) and the second tube was placed under 1 atmosphere of H_2. Both were monitored by NMR spectroscopy. Spectroscopic characterization of $Ru(IMe_4)_2(PPh_3)(P(p\text{-tolyl})_3)H_2$: ^1H NMR spectrum (500 MHz, C_6D_6): δ 7.41-7.36 (br m, $P(p\text{-}CH_3C_6H_4)_3$), δ 7.06-7.02 (br m, $P(p\text{-}CH_3C_6H_4)_3$), δ 6.88-6.81 (br m, $P(p\text{-}CH_3C_6H_4)_3$), δ 3.85 (s, NCH_3), δ 2.05 (s, CH_3), δ 1.35 (s, CH_3), δ -6.59 (t, $^2J_{HH}$ = 20.1 Hz). $^{31}P\{^1H\}$ NMR (202 Hz, C_6D_6): δ 71.6 (AB, Δν = 1239 Hz, $^2J_{PP}$ = 293 Hz, PR_3)

4.3.1.5. Reaction of **4a** with D_2

Two J. Youngs NMR tubes were prepared with **4a** (10 mg, 0.011 mmol). The second tube had PPh_3 (7.5 mg, 0.029 mmol) added, and both tubes had C_6D_6 (0.4 mL) added. Both tubes were degassed (freeze-pump-thawed, 3 cycles) and had D_2 added and the time was noted for each tube. The tubes were analysed by ^1H and $^{31}P\{^1H\}$ NMR spectroscopy periodically. Data for **4a-HD** agreed with that in 4.3.1.1. This experiment was repeated in toluene-d_8 and in THF-d_8.n Spectroscopic characterization of $Ru(IMe_4)_2(PPh_3)_2H_2$ (**4a**): ^1H NMR (500 MHz, toluene-d_8): δ 7.8-7.65 (br m, PPh_3), 7.01-6.9 (br m, PPh_3), 3.73 (s, NCH_3), 1.40 (s, CH_3), -6.47 (t, $^2J_{HP}$ = 20.63 Hz, Ru*H*). $^{31}P\{^1H\}$ NMR (202 MHz, toluene-d_8): 72.6 (s). Spectroscopic characterization of **4a-HD**: ^1H NMR (500 MHz, THF-d_8): δ 7.51-7.37 (br m, PPh_3), 7.07-6.90 (br m, PPh_3), 3.56 (s, NCH_3), 1.58 (s, CH_3), -6.80 (t, $^2J_{HP}$ = 20.53 Hz, Ru*H*). $^{31}P\{^1H\}$ NMR (202 MHz, THF-d_8): 70.4 (s).

4.3.1.6. Reaction of **4a** with D_2 in the solid state

4a (5mg, 0.006 mmol) was ground to a fine powder and stirred under 1 atm D_2 in a J. Youngs ampoule for 7 days. In a separate ampoule, the experiment was repeated but in the presence of 5 equiv. PPh_3. After 7 days, the solid in each ampoule was dissolved in C_6D_6 and analysed straight away by ^1H and $^{31}P\{^1H\}$ NMR spectroscopy.

4.3.1.7. Reaction of **4a** with D_2 with either P(*o*-tolyl)$_3$, P(C_6H_{11})$_3$, NEt_3, 6Mes, ICy, I^{t}Bu or [6MesH]BF_4

J. Youngs NMR tubes were prepared containing (i) just **4a** (10 mg, 0.011 mmol) and then with **4a** (10 mg, 0.011 mmol) and (ii) PPh_3 (15 mg, 0.057 mmol), (iii) P(*o*-tolyl)$_3$ (16 mg, 0.053 mmol), (iv) P(C_6H_{11})$_3$ (17.4 mg, 0.062 mmol) and (v) NEt_3 (3.2 μL, 0.023 mmol). All samples were dissolved in C_6D_6 (0.4 mL) freeze-pump-thaw degassed and placed under 1 atmosphere of D_2 and analysed by ^{1}H and ^{31}P NMR spectroscopy.

J. Youngs NMR tubes were prepared containing (i) just **4a** (5 mg, 0.006 mmol) and then with **4a** (5 mg, 0.006 mmol) and (ii) [6MesH][BF_4] (11.7 mg, 0.029 mmol), (iii) P(C_6D_3)$_3$ (5 mg, 0.029 mmol), (iv) 6Mes (9.2 mg, 0.029 mmol), (v) IMes (8.7 mg, 0.029 mmol), (vi) ICy (6.6 mg, 0.028 mmol) and (vii) I^{t}Bu (5.2 mg, 0.029 mmol). All samples were dissolved in C_6D_6 (0.4 mL) freeze-pump-thaw degassed and placed under 1 atmosphere of D_2 and analysed by ^{1}H and ^{31}P NMR spectroscopy.

4.3.2. Reactivity of Ru(IEt$_2$Me$_2$)$_2$(PPh$_3$)$_2$H$_2$

4.3.2.1. Isomerisation of **5b** in THF-d_8

A THF-d_8 (0.4 mL) solution of **5b** (*ca*. 5 mg) was added to a J. Youngs NMR tube. ^{1}H and ^{31}P{^{1}H} NMR spectroscopy showed the formation of small amounts of isomers **5a** and **5b** over 1 week at room temperature. Spectroscopic characterization of **5a**: ^{1}H NMR (500 MHz, THF-d_8): δ -6.63 (t, $^2J_{HP}$ = 21.13 Hz, Ru*H*). ^{31}P{^{1}H} NMR (202 Hz, THF-d_8): δ 69.3 (s). **5b**: ^{1}H NMR (500 MHz, THF-d_8): δ -7.04 (t, $^2J_{HP}$ = 20.01 Hz, Ru*H*). ^{31}P{^{1}H} NMR (202 Hz, THF-d_8): δ 67.7. **5d**: ^{1}H NMR (500 MHz, THF-d_8): δ -9.09 (t, $^2J_{HP}$ = 22.34 Hz, Ru*H*). ^{31}P{^{1}H} NMR (202 MHz, THF-d_8): δ 63.2 (s).

4.3.2.2.Reactivity of **5b** in C_6D_6

A C_6D_6 (0.4 mL) solution of **5b** (*ca*. 5 mg) was monitored by ^{1}H and ^{31}P{^{1}H} NMR periodically over 72 h. The spectra revealed a mixture of isomerization and H/D exchange reactions. **5a**: ^{1}H NMR (500 MHz, C_6D_6): δ -6.32 (t, $^2J_{HP}$ = 20.34 Hz, Ru*H*). ^{31}P{^{1}H} NMR (202 Hz, C_6D_6): δ 70.2 (s). **5b**: ^{1}H NMR (500 MHz, C_6D_6): δ -6.75 (t, $^2J_{HP}$ = 20.57 Hz, Ru*H*). ^{31}P{^{1}H} NMR (202 MHz, C_6D_6): δ 68.6 Hz (s). **5a-HD**: ^{1}H NMR (500 MHz, C_6D_6): δ -6.19 (t, $^2J_{HP}$ = 20.38 Hz, Ru*H*). ^{31}P{^{1}H} NMR (202 MHz, C_6D_6): δ 70.2 (s). ^{2}H NMR (77 MHz, C_6D_6): δ -6.3 (s, Ru*D*). **5b-HD**: ^{1}H NMR (500

MHz, C_6D_6): δ -6.62 (t, $^2J_{HP}$ = 20.57 Hz, Ru*H*). ^{2}H NMR (77 MHz, C_6D_6): δ -6.77 (s, Ru*D*)

4.3.2.3. Reaction of **5b** with D_2

A THF-d_8 (0.4 mL) solution of **5b** (5 mg, 0.005 mmol) in a J. Youngs NMR tube was degassed (freeze-pump-thawed) and had an atmosphere of D_2 added to it.

4.3.3. Reactivity of $Ru(IMe_4)_4H_2$

4.3.3.1. Reaction of **3** with C_6D_6

3 (5 mg, 8.3 mmol) was put in an NMR tube with a J. Youngs lid with C_6D_6 (0.4 mL) and monitored by ^{1}H NMR spectroscopy over 4 days. Spectroscopic characterization of **3**: ^{1}H NMR (500 MHz, C_6D_6): δ 3.79 (s, 24H, NCH_3), δ 1.82 (s, 24H, CH_3), δ -7.46 (s, 2H, Ru-*H*)

3 (5 mg, 8.3 mmol) was put in an NMR tube with C_6D_6 (0.4 mL) and C_6H_{12} (4 μL) and heated at 50 °C and monitored by ^{1}H NMR spectroscopy for 1 week. Spectroscopic characterization of **3-HD**: ^{1}H NMR (500 MHz, C_6D_6): δ 3.79 (s, NCH_xD_{3-x}), δ 1.83 (s, CH_3), δ -7.31 (s, Ru-*H*). ^{2}H NMR (77 MHz, C_6H_6): δ 3.74 (s, NCH_xD_{3-x}), δ -7.51 (s, Ru-D). Spectroscopic characterization of **3-D_2**: ^{2}H NMR (77 MHz, C_6H_6): δ 3.7 (s, CD_xH_{3-x}), δ -7.4 (s, Ru-*D*).

4.3.3.2. Reaction of **3** with toluene-d_8

3 (5 mg, 8.3 mmol) was put in an NMR tube with a J. Youngs lid with toluene-d_8 (0.4 mL) and C_6H_{12} (3 μL) and was heated at 50°C for 2 days. Spectroscopic characterization of **3**: ^{1}H NMR (500 MHz, toluene-d_8): δ 3.70 (s, 24H, NCH_3), δ 1.87 (s, CH_3), δ -7.56 (s, 2H, Ru-*H*). Spectroscopic characterization of **3-HD**: ^{1}H NMR (500 MHz, toluene-d_8): δ 3.70 (s, 24H, NCH_3), δ 1.87 (s, CH_3), δ -7.41 (s, 2H, Ru-*H*). ^{2}H NMR (77 MHz, C_6H_6): δ -7.44 (s, Ru*D*). Spectroscopic characterization of **3-D_2**: ^{2}H NMR (77 MHz, C_6H_6): δ -7.28 (s, Ru-*D*).

4.3.3.3. Reaction of **3** with H_2 in THF-d_8

3 (8 mg, 13.3 mmol) was put in a J. Youngs NMR tube with THF (0.4 mL). and freeze-pump-thaw degassed and put under an atm of H_2. Spectroscopic characterization of **3**: ^{1}H NMR (500 MHz, THF-d_8): δ 3.34 (s, 24H, NCH_3), 1.97 (s, 24H, NCCH_3═NCCH_3), -8.14 (s, 2H, Ru*H*).

4.3.3.5. Reaction of **3** with H_2 and toluene-d_8 (or C_6D_6)

A solution of **3** (5 mg, 8.3 mmol) in toluene-d_8 (0.4 mL) was freeze-pump-thaw degassed in a J. Youngs NMR tube and put under an atmosphere of hydrogen and monitored by NMR spectroscopy. NMR characterization of **3**, **3-HD** and **3-D$_2$** in tol-d_8 are noted previously. T_1 measurment of hydride resonance of **3-HD** at δ_H -7.41 was 333.0 ms. T_1 measurement of hydride resonance for **3** at δ_H = -7.56 was 336.4 ms.

4.3.3.6. Reaction of **3** with D_2 and THF-d_8

A THF-d_8 (0.4 mL) solution of **3** (10 mg, 0.02 mmol) with C_6H_{12} (6 μL) as a reference was degassed (freeze-pump-thawed) in a J. Youngs NMR tube and an atmosphere of D_2 was added. The solution was monitored by NMR spectroscopy for a week. The solvent was removed and the residue redissolved in THF-h_8. Spectroscopic characterization of **3-HD**: ^{1}H NMR (500 MHz, THF-d_8): δ 3.34 (s, NCH_3), δ 1.97 (s, CH_3), δ -7.99 (s, RuH). ^{2}H NMR (77 MHz, THF-h_8): δ -8.14. Spectroscopic characterization of **3-D$_2$**: ^{2}H NMR (77 MHz, THF-h_8): δ -7.98 (br s).

4.3.3.7. Reaction of **3** with D_2 and C_6H_6

A THF-d_8 solution (0.4 mL) of **3** (4 mg, 6.7 μmol) with C_6H_{12} (3 μL) as a reference and C_6H_6 (6 μL, 0.07 mmol) was freeze-pump-thawed degassed in a J. Youngs NMR tube and 1 atmosphere of D_2 was added. The reaction was monitored by NMR spectroscopy and the conversion from C_6H_6 to C_6D_6 was calculated from the integration values.

4.3.3.8. Reaction of **3** with D_2 and toluene-h_8

A THF-d_8 solution (0.4 mL) of **3** (5 mg, 8.3 μmol) with C_6H_{12} (3 μL) as a reference and toluene-h_8 (6 μL, 0.06 mmol) was freeze-pump-thawed degassed in a J. Youngs NMR tube and 1 atmosphere of D_2 was added. The reaction was monitored by NMR spectroscopy and the conversion from toluene-h_8 to $C_6D_{2(meta)}H_2CH_3$, $C_6D_{2(ortho)}H_2CH_3$ and $C_6D_{(para)}H_3CH_3$ was calculated from the integration values. Spectroscopic characterization of **toluene-h_8**: ^{1}H NMR (500 MHz, THF-h_8): δ 7.18 (t, $^3J_{HH}$ = 7.57 Hz, 2H, H_{meta}), δ 7.12 (d, $^3J_{HH}$ = 7.57 Hz, 2H, H_{ortho}), δ 7.08 (t, $^3J_{HH}$ = 7.4 Hz, 1H, H_{para}), δ 2.3 (s, 3H, CH_3).

4.3.3.9. Reaction of **3** with C_6D_6 and toluene-h_8

3 (10 mg, 0.02 mmol, 5 mol% relative to toluene-h_8) was added to an NMR tube with C_6D_6 (0.6 mL, 6.8 mmol), toluene-h_8 (44 μL, 0.4 mmol) and C_6H_{12} (12 μL) and was heated at 50 °C. Spectroscopic characterization of **toluene-h_8**: ^{1}H NMR (500 MHz, C_6D_6): δ 7.12 (t, $^3J_{HH}$ = 7.48, 2H, H_{meta}), δ 7.03 (t, $^3J_{HH}$ = 7.51, 1H, H_{para}), δ 7.00 (d, $^3J_{HH}$ = 7.48, 2H, H_{ortho}), δ 2.10 (s, 3H, CH_3).

4.3.3.10. Reaction of **3** with C_6H_6 and toluene-d_8

3 (5 mg, 0.01 mmol, 1.3 mol% relative to C_6H_6) was added to a J. Youngs NMR tube with toluene-d_8 (0.4 mL, 3.8 mmol), C_6H_6 (75 μL, 0.8 mmol), C_6H_{12} (6 μL) and heated at 50 °C and monitored by NMR spectroscopy.

4.4. References

1. (a) For reviews of the field; see; (b) Balcells, D.; Clot, E.; Eisenstein, O., *Chem. Rev.* **2010**, *110,* 749; (c) Ritleng, V.; Sirlin, C.; Pfeffer, M., *Chem. Rev.* **2002**, *102,* 1731; (d) Crabtree, R. H., *J. Chem. Soc., Dalton Trans.* **2001**, 2437; (e) Shilov, A. E.; Shul'pin, G. B., *Chem. Rev.* **1997**, *97,* 2879; (f) Arndtsen, B. A.; Bergman, R. G.; Mobley, T. A.; Peterson, T. H., *Acc. Chem. Res.* **1995**, *28,* 154; (g) Ryabov, A. D., *Chem. Rev.* **1990**, *90,* 403; (h) Jones, W. D.; Feher, F. J., *Acc. Chem. Res.* **1989**, *22,* 91; (i) Bergman, R. G., *Science* **1984**, *223,* 902.

2. (a) Jones, W. D.; Feher, F. J., *J. Am. Chem. Soc.* **1986**, *108,* 4814; (b) Janowicz, A. H.; Bergman, R. G., *J. Am. Chem. Soc.* **1983**, *105,* 3929; (c) Janowicz, A. H.; Bergman, R. G., *J. Am. Chem. Soc.* **1982**, *104,* 352.

3. (a) Hall, C.; Jones, W. D.; Mawby, R. J.; Osman, R.; Perutz, R. N.; Whittlesey, M. K., *J. Am. Chem. Soc.* **1992**, *114,* 7425; (b) Baker, M. V.; Field, L. D., *J. Am. Chem. Soc.* **1986**, *108,* 7433.

4. Confirmation that the higher frequency signal is indeed a Ru-H rather than Ru(η^2-HD) resonance (for example) came from analogous experiments with $Ru(IMe_4)_4H_2$ and D_2 discussed in section 4.2.1.1. since very similar resonances were recorded for the signal for **3** at δ_H -7.56 and **3-HD** at δ_H -7.41. T_1 values of 333 and 336 ms were recorded for **3** at δ_H -7.56 and **3-HD** at δ_H -7.41.

5. (a) C-H activation of N-Me groups has only been seen with metal carbonyl cluster precursors. See; (b) Cabeza, J. A.; del Rio, I.; Miguel, D.; Perez-Carreno, E.; Sanchez-Vega, M. G., *Dalton Trans.* **2008**, 1937; (c) Cabeza, J. A.; del Rio, I.; Miguel,

D.; Sanchez-Vega, M. G., *Angew. Chem., Int. Ed.* **2008**, *47,* 1920; (d) Cabeza, J. A.; Perez-Carreno, E., *Organometallics* **2008**, *27,* 4697; (e) Cabeza, J. A.; del Rio, I.; Miguel, D.; Sanchez-Vega, M. G., *Chem. Commun.* **2005**, 3956.

6. (a) Fantasia, S.; Egbert, J. D.; Jurcik, V.; Cazin, C. S. J.; Jacobsen, H.; Cavallo, L.; Heinekey, D. M.; Nolan, S. P., *Angew. Chem., Int. Ed.* **2009**, *48,* 5182; (b) Bullock, R. M.; Song, J. S.; Szalda, D. J., *Organometallics* **1996**, *15,* 2504; (c) Heinekey, D. M.; Oldham, W. J., *J. Am. Chem. Soc.* **1994**, *116,* 3137; (d) Paneque, M.; Poveda, M. L.; Taboada, S., *J. Am. Chem. Soc.* **1994**, *116,* 4519; (e) Miller, R. L.; Toreki, R.; Lapointe, R. E.; Wolczanski, P. T.; Vanduyne, G. D.; Roe, D. C., *J. Am. Chem. Soc.* **1993**, *115,* 5570; (f) Desrosiers, P. J.; Cai, L. H.; Lin, Z. R.; Richards, R.; Halpern, J., *J. Am. Chem. Soc.* **1991**, *113,* 4173.

7. Allman, T.; Goel, R. G., *Can. J. Chem.* **1982**, *60,* 716.

8. (a) Moeller, T.; Ferrus, R., *J. Phys. Chem.* **1960**, *64*; (b) triethylamine. http://pubchem.ncbi.nlm.nih.gov/summary/summary.cgi?cid=8471.

9. (a) Macgregor, S. A.; Roe, D. C.; Marshall, W. J.; Bloch, K. M.; Bakhmutov, V. I.; Grushin, V. V., *J. Am. Chem. Soc.* **2005**, *127,* 15304; (b) Jasim, N. A.; Perutz, R. N.; Whitwood, A. C.; Braun, T.; Izundu, J.; Neumann, B.; Rothfeld, S.; Stammler, H. G., *Organometallics* **2004**, *23,* 6140.

10. Burling, S.; Haller, L. J. L.; Mas-Marzá, E.; Moreno, A.; Macgregor, S. A.; Mahon, M. F.; Pregosin, P. S.; Whittlesey, M. K., *Chem.-Eur. J.* **2009**, *15,* 10912.

Chapter 5

Chapter 5: Investigation into the ability of 3, 4a and 5b to catalyse the reduction of carbon dioxide by pinacolborane

5.1. Introduction

The ability of $Ru(NHC)_2(PPh_3)_2H_2$ (NHC = IMe_4 (**4a**), IEt_2Me_2 (**5b**)) to react stoichiometrically with CO_2 as well as promote H/D exchange reactions of inert C-H bonds, led to a study of whether these compounds, as well as the all-NHC analogue **3**, could catalyse the reaction of CO_2 with a more polar E-H bond such as E=boron.

Efforts to catalytically reduce CO_2 have received much interest because of the desire to use such an abundant and atmospherically malevolent compound as a carbon based feedstock for higher value chemicals and liquid fuels.[1] There have been a considerable number of recent reports on the use of both transition metal and non-metal based catalysts for CO_2 functionalization.[2] Two particular examples from the literature pertinent to the work described herein, are the reports by Guan[3] and Sabo-Etienne[4] on the use of $Ni\{2,6\text{-}C_6H_3(OP^tBu_2)_2\}H$ and $Ru(PCy_3)_2(\eta^2\text{-}H_2)_2H_2$ respectively as catalysts for the reduction of CO_2 by boranes. The products formed are shown in Scheme 5.1.

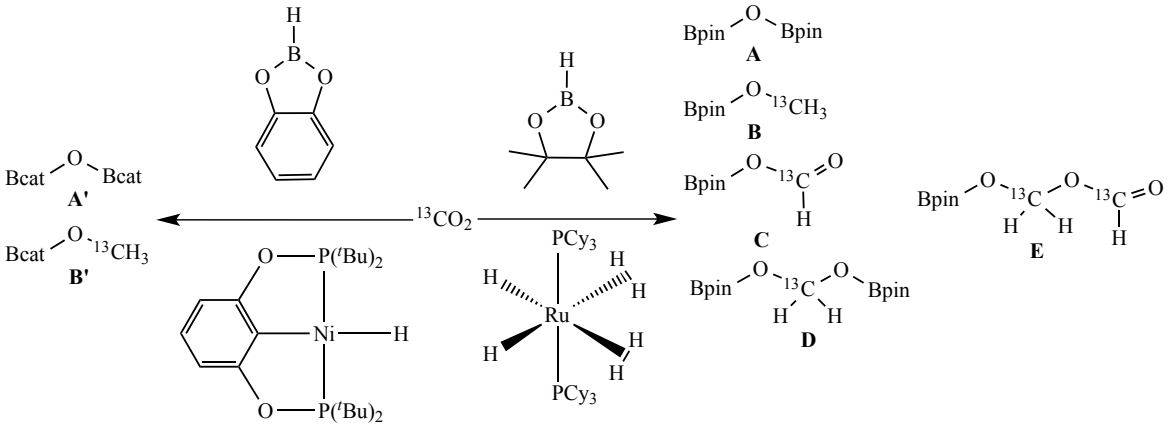

*Scheme 5.1: Products **A**-**E** formed from the reduction of $^{13}CO_2$ by HBpin / HBcat in the presence of $Ru(PCy_3)_2(\eta^2\text{-}H_2)_2H_2$ or $Ni\{2,6\text{-}C_6H_3(OP^tBu_2)_2\}H$*

The Ni-based system (Scheme 5.2) was more selective than the Ru species for the catecholborane (HBcat) products **A'** and **B'** and also more active in terms of turnover (TOF of 495 h^{-1} based on B-H) and had the ability to convert a larger excess of borane (500 equiv. *cf.* 100 equiv). A catalytic cycle has been proposed on the basis of DFT calculations and NMR observations to explain the formation of **A'** and **B'** as shown in Scheme 5.1. Thus, cycle 1 involves the insertion of CO_2 into a Ni-H bond and then cleavage by HBcat to afford HCO_2Bcat. Insertion in Ni-H, followed by the

elimination of formaldehyde affords a Ni-OBcat species which, upon reduction by a second equivalent of HBcat, yields **A'**. Further insertion of HCHO into Ni-H followed by reaction with a third equivalent of HBcat leads to the formation of **B'**.[3a,5]

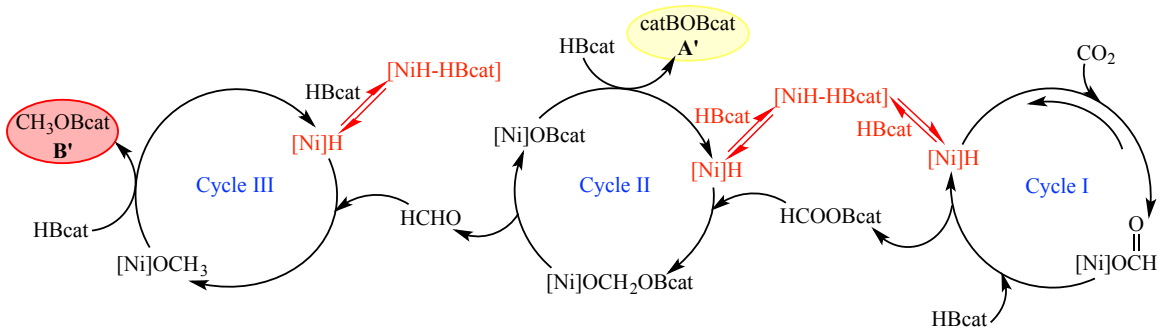

Scheme 5.2: The catalytic cycle proposed by Guan et al. for the reduction of CO_2 by HBcat with a Ni catalyst.

In the case of ruthenium, the formation of **C**, **D** and **E**, in addition to **A** and **B**, suggests that HCO_2Bpin lasts long enough to undergo a second insertion into Ru-H and react with a fourth equivalent of HBpin to allow generation of **D** and **E** (Scheme 5.3). This difference in product distribution between the Ni and Ru catalysts may be connected to the propensity of the latter to undergo facile, multiple ligand loss, to generate more than one available coordination site.[6] The formation of the acetal compound **D** suggested an intermediate {$RuOCH_2OBpin$} fragment reacting with a second equiv. of HBpin in the catalytic cycle; acetals have been key structures studied in various CO_2 reduction processes.[2r,2t,2v,7a-c] The formation of **E** represented the first time the reductive coupling of two molecules of CO_2 had been shown.[4c]

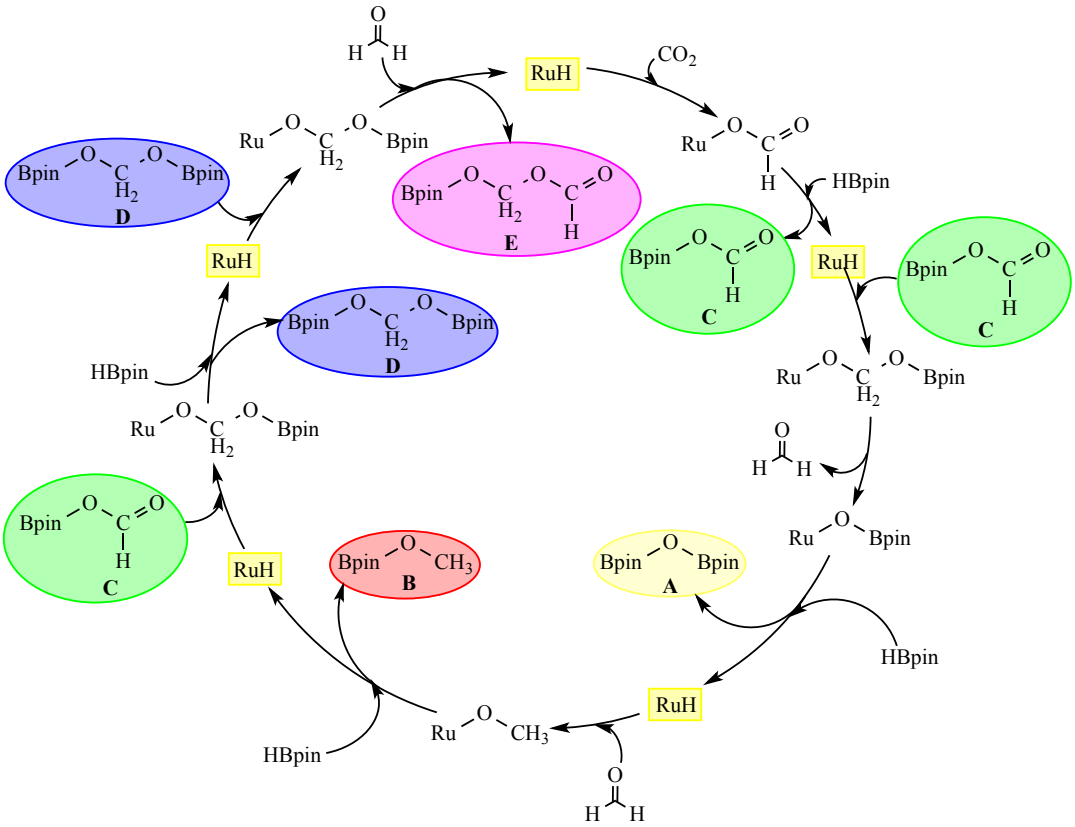

Scheme 5.3: Catalytic cycle based on the work of Sabo-Etienne for the reduction of CO_2 by HBpin with a RuH catalyst.

A key early step in any catalytic cycle for CO_2 reduction is likely to involve CO_2 insertion into a M-H bond.[7a,7b] On the basis of the reactions of **3**, **4a** and **5b** with CO_2 in Chapter 3, these complexes could be potential catalyst precursors for CO_2 reduction as they are able to insert CO_2 into the Ru-H bond (reversibly in the case of **3**). It is also known (Chapter 2) that **4a** and **5b** eliminate just a single PPh_3 ligand, suggesting that it might be possible to correlate the extent of Ru unsaturation with the formation of particular reduction products.

5.2. Results and Discussion

5.2.1. Reactivity of $Ru(IMe_4)_2(PPh_3)_2H_2$ (**4a**) and its derivatives

5.2.1.1. Reactivity of **4a** and HBpin

Heating a toluene solution of **4a** with 5 equiv. of HBpin at 70 ºC for 48 h led a colour change from orange to pale pink. Removal of the solvent and addition of hexane to the resulting oily residue gave a colourless precipitate which was identified as the dihydroborate hydride complex $Ru(IMe_4)_2(PPh_3)(H_2Bpin)H$ (**27**, Scheme 5.4) on the basis of ^{1}H, $^{31}P\{^{1}H\}$ and $^{13}C\{^{1}H\}$ NMR spectroscopy and X-ray crystallography (Figure 5.1).

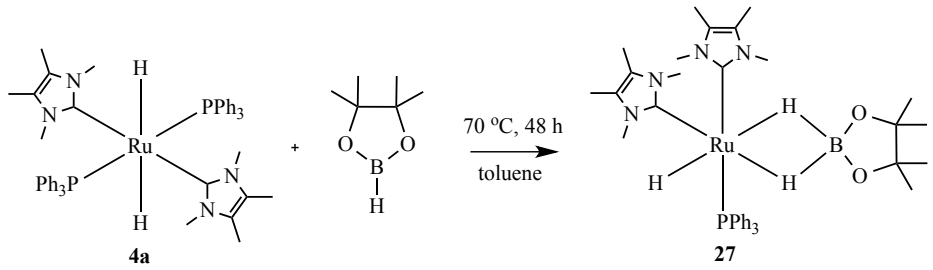

*Scheme 5.4: Reaction of **4a** with HBpin to form **27**.*

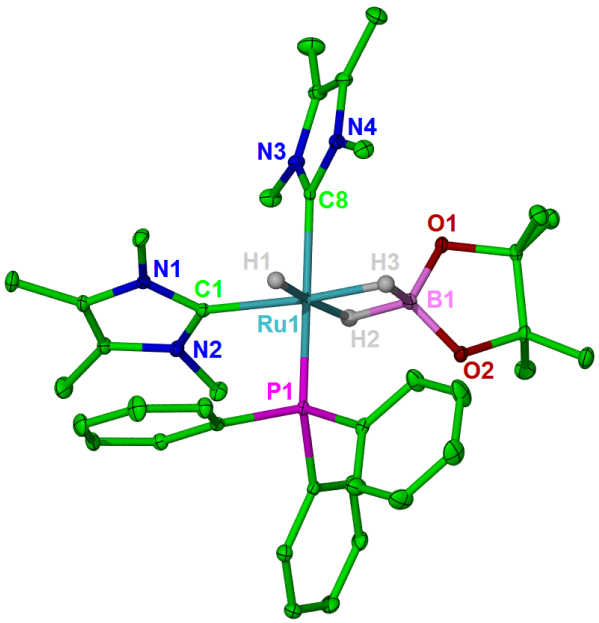

*Figure 5.1: Molecular structure of **27**. Ellipsoids are shown at the 30% level. Hydrogen atoms except for those coordinated to Ru are removed for clarity. Selected bond lengths (Å) and angles (°): Ru-C(1) 2.100(3), Ru-C(8) 2.082(2), Ru-P(1) 2.2902(5), Ru-B 2.127(2), C(8)-Ru-P(1) 169.55(6), C(1)-Ru-C(8) 92.76(7), C(8)-Ru-B 84.38(8), C(1)-Ru-B 139.85 (8).*

The X-ray structure of **27** is shown in Figure 5.1 and reveals a distorted octahedral geometry comprising of two *cis* NHC ligands and a single phosphine, which lies *trans* to the terminus of a bidentate H_2Bpin ligand. The ruthenium coordination sphere is completed by a single hydride that is *trans* to the opposite end of the boron-based ligand. All three ruthenium bound hydrogens H(1)-H(3) were located in the X-ray crystal structure with those of the Ru-H-B linkages freely refined. Notwithstanding the difficulty in accurately determining hydrogen positions using X-rays, the similarity of the B1-H2 and B1-H3 bond lengths (1.37(2), 1.43(2) Å) in **27** were consistent with the assignment as a dihydridoborate hydride complex rather than a

σ-borane dihydride species. Comparable distances in $Ru(PCy_3)_2(H_2Bpin)(HBpin)H$, which contains both dihydroborate and borane ligands[8] are shown in Figure 5.2.

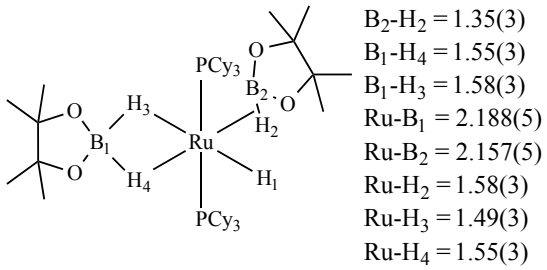

Figure 5.2: Structure of $Ru(PCy_3)_2(H_2Bpin)(HBpin)H$ with selected bond distances (Å).

The short Ru-B distance in **27** (2.127(2) Å), in combination with NMR data described below, provides some support for σ-borane coordination.[9] Sabo-Etienne has suggested that the angle between Ru, B and the middle of the O,O pinacol backbone gives the clearest indication of the ligation mode;[9c] the value of 173.7° lies midway between those of 171.5° and 177.1° for the σ-borane and dihydridoborate ligands in the complex shown in Figure 5.2.[8]

The room temperature ^1H NMR spectrum showed three low frequency resonances in a 1:1:1 ratio (Figure 5.3(a)). Two broad singlets at δ_H -6.17 and -10.06 were assigned to the two hydrogens of the H_2Bpin ligand on the basis that they sharpened upon ^{11}B decoupling (Figure 5.3(b)). A well-resolved doublet at δ_H -8.87 ($^2J_{HP}$ = 30.6 Hz) was assigned to the ruthenium hydride. In the $^{11}B\{^1H\}$ NMR spectrum, a broad singlet was apparent at *ca.* δ_B 37. The shift to higher frequency of this resonance relative to free HBpin (δ_B 28) is indicative of σ-borane character.[9c]

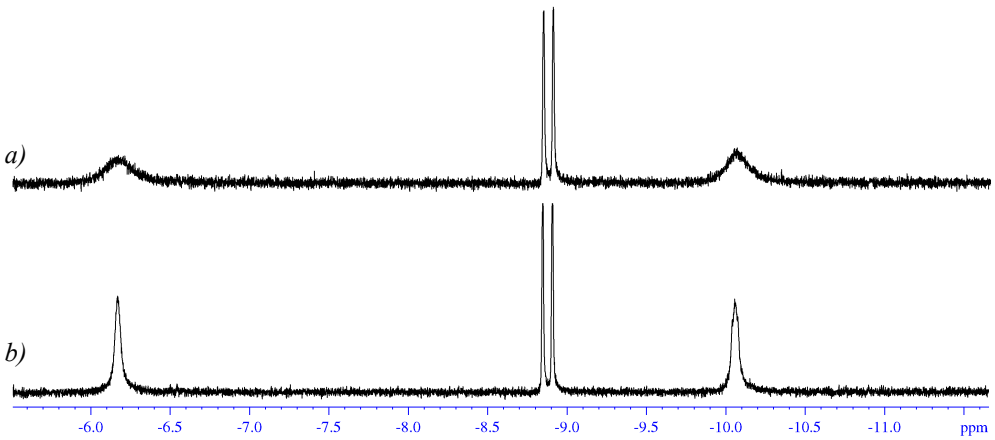

*Figure 5.3: a) Hydride regions of a) the ^1H and b) the $^1H\{^{11}B\}$ NMR spectra of **27** (C_6D_6, 298 K, 500 MHz).*

All the CH_3 groups of the IMe_4 ligands were inequivalent resulting in the appearance of eight singlets between δ_H 1.5 and 4.0 in the ^1H NMR spectrum, each of relative integral three. Four broad singlet resonances between δ_H 1.0 and 1.5, were attributed to the pinacol methyl groups.

^1H-^{31}P HSQC spectroscopy showed a correlation between the doublet hydride resonance and a singlet in the ^{31}P NMR spectrum at δ_P 61.7. A ^1H-^{13}C HMBC experiment showed correlations between the NMe proton resonances and two high frequency carbenic carbon signals at δ_C 198.5 ($^2J_{CP}$ = 11.0 Hz) and δ_C 195.0 ($^2J_{CP}$ = 90 Hz) in the $^{13}C\{^1H\}$ NMR spectrum. The magnitudes of the coupling constants supported their assignments as *cis* and *trans* to phosphine respectively.

5.2.1.2. Catalytic reduction of CO_2 using **4a**

Exposure of a C_6D_6 solution of **4a** and 25 equiv. HBpin to an atmosphere of $^{13}CO_2$ led to an immediate colour change from yellow to red through to pale orange over the course of 5 h. Representative ^1H and $^{13}C\{^1H\}$ NMR spectra recorded over this time, as well as to a time of 28 h, are shown in Figure 5.4. At early times, resonances assignable to the CO_2 reduction products, **A**, **B** and **D** were observable, along with some extremely broad signals. For example, *ca*. 1 h after $^{13}CO_2$ addition, a doublet proton resonance centered at δ_H *ca*. 9.0 was clearly visible, with a splitting of *ca*. 210 Hz and a peak width of *ca*. 19 Hz (Figure 5.4). As will be apparent throughout the rest of the chapter, the appearance of similar signals of a very broad nature are characteristic of the Ru reactions and, as yet, have not been identified.

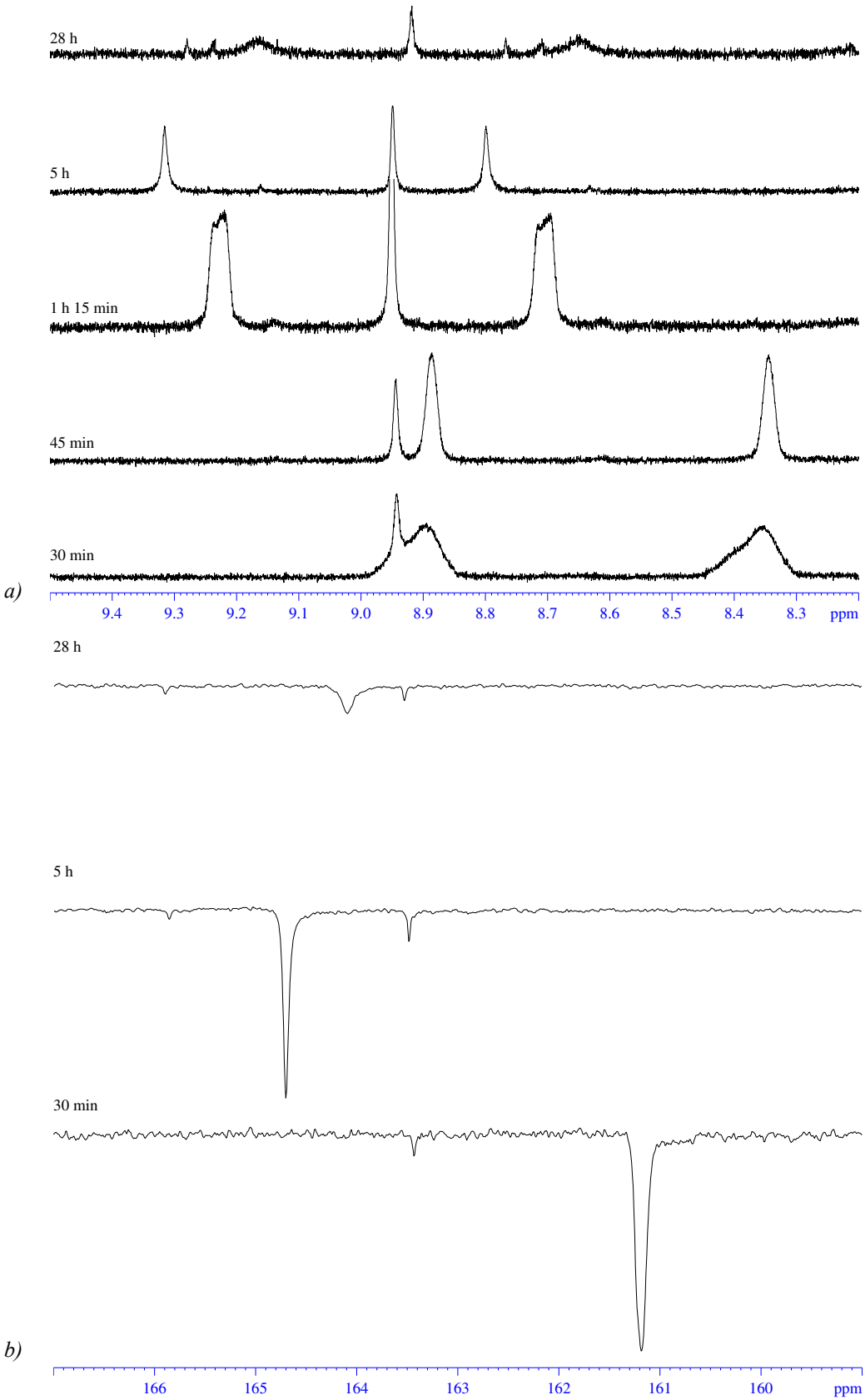

*Figure 5.4: Selected regions of a) the ^{1}H NMR spectra (C_6D_6, 298 K, 400 MHz) and b) the corresponding $^{13}C\{^{1}H\}$ NMR spectra (C_6D_6, 298 K, 126 MHz) of the reaction between **4a**, HBpin and $^{13}CO_2$ at various times.*

After the first 5 h, disappearance of the broad features allowed a more reliable calculation of the distribution of products **A**, **B** and **D** in solution (no **C** or **E** were observed, Table 5.1). These products were easily identified from their characteristic ^{1}H, ^{13}C and where possible, ^{11}B NMR signals reported by Sabo-Etienne.[4c] The boronated ether pinBOBpin (**A)** appeared as a singlet at δ_H 1.01 in the ^{1}H NMR spectrum and a broad singlet at δ_B 22 in the ^{11}B NMR spectrum. Compound **B** (pinO-$^{13}CH_3$) exhibited a characteristic $^{1}J_{HC}$ coupled doublet of 143 Hz at δ_H 3.51 (Figure 5.5a) and a singlet at δ_C 52.1 in the $^{13}C\{^{1}H\}$ NMR spectrum (Figure 5.5b).

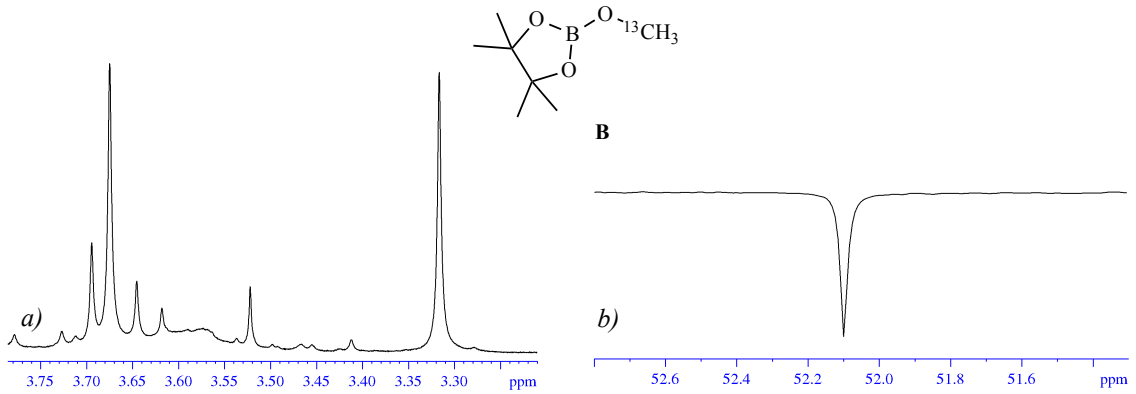

*Figure 5.5: Selected regions of a) the ^{1}H NMR spectrum and b) the corresponding $^{13}C\{^{1}H\}$ NMR spectrum showing the characteristic resonances for compound **B** (C_6D_6, 298 K, 500 MHz, 126 MHz).*

Compound **D** was identified by the presence of a doublet resonance at δ_H 5.49 ($^{1}J_{HC}$ = 167 Hz) in the ^{1}H NMR spectrum and a singlet at δ_C 85.4 in the $^{13}C\{^{1}H\}$ NMR spectrum (Figure 5.6).

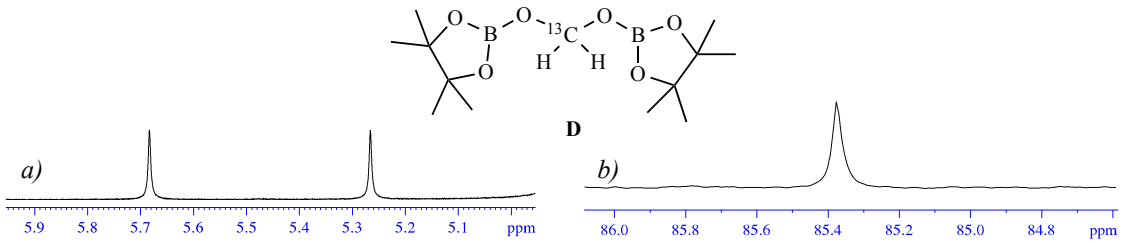

*Figure 5.6: Selected regions of a) the ^{1}H NMR spectrum and b) the corresponding $^{13}C\{^{1}H\}$ NMR spectrum showing the characteristic peaks of compound **D** (C_6D_6, 298 K, 500 MHz, 126 MHz).*

The distribution of **A**, **B** and **D** (based on integration of the ^{1}H NMR spectra) over 21 days are shown in Table 5.1. Over such a long time, the relative amounts of **A**

and **B** slowly increased at the expense of **D**. Of particular note was that after 1 month, not all of the HBpin had been consumed. No single Ru complex was present at the end of the 3 week period of reaction, although the hydride resonances characteristic of the dihydridoborate complex **27** were just about distinguishable, along with some additional unidentified hydride resonances of comparable intensity.

Time after addition of $^{13}CO_2$	Relative amounts of products (%)			
	HBpin	**A**	**B**	**D**
5 h	62	21	11	6
77 h (3 days)	50	30	14	6
7 days	48	28	19	5
14 days	46	29	22	3
21 days	30	34	19	17

*Table 5.1: Distribution of products in the catalytic reduction of $^{13}CO_2$ with HBpin in the presence of $Ru(IMe_4)_2(PPh_3)_2H_2$ (**4a**, 4 mol %).*

5.2.1.3. Catalytic reduction of CO_2 using $Ru(IMe_4)_2(PPh_3)(H_2Bpin)H$ (**27**) and $Ru(IMe_4)_2(PPh_3)(OCHO)H$ (**9**)

Given the activity of **4a** as a precatalyst for the reduction of CO_2, the products from the individual stoichiometric reactions with HBpin, **27**, and CO_2, the formate hydride complex $Ru(IMe_4)_2(PPh_3)(OCHO)H$ (**9**), were tested as catalytic precursors. At the same 4 mol% loading, **27** generated the ^1H and $^{13}C\{^1H\}$ NMR spectra shown in Figure 5.36 over the first 5 h of reaction. As before, **A**, **B** and **D** were apparent within 5 min of the addition of $^{13}CO_2$, along with broad high frequency formate like signals in the ^1H NMR spectrum and an astonishing 3 ppm wide resonance in the $^{13}C\{^1H\}$ NMR spectrum (Figure 5.7). These broad resonances did not appear at the same frequency as those from the reaction with **4a** and they diminished more quickly.

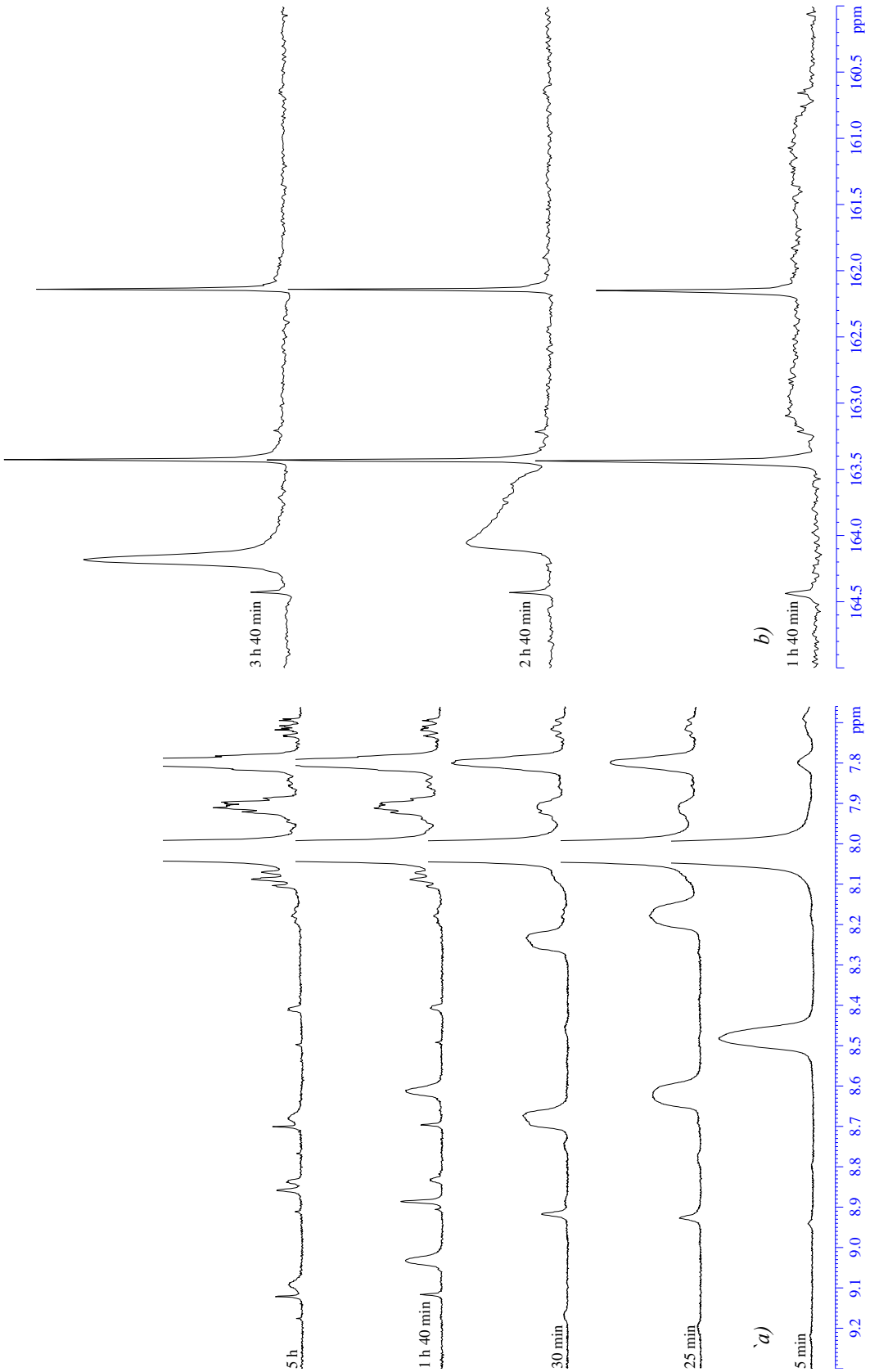

*Figure 5.7: Selected regions of a) the ^{1}H and b) $^{13}C\{^{1}H\}$ NMR spectra of the reaction of $^{13}CO_2$ and HBpin in the presence of 4 mol % **27** at various times (^{1}H, 500 MHz; $^{13}C\{^{1}H\}$, 126 MHz; C_6D_6, 298 K).*

After *ca*. 5 h the broad features had essentially vanished to leave just **A**:**B**:**D** in a ratio of 1:0.71:0.25. This ratio remained constant over *ca*. 1 week (Table 5.2), although reduction in the amount of **D** present was again apparent over a period of weeks. After 22 days, the hydride region of the ^{1}H NMR spectrum was surprisingly clean (in contrast to the reaction with **4a**) with the resonances of **27** still clearly visible.

Time after addition of $^{13}CO_2$	Relative amounts of products (%)			
	HBpin	**A**	**B**	**D**
5 h 50 min	41	31	20	8
8 days	18	41	27	14
22 days	9	51	33	7

*Table 5.2: Distribution of products from the catalytic reduction of $^{13}CO_2$ by HBpin in the presence of 4 mol % $Ru(IMe_4)_2(PPh_3)(H_2Bpin)H$, **27**.*

Broad signals were apparent when $Ru(IMe_4)_2(PPh_3)(OCHO)H$, **9** was used as the precursor (Figure 5.8). They did not appear in the same place as those seen with either **4a** or **27** and they dissipated more quickly than those seen in the reaction with **27**.

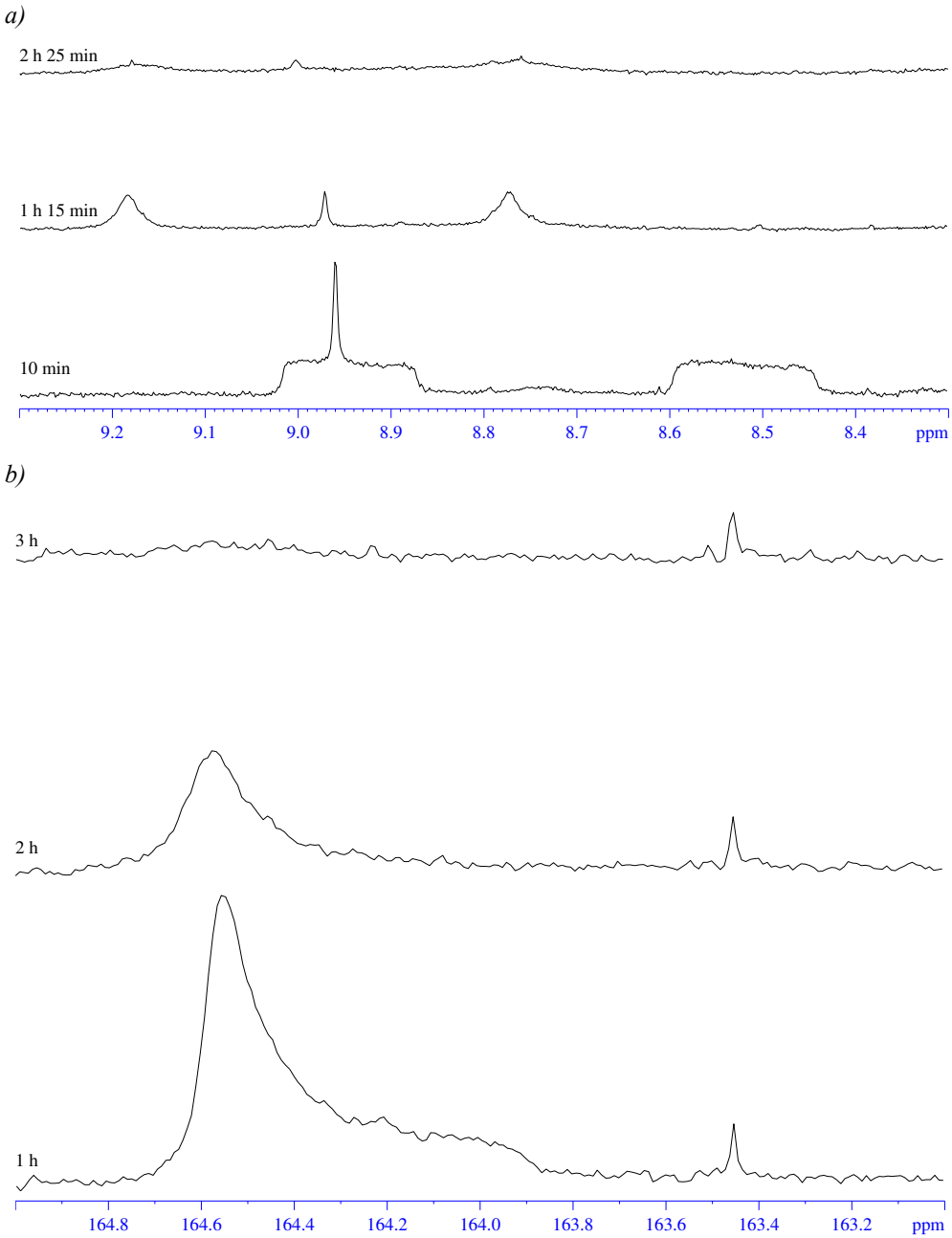

Figure 5.8: Selected regions of a) the ^{1}H NMR spectra and b) the $^{13}C\{^{1}H\}$ NMR spectra of the reaction of ***9****, $^{13}CO_2$ and HBpin at various times.*

The distribution of products **A-D** in solution over time are shown in Table 5.3. Products **B** and **D** could be seen with $^{12}CO_2$ as well as $^{13}CO_2$ incorporated, the former arising from the initial Ru precursor **9**. After 23 days, the predominant hydride containing species was **27**, however, many other hydride containing species were present in smaller quantities.

Time after $^{13}CO_2$ added	Relative amounts of products (%)			
	HBpin	**A**	**B**	**D**
5 h	13	45	31	11
14 days	22	40	32	6
23 days	10	42	42	6

*Table 5.3: Distribution of products from the catalytic reduction of $^{13}CO_2$ by HBpin in the presence of 4 mol % $Ru(IMe_4)_2(PPh_3)(OCHO)H$, **9**.*

5.2.1.4. Stoichiometric reaction of $Ru(IMe_4)_2(PPh_3)(H_2Bpin)H$ (**27**) and CO_2

Treatment of a C_6D_6 solution of **27** with 1 atm of $^{13}CO_2$ led to the very rapid consumption of **27** and formation of the formate hydride complex $Ru(IMe_4)_2(PPh_3)(\kappa^2\text{-}OCHO)H$ (**9**) as the major ruthenium containing product of the reaction. Another four, albeit minor, ruthenium hydride-containing products (**28a-d**) were also formed, as well as **A** and **B** (in a ratio of *ca*. 4:3 after 2.5 h) from the stoichiometric reduction of $^{13}CO_2$ (Scheme 5.5).

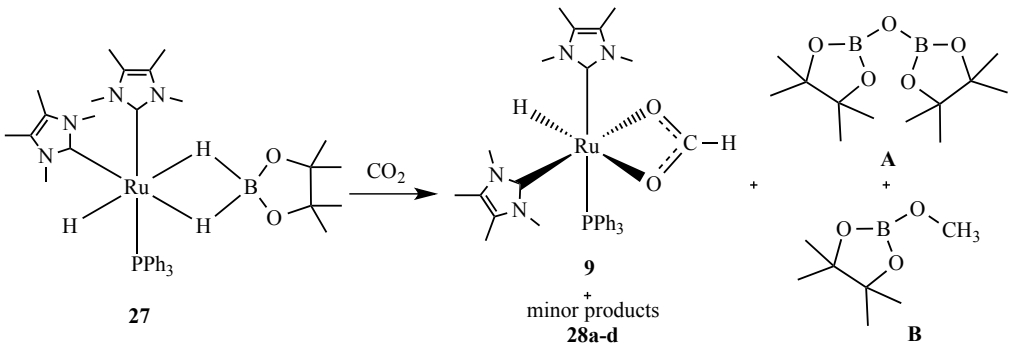

*Scheme 5.5: Reaction of $Ru(IMe_4)_2(PPh_3)H[(\mu\text{-}H)_2Bpin]$, **27** with $^{13}CO_2$ to give major product **9**, minor products **28a-d**, along with **A** and **B**.*

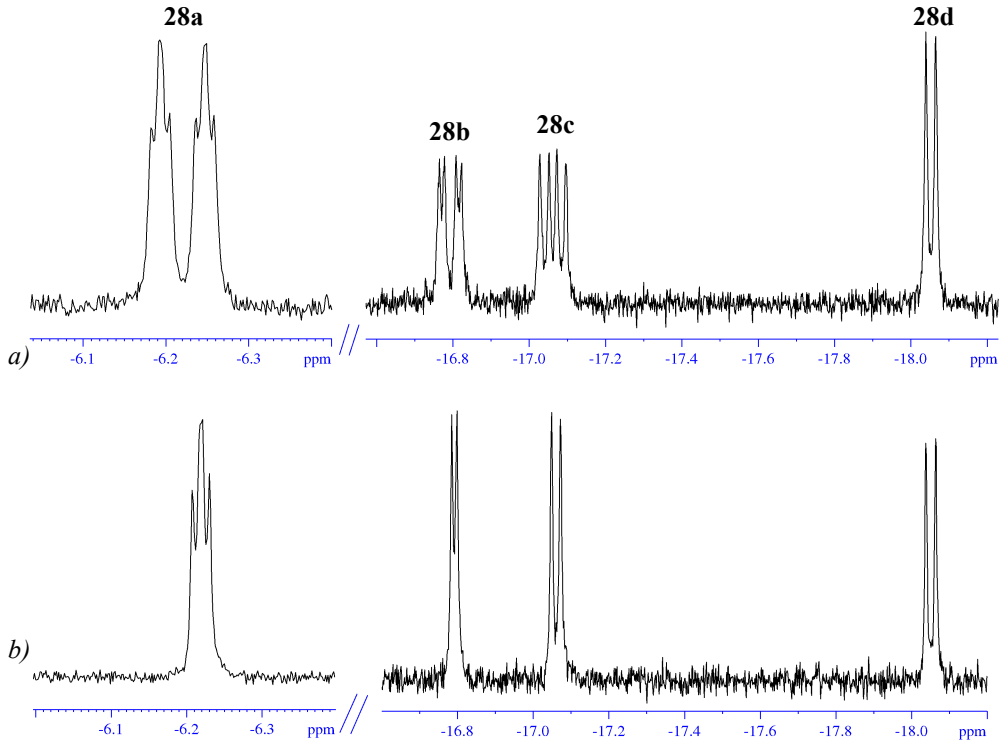

*Figure 5.9: Selected regions of a) the ^{1}H NMR spectrum and b) corresponding $^{1}H\{^{31}P\}$ NMR spectrum from reaction of **27** and $^{13}CO_2$ after 24 h (C_6D_6, 298 K, 500 MHz).*

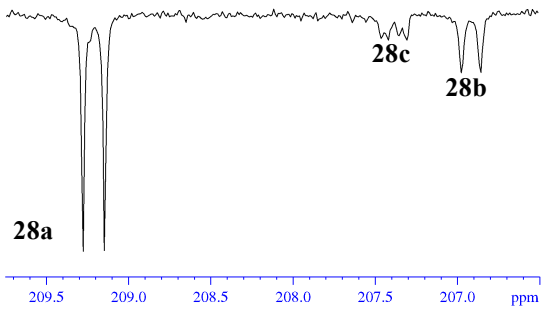

*Figure 5.10: Selected region of the $^{13}C\{^{1}H\}$ NMR spectrum of the reaction between **27** and $^{13}CO_2$ after 3 h of reaction time (C_6D_6, 298 K, 500 MHz).*

The most abundant of the minor products, **28a**, was assigned to the carbonyl formate hydride species, shown in Figure 5.11. The product showed a doublet of triplets hydride resonance at δ_H -6.22; measurement of the $^{1}H\{^{31}P\}$ spectrum (Figure 5.9b) along with ^{1}H-^{13}C and ^{1}H-^{31}P HSQC experiments afforded (i) $^{2}J_{HP}$ and $^{2}J_{HC}$ splittings of 26.4 Hz and 5.5 Hz respectively (indicative of a structure with *cis* H-Ru-P and *cis* H-Ru-CO ligands), (ii) correlation to a doublet resonance at δ_P 45.3 ($^{2}J_{PC}$ = 16.8 Hz, consistent with *cis* P-Ru-CO) and (iii) correlation to two resonances in the $^{13}C\{^{1}H\}$

NMR spectrum, a singlet at δ_C 173.9 (Ru-OCOH) and a doublet at δ_C 209.2 ($^2J_{CP}$ = 16.8 Hz, Ru-CO, Figure 5.10).[10] A relatively high frequency Ru-H resonance supports a coordinatively saturated complex, where no NHC has dissociated from **27**, implying a κ^1 bound formate in **28a**. The low concentration of **28a** ruled out the possibility of recording $^{13}C\{^1H\}$ spectra with enough signal to noise to observe the C_{NHC} resonances. Moreover, attempts to measure IR data to confirm the κ^1 binding mode of the formate ligand proved unsuccessful again due to the low concentration of the product that was generated. Formation of ^{13}CO clearly implies $^{13}CO_2$ is reduced to afford the ^{13}CO ligand.[4c]

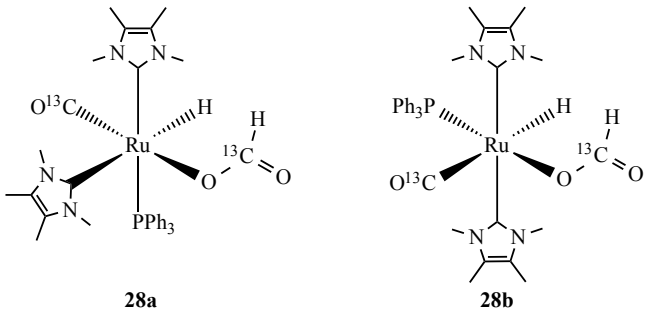

*Figure 5.11: Possible geometries of **28a** and **28b**.*

The structure of the hydride containing product with δ_H -16.79 can be suggested as the *trans*-IMe_4 complex **28b** (Figure 5.11) on the basis of *cis*-^{31}P and ^{13}C couplings to RuH (22.5 and 5.8 Hz respectively) and a *cis* $^2J_{PC}$ splitting of 14.7 Hz between the ^{31}P signal at δ_P 48.2 to a Ru-CO resonance at δ_C 206.9. Formate resonances were observed at δ_H 8.71 (^1H NMR) and δ_C 170.7 (^{13}C NMR).

The hydride containing products **28c-d** were formed in very small amounts and so could not be definitely characterized. It was apparent from the $^1H\{^{31}P\}$ NMR spectrum that they contained ^{13}CO and that **28d** did not contain a PPh_3 ligand.

5.2.1.5. Stoichiometric reaction of $Ru(IMe_4)_2(PPh_3)(OCHO)H$ (**9**) and HBpin

Treatment of **9** with an equimolar amount of HBpin formed $Ru(IMe_4)_2(PPh_3)(H_2Bpin)H$ (**27**) as the major Ru containing compound, along with **A** and **B** from the reduction of CO_2. After 24 h, the ratio of **A** to **B** was 4:1 and no free HBpin remained. This reaction resulted in the formation of more minor hydride containing products (Figure 5.12) than in the reaction of **27** with $^{13}CO_2$.

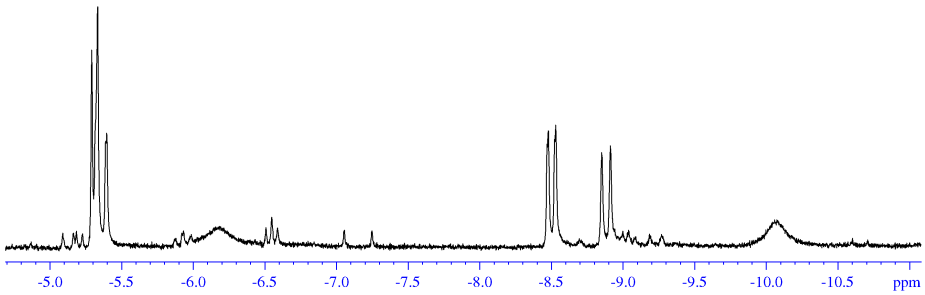

*Figure 5.12: Hydride region of ^{1}H NMR spectrum of reaction of **9** with HBpin after 48 h (C_6D_6, 298 K, 500 MHz).*

5.2.2. Reactivity of $Ru(IEt_2Me_2)_2(PPh_3)_2H_2$ (**5b**) and its derivatives

5.2.2.1. Reactivity of **5b** and HBpin

In contrast to the need for elevated temperature in the stoichiometric reaction of **4a** with HBpin described in section 5.2.1.1., HBpin reacted with **5b** at room temperature in toluene over 24 h. A near colourless precipitate of $Ru(IEt_2Me_2)_2(PPh_3)(H_2Bpin)H$ (**29**) was isolated in 58 % yield. Recrystallisation from hexane/benzene afforded single crystals appropriate for X-ray crystallography. The molecular structure of **29** is shown in Figure 5.13.

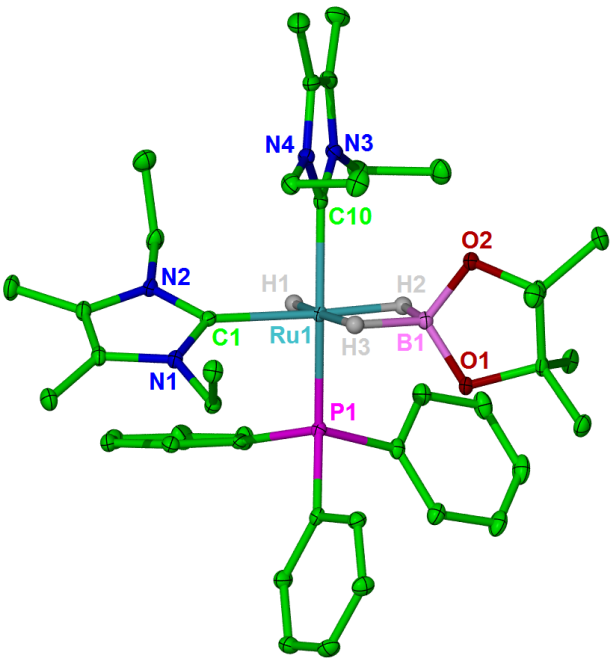

*Figure 5.13: Molecular structure of **29**. Ellipsoids are shown at the 30% level. Hydrogen atoms except for those coordinated to Ru are removed for clarity. Selected bond lengths (Å) and angles (°) in **29**: Ru-C(1) 2.113(2), Ru-C(10) 2.082(2), Ru-P(1) 2.2960(5), Ru-B 2.128(2), C(8)-Ru-P(1) 162.86(6).*

The ruthenium bound hydrogen atoms H(1)-H(3) were again located and those attached to boron freely refined. The B1-H2 and B1-H3 values of 1.51(2) and 1.42(2) Å support the same dihydridoborate hydride structure as in **27** but the same conflicting data applied, i.e. the short Ru-B distance (2.128(2) Å) and shift of ^{11}B NMR signal (δ_B 37) to a higher frequency relative to HBpin. The Ru/B/O,O angle (173.5°) was comparable to that in **27** and was again midway between those reported for σ-borane and dihydridoborate ligands.[9]

The ^{1}H NMR spectrum of **29** was essentially identical to that of **27**, with two broad Ru-H-B singlets at δ_H -6.30 and -10.69 and a doublet Ru-H resonance at δ_H -8.96 ($^2J_{HP}$ = 31.8 Hz). The NOESY spectrum (Figure 5.14) showed a correlation between the Ru-H and the lower frequency broad B-H resonance suggesting it is the one *cis* to Ru-H and *trans* to NHC. This is consistent to data previously reported for the borohydride complexes Ru(IMes)(PPh_3)(CO)(BH_4)H and Ru(IMes)$_2$(CO)(BH_4)H, where the hydride resonance for the B-H *cis* to the Ru-H is at a lower frequency than the B-H *trans* to Ru-H.[11]

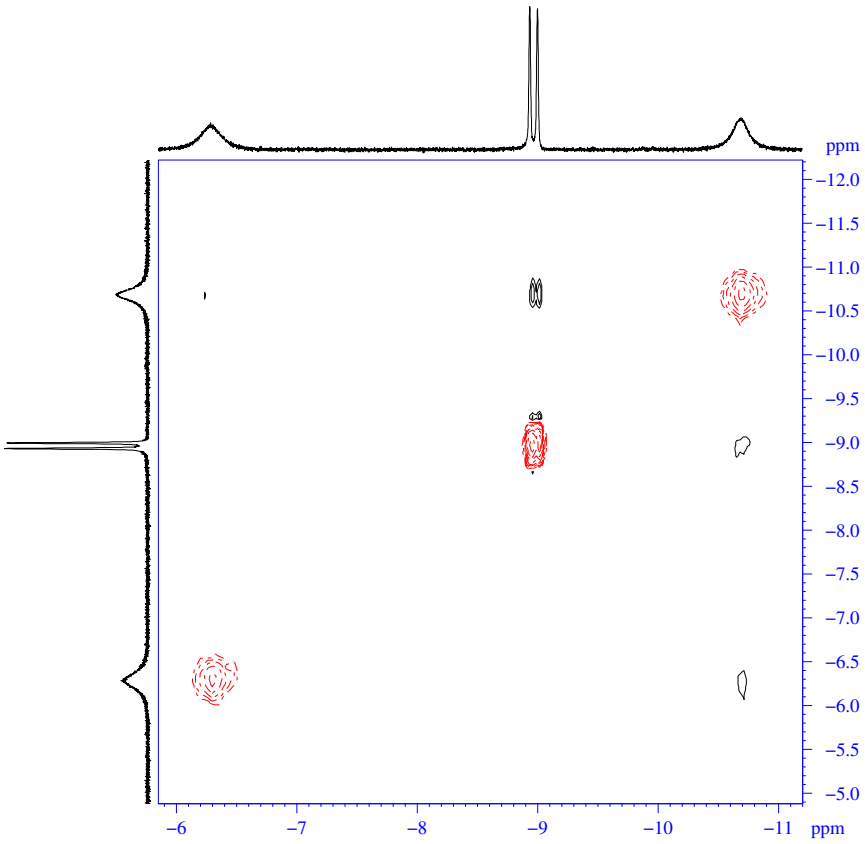

*Figure 5.14: Selected region of the NOESY spectrum of complex **29** (C_6D_6, 298 K, 500 MHz)*

At higher frequency, eight multiplets were apparent between δ_H *ca.* 6-3 (Figure 5.15) consistent with all of the methylene protons of the two IEt_2Me_2 ligands being diastereotopic. The Me resonances of the Bpin group were broad at 298 K (Figure 5.16a), but sharpened somewhat upon cooling to 273 K (Figure 5.16b), indicative of some fluxional behaviour at room temperature.

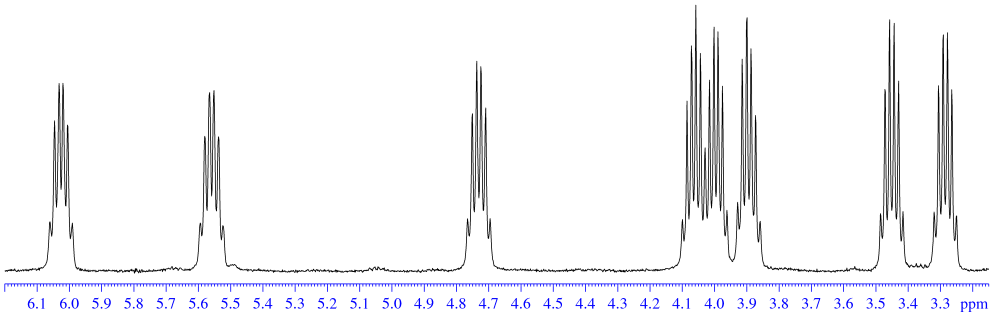

*Figure 5.15: Partial ^1H NMR spectrum of **29** showing the diastereotopic methylene resonances of the IEt_2Me_2 ligands (C_6D_6, 298 K, 500 MHz)*

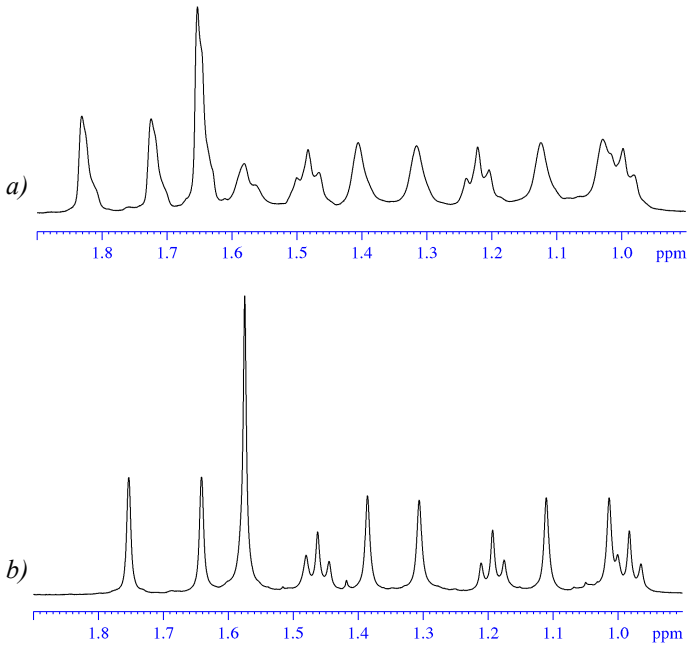

*Figure 5.16: Methyl region of the ^1H NMR spectrum of **29** at a) 298 K and b) 273 K (toluene-d_8, 400 MHz).*

Measurement of the T_1 values for the three low frequency signals at δ_H -6.30, -8.96 and -10.69 over the temperature range 298-198 K afforded $T_{1(min)}$ values at 400 MHz of 145 ms (263 K), 221 ms (268 K) and 157 ms (251 K) respectively. These values compare to the T_1 values 130 ms and 145 ms (214 K) and 131 ms and 129

ms (298 K) for Ru(H_2BH_2) in Ru(IMes)$_2$(CO)(BH_4)H and Ru(IMes)(PPh_3)(CO)(BH_4)H respectively.[11] The corresponding Ru-H values were 994 and 853 ms. In the case of **29**, the $T_{1(min)}$ of Ru-H is clearly much shorter than expected, suggesting that it contains some B-H character and vice versa. The $^{11}B\{^1H\}$, $^{31}P\{^1H\}$ and $^{13}C\{^1H\}$ NMR spectra of **29** were similar in appearance to those recorded for **27**.

5.2.2.2. Catalytic reduction of $^{13}CO_2$ using **5b**

As for the IMe_4 complexes, reduction of $^{13}CO_2$ by HBpin in the presence of Ru(IEt_2Me_2)$_2$(PPh_3)$_2H_2$ (**5b**) as the catalyst (4 mol % loading) gave broad unidentified resonances in the ^1H and $^{13}C\{^1H\}$ NMR spectra at early times, as illustrated in Figures 5.17a and 5.17b respectively.

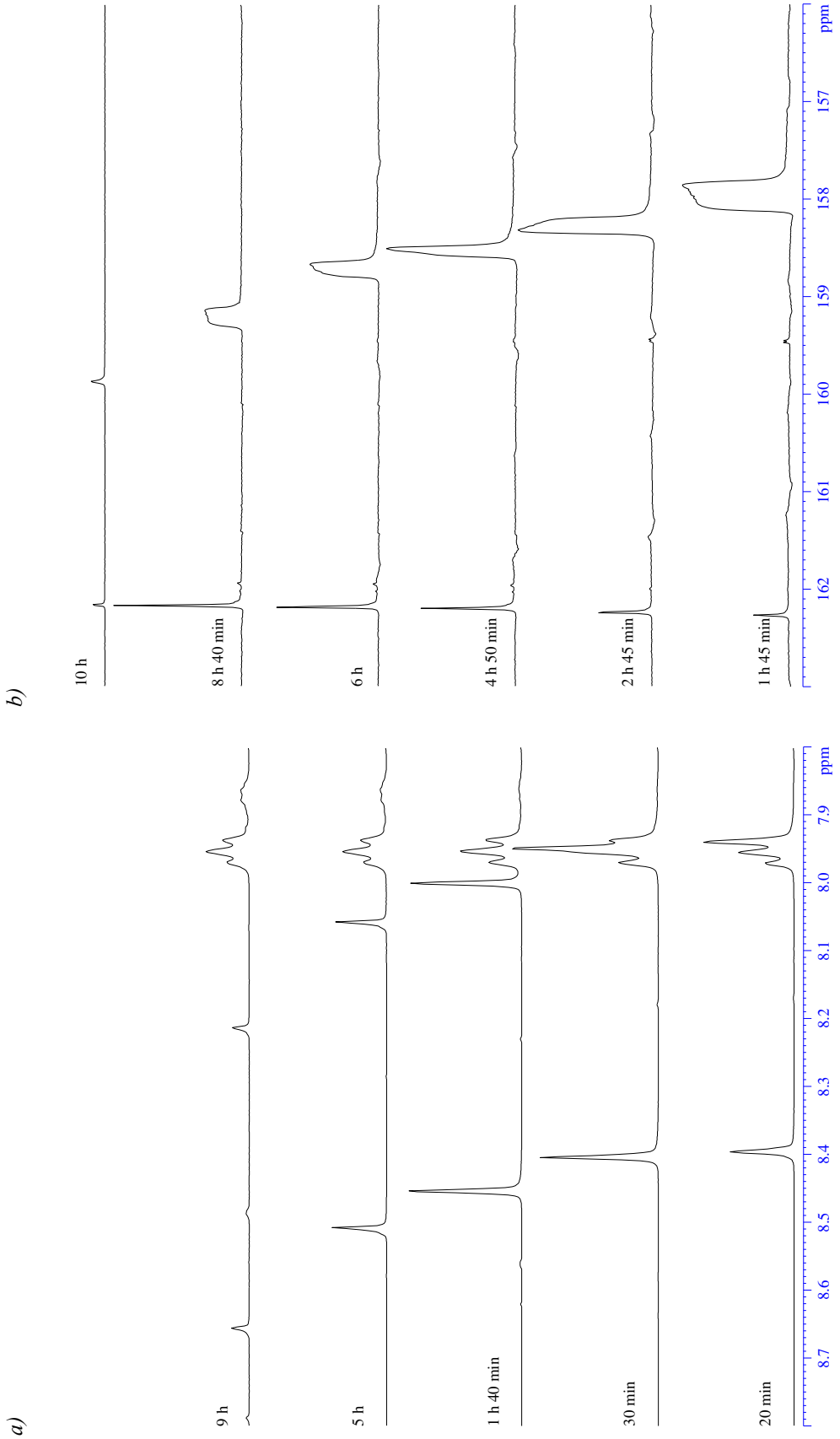

*Figure 5.17: Selected regions of the a) ^{1}H (500 MHz, 298 K) and b) $^{13}C\{^{1}H\}$ NMR (126 MHz, 298 K) spectra of a C_6D_6 solution of **5b**, HBpin and $^{13}CO_2$ at various times.*

Frustrated by the continual appearance of such signals, and an inability to characterize the species responsible due to the constant evolution over the first few hours of reaction, in the case of **5b**, further attempts were made to address this. In a separate reaction, a solution was freeze-pump-thaw degassed 1 h after addition of $^{13}CO_2$ and the volatile components condensed into a second NMR tube for analysis. As shown in Figure 5.18, the signals continued to change even in the absence of any Ru complex!

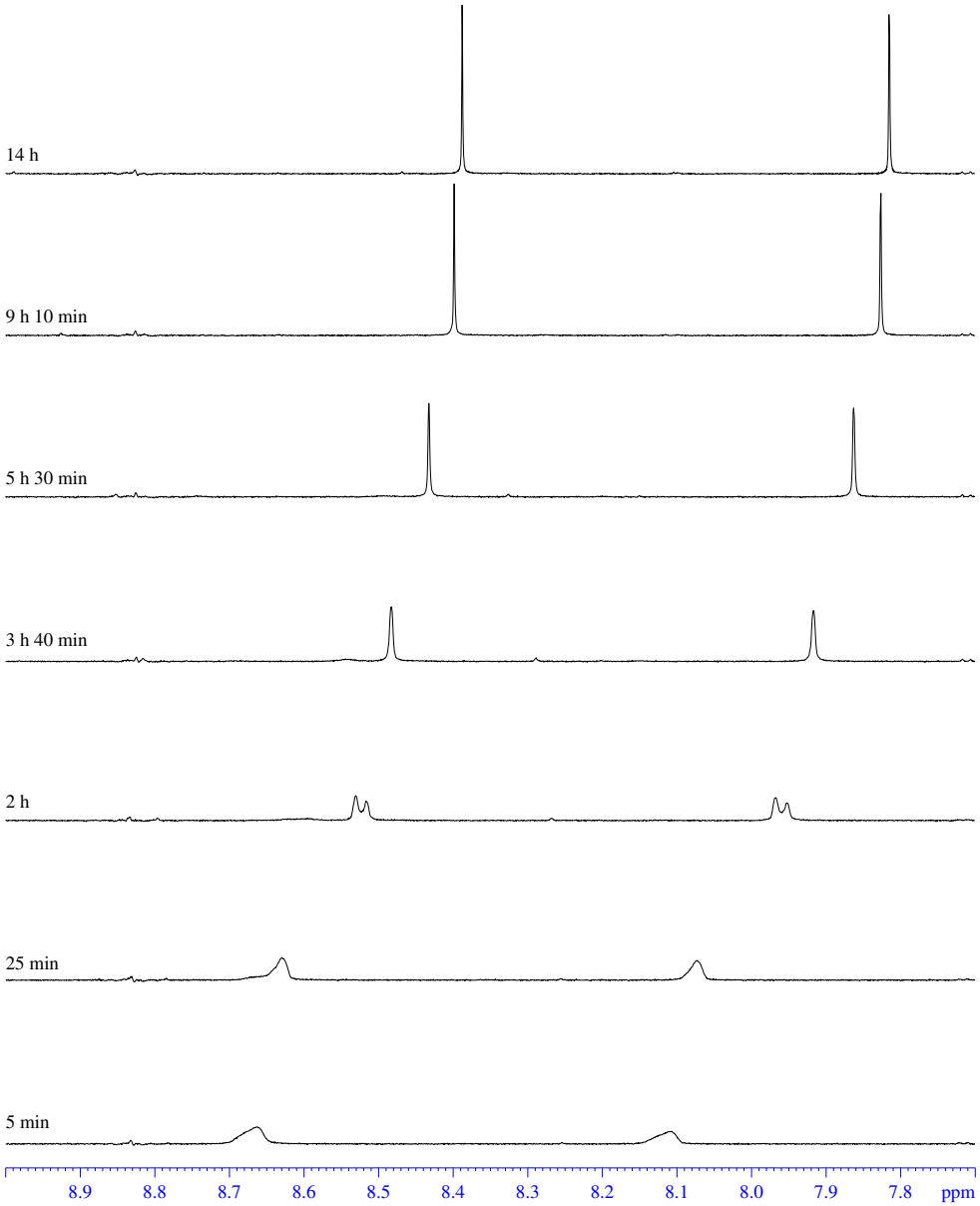

*Figure 5.18: High frequency region of the ^{1}H NMR spectrum of the volatiles from the reaction of **5b**, HBpin and $^{13}CO_2$ (C_6D_6, 298 K, 400 MHz).*

After 14 h, the ^{1}H NMR spectrum had settled down to show a single high frequency doublet at δ_H 8.11 ($^{1}J_{CH}$ = 228.5 Hz), which correlated to a singlet at δ_C 157.3 in the $^{13}C\{^{1}H\}$ NMR spectrum (Figure 5.19). These data are close to those reported for

C (^{1}H: δ_H 8.21, $^{1}J_{CH}$ = 227.3 Hz; ^{13}C: δ_C 159.7), although there was a slight discrepancy in the ^{13}C chemical shift.[4c] Efforts to definitely characterize this product as **C** by GC-MS were unsuccessful.

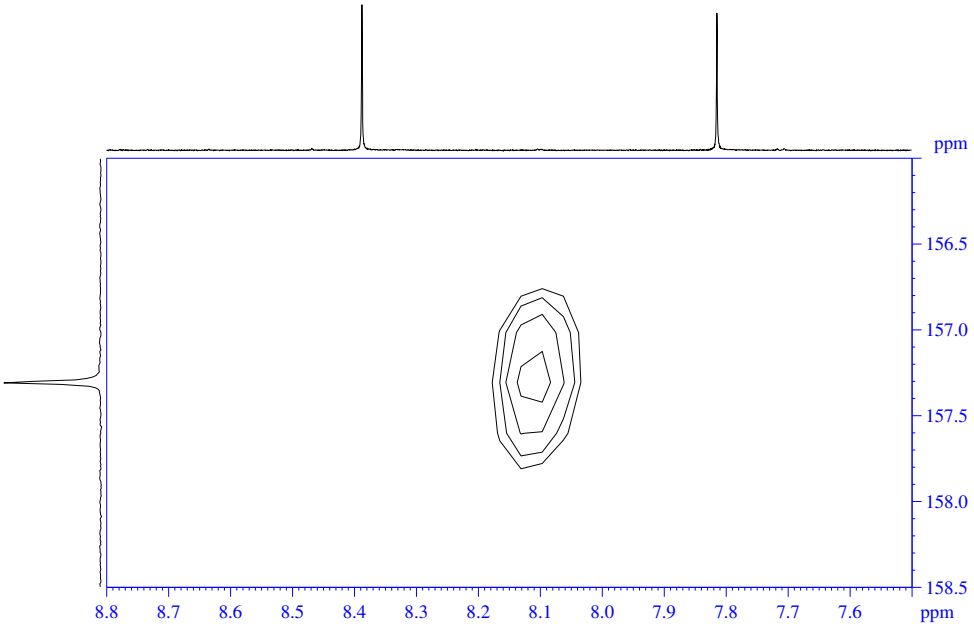

Figure 5.19: Selected region of the ^{1}H-^{13}C HSQC spectrum of the solution of volatiles 14 h after removal from ***5b*** *(C_6D_6, 298 K, 400 MHz)*

In an uninterrupted reaction of $^{13}CO_2$ and HBpin with **5b**, **A**, **B** and **D** were seen in a similar ratio to that found with the IMe_4 complexes. However, a small amount of ^{13}C-labelled **E** was apparent. Two doublet of doublet resonances were present in the ^{1}H NMR spectrum at δ_H 5.39 ($^{1}J_{HC}$ = 170.4 Hz, $^{3}J_{HC}$ = 4.4 Hz) and 7.42 ($^{1}J_{HC}$ = 228.9 Hz, $^{3}J_{HC}$ = 4.0 Hz), along with two doublets in the $^{13}C\{^{1}H\}$ NMR spectrum; the methylene at δ_C 82.5 ($^{2}J_{CC}$ = 2.3 Hz) and the formate at δ_C 159.2 ($^{2}J_{CC}$ = 2.3 Hz).

The distribution of products **A**-**E** as a function of time are shown in Table 5.4. As found before for **4a**, unreacted HBpin was still present in solution after 1 month of reaction. The hydride region of the ^{1}H NMR spectra showed that the major Ru complex in solution was $Ru(IEt_2Me_2)_2(PPh_3)(H_2Bpin)H$, **29**, along with some other small hydride resonances.

Time after $^{13}CO_2$ added	Relative amounts of products (%)			
	HBpin	**A**	**B**	**D**
5 h	46	29	20	5
7 days	31	36	28	5
15 days	30	36	30	4
22 days	26	39	31	4

Table 5.4: Distribution of products from the catalytic reduction of $^{13}CO_2$ by HBpin in the presence of 4 mol % $Ru(IEt_2Me_2)_2(PPh_3)_2H_2$, ***5b****.*

5.2.2.3. Lower pressure catalytic reduction of CO_2 with **5b**

A preliminary study was made of the catalysis with **5b** at a lower pressure of CO_2 (*ca*. 0.5 atm). Again broad resonances were seen in the ^1H NMR spectrum (Figure 5.20), however they persisted for longer than in the reaction with 1 atm of CO_2. The resonances between δ_C 157 and 164 in the $^{13}C\{^1H\}$ NMR spectrum were less broad but still shifted over time. Products **A**, **B**, **D** and **E** could be identified in the ^1H and $^{13}C\{^1H\}$ NMR spectra in a similar ratio to that seen previously. Unreacted HBpin was present in solution after 7 days and the major Ru containing product was again **29**.

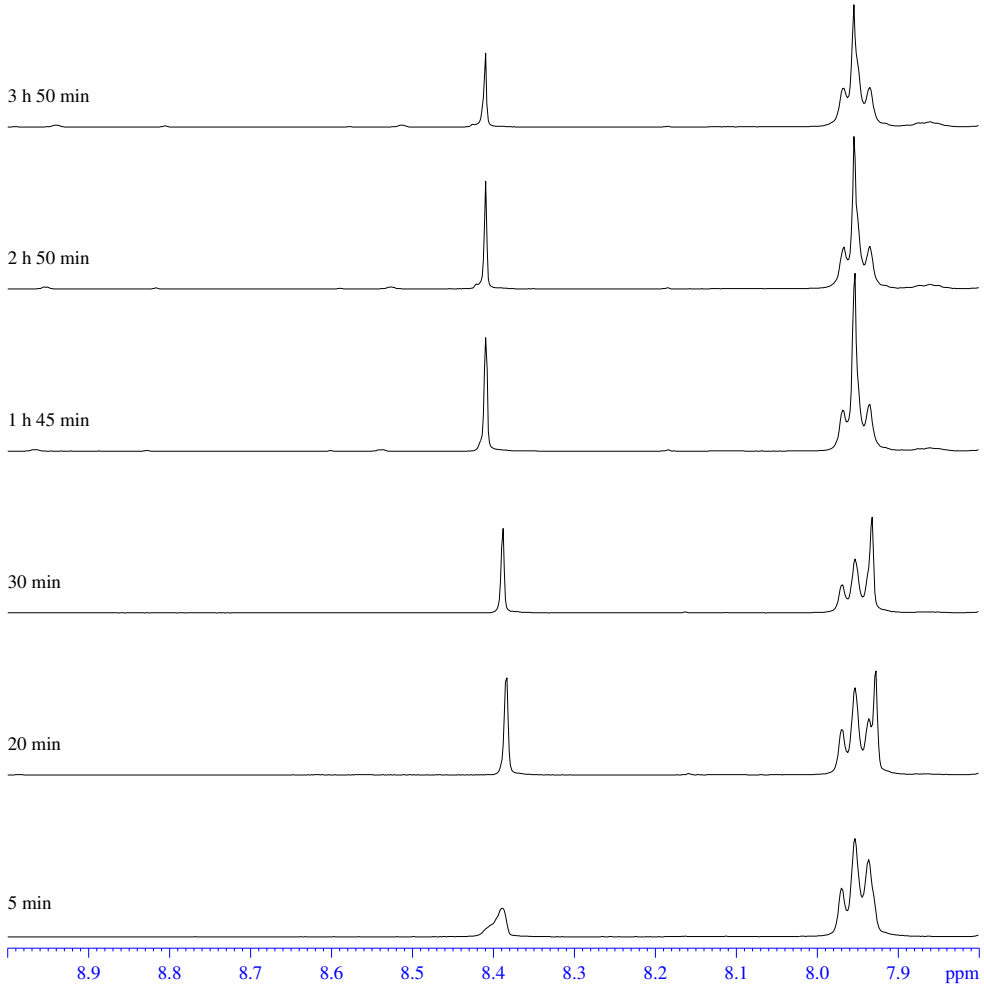

*Figure 5.20: Formate region of the ^{1}H NMR spectra of the reaction between **5b**, 25 equiv. HBpin and 0.5 atm of $^{13}CO_2$ at various times (C_6D_6, 298 K, 400 MHz).*

5.2.2.4. Catalytic reduction of CO_2 at lower loading of HBpin

The reduction of CO_2 by **5b** was repeated using 10 rather than 25 equiv. HBpin. Broad resonances were again seen between *ca*. δ_H 8-9.5 over the first 6 h of the reaction (Figure 5.21), but most noticeable was (i) the increase in the amount of **E** formed and (ii) that all of the HBpin was now consumed over *ca*. 20 h. Within 5 minutes of the CO_2 being added, **E** was present in larger amounts than either **D** or **B**. After 6.5 h, the ratio of **A**:**B**:**D**:**E** was 70:7:2:21. **E** was present for longer than previously seen but was consumed after 2 days. No **D** remained after 16 days, while the amount of **A** was higher than with 25 equiv.; less of product **B** was present.

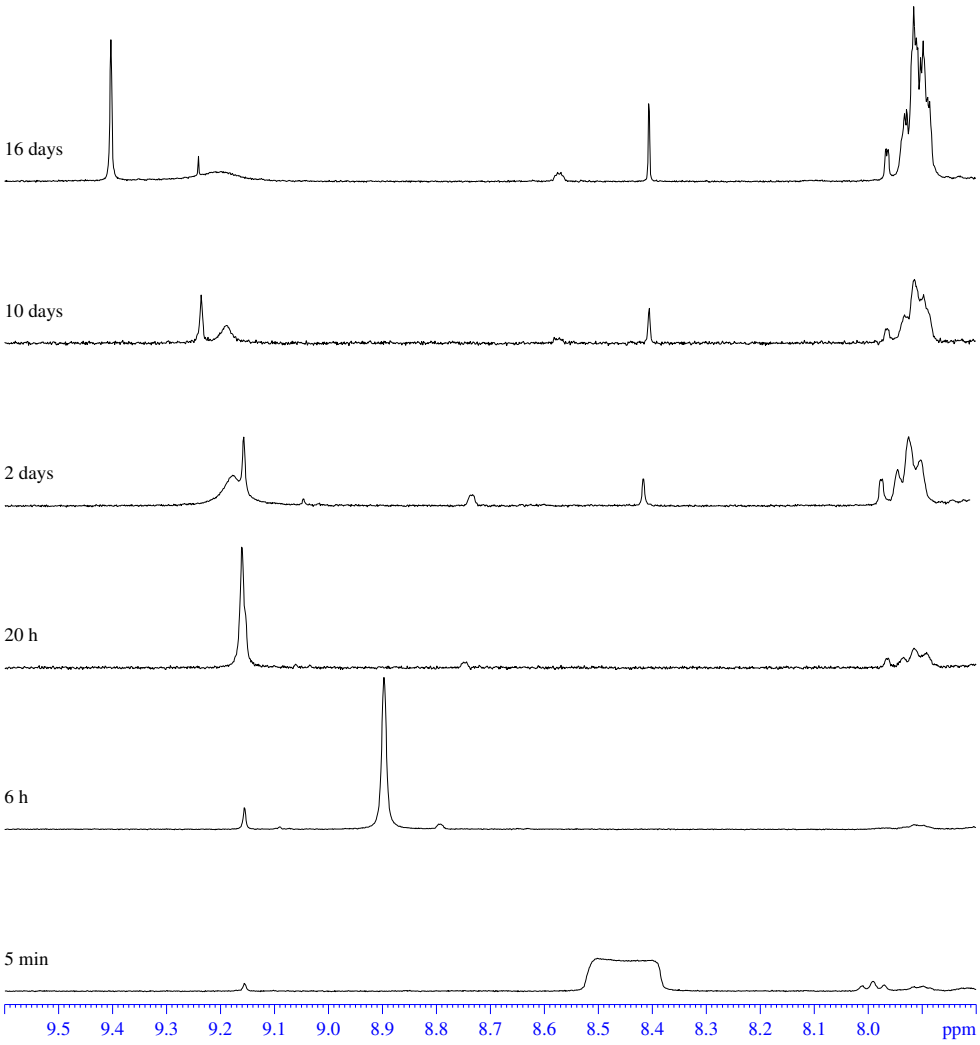

*Figure 5.21: Formate region of the ^{1}H NMR spectrum of the reaction between **5b**, 10 equiv. HBpin and 1 atm $^{13}CO_2$ (C_6D_6, 298 K, 500 MHz)*

5.2.2.5. Catalytic reduction of CO_2 using $Ru(IEt_2Me_2)_2(PPh_3)(H_2Bpin)H$ (**29**) and $Ru(IEt_2Me_2)_2(PPh_3)H(OCOH)$ (**17**)

When C_6D_6 solution of the dihydridoborate complex **29** and 25 equiv. HBpin was put under an atmosphere of $^{13}CO_2$, there was a subtle colour change from clear pale pink to colourless over a 24 h period (as with the analogous IMe_4 complex, **27**). The solution was monitored by ^{1}H, ^{11}B and ^{13}C NMR spectroscopy over 22 days. The major Ru species remaining was the dihydridoborate species **29**. The product ratio was similar to that seen with **5b**, with **E** present at early times and after 5 h the ratio between **A**:**B**:**D** being *ca*. 50:40:10. After 22 days, unreacted HBpin was still present in solution. The broad transient resonances seen at early times in both the ^{1}H and $^{13}C\{^{1}H\}$ NMR spectra were very similar to those seen when **5b** was used as the precursor.

When a C_6D_6 solution of **17** with 25 equiv. HBpin was put under an atmosphere of $^{13}CO_2$, there was a colour change from yellow to a paler yellow over a 24 h period. The solution was monitored by ^{1}H, ^{11}B and ^{13}C NMR spectroscopy over 22 days after which, unreacted HBpin was still present. The transient signals in the ^{1}H and ^{13}C NMR spectra were similar to those seen in the reaction of **29** (Figures 5.22 and 5.23). The distribution of **A**-**E** was much the same as in the reaction with the Ru precursor **29** and, as with both **5b** and **29**, product **E** was formed in small amounts at early times.

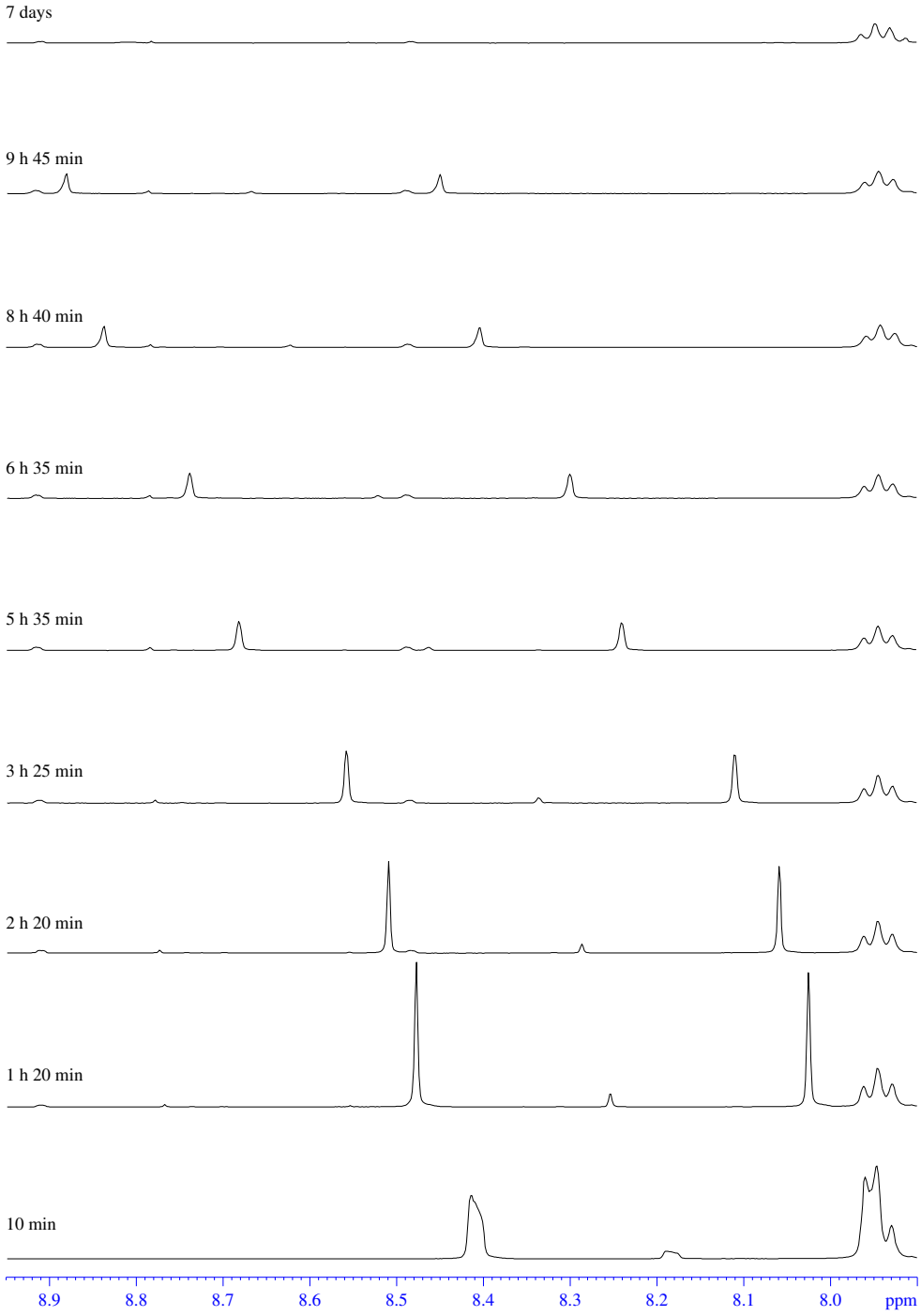

*Figure 5.22: Selected region of the ^{1}H NMR spectrum of the reaction of **17**, $^{13}CO_2$ and HBpin (C_6D_6, 298 K, 500 MHz).*

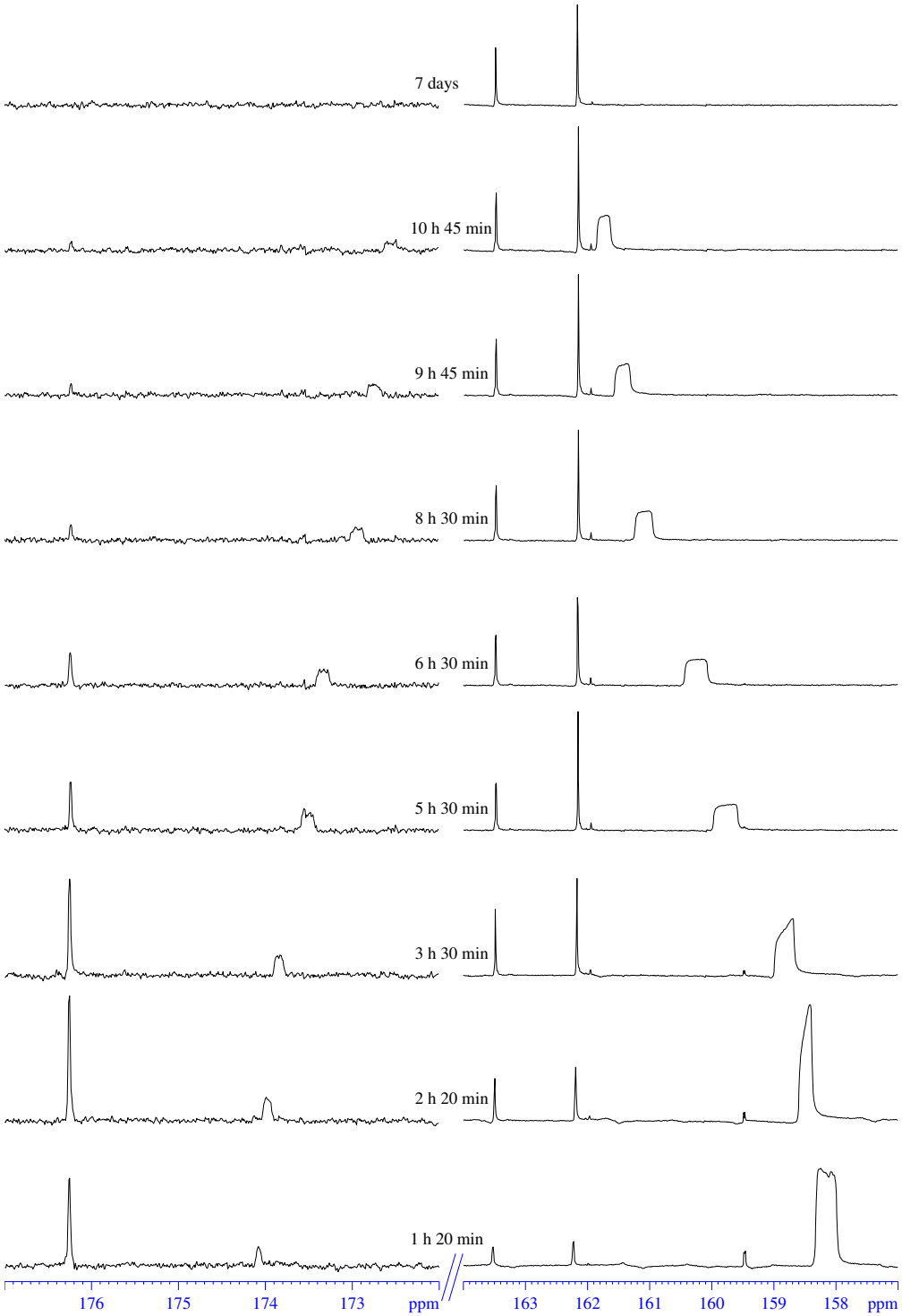

*Figure 5.23: Selected regions of the $^{13}C\{^{1}H\}$ NMR spectrum of the reaction of **17**, $^{13}CO_2$ and HBpin (C_6D_6, 298 K, 126 MHz).*

5.2.2.7. Reactivity of $Ru(IEt_2Me_2)_2(PPh_3)(H_2Bpin)H$ (**29**) and CO_2

The stoichiometric reaction between $Ru(IEt_2Me_2)_2(PPh_3)(H_2Bpin)H$ (**29**) and 1 atm CO_2 resulted in the immediate formation of the formate hydride complex $Ru(IEt_2Me_2)_2(PPh_3)H(OCOH)$ (**17**), and the reduction products **A** and **B**.

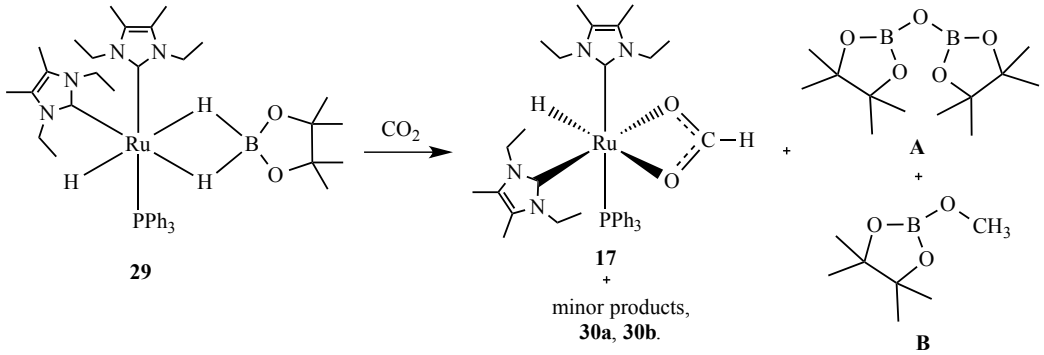

*Scheme 5.6: Reaction of **29** with CO_2 to give major product (**17**), minor products **30a-b** along with products **A** and **B**.*

No other Ru containing species were seen initially, but after 1 h, trace amounts (<3%) of two minor products (**30a** and **30b**) were apparent. These exhibited in the ^1H NMR spectrum doublet of doublet and doublet Ru-H resonances at δ_H -17.18 and δ_H -18.36 respectively, with splittings of 22.4 ($^2J_{HP}$)/12.2 ($^2J_{HC}$) and 12.8 ($^2J_{HC}$) Hz respectively. After 3 days of reaction, the hydride resonances of the minor products were most apparent, with a ratio of **17**:**30a**:**30b** of 27:1:1.3. HSQC experiments showed correlations between the hydride signal at δ_H -17.2 and a singlet resonance in the ^{31}P NMR spectrum (δ_P 47.9) and a doublet carbonyl resonance at δ_C 207.5 ($^2J_{CP}$ = 14 Hz). These data are consistent with the structure (**30a**) shown in Figure 5.24 in which, there is a PPh_3 and CO ligand coordinated to Ru and presumably a κ^1-bound formate group. This structure is in agreement with that of **28a**.

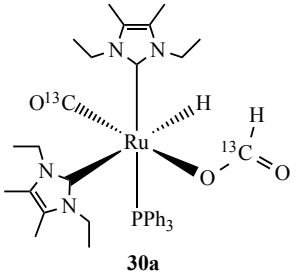

*Figure 5.24: Proposed geometry for minor product **30a**.*

In the case of **30b**, the lack of any phosphorus coupling on the hydride signal at δ_H -18.36 is suggestive of a κ^2-formate ligand to complete an octahedral coordination geometry (Figure 5.25). The presence of ^{13}C-labelled carbonyl ligand was confirmed by correlation of the hydride to a high frequency resonance at δ_C 209.3. The amount of **30b** increased as the reaction progressed, consistent with the evolution of ^{13}CO with time.

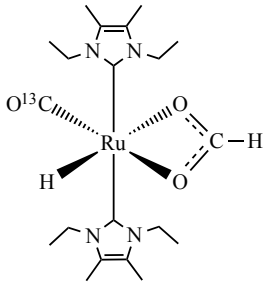

30b

*Figure 5.25: Proposed geometry for minor product **30b**.*

5.2.2.8. Stoichiometric reaction of Ru(IEt$_2$Me$_2$)$_2$(PPh$_3$)H(OCOH) (**17**) and HBpin

Addition of *ca*. 1 equiv. of HBpin to Ru(IEt$_2$Me$_2$)$_2$(PPh$_3$)H(OCOH) resulted in the immediate formation of the dihydroborate complex Ru(IEt$_2$Me$_2$)$_2$(PPh$_3$)(H$_2$Bpin)H (**29**) along with three of the reported products from the reduction of CO_2; **A**, **B** and **D** in a ratio of 57:38:5 respectively (Scheme 5.7).

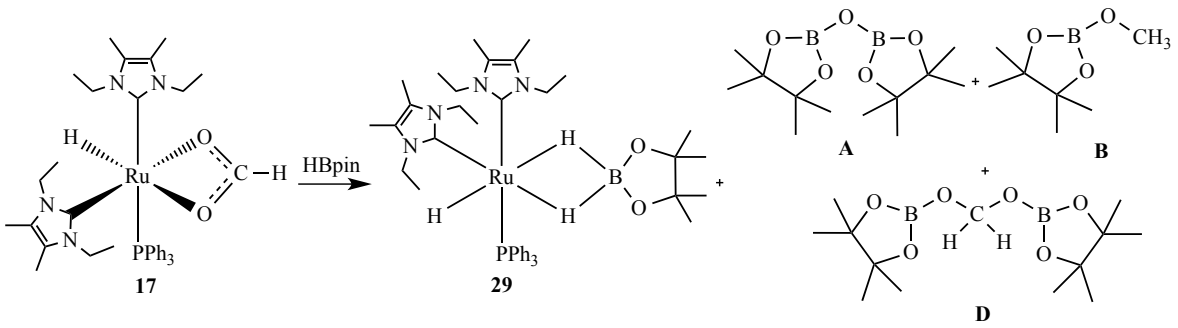

17 **29** **A** **B** **D**

*Scheme 5.7: Reaction of **17** with CO_2 to give **29**, **A**, **B** and **D**.*

5.2.3. Reactivity of $Ru(IMe_4)_4H_2$ (**3**)

5.2.3.1. Catalytic reduction of CO_2 using **3**

Addition of 1 atm $^{13}CO_2$ to a C_6D_6 solution containing **3** and 25 equiv. HBpin resulted in the appearance of ^1H and ^{13}C NMR signals for **A**, **B**, **D** and **E** within minutes, along with the by now familiar unidentifiable broad resonances (Figure 5.26).

The most significant difference in the distribution of products **A**-**E** upon using **3** rather than the mixed NHC/PPh_3 Ru complexes was the larger proportion of **E** formed at early times (before 5 h, **A**:**B**:**D**:**E** 62:23:5:10). Thereafter, the ratio of **A**:**B**:**D** was much the same (*ca*. 50:40:10). Another contrast to the IMe_4 and IEt_2Me_2 phosphine containing precursors was that all 25 equiv. of HBpin were consumed after *ca*. 5 h. At this time, the major ruthenium containing product observable in solution appeared to be the known cationic monocarbonyl complex $[Ru(IMe_4)_4(^{13}CO)H]^+$, on the basis of a doublet hydride resonance at δ_H 3.72 ($^2J_{HC}$ = 30.3 Hz).[12] The nature of the accompanying anion is unknown, although formate seems the most likely possibility.

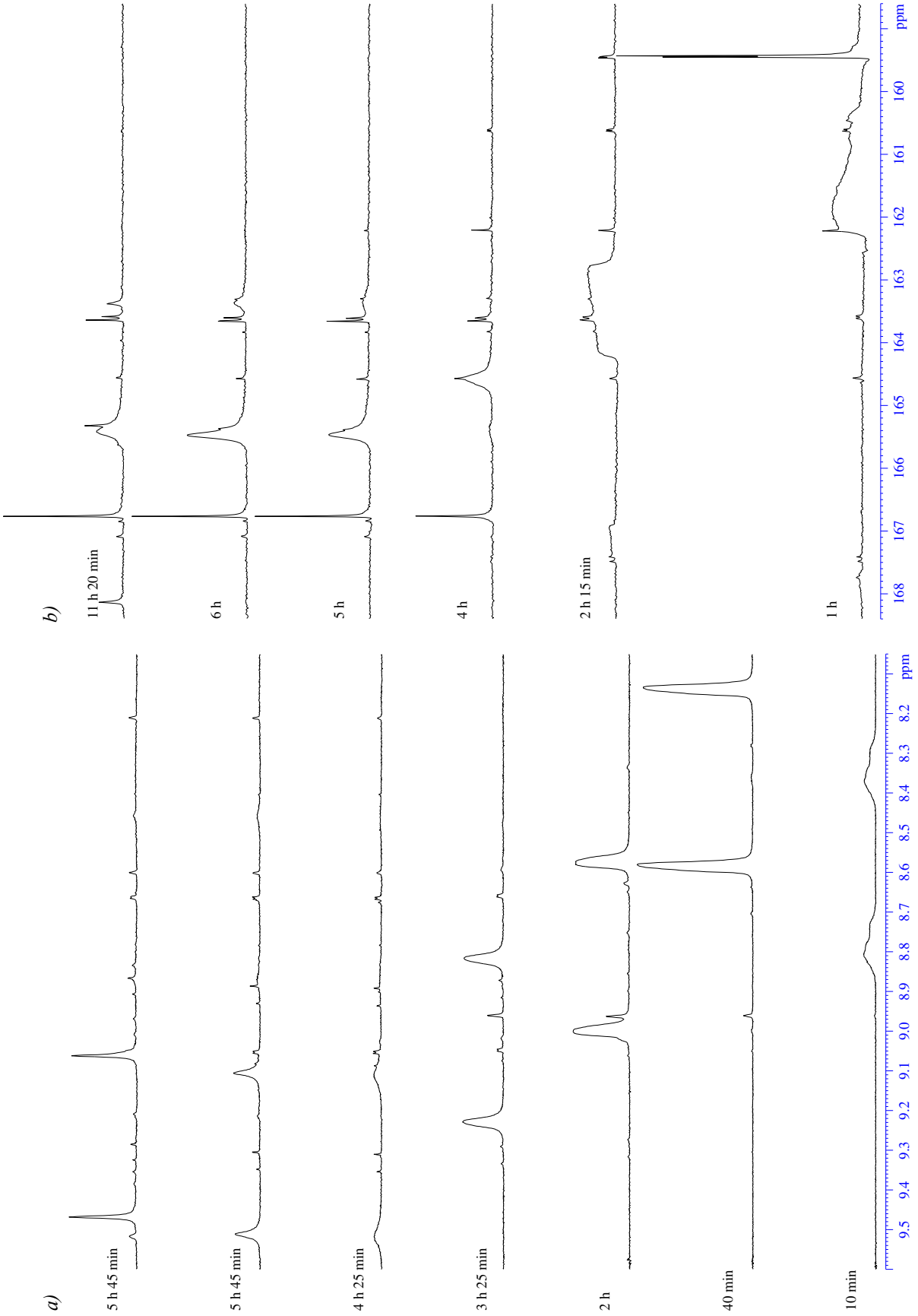

*Figure 5.26: Selected regions of a) the ^{1}H NMR (500 MHz) and b) the $^{13}C\{^{1}H\}$ NMR (126 MHz) spectra of the reaction of **3**, HBpin and $^{13}CO_2$ (C_6D_6, 298 K).*

5.2.3.2. Reaction of **3** and HBpin

In contrast to the formation of easily identifiable products upon addition of HBpin to $Ru(NHC)_2(PPh_3)_2H_2$, addition of 25 equiv. HBpin to a toluene solution of **3** only resulted in a significant broadening of the Ru-H resonance at δ_H -7.58 (almost into the baseline), with no new resonances observed (Figure 5.27).

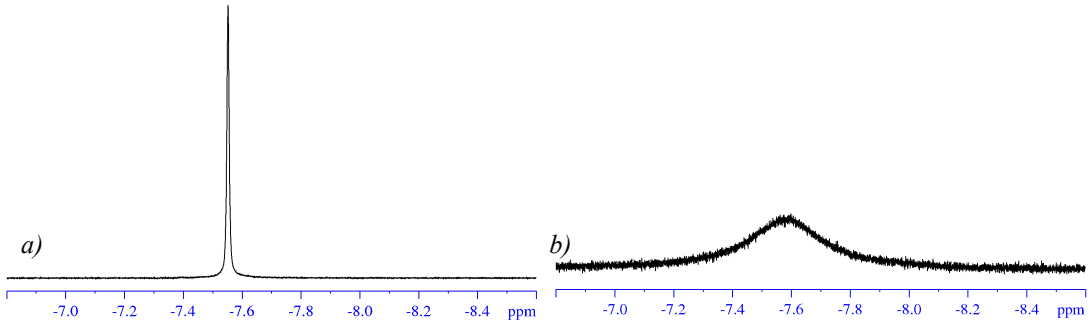

*Figure 5.27: a) Hydride region of ^{1}H NMR spectrum of **3**, b) hydride region of ^{1}H NMR spectrum of **3** with 25 equiv. HBpin (toluene-d_8, 298 K, 400 MHz)*

The hydride signal sharpened progressively upon cooling to 223 K and then broadened again and disappeared into the baseline by 193 K (Figure 5.28).

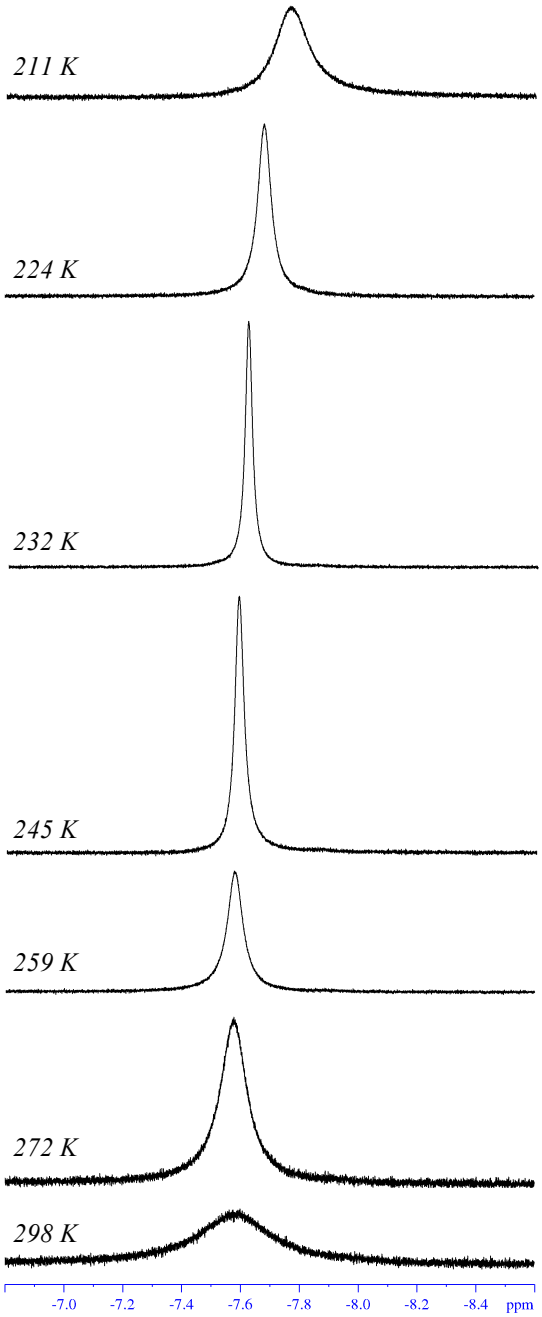

*Figure 5.28: Hydride region of the variable temperature ^{1}H NMR spectrum of a toluene-d_8 solution of **3** with 25 equiv. HBpin (400 MHz).*

5.2.4. Summary and Conclusions

$Ru(NHC)_2(PPh_3)_2H_2$ (NHC = IMe_4, IEt_2Me_2) and $Ru(IMe_4)_4H_2$ have been shown to be active catalytic precursors for the reduction of CO_2 by HBpin. In all cases, a similar series of reduction products to those reported by Sabo-Etienne (Scheme 5.1) were formed. This distribution of species was found to vary only marginally between the dihydride precursors and the species formed by the individual stoichiometric reactions of the mixed NHC-PPh_3 complexes with HBpin ($Ru(NHC)_2(PPh_3)(H_2Bpin)H$)

and CO_2 ($Ru(NHC)_2(PPh_3)(OCHO)H$, see Chapter 3). Three points warrant particular discussion.

1. *Formation of broad high frequency ^1H and ^{13}C resonances at early times:* The quite remarkable broad signals (typified by those shown in Scheme 5.7 (**27**) were a feature of all the catalytic reactions and remain unidentified. Such signals were found to propogate even in the absence of ruthenium, further hampering their identification. It is worth commenting that their appearance in some cases is reminiscent of the types of signals apparent in solid-state NMR spectra[13] although all solutions were homogeneous in appearance throughout the catalytic reactions
2. *Conversion of HBpin:* In all cases the $Ru(NHC)_2(PPh_3)$ derived catalysts were unable to bring about conversion of all 25 equiv. HBpin even over a period of 3 weeks. This contrasts to the 89 % conversion achieved by $Ru(PCy_3)_2(\eta^2\text{-}H_2)_2H_2$ at 1 mol% Ru loading over 10 h,[4c] and also to the ability of $Ru(IMe_4)_4H_2$ (**3**) to react fully over 5 h.
3. *Mechanism of reaction of **3**:* In contrast to the known ligand lability of PPh_3 in $Ru(IMe_4)_2(PPh_3)_2H_2$ (**4a**), the lack of a vacant coordination site on $Ru(IMe_4)_4H_2$ might at first sight exclude **3** from being active for CO_2 reduction. The possibility of an outer-sphere reaction of **3** with CO_2 to form $Ru(IMe_4)_4(OCHO)H$[14] and subsequent reaction with HBpin are in the process of being probed computationally.

5.3. Experimental

5.3.1. Synthesis of $Ru(IMe_4)_2(PPh_3)(H_2Bpin)H$ (**27**)

$Ru(IMe_4)_2(PPh_3)_2H_2$ (**4a**) (150 mg, 0.17 mmol) was placed in a J. Youngs resealable ampoule with HBpin (124 μL, 0.86 mmol) in C_6H_6 (20 ml) and the solution stirred at 70 °C for 96 h. Removal of the solvent left a peach coloured oil. Hexane (10 mL) was added and the suspension stirred for 1 h. After concentration to half volume, the resulting precipitate was isolated by filtration and dried in vacuo. Yield: 70 mg (40 %). Recrystallisation from benzene/hexane afforded material appropriate for X-ray crystallography and elemental analysis. ^1H NMR (500 MHz, toluene-d_8, 259 K): δ 8.06 (m, 6H, PC_6H_5), 7.13 (br, 15H, PC_6H_5), 4.02 (s, 3H, NCH_3), 3.66 (s, 3H, NCH_3), 3.13 (s, 3H, NCH_3), 2.99 (s, 3H, NCH_3), 1.55 (s, 3H, $NCCH_3{=}NCCH_3$), 1.45 (s, 3H, $NCCH_3{=}NCCH_3$), 1.43 (s, 3H, $NCCH_3{=}NCCH_3$), 1.40 (s, 3H $NCCH_3{=}NCCH_3$), 1.37 (s, 3H, CH_3(pin)), 1.26 (s, 3H, CH_3(pin)), 1.23 (s, 3H, CH_3(pin)), 1.17 (s, 3H,

CH_3(pin)), -6.17 (br s, 1H, Ru*H*), -8.91 (d, $^2J_{HP}$ = 30.2 Hz, 1H, Ru*H*), -10.05 (br s, 1H, Ru*H*); $^{31}P\{^1H\}$ NMR (202 MHz, C_6D_6): δ 61.7 (s); $^{11}B\{^1H\}$ NMR (160 MHz, C6D6): δ 36.7 (br s, $w_{½}$ = 330 Hz); $^{13}C\{^1H\}$ NMR (126 MHz, C_6D_6): δ 198.5 (d, $^2J_{CP}$ = 11.0 Hz, Ru-C_{NHC}), 195.0 (d, $^2J_{CP}$ = 89.7 Hz, Ru-C_{NHC}), 144.3 (d, $^2J_{CP}$ = 29.1 Hz, PC_6H_5), 122.6 (s, PC_6H_5), 38.0 (s, NCH_3), 36.9 (s, NCH_3), 35.5 (s, NCH_3), 35.0 (s, NCH_3), 25.4 (s, *C*pin), 25.1 (s, *C*pin), 24.8 (s, *C*pin), 9.9 (s, NCCH_3=NCCH_3), 9.6 (s, NCCH_3=NCCH_3), 9.4 (s, NCCH_3=NCCH_3), 9.3 (s, NCCH_3=NCCH_3); elemental analysis calc'd (%) for $C_{38}H_{54}BN_4O_2PRu$ (742.31): C, 61.53; H, 7.34; N, 7.55; found: C, 61.47; H, 7.21; N, 7.67.

5.3.2. Catalytic reduction of CO_2 employing Ru(IMe_4) based complexes

In a J. Young's resealable NMR tube, (**4a**, 7 mg), Ru(IMe_4)$_2$(PPh_3)(H_2Bpin)H (**27**, 10 mg) or Ru(IMe_4)$_2$(PPh_3)(OCHO)H (**9**, 10 mg) were combined with 25 equiv. HBpin in C_6D_6 (0.4 mL) and the solutions freeze-pump-thaw degassed. 1 atm $^{13}CO_2$ was introduced and the reactions monitored by multinuclear NMR spectroscopy.

5.3.3. Stoichiometric reaction of Ru(IMe_4)$_2$(PPh_3)(H_2Bpin)H and CO_2

Addition of 1 atm of CO_2 to a C_6D_6 (0.4 mL) solution of Ru(IMe_4)$_2$(PPh_3)H(H_2Bpin)H (10 mg, 0.014 mmol) in a J. Young's resealable NMR tube led to a slight colour change from an orange/yellow solution to yellow. NMR spectroscopy showed formation of **9** and three minor products **28a**, **28b** and **28c**. Selected NMR data for **28a**: ^1H NMR (500 MHz, C_6D_6): δ 8.52 (d, $^1J_{HC}$ = 192.5 Hz, 1H, Ru-OC*H*O), -6.22 (dt, $^2J_{HP}$ = 26.4 Hz, $^2J_{HC}$ = 5.5 Hz, 1H, RuH). $^{31}P\{^1H\}$ NMR (202 MHz, C_6D_6): δ45.3 (d, $^2J_{PC}$ = 16.8 Hz). $^{13}C\{^1H\}$ NMR (126 MHz, C_6D_6): 209.2 (d, $^2J_{CP}$ = 16.7 Hz, Ru-*C*O), 173.9 (s, Ru-O*C*HO). Selected NMR data with for **28b**: ^1H NMR (500 MHz, C_6D_6): δ 8.71 (d, $^1J_{HC}$ = 192.9 Hz, 1H, Ru-OC*H*O) δ -16.79 (dd, $^2J_{HP}$ = 22.5 Hz, $^2J_{HC}$ = 5.8 Hz, Ru*H*). $^{31}P\{^1H\}$ NMR (202 MHz, C_6D_6): δ48.2 (d, $^2J_{PC}$ = 14.7 Hz). $^{13}C\{^1H\}$ NMR (126 MHz, C_6D_6): δ 206.9 (d, $^2J_{CP}$ = 14.7 Hz, Ru-*C*O), 170.7 (s, Ru-O*C*HO). Selected NMR data for **28c**: ^1H NMR (500 MHz, C_6D_6): δ -17.06 (dd, $^2J_{HP}$ = 21.6 Hz, $^2J_{HC}$ = 12.1 Hz, Ru*H*). $^{31}P\{^1H\}$ NMR (202 MHz, C_6D_6): δ 47.4 (d, $^2J_{PC}$ = 12.8 Hz). $^{13}C\{^1H\}$ NMR (126 MHz, C_6D_6): δ 207.4 (dd, $^2J_{CP}$ = 14.1 Hz, $^2J_{CH}$ = 6.8 Hz, Ru-*C*O). Selected NMR data for **28d**: ^1H NMR (500 MHz, C_6D_6): δ -18.05 (d, $^2J_{HC}$ = 12.8 Hz). $^{13}C\{^1H\}$ NMR (126 MHz, C_6D_6): δ 209.2 (s, Ru-*C*O).

5.3.4. Stoichiometric reaction of $Ru(IMe_4)_2(PPh_3)(OCHO)H$ (**9**) and HBpin

Addition of 1 equiv. of HBpin (1.8 μL, 0.012 mmol) to a C_6D_6 solution of $Ru(IMe_4)_2(PPh_3)(OCHO)H$ (8 mg, 0.012 mmol) rapidly afforded a mixture of products, the major one of which was $Ru(IMe_4)_2(PPh_3)(H_2Bpin)H$, **27**.

5.3.5. Synthesis of $Ru(IEt_2Me_2)_2(PPh_3)(H_2Bpin)H$ (**29**)

Stirring a toluene (10 mL) solution of **5b** $Ru(IEt_2Me_2)_2(PPh_3)_2H_2$ (160 mg, 0.17 mmol) and HBpin (50 μL, 0.34 mmol) at room temperature for 24 h led to a colour change from orange to pale orange/pink. Removal of the solvent gave a peach-coloured oil, which upon stirring with hexane (10 mL) for 10 min, and then reduction to half volume afforded **29** as a colourless solid. Yield: 80 mg (58 %). Recrystallisation from benzene/hexane afforded material appropriate for X-ray crystallography and elemental analysis. ^{1}H NMR (500 MHz, C_6D_6): δ 8.00 (t, $^3J_{HH}$ = 8.5 Hz, 6H, $PC_6\mathit{H}_5$), 7.38 (m, 3H, $PC_6\mathit{H}_5$), 6.03 (m, 1H, $NC\mathit{H}_2CH_3$), 5.56 (m, 1H, $NC\mathit{H}_2CH_3$), 4.73 (m, 1H, $NC\mathit{H}_2CH_3$), 4.06 (m, 1H, $NC\mathit{H}_2CH_3$), 4.00 (m, 1H, $NC\mathit{H}_2CH_3$), 3.90 (m, 1H, $NC\mathit{H}_2CH_3$), 3.45 (m, 1H, $NC\mathit{H}_2CH_3$), 3.29 (m, 1H, $NC\mathit{H}_2CH_3$), 1.71 (s, 3H, $NCC\mathit{H}_3$═$NCCH_3$), 1.61 (s, 3H, $NCCH_3$═$NCC\mathit{H}_3$), 1.57 (s, 6H, $NCC\mathit{H}_3$═$NCC\mathit{H}_3$), 1.48 (t, $^3J_{HH}$ = 6.9 Hz, 3H, $NCH_2C\mathit{H}_3$), 1.39 (br s, 3H, $C\mathit{H}_3$(pin)), 1.31 (br s, 3H, $C\mathit{H}_3$(pin)), 1.18 (t, $^3J_{HH}$ = 7.3 Hz, 3H, $NCH_2C\mathit{H}_3$), 1.12 (br s, 3H, $C\mathit{H}_3$(pin)), 1.02 (br s, 3H, $C\mathit{H}_3$(pin)), 0.99 (t, $^3J_{HH}$ = 7.0 Hz, 3H, $NCH_2C\mathit{H}_3$), 0.31 (t, $^3J_{HH}$ = 7.0 Hz, 3H, $NCH_2C\mathit{H}_3$), -6.30 (br s, 1H, Ru-(μ-*H*)$_2$), -8.96 (d, $^2J_{HP}$ = 31.8 Hz, 1H, Ru-*H*), -10.69 (br s, 1H, Ru-(μ-*H*)$_2$); ^{31}P{^{1}H} NMR (202 MHz, C_6D_6): δ = 59.7 (s); ^{11}B{^{1}H} NMR (160 MHz, C_6D_6): δ 36.9 (s); ^{13}C{^{1}H} NMR (126 MHz, C_6D_6): δ 196.9 (d, $^2J_{CP}$ = 10.6, Ru-C_{NHC}), 192.3 (d, $^2J_{CP}$ = 89.3 Hz, Ru-C_{NHC}), 144.5 (d, $^2J_{CP}$ = 29.8 Hz, PC_6H_5), 138.0 (s, $^2J_{CP}$ = 12.1 Hz, PC_6H_5), 132.2 (m, PC_6H_5), 123.0 (s, $NCCH_3$═$NCCH_3$), 122.8 (s, $NCCH_3$═$NCCH_3$), 122.7 (s, $NCCH_3$═$NCCH_3$), 122.1 (s, $NCCH_3$═$NCCH_3$), 44.5 (s, NCH_2CH_3), 44.2 (s, NCH_2CH_3), 42.9 (s, NCH_2CH_3), 42.8 (s, NCH_2CH_3), 25.4 (s, CH_3pin), 25.1 (s, CH_3pin), 24.8 (s, CH_3pin), 24.7 (s, CH_3pin), 14.4 (s, CH_2CH_3), 14.1 (s, CH_2CH_3), 13.8 (s, CH_2CH_3), 9.6 (s, $NCCH_3$═$NCCH_3$), 9.5 (s, $NCCH_3$═$NCCH_3$), 9.4 (s, $NCCH_3$═$NCCH_3$), 9.3 (s, $NCCH_3$═$NCCH_3$); elemental analysis calcd (%) for $C_{42}H_{62}BN_4O_2PRu$ (797.83): C, 63.22; H, 7.83; N, 7.02; found: C, 63.21; H, 7.59; N, 7.11.

5.3.6. Catalytic reduction of CO_2 employing $Ru(IEt_2Me_2)_2$ based complexes

In a J. Young's resealable NMR tube, (**5b**, 7 mg), $Ru(IEt_2Me_2)_2(PPh_3)(H_2Bpin)H$ (**29**, 10 mg) or $Ru(IEt_2Me_2)_2(PPh_3)(OCHO)H$ (**17**, 10 mg) were combined with 25 equiv. HBpin in C_6D_6 (0.4 mL) and the solutions freeze-pump-thaw degassed. 1 atm $^{13}CO_2$ was introduced and the reactions monitored by multinuclear NMR spectroscopy.

5.3.7. Stoichiometric reaction of $Ru(IEt_2Me_2)_2(PPh_3)(H_2Bpin)H$ (**29**) and CO_2

Addition of 1 atm of CO_2 to $Ru(IEt_2Me_2)_2(PPh_3)(H_2Bpin)H$, **29** (10 mg, 0.01 mmol) in a J. Youngs resealable NMR tube resulted in immediate formation of $Ru(IEt_2Me_2)_2(PPh_3)H(OCOH)$, **17**. After 2 h small amounts (*ca*. 6 %) of complexes **30a** and **30b** with carbonyl and formate ligands were visible by NMR spectroscopy. Selected NMR data for **30a**: ^1H NMR (500 MHz, C_6D_6): δ -17.18 (dd, $^2J_{HP}$ = 22.4 Hz, $^2J_{HC}$ = 12.2 Hz, Ru*H*). $^{31}P\{^1H\}$ NMR (202 MHz, C_6D_6): δ 47.9 (d, $^2J_{PC}$ = 16.3 Hz). $^{13}C\{^1H\}$ NMR (126 MHz, C_6D_6): δ 207.5 (d, $^2J_{CP}$ = 13.8 Hz, Ru-*C*O). Selected NMR data for **30b**: ^1H NMR (500 MHz, C_6D_6): δ -18.36 (d, $^2J_{HC}$ = 12.8, Ru*H*). $^{13}C\{^1H\}$ NMR (126 MHz, C_6D_6): δ 209.3 (s, Ru-*C*O).

5.3.8. Stoichiometric reaction of $Ru(IEt_2Me_2)_2(PPh_3)H(OCOH)$ (**17**) and HBpin

Addition of *ca*. 1 equiv. of HBpin (*ca*. 1 μL, 7.0 μmol) to a C_6D_6 (0.4 mL) solution **17** in a J. Youngs resealable NMR tube resulted in a mixture of $Ru(H_2Bpin)$ containing complexes. After 24 h the major product was $Ru(IEt_2Me_2)_2(PPh_3)(H_2Bpin)H$, **29** and no free HBpin remained.

5.3.9. Catalytic reduction of CO_2 using $Ru(IMe_4)_4H_2$ (**3**)

In a J. Young's resealable NMR tube **3** (5 mg, 0.008 mmol) was combined with 25 equiv. HBpin (30 μL, 0.21 mmol) in C_6D_6 (0.4 mL). The solution was degassed (freeze-pump-thaw), prior to 1 atm of $^{13}CO_2$ being added.

5.4. References

1. (a) Vogt, M.; Gargir, M.; Iron, M. A.; Diskin-Posner, Y.; Ben-David, Y.; Milstein, D., *Chem.-Eur. J.* **2012**, *18,* 9194; (b) Omae, I., *Coord. Chem. Rev.* **2012**, *256,* 1384; (c) Czaun, M.; Goeppert, A.; May, R.; Haiges, R.; Prakash, G. K. S.; Olah, G. A., *ChemSusChem* **2011**, *4,* 1241; (d) Riduan, S. N.; Zhang, Y., *Dalton Trans.* **2010**, *39,* 3347; (e) Benson, E. E.; Kubiak, C. P.; Sathrum, A. J.; Smieja, J. M., *Chem. Soc. Rev.*

2009, *38,* 89; (f) Sakakura, T.; Choi, J.-C.; Yasuda, H., *Chem. Rev.* **2007**, *107,* 2365; (g) Aresta, M.; Dibenedetto, A., *Dalton Trans.* **2007**, 2975; (h) Omae, I., *Catal. Today* **2006**, *115,* 33; (i) Jessop, P. G.; Joó, F.; Tai, C. C., *Coord. Chem. Rev.* **2004**, *248,* 2425; (j) Arakawa, H.; Aresta, M.; Armor, J. N.; Barteau, M. A.; Beckman, E. J.; Bell, A. T.; Bercaw, J. E.; Creutz, C.; Dinjus, E.; Dixon, D. A.; Domen, K.; DuBois, D. L.; Eckert, J.; Fujita, E.; Gibson, D. H.; Goddard, W. A.; Goodman, D. W.; Keller, J.; Kubas, G. J.; Kung, H. H.; Lyons, J. E.; Manzer, L. E.; Marks, T. J.; Morokuma, K.; Nicholas, K. M.; Periana, R.; Que, L.; Rostrup-Nielson, J.; Sachtler, W. M. H.; Schmidt, L. D.; Sen, A.; Somorjai, G. A.; Stair, P. C.; Stults, B. R.; Tumas, W., *Chem. Rev.* **2001**, *101,* 953; (k) Gibson, D. H., *Chem. Rev.* **1996**, *96,* 2063; (l) Leitner, W., *Angew. Chem., Int. Ed. Engl.* **1995**, *34,* 2207.

2. (a) Wang, T.; Stephan, D. W., *Chem. Eur. J.* **2014**, *20,* 3036; (b) Fontaine, F.-G.; Courtemanche, M.-A.; Legare, M.-A., *Chem. Eur. J.* **2014**, *20,* 2990; (c) Fernandez-Alvarez, F. J.; Aitani, A. M.; Oro, L. A., *Catal. Sci. Technol.* **2014**, *4,* 611; (d) Courtemanche, M.-A.; Legare, M.-A.; Maron, L.; Fontaine, F.-G., *J. Am. Chem. Soc.* **2013**, *135,* 9326; (e) Li, Y.; Sorribes, I.; Yan, T.; Junge, K.; Beller, M., *Angew. Chem., Int. Ed.* **2013**, *52,* 12156; (f) Beydoun, K.; vom Stein, T.; Klankermayer, J.; Leitner, W., *Angew. Chem., Int. Ed.* **2013**, *52,* 9554; (g) Riduan, S. N.; Ying, J. Y.; Zhang, Y., *Chemcatchem* **2013**, *5,* 1490; (h) Berkefeld, A.; Piers, W. E.; Parvez, M.; Castro, L.; Maron, L.; Eisenstein, O., *Chem. Sci.* **2013**, *4,* 2152; (i) Courtemanche, M.-A.; Larouche, J.; Legare, M.-A.; Bi, W.; Maron, L.; Fontaine, F.-G., *Organometallics* **2013**, *32,* 6804; (j) Appel, A. M.; Bercaw, J. E.; Bocarsly, A. B.; Dobbek, H.; DuBois, D. L.; Dupuis, M.; Ferry, J. G.; Fujita, E.; Hille, R.; Kenis, P. J. A.; Kerfeld, C. A.; Morris, R. H.; Peden, C. H. F.; Portis, A. R.; Ragsdale, S. W.; Rauchfuss, T. B.; Reek, J. N. H.; Seefeldt, L. C.; Thauer, R. K.; Waldrop, G. L., *Chem. Rev.* **2013**, *113,* 6621; (k) Fan, T.; Chen, X.; Lin, Z., *Chem. Commun.* **2012**, *48,* 10808; (l) Park, S.; Bezier, D.; Brookhart, M., *J. Am. Chem. Soc.* **2012**, *134,* 11404; (m) Sgro, M. J.; Stephan, D. W., *Angew. Chem., Int. Ed.* **2012**, *51,* 11343; (n) Khandelwal, M.; Wehmschulte, R. J., *Angew. Chem., Int. Ed.* **2012**, *51,* 7323; (o) Schaefer, A.; Saak, W.; Haase, D.; Mueller, T., *Angew. Chem., Int. Ed.* **2012**, *51,* 2981; (p) Wang, W.; Wang, S.; Ma, X.; Gong, J., *Chem. Soc. Rev.* **2011**, *40,* 3703; (q) Cokoja, M.; Bruckmeier, C.; Rieger, B.; Herrmann, W. A.; Kuehn, F. E., *Angew. Chem., Int. Ed.* **2011**, *50,* 8510; (r) Berkefeld, A.; Piers, W. E.; Parvez, M., *J. Am. Chem. Soc.* **2010**, *132,* 10660; (s) Huang, F.; Lu, G.; Zhao, L.; Li, H.; Wang, Z.-X., *J. Am. Chem. Soc.* **2010**, *132,* 12388; (t) Riduan, S. N.; Zhang, Y.; Ying, J. Y., *Angew. Chem., Int. Ed.* **2009**, *48,* 3322; (u) Deglmann, P.; Ember, E.;

Hofmann, P.; Pitter, S.; Walter, O., *Chem.-Eur. J.* **2007**, *13,* 2864; (v) Matsuo, T.; Kawaguchi, H., *J. Am. Chem. Soc.* **2006**, *128,* 12362.

3. (a) Chakraborty, S.; Zhang, J.; Patel, Y. J.; Krause, J. A.; Guan, H., *Inorg. Chem.* **2013**, *52,* 37; (b) Chakraborty, S.; Patel, Y. J.; Krause, J. A.; Guan, H., *Polyhedron* **2012**, *32,* 30; (c) Chakraborty, S.; Zhang, J.; Krause, J. A.; Guan, H., *J. Am. Chem. Soc.* **2010**, *132,* 8872.

4. (a) Bontemps, S.; Vendier, L.; Sabo-Etienne, S., *J. Am. Chem. Soc.* **2014**, *136,* 4419; (b) Bontemps, S.; Sabo-Etienne, S., *Angew. Chem., Int. Ed.* **2013**, *52,* 10253; (c) Bontemps, S.; Vendier, L.; Sabo-Etienne, S., *Angew. Chem., Int. Ed.* **2012**, *51,* 1671.

5. Huang, F.; Zhang, C.; Jiang, J.; Wang, Z.-X.; Guan, H., *Inorg. Chem.* **2011**, *50,* 3816.

6. Sabo-Etienne, S.; Chaudret, B., *Coord. Chem. Rev.* **1998**, *178,* 381.

7. (a) Rankin, M. A.; Cummins, C. C., *J. Am. Chem. Soc.* **2010**, *132,* 10021; (b) Tardif, O.; Hashizume, D.; Hou, Z. M., *J. Am. Chem. Soc.* **2004**, *126,* 8080; (c) Schlorer, N. E.; Cabrita, E. J.; Berger, S., *Angew. Chem., Int. Ed.* **2002**, *41,* 107.

8. Montiel-Palma, V.; Lumbierres, M.; Donnadieu, B.; Sabo-Etienne, S.; Chaudret, B., *J. Am. Chem. Soc.* **2002**, *124,* 5624.

9. (a) Gunanathan, C.; Hoelscher, M.; Pan, F.; Leitner, W., *J. Am. Chem. Soc.* **2012**, *134,* 14349; (b) Alcaraz, G.; Sabo-Etienne, S., *Coord. Chem. Rev.* **2008**, *252,* 2395; (c) Lachaize, S.; Essalah, W.; Montiel-Palma, V.; Vendier, L.; Chaudret, B.; Barthelat, J. C.; Sabo-Etienne, S., *Organometallics* **2005**, *24,* 2935.

10. (a) Ellul, C. E.; Saker, O.; Mahon, M. F.; Apperley, D. C.; Whittlesey, M. K., *Organometallics* **2008**, *27,* 100; (b) Burling, S.; Kociok-Kohn, G.; Mahon, M. F.; Whittlesey, M. K.; Williams, J. M. J., *Organometallics* **2005**, *24,* 5868; (c) Elschenbroich, C.; Salzer, A., *Organometallics. A Concise Introduction, 2nd ed.* Weinheim, Germany, 1992; Chapter 17.9, 17.12.

11. Chantler, V. L.; Chatwin, S. L.; Jazzar, R. F. R.; Mahon, M. F.; Saker, O.; Whittlesey, M. K., *Dalton Trans.* **2008**, 2603.

12. Burling, S.; Haller, L. J. L.; Mas-Marzá, E.; Moreno, A.; Macgregor, S. A.; Mahon, M. F.; Pregosin, P. S.; Whittlesey, M. K., *Chem.-Eur. J.* **2009**, *15,* 10912.

13. Sanders, J. K. M.; Hunter, B. K., *Modern NMR Spectroscopy; A Guide for Chemists*. Oxford University Press: 1987.

14. Bernskoetter, W. H.; Hazari, N., *Eur. J. Inorg. Chem.* **2013**, 4032.

Future Work

The target molecules in the form of $Ru(IMe_4)_4H_2$ and $Ru(NHC)_2(PPh_3)_2H_2$ (NHC = IMe_4, IEt_2Me_2) have been successfully synthesized. In both cases, *trans*-dihydride isomers have been isolated, presumably as a result of the bulk of the NHC and phosphine ligands employed. It remains to be seen in the case of the mixed NHC-phosphine species whether a *cis*-RuH_2 complex can be isolated. This will be necessary if the intention to access "$Ru(NHC)_2(PR_3)_2$" is to be met. An investigation into the synthesis and reactivity of analogues of **3**, **4a** and **5b** with a bidentate carbene of phosphine could prove useful in this regard. If the hydrides were forced to be *cis*, an NHC analogue of the $Ru(dmpe)_2$ fragment might be accessible, which would potentially be a very reactive fragment for small molecule bond activation.

In terms of the chemistry of **3**, **4a**, and **5b** themselves, ongoing studies have already shown that the nucleophilic hydride character of **4a** and **5b** leads to them being active for the catalytic hydrodefluorination of aromatic fluorocarbons. Catalytic hydrogenation is another obvious angle that would be worthy of investigation.

Appendix

Appendix

Crystal data and structure refinement for $Ru(IMe_4)_2(PPh_3)_2H_2$ (4a)

Identification code	h11mkw06
Empirical formula	C50 H56 N4 P2 Ru
Formula weight	876.00
Temperature	150(2) K
Wavelength	0.71073 Å
Crystal system	Monoclinic
Space group	P21/n
Unit cell dimensions	a = 11.0200(1)Å $\alpha = 90^o$
	b = 9.3340(2)Å $\beta = 102.602(1)^o$
	c = 21.8030(4)Å $\gamma = 90^o$
Volume	2188.64(6) $Å^3$
Z	2
Density (calculated)	1.329 Mg/m^3
Absorption coefficient	0.470 mm^{-1}
F(000)	916
Crystal size	0.25 x 0.20 x 0.20 mm
Theta range for data collection	3.61 to 30.04^o
Index ranges	-15<=h<=15; -13<=k<=13; -30<=l<=30
Reflections collected	52817
Independent reflections	6407 [R(int) = 0.0538]
Reflections observed (>2σ)	5305
Data Completeness	0.997
Absorption correction	Semi-empirical from equivalents
Max. and min. transmission	0.914 and 0.830
Refinement method	Full-matrix least-squares on F^2
Data / restraints / parameters	6407 / 1 / 267
Goodness-of-fit on F^2	1.034
Final R indices [I>2σ(I)]	R1 = 0.0288 wR2 = 0.0661
R indices (all data)	R1 = 0.0408 wR2 = 0.0718
Largest diff. peak and hole	0.719 and -0.599 $eÅ^{-3}$

Notes

Asymmetric unit = ½ of a molecule – with the central Ru located at a crystallographic inversion centre. H1 located and refined at 1.6 Å from Ru1.

Crystal data and structure refinement for $Ru(IEt_2Me_2)_2(PPh_3)_2H_2$ (5b)

Identification code	k12mkw14
Empirical formula	C66 H76 N4 P2 Ru
Formula weight	1088.32
Temperature	150(2) K
Wavelength	0.71073 Å
Crystal system	Monoclinic
Space group	C2/c
Unit cell dimensions	a = 44.8210(3)Å alpha = 90°
	b = 11.5380(1)Å beta = 117.47°
	c = 25.1760(2)Å gamma = 90°
Volume	11551.59(16) $Å^3$
Z	8
Density (calculated)	1.252 Mg/m^3
Absorption coefficient	0.370 mm^{-1}
F(000)	4592
Crystal size	0.30 x 0.20 x 0.20 mm
Theta range for data collection	3.52 to 30.09°
Index ranges	-62<=h<=62; -16<=k<=16; -35<=l<=35
Reflections collected	128617
Independent reflections	16889 [R(int) = 0.0743]
Reflections observed (>2sigma)	12123
Data Completeness	0.994
Absorption correction	Semi-empirical from equivalents
Max. and min. transmission	0.930 and 0.833
Refinement method	Full-matrix least-squares on F^2
Data / restraints / parameters	16889 / 2 / 728
Goodness-of-fit on F^2	1.018
Final R indices [I>2sigma(I)]	R1 = 0.0395 *wR*2 = 0.0826
R indices (all data)	R1 = 0.0707 *wR*2 = 0.0953
Largest diff. peak and hole	1.044 and -0.718 $eÅ^{-3}$

Notes

Asymmetric unit consists of one dihydride molecule and 2 molecules of toluene. The solvent moiety containing C61 exhibited 55:45 disorder.

Hydrides H1 and H2 were located and refined at a distance of 1.6 Å from Ru1

Crystal data and structure refinement for $Ru(IMe_4)_2(PPh_3)(CO)(CO_3)$ (12)

Identification code	h12mkw13
Empirical formula	C34 H39 N4 O4 P Ru
Formula weight	699.73
Temperature	150(2) K
Wavelength	0.71073 Å
Crystal system	Monoclinic
Space group	P21/n
Unit cell dimensions	a = 12.6390(2)Å alpha = 90°
	b = 18.5257(3)Å beta = 102.4330(10)°
	c = 14.3977(3)Å gamma = 90°
Volume	3292.11(10) $Å^3$
Z	4
Density (calculated)	1.412 Mg/m^3
Absorption coefficient	0.568 mm^{-1}
F(000)	1448
Crystal size	0.50 x 0.40 x 0.40 mm
Theta range for data collection	3.97 to 27.48°
Index ranges	-16<=h<=16; -23<=k<=24; -18<=l<=18
Reflections collected	53544
Independent reflections	7522 [R(int) = 0.1228]
Reflections observed (>2sigma)	5812
Data Completeness	0.996
Absorption correction	Semi-empirical from equivalents
Max. and min. transmission	1.29 and 0.74
Refinement method	Full-matrix least-squares on F^2
Data / restraints / parameters	7522 / 0 / 405
Goodness-of-fit on F^2	1.069
Final R indices [I>2sigma(I)]	R1 = 0.0419 *wR*2 = 0.0935
R indices (all data)	R1 = 0.0634 *wR*2 = 0.1014
Largest diff. peak and hole	0.672 and -1.213 $eÅ^{-3}$

Crystal data and structure refinement for $[Ru(IMe_4)_2(PPh_3)_2H]I$ (13)

Identification code	h12mkw10
Empirical formula	C50 H55 I N4 P2 Ru
Formula weight	1001.89
Temperature	150(2) K
Wavelength	0.71073 Å
Crystal system	Monoclinic
Space group	C2
Unit cell dimensions	a = 17.8860(5)Å alpha = 90°
	b = 11.5280(4)Å beta = 112.726(2)°
	c = 12.1890(5)Å gamma = 90°
Volume	2318.13(14) $Å^3$
Z	2
Density (calculated)	1.435 Mg/m^3
Absorption coefficient	1.111 mm^{-1}
F(000)	1020
Crystal size	0.4 x 0.25 x 0.2 mm
Theta range for data collection	3.79 to 27.47°
Index ranges	-23<=h<=22; -14<=k<=14; -12<=l<=15
Reflections collected	9900
Independent reflections	5080 [R(int) = 0.0265]
Reflections observed (>2sigma)	4744
Data Completeness	0.991
Absorption correction	Semi-empirical from equivalents
Max. and min. transmission	0.804 and 0.758
Refinement method	Full-matrix least-squares on F^2
Data / restraints / parameters	5080 / 2 / 269
Goodness-of-fit on F^2	1.084
Final R indices [I>2sigma(I)]	R1 = 0.0261 *wR*2 = 0.0643
R indices (all data)	R1 = 0.0302 *wR*2 = 0.0667
Absolute structure parameter	-0.013(19)
Largest diff. peak and hole	0.511 and -0.520 $eÅ^{-3}$

Notes

H1 located and refined at a distance of 1.6 Å from Ru1.

Asymmetric unit consists of ½ of a cation and half of an anion. Ru1, H1 and I1 are located at a 2-fold rotation axis intrinsic to the space group symmetry.

Crystal data and structure refinement for $Ru(IEt_2Me_2)_2(PPh_3)_2(CO)H_2$ (14)

Identification code	h12mkw12
Empirical formula	C37 H49 N4 O P Ru
Formula weight	697.84
Temperature	150(2) K
Wavelength	0.71073 Å
Crystal system	Monoclinic
Space group	P21/n
Unit cell dimensions	a = 12.7857(7)Å alpha = 90°
	b = 19.0077(13)Å beta = 102.987(3)°
	c = 14.8084(5)Å gamma = 90°
Volume	3506.8(3) $Å^3$
Z	4
Density (calculated)	1.322 Mg/m^3
Absorption coefficient	0.527 mm^{-1}
F(000)	1464
Crystal size	0.5 x 0.4 x 0.25 mm
Theta range for data collection	4.16 to 27.47 °.
Index ranges	-12<=h<=16; -23<=k<=15; -15<=l<=14
Reflections collected	11300
Independent reflections	6035 [R(int) = 0.0382]
Reflections observed (>2sigma)	4480
Data Completeness	0.749
Absorption correction	Semi-empirical from equivalents
Max. and min. transmission	0.8943 and 0.8247
Refinement method	Full-matrix least-squares on F^2
Data / restraints / parameters	6035 / 2 / 413
Goodness-of-fit on F^2	1.026
Final R indices [I>2sigma(I)]	R1 = 0.0414 *wR*2 = 0.0795
R indices (all data)	R1 = 0.0687 *wR*2 = 0.0883
Largest diff. peak and hole	0.477 and -0.386 $eÅ^{-3}$

Notes

Hydrides located and refined at a distance of 1.6 Å from Ru1.

Crystal data and structure refinement for $Ru(IEt_2Me_2)_2(PPh_3)(\kappa^2\text{-}OCHO)H$ (17)

Identification code	p12mkw3
Empirical formula	C40 H52 N4 O2 P Ru
Formula weight	752.90
Temperature	149.9(2) K
Wavelength	0.7107 Å
Crystal system	Monoclinic
Space group	P21/n
Unit cell dimensions	a = 12.4656(6)Å alpha = 90°
	b = 12.8695(5)Å beta = 98.671(4)°
	c = 23.6891(9)Å gamma = 90°
Volume	3756.9(3) $Å^3$
Z	4
Density (calculated)	1.331 Mg/m^3
Absorption coefficient	0.499 mm^{-1}
F(000)	1580
Crystal size	0.10 x 0.10 x 0.06 mm
Theta range for data collection	3.02 to 27.48°
Index ranges	-14<=h<=16; -16<=k<=16; -21<=l<=30
Reflections collected	28448
Independent reflections	8610 [R(int) = 0.0676]
Reflections observed (>2sigma)	5478
Data Completeness	0.998
Absorption correction	Semi-empirical from equivalents
Max. and min. transmission	1.00000 and 0.96513
Refinement method	Full-matrix least-squares on F^2
Data / restraints / parameters	8610 / 43 / 494
Goodness-of-fit on F^2	1.011
Final R indices [I>2sigma(I)]	R1 = 0.0445 *wR*2 = 0.0767
R indices (all data)	R1 = 0.0935 *wR*2 = 0.0916
Largest diff. peak and hole	0.436 and -0.458 $eÅ^{-3}$

Notes

The asymmetric unit consists of one molecule of the formate complex and ½ of a benzene molecule. The latter is proximate to a crystallographic inversion centre which serves to generate the remainder of the solvent.

50:50 disorder was observed for atoms C8 and C9 , while 60:40 disorder was evident for N4 C17 and C18.

Some distance and ADP restraints were applied in the disordered regions to assist convergence.

Crystal data and structure refinement for $[Ru(IEt_2Me_2)_2(PPh_3)_2H]I$ (20)

Identification code	h12mkw8
Empirical formula	C60 H69 I N4 P2 Ru
Formula weight	1136.10
Temperature	150(2) K
Wavelength	0.71073 Å
Crystal system	Triclinic
Space group	P-1
Unit cell dimensions	a = 10.6850(3)Å alpha = 86.423(1)^o
	b = 14.1070(3)Å beta = 81.838(1)^o
	c = 18.6300(5)Å gamma = 74.350(1)^o
Volume	2675.81(12) Å^3
Z	2
Density (calculated)	1.410 Mg/m^3
Absorption coefficient	0.972 mm^{-1}
F(000)	1168
Crystal size	0.18 x 0.18 x 0.10 mm
Theta range for data collection	4.02 to 27.48^o
Index ranges	-13<=h<=13; -18<=k<=18; -24<=l<=24
Reflections collected	45106
Independent reflections	12206 [R(int) = 0.0565]
Reflections observed (>2sigma)	8833
Data Completeness	0.995
Absorption correction	Semi-empirical from equivalents
Max. and min. transmission	0.880 and 0.819
Refinement method	Full-matrix least-squares on F^2
Data / restraints / parameters	12206 / 1 / 625
Goodness-of-fit on F^2	1.014
Final R indices [I>2sigma(I)]	R1 = 0.0414 *wR*2 = 0.0899
R indices (all data)	R1 = 0.0709 *wR*2 = 0.1023
Largest diff. peak and hole	1.006 and -1.197 eÅ^{-3}

Notes

H1 located and refined at a distance of 1.6 Å from Ru1. The asymmetric unit in this structure was seen to contain 1 molecule of benzene in addition one cation and one anion.

Crystal data and structure refinement for $Ru(IEt_2Me_2)(PPh_3)_2HI$ (21)

Identification code	h13mkw8
Empirical formula	C47 H51 I N2 O0.50 P2 Ru
Formula weight	941.81
Temperature	150(2) K
Wavelength	0.71073 Å
Crystal system	Monoclinic
Space group	P21/n
Unit cell dimensions	a = 9.1740(1)Å alpha = 90°
	b = 22.0920(5)Å beta = 99.051(1)°
	c = 20.9110(5)Å gamma = 90°
Volume	4185.30(15) $Å^3$
Z	4
Density (calculated)	1.495 Mg/m^3
Absorption coefficient	1.225 mm^{-1}
F(000)	1912
Crystal size	0.30 x 0.20 x 0.10 mm
Theta range for data collection	3.71 to 27.48°
Index ranges	-11<=h<=11; -28<=k<=28; -27<=l<=27
Reflections collected	46066
Independent reflections	9431 [R(int) = 0.0542]
Reflections observed (>2sigma)	7384
Data Completeness	0.983
Absorption correction	Semi-empirical from equivalents
Max. and min. transmission	0.887 and 0.685
Refinement method	Full-matrix least-squares on F^2
Data / restraints / parameters	9431 / 1 / 507
Goodness-of-fit on F^2	1.057
Final R indices [I>2sigma(I)]	R1 = 0.0330 *wR*2 = 0.0650
R indices (all data)	R1 = 0.0526 *wR*2 = 0.0715
Largest diff. peak and hole	0.608 and -0.739 $eÅ^{-3}$

Notes

H1 located and refined at a distance of 1.6 Å from Ru1.

Hydrogen atoms attached to C5 were also readily located, but ultimately included at calculated positions proximate to the relevant maxima in the difference electron density map. Associated U_{iso} values were refined without restraints.

The asymmetric unit was seen to contain a solvent fragment which approximates ½ of a THF molecule. This moiety straddles a crystallographic inversion centre and present as 3 atoms (1 oxygen and 2 carbons) with 50% occupancy and 1 carbon with 100% occupancy. Addition of hydrogen atoms in solvent could not be achieved because of the connectivity arising from having the solvent disordered close to a space group symmetry element.

Crystal data and structure refinement for $Ru(IMe_4)_2(PPh_3)(H_2Bpin)H$ (27)

Identification code	k14mkw4
Empirical formula	C41 H57 B N4 O2 P Ru
Formula weight	780.76
Temperature	150(2) K
Wavelength	0.71073 Å
Crystal system	Triclinic
Space group	P-1
Unit cell dimensions	a = 10.5270(1)Å alpha = 83.759(1)^o
	b = 12.1350(1)Å beta = 84.669(1)^o
	c = 16.6610(2)Å gamma = 73.815(1)^o
Volume	2027.52(4) Å^3
Z	2
Density (calculated)	1.279 Mg/m^3
Absorption coefficient	0.464 mm^{-1}
F(000)	822
Crystal size	0.25 x 0.15 x 0.12 mm
Theta range for data collection	3.54 to 27.45^o
Index ranges	-13<=h<=13; -15<=k<=15; -21<=l<=21
Reflections collected	32871
Independent reflections	9176 [R(int) = 0.0604]
Reflections observed (>2sigma)	7841
Data Completeness	0.989
Absorption correction	Semi-empirical from equivalents
Max. and min. transmission	0.948 and 0.911
Refinement method	Full-matrix least-squares on F^2
Data / restraints / parameters	9176 / 37 / 502
Goodness-of-fit on F^2	1.037
Final R indices [I>2sigma(I)]	R1 = 0.0333 *wR*2 = 0.0685
R indices (all data)	R1 = 0.0445 *wR*2 = 0.0732
Largest diff. peak and hole	0.645 and -0.673 eÅ^{-3}

Notes

H1, H2 and H3 located. H1 refined subject to being located 1.6 Å from Ru1. H2 and H3 refined without constraints.

The asymmetric unit was seen to comprise ½ of a molecule of benzene, proximate to a crystallographic inversion centre. The atoms in this fragment were disordered in a 60:40 ration over 2 proximate sites.

1-2 and 1-3 carbon-carbon distances were, respectively, refined subject to being similar in the solvent. ADP restraints were also included in the minor disordered component to assist convergence.

Crystal data and structure refinement for $Ru(IEt_2Me_2)_2(PPh_3)(H_2Bpin)H$ (29)

Identification code	k14mkw3
Empirical formula	C42 H62 B N4 O2 P Ru
Formula weight	797.81
Temperature	150(2) K
Wavelength	0.71073 Å
Crystal system	Monoclinic
Space group	C2/c
Unit cell dimensions	a = 34.1430(3)Å alpha = 90°
	b = 11.98300(10)Å beta = 102.7220(10)°
	c = 20.5910(2)Å gamma = 90°
Volume	8217.69(13) $Å^3$
Z	8
Density (calculated)	1.290 Mg/m^3
Absorption coefficient	0.460 mm^{-1}
F(000)	3376
Crystal size	0.36 x 0.22 x 0.20 mm
Theta range for data collection	3.55 to 27.47 °.
Index ranges	-44<=h<=44; -15<=k<=15; -26<=l<=26
Reflections collected	66662
Independent reflections	9392 [R(int) = 0.0581]
Reflections observed (>2sigma)	7672
Data Completeness	0.997
Absorption correction	Semi-empirical from equivalents
Max. and min. transmission	0.916 and 0.833
Refinement method	Full-matrix least-squares on F^2
Data / restraints / parameters	9392 / 2 / 484
Goodness-of-fit on F^2	1.055
Final R indices [I>2sigma(I)]	R1 = 0.0322 *wR*2 = 0.0709
R indices (all data)	R1 = 0.0466 *wR*2 = 0.0779
Largest diff. peak and hole	0.819 and -0.681 $eÅ^{-3}$

Notes

H1, H2 and H3 all located in the penultimate difference Fourier electron density map. H1 refined subject to being 1.6 Å from Ru1. H2 and H3 refined subject to being similarly distanced from B1.